UNIVERSIDAD DE ANTIOQUIA

SIMULTANEOUS CATALYTIC ELIMINATION OF NITROGEN OXIDES AND ORGANOCHLORINE COMPOUNDS OVER Pd/Co CATALYSTS

Manuel José Cano Correa

Universidad de Antioquia

Facultad de Ingeniería, Departamento de Ingeniería Química

Medellín, Colombia

2020

Simultaneous catalytic elimination of nitrogen oxides and organochlorine compounds over pd/co catalysts

Manuel José Cano Correa

Tesis como requisito para optar al título de:
Doctor en Ingeniería Química

Directora: Prof. Dr. Lina María González Rodríguez

Co- Directora: Prof. Dr. Beatriz Helena Aristizábal Zuluaga

Manuel José Cano Correa.

Universidad de Antioquia
Facultad de Ingeniería
Departamento de Ingeniería Química.
Medellín, Colombia
2020.

Acknowledgements

Now that I am looking at the past, I can realize that this work would not have been possible at all without the invaluable help of a lot of people. It would be an injustice not to dedicate some lines to some of them, although at the risk that I may skip someone unintentionally.

First, I am very grateful to my entire family specially to my father Luis (R.I.P) and to my mother Inés whose teachings led me down to these paths.

I am very grateful to the Environmental Catalysis research group and all its members, especially to Prof Dr. Aída Luz Villa for allow me to be a part of the research group and the trust placed on me.

Many thanks to the director Prof Dr. Lina María González Rodríguez and co-director Prof Dr. Beatriz Helena Aristizábal Zuluaga for their valuable advices, instructions and the global guide throughout this research project.

I am very grateful to Prof Dr. Asier Aranzabal Maiztegi and to Prof Dr. Maria Pilar González Marcos for their very assertive comments on some technical details of this research, for their support and guidance during my predoctoral stay at the Chemical Technologies for Environmental Sustainability Group, University of the Basque County UPV/EHU (Bilbo, Spain).

I want to thank to Colciencias for the financial support through the project 1115-569-33782 and the scholarship to finish the last part of the doctorate program. I am also very grateful with Sapiencia, Agencia de Educación Superior de Medellín, for the financial support given for the predoctoral stay at University of the Basque County UPV/EHU (Bilbo, Spain).

Finally, I would like to dedicate some lines plenty of thanks to some colleagues and friends for help me to successfully conclude this project: Mr. Felipe Guarín for his valuable help during the experimental set-up stage of the project, Mr. Oscar Arbeláez for sharing his knowledge about the handling of some laboratory equipment and for some very precise technical advices, Mr. Mateo Giraldo for his help during the kinetic experimental stage, Mr. Juan Alberto Martín for his support and help during some laboratory experiments at the UPV/EHU, Mr. Oscar Hernandez for his moral support and personal advices during the last years of the project, Mrs. Sandra Restrepo for her honest friendship, advices and encouragement, Mrs. Selenne Ramírez for encouraging me to take the first steps in this direction, Mrs Tania Chanaga for her advices and encouragement and Mrs. Silvana Arias for her greats tips and very honest friendship during some years of the project. I am sure that I skipped a lot of people to thank them but for all who made this work possible: Many thanks!

Summary

This thesis deal with the environmental problem of the toxic emissions of dioxins, furans and nitrogen oxides to the atmosphere generated during combustion processes, especially in waste incineration plants. For the depuration of such exhaust gas pollutants, bimetallic palladium and cobalt catalysts supported on protonic mordenite (Pd/Co-HMOR) and sulfated zirconia (Pd/Co-SZ) were studied. The selective catalytic reduction of NO by CH_4 (CH_4-SCR) simultaneously with the oxidation of ortho-Dichlorobenzene (*o*-DCB) in gas phase were evaluated over the temperature range between 150 and 550 °C at atmospheric pressure. The *o*-DCB was used as a model molecule since its great structural similarity with 2,3,7,8 tetrachlorodibenzo-p-dioxin (TCDD) which is considered the most toxic dioxin congener.

The Pd/Co catalysts were characterized by several physicochemical techniques such as AAS, H_2-TPR, NH_3-TPD, BET, TGA, Raman spectroscopy, XPS, SEM/EDS, TEM/EDS and *in-situ* FTIR spectroscopy studies, in order to identify the nature of the active species responsible of their activity and stability in the simultaneous reactions. Some catalytic analysis and characterizations were performed only for Pd/Co-HMOR catalyst, since this showed the better catalytic performance in the simultaneous reactions.

The catalysts were tested under several operation conditions including the presence of water vapor (6%) and oxygen (10%), since these components are unavoidably present in the gas exhaust of any combustion processes. The Pd/Co-HMOR presented a better catalytic performance than Pd/Co-SZ in terms of activity and durability, for the simultaneous reactions. The Pd/Co-HMOR showed the higher conversions at 500 ºC, 40% and 99% for NO and *o*-DCB, respectively, in the case of Pd/Co-SZ catalyst the higher conversion of NO and *o*-DCB were 25% and 99%, respectively at 550 ºC. Both catalysts were highly stable for the *o*-DCB oxidation, however in the case of CH_4-SCR, the Pd/Co-SZ almost completely

deactivated after only 7 hours of continuous operation while the Pd/Co-HMOR catalyst showed a better stability performance although the NO conversion decayed by 50% after 23 h of continuous operation. The main cause of catalyst deactivation identified for Pd/Co-SZ catalyst was the loss of the sulfate group leading to the formation of the monoclinic phase of zirconia, while in the case of Pd/Co-HMOR catalyst the formation of PdO clusters explains the loss of the activity towards the CH_4-SCR of NOx reaction.

The *in-situ* FTIR study of the Pd/Co-HMOR and the comparison between the reaction rate measurements of single and simultaneous reactions showed that Co^{2+} Lewis sites and Brønsted acid sites are common active sites for both reactions, but there is a competition for these active sites during simultaneous reactions.

Pd/Co-HMOR catalyst has a potential use in the selective catalytic reduction of nitrogen oxides by methane simultaneously with the catalytic oxidation of *o*-DCB under wet and lean conditions. From a technical point of view, these results open a new research field on this topic due to the possibility of the replacement of conventional NH_3-SCR of NOx over vanadium-tungsten which present some risks related with the use of ammonia. The use of methane instead of ammonia as NOx reductant is a desired alternative, since the methane is widely available, easy of handle and relatively cheap.

Table of Contents

List of Figures

List of Tables

Chapter 1 Introduction

The incineration is an alternative method for dealing with the municipal, medical and hazardous wastes. However, during the thermal processing several harmful compounds may be formed and emitted to the atmosphere unless the incineration plant accounts with appropriate technology for the cleaning of exhaust gases [1]. Nitrogen oxides (NOx), dioxins and furans are among the most problematic pollutants, the harmful effects of these compounds on the environment and human health are well known [2–4].

Since 1970's emission reduction policies of pollutants from flue gases in stationary sources have become increasingly stringent in several countries, especially in Japan, the United States (U.S) and Germany [3]. In this sense, the Gothenburg Protocol signed by 29 European countries together with U.S and Canada urges to set national emission ceilings for 2010 up to 2020 for NOx, SO_2, NH_3 and volatile organic compounds (VOCs) which are recognized as air pollutants causing of adverse effects on human health and environment, besides emission of these compounds are treated as a transboundary problem because they and their derivatives may travel long distances in the atmosphere affecting areas far away from the emission points [5,6].

Dioxins and nitrogen oxides are hazardous and highly toxic compounds formed as unwanted by-products of several processes [1]. Dioxins refers to polychlorinated dibenzodioxins (PCDD) and dibenzofurans (PCDF), two families of organic solids compounds with high melting points and low vapor pressures [7]. They are highly stable molecules classified as persistent organic pollutants, these compounds tend to bio-accumulate through the food chain

and can cause a variety of toxic responses in the exposed organisms such as carcinogenicity, immunotoxicity and adverse effects on reproduction, development, and endocrine functions [8,9]. In general PCCDs consist in two benzene rings linked by two oxygen atoms and PCDFs consist in two benzene rings but linked by a carbon bond on one side and an oxygen bridge on the other [7]. Depending on the position of chlorines inside the cyclic molecule there are 210 different possible compounds (135 PCDF and 75 PCDD), however special PCDDs/PCDFs congeners having chlorines at 2,3,7,8 positions have been identified as the most toxic and bioactive molecules to exposed organisms, they form a group of seventeen molecules (7 PCDDs and 10 PCDFs) which are called "toxic congeners" [10,11]. Not all these compounds have the same toxicity, the 2,3,7,8-tetrachlorodibenzo-p-dioxin (TCDD) is considered the congener with the greatest toxic potential [12] even catalogued as a "known" human carcinogen by the World Health Organization [7]. PCDDs/PCDFs have been detected as side products from several industrial thermal processes including incineration of municipal [13,14], hazardous [15] and medical [16] wastes, combustion of coal in power plants [17], metallurgical processes such as smelting [18] and in some chemical process where chlorine is involved as raw material [19]. Emission of dioxins to environment has become a problem of global great concern, in this sense several nations signed the International Stockholm Convention on Persistent Organic Pollutants [20] in which they committed to inventory and reduce the emissions of these kind of hazardous compounds including PCDDs/PCDFs. Besides, several countries have set stringent environmental regulations to the emissions of dioxins, for example a limit value of 0.1 ng (TEQ)/Nm^3 (i.e., International Toxicity Equivalents per Nm^3) has been adopted by several European countries and Japan [7][21].

Nitrogen monoxide (NO) and nitrogen dioxide (NO_2) commonly named as nitrogen oxides (NOx) are the source of several environmental issues including acid rain, photochemical smog, global warming, tropospheric ozone, ozone layer weakening [3,22,23] and even have been associated with increased rates of cardiac mortality and morbidity [4]. NOx are formed during the combustions processes in several stationary sources such as power plants, waste incinerators, refineries, iron ore sintering and so on, also they are generated from mobile sources during the combustion of gasoline and diesel in vehicles and airplanes [3,24]. NOx emissions are considered an environmental problem of great global concern, since 1970's

emission reduction policies of pollutants in flue gases from stationary sources has gradually evolved in several countries, especially in Japan, the United States (U.S) and Germany [3]. According with the Gothenburg Protocol urges to set national emission ceilings for 2010 up to 2020 for NOx, SO_2, NH_3 and volatile organic compounds which are recognized as air pollutants causing of adverse effects on human health and environment; besides emission of these compounds are treated as a transboundary problem because they and their derivatives may travel long distances in the atmosphere affecting areas far away from the emission points [5,6].

V_2O_5–WO_3/TiO_2 catalysts are widely used in stationary applications and have shown to be effective for the catalytic oxidation of PCDDs/PCDFs simultaneously with the selective catalytic reduction of NOx by ammonia (NH_3–SCR) [1,25,26], however there are some important drawbacks: The ammonia is a high corrosive, toxic and hard to handle gas as well its oxidation may generate more NOx [27]; vanadium-based catalysts may release volatile and toxic VOx to the environment [23], and the catalysts are also susceptible to deactivation by the depositions of ammonia salts [28], the presence of incomplete combustion products and coking [29].

The selective catalytic reduction of NOx by methane (CH_4–SCR) is considered a promising alternative to the traditional NH_3–SCR because the high availability, ease of handling and relative low cost of methane [30]; furthermore, CH_4 is the main component of natural gas, used in several power plants, industrial furnaces and residences with supply infrastructure in many countries [31]. In this work, bimetallic palladium and cobalt catalysts supported on protonic mordenite (Pd/Co-HMOR) and sulfated zirconia (SZ) were studied for the combined CH_4-SCR and *o*-DCB oxidation as an alternative to the conventions NH_3-SCR technology based on vanadium-tungsten supported catalysts.

1.1 Nitrogen Oxides (NO_X)

The emission of nitrogen oxides (NOx: NO and NO_2) to the atmosphere is considered an environmental problem of great global concern, these compounds are the source of several environmental issues including acid rain, photochemical smog, global warming, tropospheric ozone, ozone layer weakening [3,22,23] and even have been associated with increased rates

of cardiac mortality and morbidity [4]. According to the Emissions Database for Global Atmospheric Research (EDGAR inventory) [32], the NOx emitted globally by the year 2000 was about 30.3 Tg yr^{-1} (1 Tg = 10^{12} g).

NOx are formed during the combustion processes in several stationary sources such as power plants, waste incinerators, refineries and others, also they are generated from mobile sources during the combustion of gasoline and diesel in vehicles and airplanes [3,24]. Other sources of NO_X are the lightening oxidation of NH_3 produced by microbial decomposition of proteins in the soil and the volcanic activity [3].

In waste incineration plants, NO is the primary form of nitrogen-oxygen product emitted [33], later at lower temperatures and in presence of oxygen is oxidized to produce NO_2 according with reaction R. 1-1 [34], depending on the combustion temperature NO_2 can also be delivered directly from the combustion to the atmosphere. The equilibrium constant for this reaction presents high values at low temperatures and vice versa.

$$2NO + O_2 \leftrightharpoons 2NO_2 \qquad \text{R. 1-1}$$

From a thermodynamic point of view, nitrogen monoxide is unstable with respect to its decomposition into N_2 and O_2 elements ($\Delta G_{298\,K} = -173$ kJ mol^{-1}, see R. 1-2) [35], however the reaction is inhibited by a high activation energy (~335 kJ mol^{-1}) therefore, very high temperatures (1100–1200 ºC) or a suitable catalyst are required for the decomposition [3,36].

$$NO \rightarrow \frac{1}{2} N_2 + \frac{1}{2} O_2 \qquad \text{R. 1-2}$$

For the formation of the NO_X during the combustion process a source of nitrogen is required. There are two possibilities, the nitrogen present in the combustion atmosphere and the nitrogen compounds bounded to the fuel, the reaction mechanisms leading the NOx formation depend on the nitrogen source and reaction conditions [37]. Accordingly, three mechanism for NO_X formation has been identified: thermal NO, prompt NO and fuel NO [3,33,38].

Thermal NO implies the gas phase reaction between atmospheric molecular nitrogen and oxygen at high temperatures; fuel NO is formed by the oxidation of Fuel-Bound Nitrogen

(FBN), and prompt NO results from reactions between nitrogen on atmosphere and hydrocarbon radicals forming volatile-N species (gaseous intermediates), which are oxidized to NO [3,34]. A short review of these reaction mechanisms is presented below.

1.2 Reaction mechanism for NO_X formation

1.2.1 Thermal NO

In the combustion of fuels that not contain FBN, the oxidation of atmospheric nitrogen by thermal mechanism is the major source of NO_X [39]. This mechanism requires high temperatures to break the molecular N_2 of the atmosphere into atomic nitrogen N* + N* [38]. The following mechanism was proposed by Zeldovich [3,33]:

$$N_2 + O^* \leftrightharpoons NO + N^* \qquad \text{R. 1-3}$$

$$N^* + O_2 \leftrightharpoons NO + O^* \qquad \text{R. 1-4}$$

$$N_2 + O_2 \leftrightharpoons 2NO \qquad \text{R. 1-5}$$

The thermal mechanism is commonly referred to as the Zeldovich mechanism. There is an additional step propose by Lavoie [40]:

$$N^* + OH \leftrightharpoons NO + H^* \qquad \text{R. 1-6}$$

The reaction R. 1-3 has a high activation energy and controls the reaction rate of thermal NO formation, temperatures above 1500 °C are required to initiate the chain reaction of O* and N* radicals [34].

1.2.2 Fuel NO

Fuel NO is formed more easily than thermal NO because the triple bond in the molecular nitrogen is harder to break than the N-H and N-C bonds [41]. Fuel NO is the main mechanism of NO formation in flames containing FBN and typically accounts for more than 80% of NO formed in these kind of systems [41]. During the combustion of heavy fuels such as heavy oils, coal, coke and biomass, the FBN may evolve as NO_X and eventually as N_2O [3,42].

During fuel combustion, some FBN may undergo some thermal decomposition generating several NO precursors, these will be low molecular weight nitrogen compounds or radicals (NH_3, NH_2, NH, HCN, CN etc.) [33].

NH_i species under oxidizing conditions react with molecular oxygen and oxygen containing radicals O* and OH* to form nitric oxide according to reactions R. 1-7 to R. 1-9. Under oxygen-poor conditions, NH_i radicals react with nitrogenous component to form molecular nitrogen N_2 according to reaction R. 1-10, in this specific condition, the fuel NO formation is inhibited because of the low concentration of oxidizing radicals [37].

$$NH_i + O_2 \leftrightharpoons NO + H_iO \qquad \text{R. 1-7}$$

$$NH_i + OH \leftrightharpoons NO + H_{i+1} \qquad \text{R. 1-8}$$

$$NH_i + O \leftrightharpoons NO + H_i \qquad \text{R. 1-9}$$

$$NH_i + NO \leftrightharpoons N_2 + H_iO \qquad \text{R. 1-10}$$

According with this, in fuel-rich regions the FBN compounds will be reduced to N_2 rather than oxidized to NO and in fuel-lean regions these species will be generally oxidized to form NO [37]. In this way, the yields to NO and N_2 will depend mainly on the local Air/Fuel ratio; at a sufficient residence time in a very fuel-rich gas, the FBN will convert preferentially to N_2 and lesser extent to NO [43]. Control the environmental in which the FBN compound will be released from the fuel could be the first step to control the NO formation and emission [37]. In brief, fuel NO mechanism can be described as follows:

$$C(N) \rightarrow I(N) \qquad \text{R. 1-11}$$

$$I(N) + O \text{ (or } O_2, OH) \rightarrow NO + \ldots \qquad \text{R. 1-12}$$

Where C(N) represents the FBN, I(N) denotes intermediate species such as CN, HCN, NH and NH_2 [3].

1.2.3 Prompt NO

The formation of NO by this mechanism begins with the breaking of the triple bond of molecular nitrogen (N≡N) stimulated by some hydrocarbon radicals derived from burned hydrocarbons (CH_i with i=0, 1, 2). The activation energies of the reactions involved in this mechanism are much lower than those involved in the thermal NO mechanism and can occur at much lower temperatures (below 750 ºC). However, the prompt NO is responsible for just a small part of the overall NO formation, especially for the combustion of solid fuels such as coal or waste [37].

This mechanism takes place in combustion systems in the area of the flame front (reaction zone) under fuel-rich conditions [37]. Fenimore [44] reported the formation of nitric oxide by this mechanism in hydrocarbon flames (ethylene, methane or propane) with $N_2 - O_2$ mixtures and proposed that attacks of carbon or hydrocarbon radicals on nitrogen molecules may produce atomic nitrogen which can be oxidized to NO according with reactions R. 1-13 and R. 1-14 [44]. Another possible reaction has been proposed in which the intermediate NCN instead of HCN is formed according with reaction R. 1-15 [45,46]

$$CH + N_2 \rightarrow HCN + N \qquad \text{R. 1-13}$$

$$C_2 + N_2 \rightarrow CN + CN \qquad \text{R. 1-14}$$

$$CH + N_2 \rightarrow NCN + H \qquad \text{R. 1-15}$$

Miller and Bowman [39] considered several hydrocarbon radicals such as CH, CH_2, C_2, C_2H and C proposed on different works as possible intermediates in the prompt NO mechanism. They studied several possible elementary reactions and concluded that reaction R. 1-13 is a significant rate-limiting step for prompt NO production under the researched conditions.

1.3 Dioxins and furans

Dioxins refers to polychlorinated dibenzodioxins (PCDD) and dibenzofurans (PCDF), two families of organic solids compounds with high melting points and low vapor pressures [7]. These molecules are highly stable and lipophilic, which is why they tend to bio-accumulate through the food chain and may cause a variety of toxic responses to the exposed organisms such as such as carcinogenicity, immunotoxicity and adverse effects on reproduction, development, and endocrine functions [8,9].

Structurally the PCDDs consist of two benzene rings linked by two oxygen atoms and PCDFs consist in two benzene rings but linked by a carbon bond on one side and an oxygen bridge on the other [7], the position of the chlorine atoms inside these cyclic structures (see Figure 1) result in 210 different possible compounds (135 PCDF and 75 PCDD), however special PCDDs/Fs congeners having chlorines at 2,3,7,8 positions have been identified as the most toxic and bioactive molecules to exposed organisms, they form a group of 17 molecules (7 PCDDs and 10 PCDFs) which are called “toxic congeners” [10,11]. Not all the toxic congeners have the same toxicity, the 2,3,7,8 tetrachlorodibenzo-p-dioxin (TCDD) is

considered as the congener with the greatest toxic potential [47] even catalogued as a "known" human carcinogen by the World Health Organization [7].

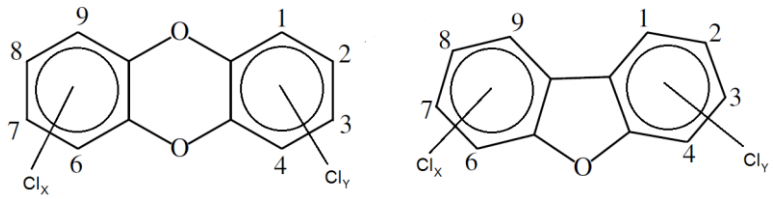

Figure 1 Structure of A) PCDD and B) PCDF. On both cases the number of chlorines in the structure must satisfy: X = 0 to 4, Y = 0 to 4 and X + Y ≥ 1 [48].

PCDD/Fs are generated unintentionally as by-products from different industrial process such as municipal, hazardous and medical waste incinerators, crematories, metallurgic, paper, pulp and chlorine-chemical industries [7,49]; however, most of the chemical and physical mechanism identified for dioxins formation are related to combustion processes in presence of chlorine-containing materials.

The emission of dioxins to the environment has become a problem of global great concern, in this sense several nations signed the International Stockholm Convention on Persistent Organic Pollutants [20] in which they committed to inventory and reduce the emissions of these kind of hazardous compounds among which PCDD/Fs are included. Besides, several countries have set stringent environmental regulations to the emissions of dioxins, for example a limit value of 0.1 ng (TEQ)/Nm^3 (i.e., International Toxicity Equivalents per Nm^3) has been adopted by several European countries and Japan [7]. Next a review about the reaction mechanisms for PCDD/Fs formation is presented.

1.4 Reaction mechanisms for PCDD/Fs formation

During combustion of organic substances in presence of chlorine under certain conditions, carbon, hydrogen and chlorine can combine to form PCDD/Fs compounds [12,50]. In the case of waste incineration, when flue gases leave the primary combustion chamber the compounds cool down from temperatures around 1000 °C to ambient, during this cooling process is known [50] that some molecular rearrangements may promote the formation of dioxins, mainly at temperatures between 250°C to 650 °C, according to the general reaction R. 1-16:

$$Cl_2 + \text{organic molecules} \rightarrow \text{PCDD/Fs} + \text{Cl-R} \qquad \text{R. 1-16}$$

Although the mechanisms for PCDD/Fs formation have been widely studied they are not fully understood yet. In general, the formation of these compounds may occur by homogenous pathways at high temperatures (500 – 800 ºC) or by heterogenous pathways at lower temperatures (200 – 400 ºC) [12,50–52].

1.4.1 Homogeneous paths (500–800 ºC)

Several reactions in gaseous phase in the temperature range of 500 to 800 ºC can produce PCDD/Fs, it has been shown that PCDD/Fs formation by homogeneous pathways can correlated with various possible precursors such as polychlorinated benzenes or polychlorinated phenols or formed by condensation from aliphatic hydrocarbons. According to the available precursors, four pathways have been identified [12], the cyclization of polychlorobiphenyls, the cyclization of polychlorodiphenyl ethers, the chlorination of dibenzofuran and the dechlorination of octachlorodibenzo-p-furan.

1.4.2 Heterogeneous paths (200–400 ºC)

PCDD/Fs formation is catalyzed by certain metals such as copper [12,51] present in the soot or fly ash particles at relative low temperatures from 200 to 400 ºC [12,51]. The precursor may be chlorine compounds such as chlorophenols or chlorobenzenes. In general, the formation of PCDD/Fs by this path can be divided in four steps: 1) formation of ashes products of incomplete combustion (PIC), carbon monoxide, volatile compounds and organic radicals. 2) Formation of surface-active compounds with adsorbed PCDD/Fs precursors, transition metals, their salts and oxides. 3) Occurrence of complex organic (radical) reactions. 4) Partial desorption of products from the surface [50].

The formation of PIC compounds is higher at temperatures about 750 °C in lean conditions. Mechanisms of these reactions are of radical type and involve halogenation, radical combustion and disproportionation. For instance, the combustion of 1,2-dichlorobenzene gave the following PIC compounds: Chlorinated benzenes (from mono to penta), chlorophenols, chlorinated biphenylenes, chlorinated polyaromatic compounds (mono-octa) and numerous condensed aromatic compounds, in particular naphthalenes and benzoic acid derivatives [50].

The PCDD/Fs can be also formed by another pathway known as *de novo synthesis* [12,50,53] from precursors such as elemental carbon, short chain compounds (acetylene and ethylene), polystyrene, cellulose and PVC in presence of oxygen and chlorine-containing materials by gas-solid reactions mainly catalyzed by $CuCl_2$ at temperatures between 200 and 400 ºC. Hence, these reactions occur far from the combustion chamber and are favored during the cooling process of the gas.

The net rate of PCDD/Fs production will be the difference between the rates of formation and thermal destruction. Taking in account that thermal destruction of PCDD/Fs requires higher activation energies than thermal formation, then the rate of production has a maximum at certain temperatures (about 300 °C) [12].

1.5 Non-catalytic control systems for NOx emission.

NOx emissions can be partially controlled during the combustion process by modifying some operational variables to reduce the NOx formation, however these primary measures do not completely prevent its formation then other post-combustion techniques for the treatment of the flue gas are needed to complement the removal of NOx and avoid the emission to the atmosphere.

1.5.1 Control of the furnace operating conditions

This control strategy search to avoid the NOx formation by modifying some combustion variables within the combustion zone [54]. Strategies, such as, reduce the combustion temperature, create an O_2-deficient stoichiometric condition or vary the residence time within various parts of the combustion zone, may lead to decrease NOx emission about 30 to 40% by lowing the NOx formation [3,54,55].

These strategies are less costly than post-combustion techniques since not additional equipment is required [56]. However, there are some side effects such as the increase of carbon in ashes and greater CO formation [3]. In general, exhaust gas treatment methods are preferred for NOx control instead of combustion modifications techniques because they are versatile and can be applied in a wide range of systems [35].

1.5.2 Addition of metal chelates

Some metal chelates, such as ferrous ethylenediaminetetraacetate (Fe(II)*EDTA), increases the NO adsorption by reacting to produce ferrous nitrosyl complex (Fe(II)*EDTA*NO). The resulting spent scrubber solution is then biologically treated to remove the nitrosyl adduct (bound nitric oxide) from the ferrous EDTA and to reduce the oxidized ferric EDTA (Fe(III)EDTA-) to ferrous form which is active for NOx scrubbing. Reported efficiency for this technique is about 75% of NOx removal [3,35].

1.5.3 Selective non-catalytic reduction (SNCR) of NOx

The injection of a reductant directly into the furnace at high operation temperatures (850 – 1175 ºC) can reduce the NOx to N_2 and O_2. The reductant mixes with the flue gas stream containing NOx and selectively reacts with them leaving the oxygen required in the furnace almost untouched [54].

In most of full-scale applications, the reductant is either NH_3 or $CO(NH_2)_2$ although in some laboratory and pilot scale experiments cyanuric acid has been also studied as a potential reductant [3,54]. Some advantages of the technology include its simplicity, ease of installation on existing plants, low capital and operational costs, applicability to all types of stationary-fired equipment and is practically unaffected by fly ash [54]. However, the main drawback of SNCR is its low efficiency which ranges from 30% to 75% [3,22], there are also risks of N_2O emissions and in the case of $CO(NH_2)_2$ some CO can be also generated [22].

1.6 Non-catalytic control systems for PCDD/Fs emissions.

The primary measures to reduce the formation of PCDD/Fs consist of controlling some variables such as residence time, temperature of the post-combustion chamber and control of the air during the combustion process. However, these measures do not avoid the formation of PCDD/Fs completely and secondary measures are also needed to implement in the post-combustion zone.

1.6.1 Control of the temperature-time profile of flue gases

Dioxin formation by de novo synthesis occur mainly in the post-combustion region of incinerators at temperatures between 200 and 500 ºC with a maximum formation rate around 300 ºC [53]. Therefore, a decrease in dioxins formation can be achieve by reducing the flue

gas residence time in the post-combustion zone and decreasing the temperature to below 260 ºC quickly [57]. There are several studies [58–62] which results confirm the reduction effect in dioxin formation by quickly quenching and lower flue gas residence time techniques.

The effect of cooling rates on PCDD/Fs formation is evident. In a waste heat boiler, the flue gas cooling rates are usually in the range of 100 – 200 ºC/s, and the PCDD/Fs level at boiler outlet is typically 5 ng-TE/Nm^3. To achieve a PCDD/Fs level of 1 ng-TE/Nm^3 at boiler outlet, a cooling rate in the range of 500 – 1000 ºC/s is probably necessary. However, in practice, such a high cooling rate is difficult to reach as the volume of flue gases is usually large [53].

1.6.2 High-temperature separation of fly ashes

Since the PCDD/Fs formation at low temperatures (200 – 400 ºC) are catalyzed by certain metal components in the fly ash surfaces such as Cu and Fe, it could be expected a reduction in the generation of PCDD/Fs by separating out the fly ashes from the flue gases prior to the low temperature zone [53,57]. Fangmark et al [59,63] researched about this potential technique in a laboratory-scale fluidized bed reactor fueled by a synthetic fuel and removing the fly ashes at the entrance of the post-combustion zone by either a) using a cyclone in the post-combustion zone for fly ash separation or b) using a cyclone followed by a filter. However, the results were not the expected and not dioxin reduction was obtained by this technique, probably because some small particles may even pass through the fly ash separation units. Therefore, this does not seem to be a promissory control system and research about this technique are rare nowadays [57]

1.6.3 Injection of additives

The addition of sulfur compounds such as SO_2, ammonia and amines can inhibit the catalytic activity of the metals in the fly ashes because they are strongly adsorbed forming stable metal complexes inactive to catalyst the PCDD/Fs formation [53,57,64]. Dickson et al [65] studied several inhibitors finding that two polyfunctional amines (2-aminoethanol and triethanolamine) were the most effective to reduce the PCDD/Fs and suggest that the effect of these compounds may be due to their ability to form poly-dentate ligand complexes with the metallic active sites on the fly ash surface. Some alkaline sorbents such as CaO, $CaCO_3$, $Ca(OH)_2$, prevent the HCl decomposition to Cl_2 which inhibits the generation of chlorine

compounds [53,57]. However, the experimental results are divergent and controversial, it was reported [53] that the addition of alkaline sorbents resulted in a decrease of the HCl concentration but the PCDD/Fs level could be increased, decreased or remain unchanged. The addition of strong oxidants such as hydrogen peroxide or ozone in the post-combustion zone is expected also to help in the oxidation of organic compounds including the PCDD/Fs in the flue gasses [53]. The injection of methane in the burning or post-combustion zone can effectively inhibit the PCDD/Fs formation by increasing the concentration of free radicals which promote the oxidation of dioxins [57].

1.6.4 Fabric filter and electrostatic precipitators

These control devices are used to remove the particulate matter generated during the waste incineration. In the flue gas stream the PCDD/Fs can exist in the gaseous form or can be adsorbed onto the solid particulate matter. The fabric filters can remove the solid phase PCDD/Fs and any vapors also adsorbed on the particle matter. The fabric filters are made of woven fiberglass material, it is sensitive to acid gas because of this they are usually operated in combination with spray dryer adsorption of acid gases. The porosity of the fabric allows the bags to retain particulate matter sizes down to less than 1 μm [7]. The fabric filters can remove solid phase PCDD/F however gas phase PCDD/Fs is not retained by the filters and must be removed by other techniques such as adsorption onto activated carbon or by catalytic oxidation [66].

The electrostatic precipitators (ESP) are generally used to collect particulate matter by introducing a strong electrical field in the flue gas stream which charges the particles flowing with the flue gases, then large collection plates receive an opposite charge to attract and collect the particles. It is known [7] that PCDD/F formation may also occur in the ESP unit operated in a temperature range of 150–300 °C. Thus, although ESP can remove particulate matter containing PCDD/Fs the formation can result in a net increase in PCDD/Fs emissions [7]. Chang et al observed [67] a severe increase in the PCDD/Fs concentration after the ESP unit of an incinerator in Taiwan operating at 248 °C which was attributed to *de novo synthesis*. Below 200 °C the PCDD/Fs formation in the ESP is attributed to de novo synthesis promoted by the high voltage applied to the particles [68].

1.6.5 Dry and wet scrubbers

The dry scrubbers are designed to remove the acid gases and particulate matter from the post-combustion gases. Typically, the system consists in a scrubber reactor vessel where the hot combustion gases are atomized with a hydrate lime slurry injected at a controlled velocity. The water in the slurry evaporates quickly by the mixing with the hot combustion gases and the heat of evaporation causes a rapid decrease of the combustion gases temperature. About 70% of the acid gases can be neutralized by the hydrated lime. Finally, a solid consisted of particulate matter and hydrated lime, settles to the bottom of the reactor vessel. The dry scrubber in combination with fabric filters have achieved greater than 95% reduction and control of PCDD/Fs in municipal solid waste incinerators [69].

Wet scrubbers designed for acid gas can partially remove particulate matter in the flue gas. These devices consist of two-stage scrubbers, the first removes the HCl and the second remove SO_2. Water is used to remove the HCl, and caustic or hydrated lime is added to remove SO_2 from combustion gases [69]. The PCDD/Fs levels can be increased after the wet scrubber unit as reports Löthgren [70] which was attributed to the so called memory effect, where dioxins are adsorbed on scrubber plastic parts when the emission from the incinerator is high and desorbed slowly when the plant is running under more stable conditions. Additionally, it is known that wet scrubbers do not remove vapor-phase PCDD/Fs since they are not water soluble [71].

1.6.6 Activated carbon adsorption

The PCDD/Fs can also be removed by adsorption onto powdered activated carbon which is injected into the exhaust flue gas stream and subsequently removed with the residual dust by using an electrostatic precipitator or a fabric filter placed downstream [57]. Although a removal efficiency higher than 95% can be achieved by this technique, however the adsorption onto activated carbon does not destroy the PCDD/Fs leaving large amounts of solid residues which are highly contaminated with dioxins. This technique can also remove mercury and is effective at low temperatures where the catalysts are generally ineffective but the large amount of activated carbon required increases considerably the operational costs [57,66].

1.6.7 Dioxin destruction by electron irradiation

This technology uses an electron beam for dioxin destruction [57], it has been reported [72] that combination of electron beam radiation and hydrated lime $Ca(OH)_2$ can remove HCl, SO_2, NO_X and chlorine compounds in exhaust gases, however in such study, only 40% of PCCDs and about 70% of PCDFs were decomposed by the irradiation. In another research Hirota et al [73] reported a significant decomposition for PCDDs and isomers as results of oxidation reactions with OH radicals yielded by electron-beam irradiation, however in the case of PCDFs the formation of lower chlorinated isomers having a toxic equivalent factor was also observed at lower doses [73].

1.7 Catalytic technologies for the abatement of NOx and PCDD/Fs

1.7.1 Selective catalytic reduction with ammonia (NH_3–SCR)

One of the most widespread technologies for the NOx abatement is the selective catalytic reduction of NOx by ammonia (NH_3-SCR) in an oxidant atmosphere over vanadium oxide catalyst supported on titanium oxide and promoted by tungsten or molybdenum oxides (V_2O_5-WO_3/TiO_2 or V_2O_5-MoO_3/TiO_2). This technology allows the reduction of NOx with NH_3 into N_2 and H_2O according to the reactions R. 1-17 to R. 1-19 [1,30]. Generally, the catalyst shape is in the form of extruded ceramic monoliths or deposited on a plate structure [74].

The active phase of the vanadium oxides catalysts for the NH_3-SCR have been attributed to the various oxidation states of vanadium, the different coordination geometries of oxygen atoms and the presence of Brønsted acidity [75–77]. The tungsten or molybdenum are promoters added to stabilize the anatase form of titanium (high surface area) preventing the conversion to rutile phase (low surface area) which causes irreversible deactivation of the catalyst, the promoters also favors the spreading of the vanadium and increases the Brønsted acidity [74,78].

Depending on the location of the catalytic reactor unit there are three system configurations which are commonly referred as high-dust, low-dust and tail-end systems [79]. In the high-dust position of the SCR unit is located upstream of the particulate control devices, the main advantage of this configuration is the low energy consumption since the flue gases are usually

within the optimum temperature window for the NH_3-SCR of NOx, however the catalyst is exposed to a high level of particulate matter and SO_2 which implies a high probability of catalyst deactivation, in general, this configuration can be applied when the dust and SO_2 content in the flue gases are sufficiently low to allow the direct feed to the SCR unit [80]. In the low-dust configuration the SCR unit is located downstream of the ESP where most of the dust is removed before to entering the catalytic reactor, this configuration increases the catalyst life time by minimizing the concentration of particulate matter in the SCR reactor. Although the temperature of the flue gases slightly drops after pass through the ESP unit, usually no reheating is needed for the NH_3-SCR. In the tail-end configuration the SCR unit is placed at the end, downstream of all air pollution control system (APCS) which implies a considerable drop in the flue gas temperature therefore the reheated of the gases is needed before the NH_3-SCR which increase de operational costs. However, this increases in operational costs is in part offset by reduction of catalyst costs due to an increase in the catalyst life time and lower catalysts requirements, the tail-end SCR typically require only 2 layers of catalysts although some use four half-layers of catalyst to allow for greater flexibility for catalyst replacement [79].

Experimental evidence suggests a Eley-Rideal type mechanism for the NH_3-SCR, in which the ammonia is strongly chemisorbed onto the active sites of the catalyst, where it reacts while the NO reacts in gaseous phase or weakly adsorbed [30]. The overall NH_3-SCR involves desires (R. 1- to R. 1-19) and undesired (R. 1-20 to R. 1-23) reactions, as follow [3,27,81]:

R. 1-17	$4NO + 4NH_3 + O_2 \rightarrow 4N_2 + 6H_2O$	Desired selective reduction of NO.
R. 1-18	$2NO_2 + 4NH_3 + O_2 \rightarrow 3N_2 + 6H_2O$	Desired selective reduction of NO_2.
R. 1-19	$6NO + 4NH_3 \rightarrow 5N_2 + 6H_2O$	Desired selective reduction of NO in the absence of O_2.
R. 1-20	$4NO + 4NH_3 + 3O_2 \rightarrow 4N_2O + 6H_2O$	Unselective reduction of NO to form the undesired nitrous oxide.

R. 1-21	$2NH_3 + 3/2O_2 \rightarrow N_2 + 3H_2O$	Undesired oxidations of ammonia by the oxygen instead of NO.
R. 1-22	$2NH_3 + 2O_2 \rightarrow N_2O + 3H_2O$	Undesired oxidation of ammonia by oxygen to form undesired nitrous oxide.
R. 1-23	$2NH_3 + 5/2O_2 \rightarrow 2NO + 3H_2O$	Undesired oxidation of ammonia by oxygen could lead to more NO.

The system is considered selective when molecular nitrogen is produced through reactions R. 1- to R. 1-19, that is when N_2 is produced with a selectivity close to 100% and the ratio of converted moles of NO and NH_3 is 1 [81,82]. Typical conditions for a selective reduction requires a NH_3/NO ratio close to 1, low percent of oxygen in the media and operation temperatures between 200 and 400 °C [30,81]. On the other hand unselective behavior occurs when the ratio of converted NO and NH_3 moles is lower than 1 which implies that ammonia is being oxidized through reactions R. 1-21 to R. 1-23 [81].

1.7.2 Catalytic oxidation of PCDD/Fs and other chlorinated compounds

The catalytic removal of PCDD/Fs consist of achieve the deep oxidation of these compounds into H_2O, CO_2 and HCl according to the stoichiometric equations R. 1-24 and R. 1-25 [1,28,80,83]. The main advantage of the catalytic oxidation technique is the real destruction of the molecules into less harmful compounds in contrast with adsorption techniques where the PCDD/Fs are only transfer from the vapor phase to a solid residue and additional treatments are required before the final disposal of the waste solids [80].

R. 1-24 $C_{12}H_nCl_{8-n}O_2 + (9 + 0.5n)O_2 \rightarrow (n-4)H_2O + 12CO_2 + (8-n)HCl$

R. 1-25 $C_{12}H_nCl_{8-n}O + (9 + 0.5n)O_2 \rightarrow (n-4)H_2O + 12CO_2 + (8-n)HCl$

A reduction of about 90% of PCCD/Fs concentration after the NH_3-SCR units of various municipal wastes incinerators in Europe was reported [84] in 1992, from this finding a relationship between the NO reduction and the decrease of the PCDD/Fs concentration was elucidated. Nowadays, it is well known [1,26,85–87] that commercial V_2O_5-WO_3/TiO_2 catalysts originally designed for the NH_3-SCR are also effective in the deep oxidation of PCDD/Fs at the same temperature window of the NOx reduction. This catalytic technology

has proved to reduce the gas concentration of PCDD/Fs through deep oxidation to below 0.1 ng TEQ/Nm^3 [86]. Other studies have shown [88] that vanadium-based catalysts such as V_2O_5/TiO_2 or V_2O_5/Al_2O_3 catalysts can also oxidize the *ortho*-dichlorobenzene (*o*-DCB), this compound is usually used as a model molecule to study the catalytic oxidation of PCDD/Fs due to the high toxicity of this compounds [83].

Catalytic oxidation of several Cl-VOCs such as 1,2-dichloroethane, dichloromethane, trichloroethylene and *o*-DCB over H-zeolites and metal loaded H-zeolites has been also studied and widely reported [89–93]. The activity of H-type zeolites such as H-FAU, H-BEA, H-MFI, and H-MCM-22 has been related [90,93] to the presence of Brønsted acid sites and the confinement effect that the micropores exert on the molecules to be oxidized. Co-HMOR and Pd/Co-HMOR catalysts have been reported as active for the *o*-DCB oxidation [47,90,92], the active sites have been attributed [90] to the presence of both Brønsted and Co^{2+} Lewis acid sites, and the similarity in size between the zeolite pores and the o-DCB molecule which contributes to increase the adsorption strength because of the confinement effect. Pd/Co-HMOR catalysts have also been reported [94–98] as active for the selective catalytic reduction of NOx with CH_4 (CH_4-SCR) under lean and wet conditions, which makes it an interesting option for the simultaneous abatement of NOx and chlorinated compounds.

1.7.3 Combined NH_3–SCR of NOx and catalytic oxidation of PCDD/Fs

Since the catalysts used for NH_3-SCR of NOx are also active for PCDD/Fs oxidation at the same temperature window, the combined catalytic elimination of these compounds in a single catalytic reactor has been widely implemented to clean the waste gases from stationary sources [85], this process is commonly known as dDInOX. In Europe and Japan, commercial V_2O_5-WO_3/TiO_2 catalysts have been applied in municipal solid waste incinerators (MSWIs) to remove PCDD/Fs and NOx simultaneously [26,66]. The commercial catalysts used only for NH_3-SCR must be optimized to carry on the PCDD/Fs oxidation simultaneously, this can be achieve by using higher vanadium loadings which increases the potential oxidation of the catalysts [99]. The increase in the oxidation efficiency towards other chlorinated compounds such as *o*-DCB by increasing the vanadium loading in a series of V_2O_5/TiO_2 catalysts was also reported by Krishnamoorthy et al [88].

The reactions towards the NH_3-SCR of NOx simultaneously with the catalytic oxidation of PCCD/Fs occur in a temperature range from approximately 200 to 300 °C and the removal efficiencies of both pollutants increment with increasing temperature [1,26]. According to the operational temperature high reduction of both pollutants may be achieved, Liu et al reported [26] removal efficiencies for PCDD/Fs and NOx of 97.24 and 90.3%, respectively in a catalytic reactor unit of a pilot-scale plant operated at 300 °C, however at 220 °C an inhibiting effect of the NH_3-SCR on the decomposition of PCDD/Fs was observed.

1.8 Pd-Co catalysts for selective catalytic reduction of NOx with CH_4 and oxidation of chlorinated compounds as an alternative to the NH_3-SCR technology

Although the V_2O_5-WO_3/TiO_2 catalysts have proved to be effective for the catalytic oxidation of PCDD/Fs simultaneously with the NH_3–SCR of NOx at relative low temperatures and in presence of oxygen [85], there are some drawbacks. The ammonia is a high corrosive, toxic and hard to handle gas which unselective oxidation may even lead to the formation of NO and N_2O and the vanadium-based catalyst are susceptible to deactivation by the deposition of ammonia salts [28]. Alternative catalytic systems using other reductants than ammonia such as hydrocarbons instead of ammonia were studied in the 70's [100] however, the first attempts resulted in non-selective catalysts that led to the combustion of hydrocarbons in the presence of oxygen, then a large hydrocarbons excess was required to consume the O_2. Consequently, the NH_3-SCR technology became in the more attractive commercial solution to the NOx abatement from stationary sources [101].

Co-zeolites catalysts were the first reported as active for selectively reduce the NO with CH_4 in presence of oxygen at 400 °C [101], since then several metal load zeolites have been also reported as active for this reaction [102–111]. The selective catalytic reduction of NOx by methane (CH_4–SCR) is considered a promising alternative to the traditional NH_3–SCR technology because of the high availability, ease of handing and relative low cost of methane [112]; moreover, methane is the main component of natural gas used in several power plants, industrial furnaces and residences with supply infrastructure in many countries and even can represent an alternative fuel for automotive vehicles [113,114].

The overall stoichiometric reactions for the CH_4–SCR process can be summarized as follow [101,106]:

R. 1-26	$CH_4 + 2NO + O_2 \rightarrow N_2 + CO_2 + 2H_2O$	Reduction of NO.
R. 1-27	$2NO + O_2 \rightarrow 2NO_2$	Oxidation of NO to NO_2.
R. 1-28	$CH_4 + 2NO_2 \rightarrow N_2 + CO_2 + 2H_2O$	Reduction of NO_2.
R. 1-29	$CH_4 + 2O_2 \rightarrow CO_2 + 2H_2O$	Oxidation of methane.

Since Li and Armor reported [101] the effectiveness CH_4-SCR of NO in presence of oxygen over a Co-ZSM-5 catalyst, other cobalt exchanged protonic zeolites such as Co-FER, Co-MFI and Co-MOR have been also reported [115–118] as active for the reduction. Co^{2+} cations (Co-α, Co-β and Co-γ type ions), oxide-like Co species and Co-oxide clusters have been identified in several studies as active species [115–119]. However, there is controversy about the specific roles that Co-species and Brønsted acid sites have during the reaction. In general, there is consensus about the role of Co-oxo and oxide-like Co species which is to oxidize the NO to NO_2, but there are different opinions about the role of Co^{2+} cations and the protonic acidity. According to Kaucký et al [115] the protons and oxide-like Co species in Co-zeolites oxidize the NO to NO_2 but they own activity in the CH_4-SCR is low while the Co^{2+} ions in specific sites (α-type Co ions in MOR and FER, and β-type Co ions in MFI) are responsible for the reduction by methane. Similarly, Lónyi et al [120] propose bifunctional mechanism in which the NO is oxidize to NO_2 by O_2 over Co-oxo species and Brønsted acid sites while the reduction reaction by CH_4 takes place over Co^{2+}/$[Co\text{-}OH]^+$ ions. In contrast, Yan et al [121] suggest that the Co cations act in the oxidation of NO to NO_2 while the protons are responsible of the reduction step.

Catalyst of palladium exchanged with H-ZSM-5 and HMOR have been also reported [108,109,122] as active and selective for the CH_4-SCR. The Pd dispersion in these catalytic systems is considered as one of the key factors towards the selectivity to the reduction of NO instead of the methane oxidation. Ali et al reported [123] that Pd supported on non-acidic materials are totally unselective for NO conversion but very active for methane combustion, in contrast low loading Pd catalysts supported on acidic materials such as H-ZSM-5, H-Mordenite (HMOR) and sulfated zirconia (SZ) present a higher selectivity. Similarly,

Misono et al found [109] that Pd ion-exchanged Na-ZSM-5 is inactive for the NO reduction while Pd ion-exchanged H-ZSM-5 is active, on this basis the presence of Brønsted acidity was considered essential for the CH_4-SCR of NO in presence of oxygen having a double role, one is to contribute with the Pd dispersion and the other is the direct involvement in the reaction. The Pd states of Pd/H-ZSM-5 and Pd/Na-ZSM-5 catalysts showing high and poor activity towards the CH_4-SCR, respectively were analyzed by Koyano et al [122]. Pd atoms in the active catalysts were found mostly in the isolated Pd^{2+} state and distributed almost uniformly in the zeolite framework while in the inactive samples the Pd was found as PdO particles on the external surface, the activity and selectivity for the CH_4-SCR were then attributed to the isolated Pd^{2+} ions in the zeolite micropore of Pd/H-ZSM-5 while PdO particles observed in Pd/Na-ZSM-5 were considered as active mainly for the CH_4 oxidation. The acidity of the support on Pd based catalysts was related [123] with the morphology of the oxidized Pd species after exposition of the samples to an oxidant reaction mixture containing CH_4, NO and O_2, on acidic supports Pd atoms are rapidly oxidized to Pd^{2+} ions while on non-acidic supports they are transformed into PdO clusters, these are active for CH_4 oxidation. Therefore, the presence of acid sites seems to be one of the key factors determining the activity and selectivity of Pd-zeolites catalysts towards the CH_4-SCR.

On the other hand, the catalytic oxidation of PCDD/Fs is commonly studied by using less toxic and dangerous chlorinated compounds such as 1,2-dichloroethane, dichloromethane, trichloroethylene and *ortho*-dichlorobenzene (*o*-DCB) [83,89–91]. Particularly, the *o*-DCB has been frequently used as a model compound, since is known [83,90] to be an important precursor of PCDD/Fs and it presents a special structural similarity with 2,4,7,8 TCDD, the most toxic dioxin congener.

It is generally recognized that noble metals are powerful oxidation catalysts, they generally exhibit a high activity towards the oxidation of Cl-VOCs [124–126]. However, they may susceptible to being deactivated due to formation of inorganic chlorides by reacting with HCl and Cl_2 [83,124,127]. Furthermore, noble-metal chloride species may also cause chlorination of organic compounds besides their oxidation [124]. In contrast, transition metal oxides (Cr, Mo, Fe and Co) are generally more resistant to deactivation, but their destruction activity is

often lower [83,125]. Zeolites such as H-FAU, H-BEA, H-MFI, H-MCM22, H-MOR, H-ZSM5, H-Y and ITQ2 have been also studied [83,89–93,125,126,128] in the Cl-VOC oxidation, the activity of these materials has been related with some physical and chemical characteristics such as the existence of strong Brønsted acid sites, the confinement effect of the molecules in the micropores and the thermal stability [89–91,93,126,128,129]. It seems that the presence of both Brønsted and Lewis acid sites may favor the activity of the catalyst, in this sense, Scirè et al [91,126] reported that the chloroaromatic oxidation over Pt/Zeolite samples having both Brønsted and Lewis acid sites showed a higher activity than the obtained over Pd/γ-Al_2O_3 catalysts containing Lewis acids sites only, which suggests a cooperative effect between both acid sites.

Supported bimetallic catalysts of Co and Pd have been reported as active for both CH_4-SCR of NOx and the oxidation of Cl-VOCs. Ogura and coworkers [130] found that incorporation of Co to Pd/H–ZSM-5 resulted in a marked increase of catalytic activity and durability, leading to stable NO conversion lasting more than 40 h in presence of steam, later they suggested [131] that Co incorporation into Pd/H-zeolites enhances the zeolite acidity, stabilizing the isolated Pd^{2+} and minimizing the residual ion-exchangeable sites, which avoids zeolite framework collapse and dealumination from the zeolite framework, maintaining ion-exchange sites for the isolated Pd^{2+}. Pieterse and coworkers [96] tested Co–Pd bimetallic catalysts supported on different H–zeolites structures (ZSM-5, MOR, FER and BEA) in presence of water and oxygen, the catalyst based on MOR and ZSM-5 were the most active. Although initially ZSM-5 supported catalyst showed higher activity than HMOR it was severe deactivated during the first 50 h on stream while HMOR based catalyst maintained the highest SCR activity over the longest period. Córdoba et al [97] also reported a high CH_4–SCR activity at 500 ºC over Pd/Co–HMOR and improved stability under hydrothermal conditions compared to Co or Pd-Mordenite catalysts, reported by other researchers [31,132,133]. On the other hand, synergistic effects between Pd and Co supported on H-MOR and sulfated zirconia (SZ) towards the *o*-DCB oxidation under wet conditions were reported by Aristizábal et al [47], the incorporation of 0.2 %wt. Pd resulted in the increase of the catalytic activity from about 30% observed in the monometallic sample to 90% in the bimetallic Pd/Co-HMOR catalyst at 450 °C. It was suggested that the

incorporation of Pd into the Co-HMOR favors the formation of Co-oxo species under wet reaction conditions, these species are considered active for the *o*-DCB oxidation.

Few works are reported for the simultaneous abatement of NOx and PCDD/Fs [28,99,134,135], some of these studies are dedicated to investigate the simultaneous reactions over the commercial V_2O_5–WO_3/TiO_2 catalysts by NH_3-SCR [28,99]. Recently, catalysts based on ZSM-5 zeolite have been proposed [134,135] for the simultaneous removal of NO (by SCR) and o-DCB as model molecule of PCDD/Fs (by catalytic total oxidation); however, the NH_3 is also used as reducing agent.

According to the presented background and considering that the CH_4-SCR of NOx represents a promising alternative to the conventional NH_3-SCR technology in the present work we propose to study the feasibility of the Pd/Co-HMOR and Pd/Co-SZ catalysts to carry out the CH_4-SCR of NOx simultaneously with the o-DCB oxidation under lean and wet conditions.

1.9 Discussion about the nature of the acid sites

1.9.1 Supported mordenite catalyst

Zeolites are crystalline aluminosilicates minerals having a three–dimensional framework structure which form uniformly sized pores of molecular dimensions [136]. These materials can selectively adsorb certain molecules that fit snugly inside the pores while exclude large molecules that do not fit, because of this zeolites are considered as molecular sieves [136].

Most of the synthetic zeolites are obtained by dissolving a source of alumina and a source of silica in a strongly basic aqueous solution. Variables such as the solubility, the silica–to–alumina ratio, the nature of the cation, and the synthesis temperature of the resultant gel determine what structure is formed [136]. The huge industrial needs of zeolites promoted the use of synthetic zeolites instead of the natural ones since these were not enough to completely meet the demand [137].

The basic structure of zeolites consists of silicon (Si^{+4}) and aluminum (Al^{+3}) cations which are tetrahedrally linked each other by the sharing of oxygen anions (O^{-2}), thus forming a three–dimensional tetrahedral framework [138], basic structure of zeolites can be schematized as is shown in Figure 2. Since in the structure, four anions of oxygen are linked

with one aluminum cation (+3) a negative net charge is produced (see Figure 3), then in order to keep the neutrality of the matter some extraframework cations are required as compensation charges (both inorganic or organic cations are able to satisfy this requirement) [138].

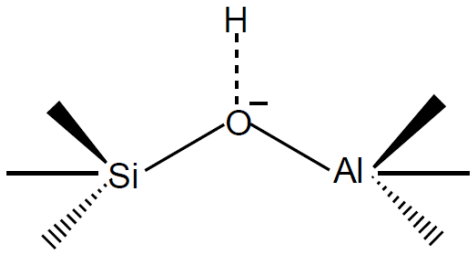

Figure 2 General tetrahedral framework of zeolites [139].

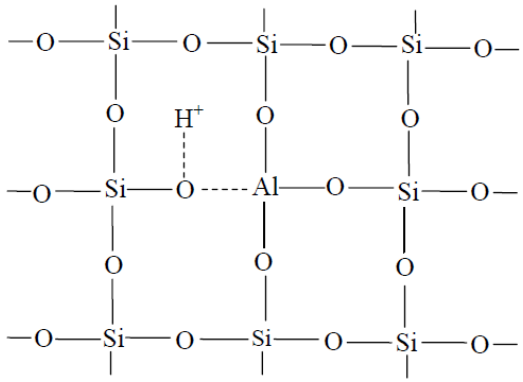

Figure 3 Schematic representation of a negative charge balanced by a proton [140].

When a zeolite has equal number of aluminum and silicon atoms, each oxygen atom is linked to one aluminum and to one silicon atom, and the cavities contain the maximum density of exchangeable cations, these kinds of zeolites are interesting as ion exchangers and adsorbents. Catalytic applications usually require high silica zeolites with cationic protons residing at well–separated exchange sites. High silica content of the framework makes it resistant to high temperatures while high dispersion of acidic protons assures that each proton has the maximum strength [136].

The mordenite is a high-silica zeolite having an orthorhombic crystalline structure with two types of channels running parallel along the [001] crystallographic direction (see Figure 4):

large 12-MR channels (6.5 Å x 7.0 Å) and compressed 8-MR channels (2.6 Å x 5.7 Å) which are connected by perpendicular 8-MR "side pockets" (3.4 Å x 4.8 Å) running along [010] direction [138,141]. Notwithstanding the 2-dimensional channel structure of mordenite, the side pocket running along [010] direction present narrow-necked obstructions that do not allow the flow of molecules through it, therefore the channel system of mordenite is effectively 1-dimmensional and the diffusion of molecules through the zeolite occurs only along the channels in the [001] direction [138,141].

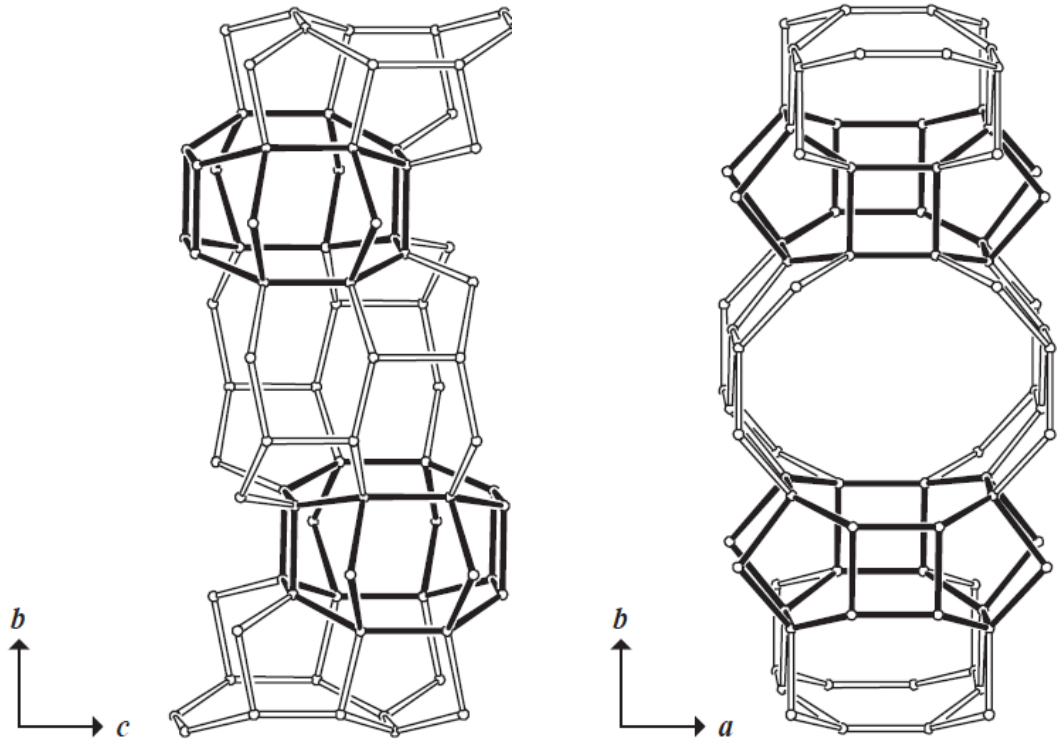

Figure 4 Structure of the mordenite [142].

From a catalytic point of view, the surface acidity is one of the most important properties of zeolites [136]. Many hydrocarbon reactions can be catalyzed by either Brønsted and Lewis acids sites both present in the zeolites lattice structure [143]. Some of these industrial hydrocarbon transformations include, isomerization of light gasoline, hydrocracking of heavy petroleum distillates, FCC process, alkylation of benzene with ethane or propene, disproportionation of toluene, isomerization of xylenes and numerous others [136,143].

A Brønsted acid site (proton donator) is the result of a proton (H^+) loosely bound to an oxygen anion bridging Al and Si atoms [143] as is shown schematically in Figure 2. The proton with a positive charge balances the negative charge resulting from the substitution of a quadravalent Si (+4) atom for a tervalent Al (+3) in the lattice as is shown in Figure 3 [143]. It is generally accepted that these bridging hydroxyl groups Al–(OH)–Si also known as SiOH groups (silanol group) are responsible of the strong acidic sites of protonic zeolites [140,144]. On the other hand, a Lewis acid site (electron acceptor) is characterized by the absence of the hydroxyl group between the Al and Si atoms; the Al atom and its Si neighbor are even more so positively charged (total formal charge of +1), thus facilitating the bonding of an electronically rich species to the Lewis acid site [143].

Lewis acid sites may be converted to Brønsted acid sites in the presence of proton donor species such as water and hydrogen halogenides [144], similarly Brønsted acid sites may be switched to Lewis acid sites through dehydration of the aluminosilicate surface [143]. At temperatures of 500 ºC the protons of the Brønsted acid sites are lost as water molecules followed by the formation of the corresponding Lewis acid sites; this is shown in schematically in Figure 5.

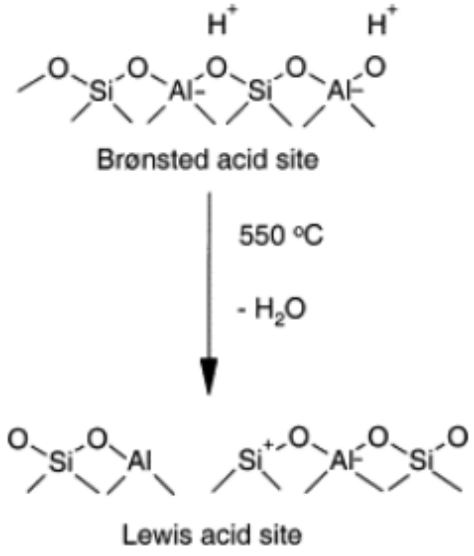

Figure 5 Brønsted and Lewis acid sites [145]

1.9.2 Supported sulfated zirconia catalyst

Sulfated zirconia (SZ) is how zirconium oxide is commonly known when it has been modified with sulfate anions to create high acidic catalysts. These materials have shown higher catalytic activity and have been widely used to catalyze a wide variety of reactions of industrial importance such as, methanol conversion to hydrocarbons, hydrocarbon isomerization, alkylation, nitration, cyclization, Fischer-Tropsch reaction, hydrogen peroxide production and others [146]. The active SZ is based on tetragonal zicornia as the prevailing phase while the more stable monoclinic phase results much less active [147].

The water is almost unavoidably present at zirconia surfaces, since many syntheses of zirconia catalysts are made in aqueous solution, and the handling of SZ under normal laboratory conditions leads to water adsorption on the surface depending on the temperature and partial pressure of the water. Surface hydroxyl groups are formed from the water and even during calcination procedure the zirconia loses only a part of the hydroxyl groups [147].

Several studios have been conducted in order to understand how sulfation enhances the surface acidity of zirconia, however the exact structure of the active sites and their nature (Lewis or Brønsted type) is a subject of intense debate and several models have been proposed. One of the models involves a sulfate bridging across two Zr atoms, as is shown in Figure 6. The Lewis acid strength in this structure result remarkably greater by the inductive effect of S=O in the complex. In the absence of water, the Lewis acid sites would prevail, but they may be converted into Brønsted acid sites via proton transfer [148].

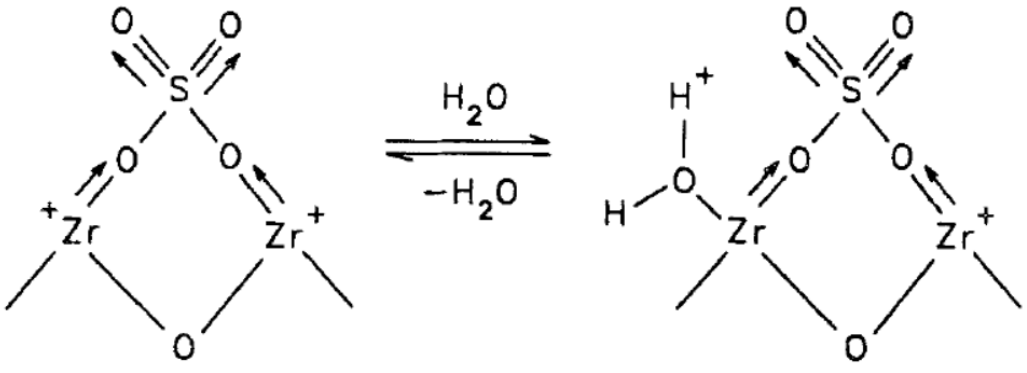

Figure 6 Model of acids sites of SZ [148].

Another structural model proposed is presented in Figure 7, in the presence of water the Brønsted acidity is generated which is attributed to the formation of S–O–H groups [148].

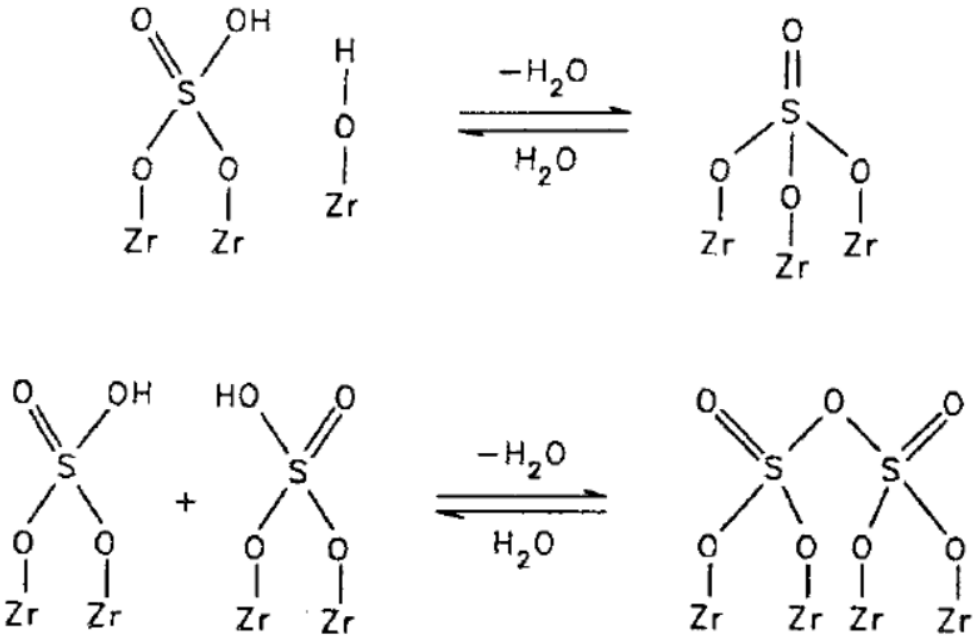

Figure 7 Model of acids sites of SZ [148].

Another model considers that the hydroxyl group is bonded to a Zr atom adjacent to the Zr atom to which a sulfate group is chelated (see Figure 8). The proton donating ability of the hydroxyl group on the zirconia surface is strengthened by the electron-inductive effect of the S=O double bounds in the sulfate group. The structural models show here are illustrative of the acid sites present in the SZ catalysts but there is not one definitive, each model is the results of the characterization of the catalysts by techniques such as IR spectroscopy of adsorbed bases, however the exact structure of the active sites remains as a subject of debate [146].

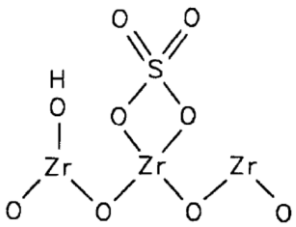

Figure 8 Model of acids sites of SZ [148].

1.10 Objectives

1.10.1 General objective

Evaluate supported Pd/Co monolithic based catalysts for the simultaneous removal of ortho-dichlorobenzene(*o*-DCB) and nitrogen oxides in the presence of methane, water and oxygen.

1.10.2 Specific objectives

- Determine the physicochemical properties of Pd/Co-HMOR and Pd/Co-SZ catalysts in powder and monoliths.
- Evaluate the performance of the synthesized catalysts in the selective catalytic reduction of NOx with methane simultaneously with catalytic oxidation of o-DCB in gas phase.
- Determinate the effect of space velocity, temperature, initial concentrations of the reactants and water and oxygen concentration on the activity of the catalysts.
- Evaluate the stability of the Pd-Co/HMOR catalyst under the best reaction conditions.
- Determine a kinetic model for NOx reduction and o-DCB oxidation.

Chapter 2 Methodology

2.1 Powder catalyst synthesis

The Co and Pd/Co catalysts supported on protonic mordenite were prepared according to the procedure previous reported by Córdoba et al [97]. Na-MOR (Si/Al = 6.5 from Zeolyst) was first transformed into NH_4–form by ion exchange with 100 mL of 1 M NH_4Cl per gram of zeolite at 80 ºC for 24 h under reflux. Co–HMOR was prepared by ion exchange of NH_4–MOR with 100 mL g^{-1} of 0.09 M cobalt acetate solution per g of zeolite for 20 h at 70 ºC under reflux. After the ion exchange procedure, the sample was rinsed with deionized water, filtered and heated in flowing He up to 500 ºC at a rate of 2 ºC/min and held at this temperature for 4 h. The Pd/Co–HMOR catalyst was obtained by incipient wetness impregnation with an aqueous solution containing the required amount of $Pd(NH_3)_4Cl_2 \cdot H_2O$ to obtain a Pd loading of about 0.1 – 0.15 wt.%. After drying at 60 ºC, the catalyst was heated in flowing argon at 2 ºC min^{-1} up to 500 ºC and held 4 h at this temperature and then allowed to cool at room temperature.

Pd/Co catalyst supported on sulfated zirconia was prepared following a previous reported procedure [102], 6.5 mL of zirconium butoxide $Zr(OC_4H_9)_4$ (Aldrich) was added to 22.5 mL of cyclohexane at 60 °C. The solution was stirred for 1 h and then cooled down to 3 °C. Then, a solution of distilled water (4 mol/mol Zr) and sulfuric acid (0.48 mol/mol Zr) was added dropwise with constant stirring, until the mixture became hard to stir. The resulting gel was aged for 24 h at room temperature without stirring. Then, the aged gel was dried at 70 °C and calcined in static air at 600 °C during 4 h. Co–SZ samples were obtained with a similar

procedure using a solution of 0.2 g of cobalt acetate in 5.5 mL of ethanol added to a mixture of 17 mL of cyclohexane and 6.5 mL of zirconium butoxide. The incorporation of Pd was performed also by incipient wetness impregnation equal to the followed for Pd/Co-HMOR catalyst.

2.2 Monolithic catalyst

The word "monolith" is derived from the Greek *mono, "single" and lithos, "rock"* and means "composed of a single rock" [149]. Monolithic structure refers to a continuous unitary framework containing many narrow parallel straight channels (like a honeycomb) made of ceramic or metallic materials. The number of channels, their diameters and wall-thickness determine the cell density (the number of channels per unit area) which range from 9-600 cpsi (cells per in^2) [143,150]. Although channel shapes may be square, rectangular, hexagonal or triangular, the square channels are the most common geometry used [143]. Monolithic catalysts are obtained by the incorporation of a catalytic active phase to the walls of a monolithic structure, this is schematized in Figure 9 [149,151–153].

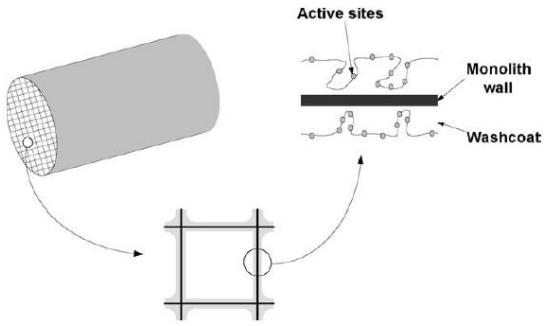

Figure 9 Schematic representation of a monolithic catalyst [153].

Monolithic catalysts exhibit several engineering design advantages in comparison with the conventional fixed-bed catalytic reactors that have led to their widespread use for environmental applications. The large open frontal area of monolithic reactors giving access to straight channels results in very little resistance to flow and hence in an extremely low-pressure drop in comparison with pellet-type catalysts. This is essential for end-of-pipe technology used in exhaust systems and for treating stack gases [154]. The lower the pressure drop also translates to lower compressor costs for stationary applications and to greater power savings for mobile sources [155]. The open channels of the monoliths are also less sensitive

to fouling due to the small particles can easily flow along the channels, only large one can block a complete channel but can be removed by an upstream filter [152]. This feature allows monolithic catalysts to be used in high dust environments as is the case of incineration plants [150].

The most direct preparation method of monolithic catalysts is by extruding the monolith from a catalytic material [154], in this case, the active phases or their precursors are mixed with other components that constitute the catalyst before its extrusion in the monolithic shape [156]. By this method a high catalyst loading can be achieved because almost the entire wall is made up of catalyst and not mostly of an inert support structure such as cordierite [154]. The monolithic catalysts thus obtained present some inaccessible active sites, which are buried in the walls lowering the effectiveness of the catalyst, this is particularly relevant when the cost of the catalytic material is high as in the case of noble metals. On the other hand, washcoated monolithic catalysts are prepared by coting the monolithic structure with a thin film of a porous material which serves for the dispersion of the active phases or by coating the monoliths with a ready-made catalyst [156]. In general, it is recommended to extrude the monolith from an inert material or a catalyst support in which the catalyst is subsequently coated [154].

The most common ceramic material for the preparation of monolithic catalysts is cordierite because it presents a high mechanical strength, high temperature resistance and low thermal expansion coefficient. The monoliths have become one of the most chosen catalytic supports in almost all environmental applications use of monolithic reactors is widely used in catalytic pollution control field. Most of the applications of monolithic reactors is one of the choicest options as catalyst supports for environmental applications. The use of metal or ceramic monoliths depends on the application.

2.2.1 Minimonoliths of cordierite

A commercial cordierite straight-channels monolithic structure (from Corning Inc.) of 400 cpsi was carefully and conveniently cut to obtain minimonoliths of 10 mm x 10 mm x 12 mm (36 channels).

2.2.2 Preparation and treatment of cordierite minimonoliths

Before the washcoating of the Pd/Co-HMOR powder catalyst, the minimonoliths were immersed in 20% w/w HNO_3 solution for 5 hours and subsequently washed with deionized water until neutral pH. The nitric acid treatment of cordierite increases its specific surface area and reduces the thermal expansion coefficient [156]. Afterwards, minimonoliths were immersed in acetone for 2 h, then dried at 100 °C. Finally, they were calcined in static air with a heating rate of 2 °C/min up to 600 °C for 2 h.

2.2.3 Incorporation of the active phase

The washcoat slurry was prepared as follows: powder Pd/Co-HMOR catalyst was slurred into deionized water to obtain 30 wt. % solids. The slurry was mixed in a ball mill (Restch PM 100) for 36 h at 200 rpm in 15 continuous cycles (each cycle consisted of 1 h work and 1 h rest) at room temperature. The milling of the slurry is an important step since the coating adherence increases as the size of aggregates decreases [156], big aggregates would result in a poor adhesion since they cannot enter inside the cordierite pores.

Mini-monoliths were washcoated as follows: (1) The ball-milled slurry was stirred at 800 rpm using a mixer (Ultra-turrax T25); (2) minimonoliths were dipped into the slurry for 10 s; (3) excess slurry was softly blown off with compressed air (5 psi) avoiding shaking the mini-monolith in order to keep the washcoat uniformity; (4) samples were dried in a conventional oven at 120 ºC for 2 h. The steps 2 to 4 were repeated until a 15 wt % washcoat loading was achieved. Finally, the mini-monolithic catalysts were calcined in air at 2 ºC/min from room temperature to 600 ºC for 2 h. This last step is crucial, since the calcination binds the washcoat safely to the monolith walls, the calcination temperature must be at 550 °C or higher in order to get a good coating adherence [157].

2.2.4 Resistance tests for evaluation of the washcoat adherence

Thermal and mechanical resistance tests were performed in order to evaluate the washcoat adherence to the minimonoliths walls. In the thermal tests, the samples were heated and cooled abruptly by using a tubular quartz reactor placed on a mobile support which instantaneously in or out from the tubular furnace kept at 500 °C. Using this assembly, the mini-monoliths were exposed to the high furnace temperature for 10 minutes and

subsequently exposed to ambient temperature for other 10 min. This operation was repeated during 10 cycles in order to determine the thermal shock resistance. In the mechanical test, the mini-monoliths underwent ultrasonic vibration in an aqueous medium for 1 h using a Branson 3510 ultrasonic vibration equipment.

Four tests were carry out as follows: (1) Only thermal test; (2) only mechanical test; (3) one mechanical test followed by one thermal test and (4) one thermal test followed by one mechanical test. The degree of erosion was measured by the decrease of mini-monoliths weight before and after each test, as reported in similar works [156,158].

2.3 Experimental Set-up

Catalytic reactions were carried out at atmospheric pressure (0.84 atm) in a quartz tube reactor (3/8" OD) containing a quartz frit to hold either the powder or mini-monolithic catalysts. The reactant gases (NOx/He: 5000 ppm (90% NO and 10% NO_2), CH_4/Ar: 5%, O_2 UHP, Ar UAP) were fed using electronic mass flow controllers (Brooks 5850E) and mixed in line before entering the reactor, Ar was always used as balance gas. The water vapor and *o*-DCB were introduced into the reactant mixture by means of two saturators composed of a sealed glass bubbler with a medium-pore frit immersed on the liquid deionized water and *o*-DCB, respectively, in both saturators Ar was used as carrier gas. The volumetric flow rates through the saturators were calculated by the Equation 2-1. In the case of water vapor the saturator was heated to increase the vapor pressure and to decrease the volumetric flow rate in the saturator conveniently, the temperature was controlled by a temperature controller. The tubing between the water saturator and the reactor was thermally well isolated. The experimental set-up scheme is presented in the Figure 10.

$$F_{sat} = \frac{C * 10^{-6} * F_t * P_0}{P_v} \quad \text{Equation 2-1}$$

Where,

F_{sat}: Volumetric flow throughout the saturator to obtain the desired concentration in the gas mixture (mL/min).

C: Desired concentration of water vapor or *o*-DCB in the gas mixture (ppm_v).

F_t: Total volumetric flow rate of the reactant gas mixture (mL/min).

P_0: Atmospheric pressure (kPa).

P_v: Vapor pressure of the water or *o*-DCB (kPa).

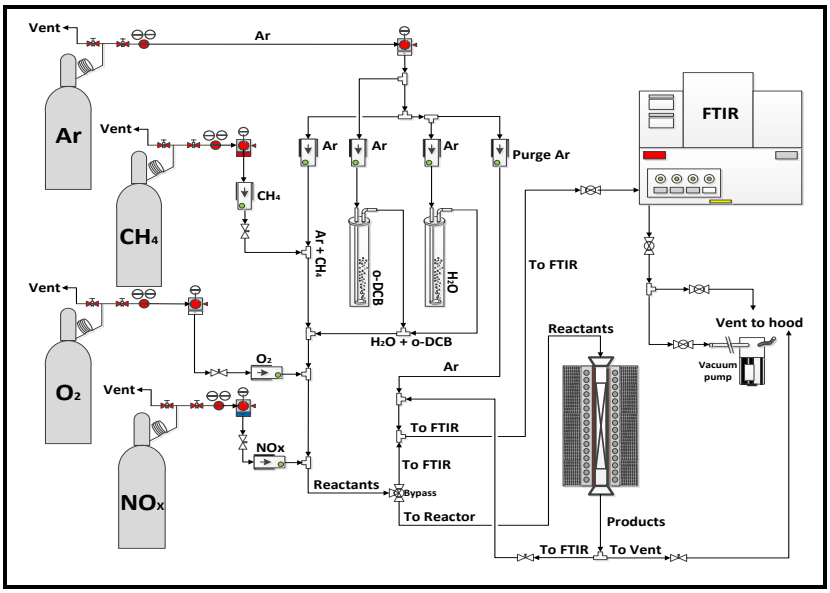

Figure 10 Experimental set-up

The concentrations of the gases were analyzed online by a FTIR gas analyzer (Thermofisher scientific, model AntarisTM IGS–USB) equipped with a MCT detector, KBr beamsplitter, 2 m pathlength gas cell, 200 mL gas cell volume and a ZnSe window. Data were collected with a spatial resolution of 0.5 cm^{-1} and 32 scans were collected for each sampling. Gas cell was operated at atmospheric pressure and the temperature was fixed at 150 ºC in order to avoid condensation of the reactants inside the gas cell. A quantification model was developed by taking several spectrums of known gas mixtures and adjusting the absorbance and concentrations data by means of classical least square model, the software TQ Analyst 9.4.45 (Thermo Fisher Scientific Inc.) was used for this purpose, in Table 1 is shown the spectrum range analyzed for each compound . The o-DCB, NO and CH_4 conversions were calculated as follow:

$$x_{NOx} = \frac{([NO] + [NO_2])_0 - ([NO] + [NO_2])_f}{([NO] + [NO_2])_0} * 100 \qquad \text{Equation 2-2}$$

$$x_{CH_4} = \frac{[CH_4]_0 - [CH_4]_f}{[CH_4]_0} * 100$$ Equation 2-3

$$x_{o-DCB} = \frac{[o-DCB]_0 - [o-DCB]_f}{[o-DCB]_0} * 100$$ Equation 2-4

Where 0 represents the initial concentration before entering to the reactor and f represents the effluent concentration.

Table 1 Infrared spectrum range used for quantification of compounds.

Compound	**Spectrum range (cm^{-1})**
NO	1899.00 – 1901.00
NO_2	1663.54 – 1548.08
CH_4	2872.16 – 2888.12
o-DCB	753.55 – 754.03
CO	2144.70 – 2149.04
CO_2	2380.21 – 2392.75 2344.53 – 2351.52

2.4 Physico-Chemical Characterization Techniques

2.4.1 Atomic Absorption Spectroscopy (AAS)

The atomic absorption spectroscopy is widely used to determine the bulk atomic composition of catalysts [143]. In this technique the analyte must be first vaporized to convert the element of interest into gaseous atoms, usually by application of heat to a cell called atomizer. The free gaseous atoms absorb electromagnetic radiation at specific wavelength (emitted from a light source) to produce a measurable signal. The elemental concentration is determined from the fact that the absorption signal is proportional to the concentration of those free absorbing atoms in the optical path. The light source is usually a hollow cathode lamp containing the element of interest and an anode within an enclosed glass tube filled with an inert gas at low pressure [159]. Elemental composition of Pd and Co were determined in an Atomic Absorption Spectrometer Philips (Model PU–9100X).

2.4.2 X-Ray Diffraction

X-ray powder diffraction (XRD) is the main technique for the study of the bulk structure of crystalline materials. Crystalline phases present in the catalysts, supports and active phases can be identified by this technique. A powder diffraction pattern contains structural information which has been used essentially as a fingerprint, for crystal phase identification purposes in the characterization of heterogenous catalyst [160].

The pass of X-ray radiation through matter result in the physical phenomena of the scattering of the radiation. If the material is crystalline (the atoms are arranged in an orderly and periodic way in space forming planes) and the separation of the crystalline planes is the same magnitude as the wavelength (λ) of the X-rays, then constructive and destructive interference will occur. This results in diffraction where X-rays are emitted at characteristics angles based on the spaces between the crystalline planes, which are of comparable magnitude to the incident wavelength of the X-ray radiation. The relationship between the wavelength, atomic spacing and angles is given by the Bragg equation (Equation 2-5) [140].

$$n\lambda = 2d \sin\theta \qquad \text{Equation 2-5}$$

Where, n is the order of reflection ($n = 1, 2, 3\ldots$), λ is the wavelength of x-ray (Å), d is the lattice distance (Å) and θ is the angle of diffraction (°).

A limitation of the XRD technique is the lack of sensitivity in detecting a low amount of a given phase in a mixture, therefore it might be greatly underestimated or even overlooked. This limitation is even more severe in the case of heterogenous catalysts. The limit of detection of a metal phase depends upon several factors, the weight fraction, the square of the atomic number, the size of the particles, and the intensity of the continuous scattering from the support, then is difficult to define a general limit concentration or a limit of size under which the phase can no longer be detected [161].

XRD technique was used in this research to identify changes in the structure of the mordenite because of the protonation and the incorporation of the metals (Pd and Co) in the zeolite and due to the thermal and chemical reactions in the case of the used catalysts. XRD patterns were obtained in a XPert PANalytical X-ray diffractometer Empyrean Series II equipped with a PIXcel 3D detector using Cu Kα radiation (λ= 1.54 nm) with a Ni filter at 45 KV and

40 mA, the scan step was 0.039º, the rate 2º/min and the scanning ranges were of 2θ = 5–50°.

2.4.3 Low Temperature N_2 Adsorption

The internal surface and porous structure are among the most fundamental properties of heterogeneous catalysts, since the catalytic process take places on the active sites which are distributed throughout the internal solid surface. The diffusion of the reactants and products throughout the pores depends on the pore size and structure. The size and number of pores determine the internal surface area. High surface areas (high density of small pore sizes) are convenient to maximize the dispersion of catalytic components. However, small pore sizes can lead to resistance to the diffusion of the molecules [143].

The textural properties of catalysts are commonly determined by the physisorption of a chemical inert gas on the surface of solid substances [140]. Nitrogen adsorption at boiling temperature (77 K) is the most widely used technique to determine the catalyst surface area and to characterize its porous texture. The method is based on the determination of the adsorption isotherm which relates the nitrogen adsorbed volume against the relative pressure at equilibrium [162].

The BET model, proposed by Brunauer, Emmett and Teller is widely used to interpret the adsorption isotherm data and to determine the surface area of a solid samples. The model relates the nitrogen adsorbed volume with the monolayer volume on the surface of a solid at the relative equilibrium pressure by the Equation 2-6 [163].

$$\frac{p}{v_{ads}(p_0 - p)} = \frac{1}{v_m c} + \frac{c - 1}{v_m c}\frac{p}{p_0} \qquad \text{Equation 2-6}$$

Where, p is the equilibrium pressure, p_0 is the saturation pressure of the adsorbate, v_m is the monolayer volume of the adsorbate and c is a parameter. The plot of $\frac{p}{v_{ads}(p_0-p)}$ against $\frac{p}{p_0}$ should give a straight line, whose intercept is $\frac{1}{v_m c}$ and whose slope is $\frac{c-1}{v_m c}$, from here the two constants v_m and c can be known [163]. The surface area of the solid can be then derived from the Equation 2-7 [162]:

$$A_s = (v_m/22414)N_a\sigma \qquad \text{Equation 2-7}$$

Where, v_m is the monolayer volume, N_a is the Avogadro number and σ is the area covered by one nitrogen molecule. The σ value generally accepted is 0.162 nm^2 [162].

The low temperature N_2 adsorption experiments for the catalyst samples were carried out in an AutoChem II 2920 instrument (Micromeritics) equipped with a Thermal Conductivity Detector (TCD). Specific surface areas of samples were measured by nitrogen adsorption at 77 K and data were interpreted by using the Brunauer–Emmett–Teller (BET) modeling equation. N_2 adsorbed was previously calibrated by injecting known amounts of a mixture of 30% N_2/He and correlating them with the respective integrated TCD profiles.

2.4.4 Temperature programed reduction under hydrogen (H_2-TPR)

The temperature programmed reduction (TPR) is a widely used technique for the characterization of the reducible species of a catalyst. In a typical TPR experiment, the catalyst sample to analyze is placed in a fixed-bed reactor and exposed to a reducing gas mixture (typically H_2 diluted in an inert gas) while the temperature is increased according to a linear temperature program. The difference between the inlet and outlet concentration of the gas reducing mixture is measured as a function of time using a thermal conductivity detector (TCD). As result, a TPR profile of consumed H_2 in function of the reduction temperature is obtained. The interpretation of the TPR profile reveals qualitative information about the oxidation state of the reducible species present in the catalysts [164]. The total amount of hydrogen consumed gives the degree of the reduction α of the catalyst determined by the Equation 2-8 [165].

$$\alpha = \frac{n_r}{n} = \frac{n_{H_2}}{n} \cdot \frac{z}{2} \quad \text{Equation 2-8}$$

Where, n is the amount of reducible species in moles, n_r is the amount of the actually reduced species in moles, n_{H_2} is the amount of the consumed hydrogen in moles and z is the formal charge of the metal ion. In the case of metal oxides, water is formed as byproduct and must be removed upstream of the TCD to prevent unwanted signals and the damage of the filaments inside the detector, this can be achieved by passing the gas stream through a cold trap. Samples which undergo thermal decomposition or thermal desorption cannot be effectively studied by the TPR technique [165].

H_2–TPR of fresh samples were obtained by flowing 50 mL min^{-1} of a mixture 10% H_2/Ar and heating from 100 to 1000 ºC using a heating rate of 5 ºC min^{-1}. Before H_2–TPR analysis, the samples were calcined under 50 ml min^{-1} of a flowing mixture of 5% O_2/Ar at 500 ºC for 1 h. Then, the fresh samples were cooled to room temperature under a constant flow rate of pure Ar (50 ml min^{-1}). In the case of used catalysts, the samples were only dried at 150 ºC in flowing He for 1 h and then cooled to room temperature before TPR experiment run. Some of the H_2–TPR profiles presented convoluted peaks, in such cases the curves were fitted by two or even three Gaussian functions to separate each peak, for this Origin software was used for data processing. In all cases the correlation coefficient was at least 0.9.

2.4.5 Temperature programmed desorption of ammonia (NH_3-TPD)

Surface acidity is one of the most important chemical properties of the catalysts. The Brønsted and Lewis acid sites in solid acid catalysts such as zeolites and metal oxides catalyze many reactions, especially in organic chemistry [166]. TPD of a base such as ammonia, amines or pyridine is a widely used method to obtain information about the density and strength of acid sites on the surface of a solid [167].

In a typical TPD experiment, a small amount of catalyst (10 – 200 mg) is contained in a reactor which can be heated at a linear rate, the temperature is measured by a small thermocouple inserted in the catalyst. The catalyst is first degassed by heating in a flowing inert gas such as Ar or He. After pretreatment, the sample is saturated with the gaseous base, usually ammonia at 100 ºC or at a lower temperature. Then the physiosorbed molecules are evacuated with an inert gas. The programmed desorption begins by raising the temperature linearly with time in a flowing inert gas stream. The concentration of the desorbing gas in the effluent stream is usually measured by a thermal conductivity detector downstream [168]. NH_3–TPD was used to determine the total acidity of the catalysts. Before the programmed desorption the samples were pretreated in flowing Ar (50 mL min^{-1}) for 1 h at 250 ºC, then cooled to 50 ºC in flowing Ar. The saturation adsorption of ammonia was performed at 50 ºC by flowing 50 mL min^{-1} of a gas mixture 0.3% NH_3/He for 90 min. In order to remove any physical adsorbed ammonia, the samples were flushed with 50 mL min^{-1} of He for 1 h. Desorption of ammonia was obtained by rising the temperature (10 ºC min^{-1}) up to 1000 ºC in flowing He. Some of the NH_3–TPD profiles presented convoluted peaks, in such cases the

curves were fitted by two or even three Gaussian functions to separate each peak, for this Origin software was used for data processing. In all cases the correlation coefficient was at least 0.9.

2.4.6 Transmission Electron Microscopy (TEM)

Transmission electron microscopes are complex optical systems analogous to the ordinary optical microscopes with the difference that highly accelerated electron beams are used (200 – 300 kV) instead of light [169]. These microscopes can produce high-magnification images of thin samples by probing with a high-energy electron beam and collecting the electrons that have been scattered in the forward direction, that is, they operate in transmission [170]. In general, a transmission electron microscope operates as follow, the electrons are emitted from the electron gun (tungsten filament) and accelerated by a potential difference. The electrons are focused with a series of electromagnetic lenses to form a parallel beam which goes through the thin sample. The system must operate in ultra-high vacuum, which is achieved with a series of pumps [169]. The magnified images of the sample are formed by combining the transmitted electrons by means of an electromagnetic objective lens. The lens produce a 2D diffraction pattern of the sample in its focal plane and these diffracted beams recombine to form the image in the image plane [171].

Elemental analysis on the solid surface can be performed by Energy-Dispersive X-ray Spectroscopy (EDS), which is the most commonly used analytical technique in a microscope [171]. The incident electron beam causes the ejection of electrons from atoms of the sample leading to X-ray emission that can be analyzed with a solid-state energy-dispersive detector [171,172]. Since each element has a unique pattern of X-ray lines from the K, L and M shells, then the qualitative analysis by this method is straightforward. Besides, the software provided by most of the manufacturers also allows to obtain a semi-quantitative analysis of the elements present in the sample [171].

Transmission electron microscopy (TEM) analyzes were performed on a Tecnai F20 Super-Twin TMP instrument with FEG (Gatan UltraScan® 1000XP-P camera, 0.1 nm point resolution operated at 200 kV), the chemical analyzes were performed by Energy-dispersive X-ray spectroscopy (EDS) with a detector Oxford Instruments X-MaxN. The samples for the TEM/EDS analysis were dispersed in ethanol and kept in an ultrasonic bath for 20 min, a

drop of this suspension was spread out onto a TEM cooper grid (200 Mesh) covered by a holey carbon film followed by drying under room conditions.

2.4.7 Scanning Electron Microscope (SEM)

The scanning electron microscopy allows to study the morphology and topography of a solid surface and combined with the energy dispersive X-ray spectroscopy (EDS) allows to analyze the elemental distribution on the solid surface. In a scanning electron microscope, the sample is irradiated with a beam of high-energy electrons (30 – 50 kV). The incident electron are decelerated on the solid sample generating a variety of signals: secondary electrons, backscattered electrons, diffracted backscattered electrons, photons, visible light and heat [169]. The image is formed by either secondary electrons or backscattered electrons emitted from the area irradiated by the scanning electron probe. The most commonly used imaging mode make use of the secondary electrons which are low-energy electrons (0 – 100 eV) easy to collect by a biased scintillator. The low energy electrons have a small mean free path, which guaranties that the electron signal comes from the surface region of the sample. The number of electrons emitted depends on the angle between the sample and the electron beam and the detector. Orthogonal angles result in a large fraction of secondary electrons escaping from the sample and collecting by the detector generating bright in an SEM image. On the other hand, only a small fraction of secondary electrons can escape and be collected from horizontal surface with respect to the beam resulting in less brightness images. The backscattered electrons have much larger energies (1 – 30 keV) make them more difficult to collect than the secondary electrons. Therefore, the signal is less sensitive to surface topography, and instead the image intensity depends on the composition of the sample [171]. Then, the morphology and topography of the sample are revealed by the secondary electrons while contrasts in composition in multiphase samples is showed by the backscattered electrons. The elemental distribution analysis by EDS is determined based on the characteristic X-ray photons emitted which allows the identification of the atoms present in the sample [169].

Fresh and used minimonolithic catalysts were characterized by SEM-EDS in order to analyze the changes in the morphology and element distributions on the coated walls. For the analyzes, longitudinal cuts of the monoliths were made with a precision cutter Buchler Isomet

® 1000 model 112180. The samples were analyzed in a microscope JEOL model JFM-6490LV.

2.4.8 Raman Spectroscopy

Raman spectroscopy is a vibrational technique based on the inelastic scattered light from a sample when a high energy photon from an incident light strikes a molecule and produce a scattered photon [173]. This is a widely used technique for the catalyst characterization of supported and bulk metals, oxides and supported oxides [174]. This spectroscopy technique has several advantages, the sample handling and preparation requirements are minimum; the required sample volume depends only on the diameter of the focused laser beam, which is of the order of a micron and the water is a weak Raman scatter molecule, so the spectra present very little interference due to the presence of water [175]. The information depth of Raman spectroscopy depends strongly on the optical properties of the sample and should typically be of the order of 2 nm [174]. The Raman spectrum is considered as a fingerprint tool very useful for qualitative analysis of unknown samples or components [176].

There are two types of light scattering when a molecule is irradiated with a monochromatic light, the elastic and inelastic scattering. The elastic scattering occurs when the photon frequency does not shift or change its wavelength and energy (Rayleigh scatter). On the other hand, the inelastic scattering results in a frequency shift of the incident photon due to excitation or deactivation of molecular vibrations [177]. When the out coming scattered light has a lower frequency than the incident photon is known as Stokes Raman scattering and when it has a higher frequency is known as anti-Stokes Raman scattering [173]. Stokes shifted Raman bands involve the transitions from lower to higher energy vibration levels of the molecules, these bands are measured in conventional Raman spectroscopy. The anti-Stokes bands are much less intense than the Stokes bands and are measured with fluorescing samples because fluorescence causes interference with Stokes bands. The observation of Raman scattering signals of a sample requires a change in polarizability during molecular vibration, otherwise no Raman spectrum is obtained. This change will be the result of the displacements of the constituent atoms from the equilibrium position as the result of the molecular vibrations [173].

In this research, Raman spectra of fresh and used catalysts were collected in a Horiba Jobin Yvon Labram HR spectrometer using a 633 nm He–Ne laser, no special preparation procedures were required for the analysis of the samples.

2.4.9 X-ray Photoelectron Spectroscopy (XPS)

The performance of solid catalysts greatly depends on the chemical composition on the surfaces of the solid phase. X-ray photoelectron spectroscopy is one of the most widely used methods for surface chemical analysis, it allows to analyze quantitatively the chemical composition in the surface region and to identify different chemical states of an element. Here, chemical composition in the surface region refers to the identification of the atomic species present in the first or second outermost atomic layers of the solid surface [178].

XPS is based on the photoelectric effect, the surface sample is irradiated by an X-ray source in an ultrahigh vacuum environment, as a result of this, an electron belonging to an inner shell of an atom is excited and escaped into the vacuum [169,178]. The emission process has been explained by a three-step model, in which the first step corresponds to the absorption of an X-ray photon and promotion of an electron from its ground state to the final state above the fermi level. In the second step the electron is transported to the surface and the third step is the escape of the electron into the vacuum. Since the electron is generated within the potential of the solid, its wave function contains contributions from the solid even after it has escaped into the vacuum. The kinetic energies of the emitted electrons are measured using an electrostatic charged-particle energy analyzer [179]. The electron binding energies can be calculated from Equation 2-9.

$$E_b = h\nu - E_k - \Phi \quad \text{Equation 2-9}$$

Where,

E_b is the electron binding energy in the solid.

$h\nu$ is the energy of the incident photon.

E_k is the kinetic energy with which the photoelectron is emitted.

Φ is the difference in work function between the sample and the detector material assuming that there is no charge at the sample surface.

The surface atoms are identified by their specific electronic binding energies. The atomic core level binding energies also depend on the environment, particularly from the oxidation state [169]. These chemical shifts can reach values up to about 4 eV and are therefore the basis for chemical analysis with XPS. The binding energies generally increase with increasing oxidation state [178].

X-ray photoelectron spectroscopy (XPS) experiments were carried out in a SPECS X(NAP-XPS) electron spectrometer equipped with a PHOIBOS 150 1D-DLD analyzer and a monochromatic Al-Kα (hν = 1486.7 eV) X-ray source operated at 13 kV and 100 W. The analyzer was operated with a pass energy of 90 eV for the survey spectra and 30 eV for the high-resolution spectra. The binding energies were measured within precisions of 1 eV for the survey spectra and 0.1 eV for the high-resolution spectra. The data treatment was performed with the Casa XPS program (Casa Software Ltd., UK). All XPS spectra were corrected using the C 1s line at 284.5 eV.

2.4.10 In-situ FT-IR spectroscopy

The infrared spectroscopy is a vibrational technique based on the energy transitions of a molecule exposed to infrared radiation. The energy of infrared radiation is too low to affect the electrons within an atom, but instead it can affect the vibrational, translational and rotational energy transitions of a molecule. Since a molecule's movements are unique to its structure then measurement of these transitions can be used for compound characterization. The condition for a molecule to show infrared absorption is that a vibration must cause a change in the dipole moment of the molecule, therefore homonuclear diatomic molecules are "infrared-inactive" because its dipole moment is always zero [180].

The *in-situ* FT-IR spectroscopy refers to the study of a catalyst and adsorbed species in presence of the reactants under real high-temperature reaction conditions or at lower temperatures. This technique is widely used to establish correlations among the surface species and the catalytic properties of the catalysts [181]. It also contributes to determine the nature of the adsorbed species, the formation of some intermediates, the interactions of the active sites with the adsorbed species and its strength, the identification of the active sites and possible causes of catalyst poison.

Transmission infrared (IR) spectra were obtained using an Agilent Technologies Cary 600 series FT-IR spectrometer equipped with a liquid N_2 cooled high sensitivity MCT detector. A stainless-steel IR transmission cell (HTHP Specac) with an effective path length of 30 mm between two IR-transparent ZnSe windows was used to conduct the in-situ experiments. The samples were in the form of self-supported discs of approximately 1 cm diameter which were prepared by pressing about 25–30 mg of each powder sample to study. The thermal treatment was performed with a heater block assembly inside the cell which has a special hole at the center where the sample disc is placed to be exposed to the infrared beam, the temperature was monitored with a thermocouple located in close proximity to the sample and controlled using a PID controller (WEST 6100+). Before each adsorption experiment, the catalysts samples were pretreated *in situ* with flowing Ar at 360 ºC (5 ºC/min) for 2 h. Then, the sample was cooled in flowing Ar to the temperature of the adsorption experiment and the spectrum of the pretreated sample was used as background. The spectra were collected with a spatial resolution of 4 cm^{-1} and 128 scans were recorded per spectrum. In all the spectra here presented the IR spectrum of the clean catalyst surface was subtracted.

2.5 Kinetic study

Chemical kinetics refers to the study of reaction rates and mechanism. For homogeneous reactions, the reaction rate $(-r_A)$ is commonly defined as the number of moles of A reacting per unit time per unit volume $(mol/dm^3 \cdot s)$, in the case of heterogeneous reactions the reaction rate $(-r'_A)$ is expressed as the number of moles of A reacting per unit time per unit mass of catalyst $\left(mol/s \cdot g_{catalyst}\right)$ [182].

One of the main objectives of a kinetic study is to parameterize the reaction rate as a function of state variables such as temperature, pressure and concentration of the reactants, which will result in an algebraic equation known as the rate equation or rate law [182,183]. This equation is used to predict the reaction rate for any set of conditions, the accuracy of the prediction will depend on the functional form used for the parameterization and how close the set of conditions are to those used for determining the parameters [183]. The kinetic studies also provide elements that allow to propose a possible mechanism and the reaction rate equation obtained allows to describe the experimental data. The reaction mechanism is just a theory

to explain the results observed in the experiments, however for reactor design purposes it is not mandatory to know the mechanism of the reaction, what is really needed is to have a satisfactory rate equation [184].

In heterogeneous catalytic reactions, the mechanism typically involves an adsorption step, a surface reaction step and a desorption step [182]. Two main models are commonly used to explain the mechanism of a heterogeneous reaction, the *Langmuir–Hinshelwood* and the *Eley–rideal* mechanisms. In the *Langmuir–Hinshelwood* model the two reacting species are chemisorbed on the catalyst surface before the reaction takes place, while in the *Eley–rideal* mechanism one species reacts directly from the gas phase with the chemisorbed species on the active sites [185].

2.5.1 Data acquisition and reaction rate equation

Kinetic experiments for both powder and mini-monolithic reactors were carried out in a continuous-flow tubular reactor operated in differential conditions, several experiments varying the flow of reactants and the catalyst weight were carried out in order to obtain low conversions. Thus, the heat of reaction release per unit volume is negligible and the reactor can be considered as isothermal. A differential reactor can be considered gradientless, namely the reactant concentration through the reactor is approximately constant and the reaction rate is considered spatially uniform within the reactor [182]. Therefore, the design equation will be similar to the CSTR (Continuous–stirred tank reactor) design equation. A steady-state mole balance on reactant A gives:

$$F_{A0} - F_{Ae} + r'_A W = 0 \qquad \text{Equation 2-10}$$

Where,

F_{A0}: molar flow rate of the specie A into the reactor system (mol/s)

F_{Ae}: molar flow rate of the specie A to the exit of the reactor (mol/s)

r'_A: rate of formation of A per gram of catalyst ($mol \cdot g^{-1} \cdot s^{-1}$)

W: mass of the solid catalyst (in grams).

Solving for $-r'_A$*:*

$$-r_A' = \frac{F_{A0} - F_{Ae}}{W} \quad \text{Equation 2-11}$$

Assuming a constant volumetric flow rate (Q) through the reactor, the reaction rate equation for the specie A can be written in terms of the inlet (C_{A0}) and outlet (C_{Ae}) concentrations of A to the reactor, as follow:

$$-r_A' = \frac{Q(C_{A0} - C_{Ae})}{W} \quad \text{Equation 2-12}$$

Finally, from Equation 2-12 the rate of reaction can be expressed in terms of the conversion of the specie A:

$$-r_A' = \frac{QC_{A0}}{W}\frac{(C_{A0} - C_{Ae})}{C_{A0}} \quad \text{Equation 2-13}$$

$$-r_A' = \frac{F_{A0}X_A}{W} \quad \text{Equation 2-14}$$

Where,

X_A: conversion of the specie A.

In the previous equations the A specie may represent either NO, CH_4 or *o*-DCB.

Since a very small amount of catalyst and large volumetric flow rates are used in kinetic experiments, the concentration difference $C_{A0} - C_{Ae}$ becomes quite small and the rate of reaction determined from the Equation 2-12 can be obtained as a function of the reactant concentration in the catalyst bed, namely $-r_A' = f(C_{Ab})$ by varying the inlet concentration. However, the concentration of the specie A through the bed is unknown, this can be approximated by the arithmetic mean of the inlet and outlet concentrations as follow,

$$C_{Ab} = \frac{C_{A0} + C_{Ae}}{2} \quad \text{Equation 2-15}$$

Since very little reaction takes place within the bed then the concentration of the specie *A* through the bed can be approximated to the inlet concentration ($C_{Ab} \approx C_{A0}$) and the reaction

rate equation in terms of specie A will be a function of the initial concentration of that specie (C_{A0}), namely $-r'_A = f(C_{A0})$ [182].

Accordingly, the Equation 2-14 was used to calculate the experimental reaction rates, the specie *A* may represent either *o*-DCB, CH_4 or NO depending on the reaction under study.

The initial molar flow rate for each specie A (F_{A0}) in mol/min corresponds to the product of the initial molar concentration of the specie A (C_{A0}) times the volumetric flow rate (Equation 2-16):

$$F_{A0} = C_A Q \qquad \text{Equation 2-16}$$

Considering gas ideal behavior, the molar flow rate of each specie A can be calculated in terms of the initial molar fraction of the specie A in the reaction mixture, y_{A0}:

$$F_{A0} = \frac{P * y_{A0} * Q}{R * T} \qquad \text{Equation 2-17}$$

$$y_{A0} = \frac{C_{A0}}{10^6} \qquad \text{Equation 2-18}$$

Where,

P: Pressure ($P = 0.84\ atm$)

Q: volumetric flow rate through the reactor (L/s)

y_{A0}: initial molar fraction of specie A in the reaction mix

C_{A0}: initial concentration of specie A (ppm_v)

R: universal gas constant $\left(0.082\ \frac{atm*L}{mol*K}\right)$

T: temperature (K)

Before the reactions take place on the active sites located inside a catalyst particle, the reactants must diffuse through two regions to reach those active sites. In the first region, the species diffuse through the boundary layer between the bulk fluid and the external surface of the catalyst pellet, the transport phenomena in this region are commonly referred to as external or interphase transport effects. In the second region, the reactants diffuse inside the pores of the catalysts particle, in this region the transport phenomena are known as internal, intraphase or intraparticle transport effects [186].

In any kinetic study, the experimental data must be obtained under appropriate reaction conditions that guarantee the absence of external and internal diffusional limitations, thus the collected data will correspond to chemical events exclusively (adsorption, surface reaction and desorption) and the reaction system will be in the kinetic control regime [182]. The experimental data obtained under these conditions can be used to obtain reliable intrinsic kinetic parameters of the rate law [182,187–190]. The methodology followed to determine the reaction conditions that ensured the absence of diffusional limitation problems in the kinetic experiments is summarized below.

2.5.2 External diffusional limitations

The Mear's criterion (Equation 2-19) is commonly used to analyze if external mass transfer phenomena limits or not the observed reaction rate [188]:

$$\frac{-r_A' \cdot \rho_b \cdot R \cdot n}{k_c \cdot C_{Ab}} < 0.15 \qquad \text{Equation 2-19}$$

Where,

r_A': The observed rate of disappearance of species *A* per mass of catalyst [kmol/kg cat·s]

ρ_b: Bulk density of catalyst bed [kg/m^3]

$\rho_b = (1-\phi)\rho_c$, where, ϕ: porosity and ρ_c: solid density of catalyst pellet

R: Catalyst particle radio [m]

n: reaction order

k_c: mass transfer coefficient [m/s]

C_{Ab}: solid catalyst density [kmol/m^3]

If Equation 2-19 is satisfied, then the external mass transfer limitations can be neglected and there are no concentrations gradients between the bulk gas and external surface of the catalyst pellet. However, the application of the Mear's criterion involves the estimation of the coefficient of diffusion of the reactants using empirical correlations, which may present deviations from the real values, as alternative the diffusional problems can be evaluated experimentally.

When the linear velocity of the reactants is high enough, the boundary layer around the catalyst particle becomes very small, no concentration gradients of the reactants will be observed between the bulk fluid and the catalyst surface. According to this, the presence of external mass diffusion limitations under the reaction conditions can be studied experimentally by varying the linear velocity of the reactant mixture but keeping the concentration and the spatial velocity (W/F) of the reactants constant, The absence of external diffusion problems is consider if there are constant conversions in the velocity range [187,190,191].

2.5.3 Internal diffusional limitations

The Weisz–Prater criterion (Equation 2-20) is commonly used to study the internal diffusional limitations. This criterion uses the experimental rate of reaction, to determine if the intraparticle diffusion is limiting the reaction [190].

$$C_{WP} = \frac{-r'_{A\,(obs)} \cdot \rho_c \cdot R^2}{D_e \cdot C_{As}} \leq 1 \qquad \text{Equation 2-20}$$

Where,

$r'_{A\,(obs)}$: The observed rate of disappearance of species A per mass of catalyst [kmol/kg cat·s];
ρ_c: Density of catalyst [kg/m^3];
R: Catalyst particle radio [m];
D_e: Effective diffusivity [m^2/s];
C_{As}: Concentration of reactant A [kmol/m^3].

When $C_{WP} \gg 1$ then internal diffusion limits the reaction severely.

The application of the Weisz–Prater criterion requires the estimation of the effective diffusivity, because of the high complexity of the reaction mixture this estimation implies very high errors. Instead, the internal diffusional limitations can be also studied experimentally. This is done by studying the effect of the catalyst particle size on the experimental reaction rate, the absence of internal diffusion limitations is evidenced in the particles size range where the activity of the catalyst does not change significantly [187].

2.5.4 Approximation to rate law equations

2.5.4.1 Approximation to a rate law equation for o-DCB oxidation reaction

The approximation to the rate law equation for *o*-DCB oxidation reaction was obtained by varying the *o*-DCB concentration between 200 and 800 ppm in presence of water vapor (6%), CH_4 (2500 ppm) and NO (1000 ppm), the experiments were carried out at 500 ºC with excess of oxygen (10% O_2) so the reaction rate of *o*-DCB oxidation can be considered independently of the oxygen concentration. As an approximation to the rate law for *o*-DCB oxidation it was supposed a kinetic equation of the power law type depending on the concentration of *o*-DCB, Equation 2-21, the linearization by taking logarithms leads to the Equation 2-22 which represents a line and its slope indicates the reaction order [182]. For the adjustment of the experimental data to the linearized expression the classical least squares method was used, the data processing was performed in the statistic software R version 3.4.2.

$$-r'_{\mathrm{o-DCB}} = k \cdot C_{o-DCB}^{n} \qquad \text{Equation 2-21}$$

$$ln\,(-r'_{\mathrm{o-DCB}}) = ln\,(k) + n \cdot C_{o-DCB} \qquad \text{Equation 2-22}$$

2.5.4.2 Approximation to a rate law equation for the CH_4-SCR reaction

The experiments were carried out at 500 ºC in the presence of water vapor (6%), oxygen (10%) and *o*-DCB (600 ppm). The concentrations of CH_4 and NO were varied in the 1200 – 3000 ppm and 400 – 800 ppm ranges, respectively. The approximation to a reaction rate law for CH_4-SCR of NO was attempted according to the least-squares analysis [182], the use of this method for data analysis allows to determine the best values of the rate law parameters from a series of measurements where three or more parameters are involved. It is assumed that the reaction rate law can be expressed as a power law equation involving the concentration of the reactants and the reaction rate constant, Equation 2-23, the linearization by taking logarithms on both sides leads to the Equation 2-24

$$-r'_{NO} = k \cdot C_A^{\alpha} \cdot C_B^{\beta} \qquad \text{Equation 2-23}$$

$$ln\,(-r'_{\mathrm{o-DCB}}) = ln\,(k) + \alpha \cdot C_A + \beta \cdot C_B \qquad \text{Equation 2-24}$$

The experimental data can be fitted to the Equation 2-24 using a multiple linear regression model where the resulting regression coefficients will correspond to the values of $ln\,(k)$, α

and β. Here, C_A represents the concentration of CH_4 and C_B the concentration of NO, α is the order of the reaction regards to CH_4 and β is the order of reaction regards to NO. The experimental data fit was performed in the statistic software R version 3.4.2.

2.5.5 Determination of apparent activation energies

The dependence of the specific reaction rate constant with respect to temperature can be determined by the Arrhenius equation, as follow [182]:

$$k_A(T) = Ae^{-E/RT} \qquad \text{Equation 2-25}$$

Where,

$k_A(T)$: The specific reaction rate constant at temperature T for the reacting specie A.

A: Preexponential factor or frequency factor.

E: Activation energy (J/mol or cal/mol).

R: Gas constant = 8.314 J/mol·K = 1.987 cal/mol·K

T: Absolute temperature (K).

The activation energy E has been interpreted in different ways, one of the most accepted is that it corresponds to the minimum energy that must be possessed by reacting molecules before the reaction will occur, this interpretation is derived from the kinetic theory of gases, since the factor $e^{-E/RT}$ gives the fraction of the collisions between molecules that together have this minimum energy E [182].

Experimentally, the apparent activation energy can be obtained from the Equation 2-26 by computing the slope of the graph $\ln(-r_A)$ vs $\frac{1}{T}$ [182].

$$\ln(-r_A) = \ln(A * C_A^n) - \frac{E}{R}\left(\frac{1}{T}\right) \qquad \text{Equation 2-26}$$

Chapter 3 Activity, durability and characterizations of the powder catalysts.

3.1 Catalytic activity tests

The NO, CH_4 and *o*-DCB conversions were analyzed as a function of temperature over the 150 to 550 ºC range under lean, dry and wet conditions, with the variation of the $[CH_4]/[NO]$ ratio from 1 to 4 keeping constant the other reaction parameters. The catalyst showed a similar conversion-temperature profiles with differences in the activity according to the $[CH_4]/[NO]$ ratio, depending on the temperature range the catalytic activity can be summarized as follow. From 150 to 350 ºC **(zone I)** the catalyst presents very low conversions, in the 350–500 ºC range **(zone II)** the catalytic activity trends to increase and from 500 to 550 ºC **(zone III)** the *o*-DCB and CH_4 conversions continue increasing while the NO conversion decreases significantly.

In the Figure 11 the results for the [CH_4]/[NO] ratio of 1 are shown. Although Pd/Co–HMOR shows a conversion of about 20% at 150 ºC, it decays at 250 ºC but above this temperature o-DCB conversion tends to raise with increasing temperature. The initial *o*-DCB conversion at 150 ºC cannot be associated with any oxidation process since not CO nor CO_2 were detected in the exhaust gases, this result might be explained by the o-DCB physisorption in the catalyst at low temperature (150 ºC) and the subsequent desorption at 250 ºC resulting in the lower conversion observed at this temperature. Similar results were obtained in the cases of [CH_4]/[NO] ratios of 2 and 4 as is shown in Figure 12 and Figure 13, respectively. Although for all the [CH_4]/[NO] ratios, the NO and *o*-DCB conversions increased slightly in the **zone I** in the presence of water, the differences were not significant respect to the dry conditions. On the contrary, in the **zone II** the presence of water vapor (6%) in the feed led to a significant increase in the *o*-DCB conversions and a higher CO_2 formation regards to the dry conditions for all [CH_4]/[NO] ratios. The promoting effect of water vapor was observed previously during the oxidation of *m*-DCB and *o*-DCB (independently) over a V_2O_5/TiO_2 catalyst [192], and in the oxidation of C_6H_5Cl over Pt-HFAU(5) [193] and Pt/Al_2O_3 [194] catalysts, and in the oxidation of C_2HCl_3 over Pt/Al_2O_3 (improving the activity) and Pd/Al_2O_3 catalysts (improving the selectivity to HCl) [195]. Moreover, it has been reported [47,195–197] that the presence of water has an inhibiting effect on chlorinated by-product formation during the oxidation of chlorinated compounds. In this sense, Aristizábal et al reported [47] that the *o*-DCB oxidation over Pd/Co-HMOR catalyst in the presence of water led to higher selectivity to CO_2 formation and to lower traces of polychlorinated benzenes (Cl = 2–6) as by-products in comparation to dry reaction conditions. It seems that the water can act as a hydrogen-supplier compound able to remove Cl anions left on the catalyst surface after the oxidation of the aromatic ring to form HCl and OH^- by the reaction: $H_2O + Cl^- \rightleftharpoons HCl\uparrow + OH^-$ [47,83,197]. Additionally, water can also react with chlorine to produce HCl by Deacon reaction: $H_2O + Cl_2 \rightleftharpoons 2HCl + \frac{1}{2}O_2$, in which HCl formation is thermodynamically favored with temperature [195]. The formation of surface chlorine anions and Cl_2 is highly undesired because of their capacity to participate in the chlorination of adsorbed chlorobenzene, leading to the formation of undesired polychlorinated benzenes [47]. The hypothesis of the Cl^- removal from the catalyst surface by water is consistent with the higher

selectivity to CO_2 observed under wet conditions in **zones II** and **III** (Figure 14), besides the chemical analysis by EDS/TEM of used samples during 30h at 500 ºC under dry and wet conditions (see Figure 15 and Table 2) showed the presence of Cl atoms in the sample used under dry conditions with a Cl/Pd atomic ratio of 1.7, which strongly suggests the formation of $PdCl_2$ in the catalyst, while not traces of chlorine atoms were detected by this technique in the sample used under wet conditions, this reinforces the hypothesis of Cl anions removal by the water vapor during the reaction.

The CO_2 and CO can be generated from the CH_4-SCR or *o*-DCB oxidation which difficult the analysis of the influence of the water in the selectivity of the *o*-DCB oxidation to CO_2 or CO. Despite this, the analysis of the CH_4 conversions at 400 ºC gives some insights, since at this temperature not significant differences in the CH_4 conversions between dry and wet conditions were found for all the $[CH_4]/[NO]$ ratios. In the presence of water the *o*-DCB conversion is remarkably increased as CO_2 production in each case (see Figure 11 to Figure 13 parts A and B), this suggests that the increase in the CO_2 formation under wet conditions at this temperature is due to a high selectivity of the *o*-DCB oxidation to CO_2 which is in agreement with previous studies [47,192,195]. Figure 14 shows the $[CO_2]/[CO]$ ratio as function of temperature and $[CH_4]/[NO]$ ratio for both dry and wet conditions. In **zone I** not significant differences in the $[CO_2]/[CO]$ ratio between dry and wet conditions were found, however in **zones II** and **III** the $[CO_2]/[CO]$ ratio has higher values in the presence of water vapor with respect to the dry conditions for each $[CH_4]/[NO]$ ratio. The decrease in the amount of the CO generated by the addition of water can be attributed to dissociation of water on the catalyst surface which results in OH^- species able to oxidize the CO to CO_2 by the water gas shift reaction (WGSR), as was proposed by González et al [195]. Additionally, the OH^- species are also generated during the removal of Cl anions by the water [47,83,197]. In the **zone III**, no significant differences were observed in the *o*-DCB conversion between dry and wet conditions, these results are contrary to the reported by Aristizábal et al [47], who studied the oxidation of o-DCB (alone) over a similar catalyst system, they reported that the presence of water increases the *o*-DCB conversion even at high reaction temperatures (above 475 ºC). To explain this difference, we must consider that in the present study the o-DCB oxidation occurs simultaneously with the SCR of NO by CH_4 and above 475 ºC, both the NO

reduction and the oxidation of CH_4 and *o*-DCB molecules give rise to the generation of water, although the water generated was not quantified, at least 2000, 4000 and 8000 ppm of water are expected for the [CH_4]/[NO] ratio of 1, 2 and 4, respectively. Although the amount of water generated in each case is not enough to turn the dry condition into an *in-situ* wet condition (60000 ppm), probably is enough to emulate the effect that the water have into the catalysts.

The NO conversion-temperature profiles display a volcano-shaped curve with the maximum NO conversions at 500 ºC (limit between **zone II** and **III**) in all cases. In **zone II**, both the conversions of CH_4 and NO tend to increase with temperature, but in **zone III** the conversion of NO drops with increasing temperature while the conversion of CH_4 continues to increase, as does the CO_2 generated. These facts can be attributed to the non-selective oxidation of methane by O_2 above 500 ºC, since the decrease of the reductant (CH_4) by the combustion with O_2 is expected to decrease the rate of NO reduction. The CH_4-SCR competes with the methane combustion and as the temperature increases beyond 500 ºC the methane oxidation is strongly favored over the CH_4-SCR. Similar results were reported by Gélin et al [198] in the CH_4-SCR over Pd-H-ZSM-5 catalysts and by Azambre et al [199] during the CH_4-SCR over Pd-based catalysts. The presence of water slightly increased the catalytic activity of the catalyst in the temperature range. This was an unexpected result since it has been reported [97,199,200] that the presence of water in the feed tends to decrease the CH_4-SCR activity by inhibiting the adsorption of NO and CH_4 [199]. Considering that in this case both the *o*-DCB oxidation and the CH_4-SCR occur simultaneously, the positive effect of water vapor in the CH_4-SCR can be a consequence of the removal of Cl^- anions from the catalyst surface, other possibility is that the water may affect the methane combustion [94], leading it to react more selectively with NO instead of oxygen molecules. Additional analysis of the effect of water in both reactions will be presented in the kinetic study. Both under wet and dry conditions, above 400 ºC the increase of methane concentration results in an increase of NO conversion, but below this temperature not significant differences are observed (see Figure 11 to Figure 13), this result is consistent with the competitive reaction between CH_4-SCR and methane combustion by O_2.According with the results obtained, the optimum temperature for the CH_4-SCR combined with the *o*-DCB oxidation is 500 ºC with the

following compositions: [CH_4] = 4000 ppm, [NOx] = 1000 ppm, [o-DCB] = 600 ppm, [O_2] = 10%, [H_2O] = 6% and with a gas hour space velocity of 60,000 h^{-1}. These conditions were selected for the durability test of the catalyst, the results are part of a published work presented in the section 3.3.

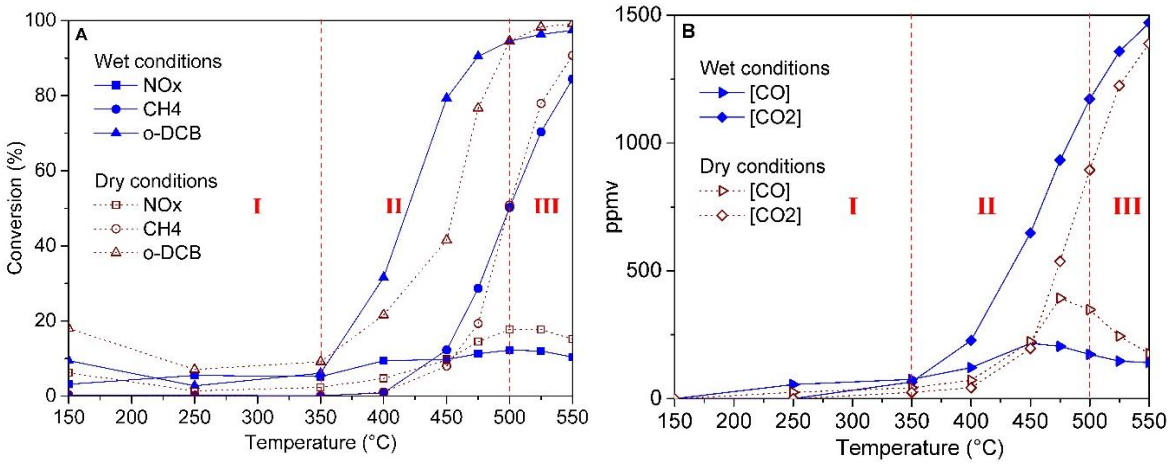

Figure 11 Activity of the catalyst [CH_4]/[NO] = 1. Reaction conditions: [CH_4] =**1000 ppm**, [NO] =1000 ppm, [NO_2] =111 ppm, [o-DCB] =600 ppm, [O_2] =10%, [H_2O] = 0% (open symbols) or 6% (filled symbols), GHSV= 60,000 h^{-1}.

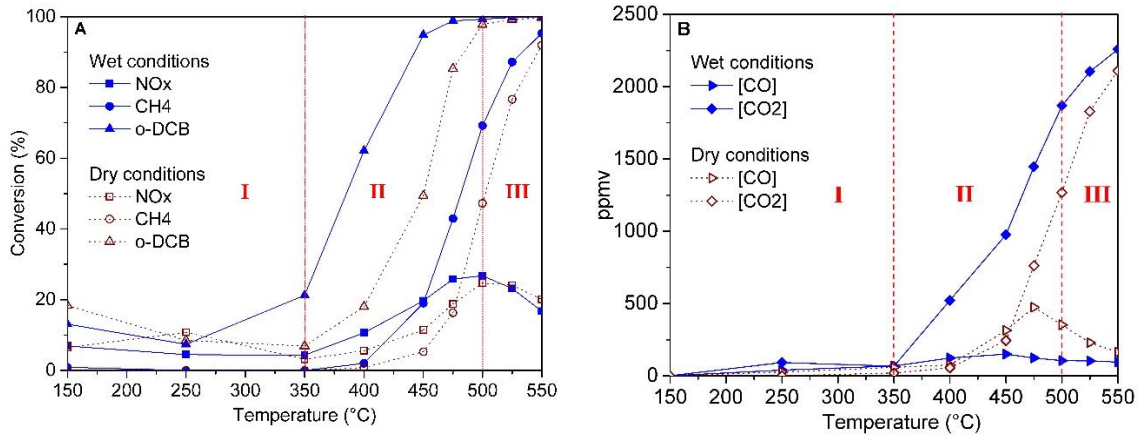

Figure 12 Activity of the catalyst [CH_4]/[NO] = 2. Reaction conditions: [CH_4] = **2000 ppm**, [NO] =1000 ppm, [NO_2] =111 ppm, [o-DCB] = 600 ppm, [O_2] = 10%, [H_2O] = 0% (open symbols) or 6% (filled symbols), GHSV= 60,000 h^{-1}.

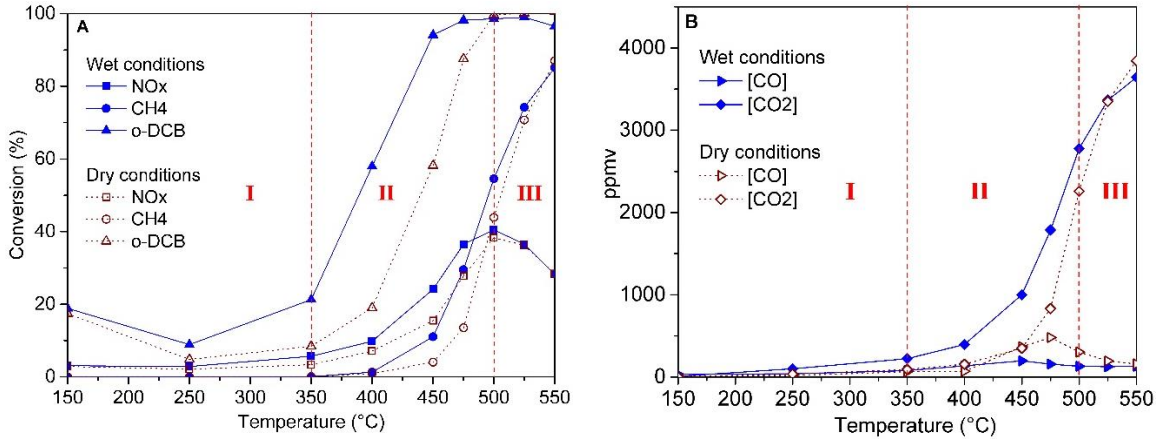

Figure 13 Activity of the catalyst $[CH_4]/[NO] = 4$. Reaction conditions: $[CH_4]$ = **4000 ppm**, [NO] =1000 ppm, $[NO_2]$ =111 ppm, [o-DCB] = 600 ppm, $[O_2]$ = 10%, $[H_2O]$ = 0% (open symbols) or 6% (filled symbols), GHSV= 60,000 h^{-1}.

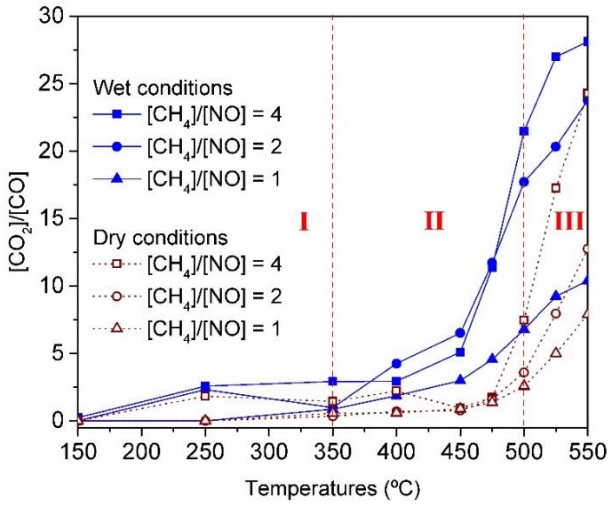

Figure 14 $[CO_2]/[CO]$ ratio as function of $[CH_4]/[NO]$ ratio and temperature for wet and dry conditions.

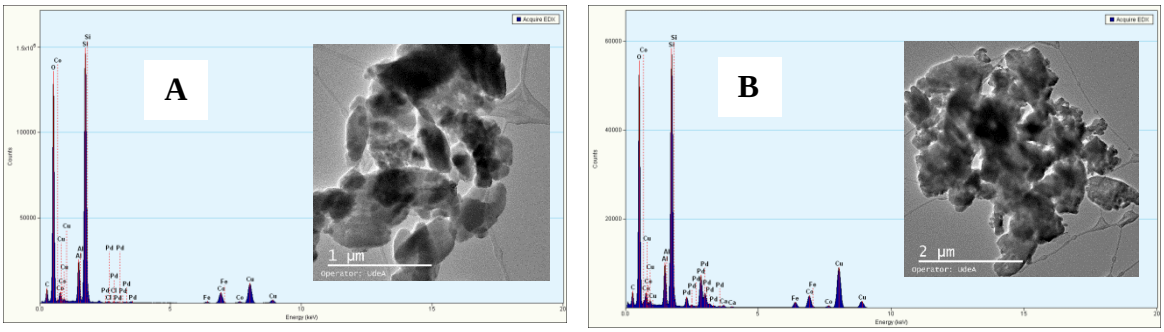

Figure 15 TEM images of used samples during 30 h. Reaction conditions: [CH_4] =4000 ppm, [NO] =1000 ppm, [NO_2] =111 ppm, [o-DCB] = 600 ppm, [O2] = 10%, [H_2O] = 0 (**A**) or 6% (**B**), GHSV =60,000 h^{-1}.

Table 2 EDS analysis of Pd/Co-HMOR samples used during 30 h under dry and wet conditions.

Element	Used Pd/Co-HMOR (Dry conditions)			Used Pd/Co-HMOR (wet conditions)		
	Weight %	**Atomic %**	**Uncertainity. %**	**Weight %**	**Atomic %**	**Uncertainity %**
O	51,49	66,05	0,05	48,12	63,501	0,06
Al	6,35	4,83	0,01	6,77	5,301	0,01
Si	37,73	27,57	0,03	38,62	29,03	0,04
Cl	**0,18**	**0,1**	**0,00**	**N.D.**	**N.D.**	**-**
Co	3,89	1,35	0,01	4,59	1,64	0,01
Pd	0,33	0,06	0,00	1,58	0,31	0,01

N.D.: Not detected.

The effect of oxygen concentration on catalyst activity was studied under wet conditions from 150 to 550 ºC. In the Figure 16 the NO, CH_4 and *o*-DCB conversions for three different concentration of oxygen (0, 5 and 10%) are displayed. Although in the presence of 5% oxygen in the stream the conversion-temperature profile of NO shows a volcano-shape curve peaking at 500 ºC, similar to the obtained in the presence of 10% oxygen, the conversions between 450 and 525 ºC drop significantly while at lower temperatures there are not significant differences. In the case of *o*-DCB, the decrease in the oxygen concentration from 10 to 5% results in the drop of conversions in the temperature range from 350 to 450 ºC but in the high temperature range no significant differences are observed. In the absence of oxygen, while no conversion of CH_4 was observed, the NO conversion increased significantly and the conversions of o-DCB showed a considerable decrease with respect to

those observed in the presence of oxygen at both concentrations 5% and 10%. This lead to consider the possibility of *o*-DCB oxidation by the NO and NO_2 (that is presented in the stream) in the absence of oxygen, however the CO and CO_2 generated may be arise from CH_4 or the *o*-DCB. In this sense, the possible chemical interactions between the *o*-DCB and NO or NO_2 in the absence of CH_4 and O_2 under wet conditions were studied over the catalyst in the temperature range from 150 to 550 ºC, the results are shown in the Figure 17. Evidently the NO combined with NO_2 may oxidize the *o*-DCB, the conversion profiles of both compound result quick similar to the observed in the presence of CH_4 (Figure 16) but the generation of CO and CO_2 is below what was expected for the conversion level reached, which means that there are other by-products formed during the reaction. The FT-IR spectra of the products in the absence of oxygen (Figure 18) revealed two bands at 3337 and 3284 cm^{-1} which were not detected when the oxygen was presented. It is known that the primary amines present two sharp N-H stretching bands near 3335 cm^{-1} [201]. Asymmetric and symmetric N–H stretching bands at 3355 and 3284 cm^{-1} have been reported for primary amines [202]. According to this, the formation of some amine compounds in the absence of oxygen seems highly probably. Notwithstanding, in the absence of oxygen the *o*-DCB and CH4 are preferentially oxidized and not amine compounds are detected.

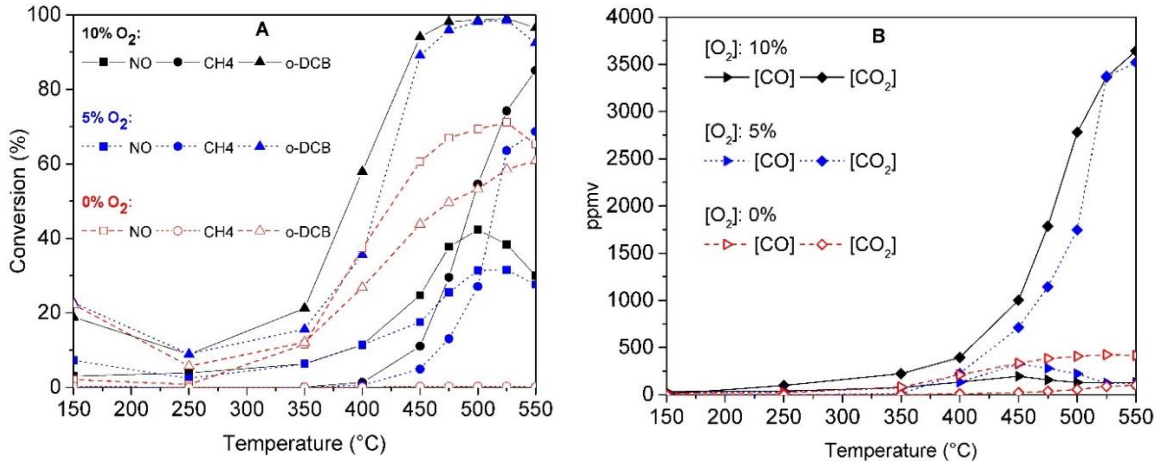

Figure 16 Effect of the oxygen concentration in the activity of the catalyst under wet conditions. Reaction conditions: [CH_4] = 4000 ppm, [NO] =1000 ppm, [NO_2] =111 ppm, [o-DCB] = 600 ppm, [O_2] = 0, 5 or 10%, [H_2O] = 6%, GHSV= 60,000 h^{-1}.

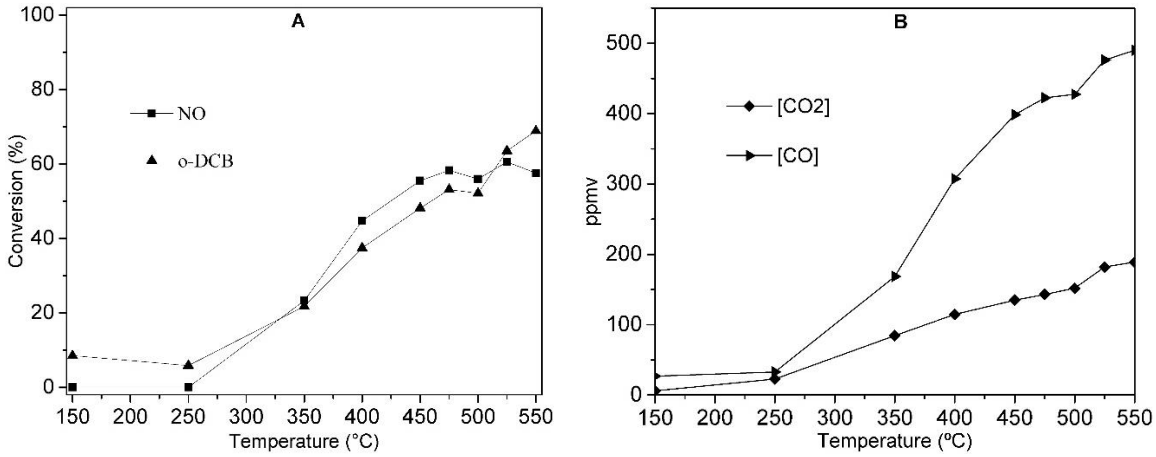

Figure 17 Effect of the oxygen concentration in the activity of the catalyst under wet conditions. Reaction conditions: [CH_4] = 0 ppm, [NO] =1000 ppm, [NO_2] =111 ppm, [o-DCB] = 600 ppm, [O_2] = 0%, [H_2O] = 6%, GHSV= 60,000 h^{-1}.

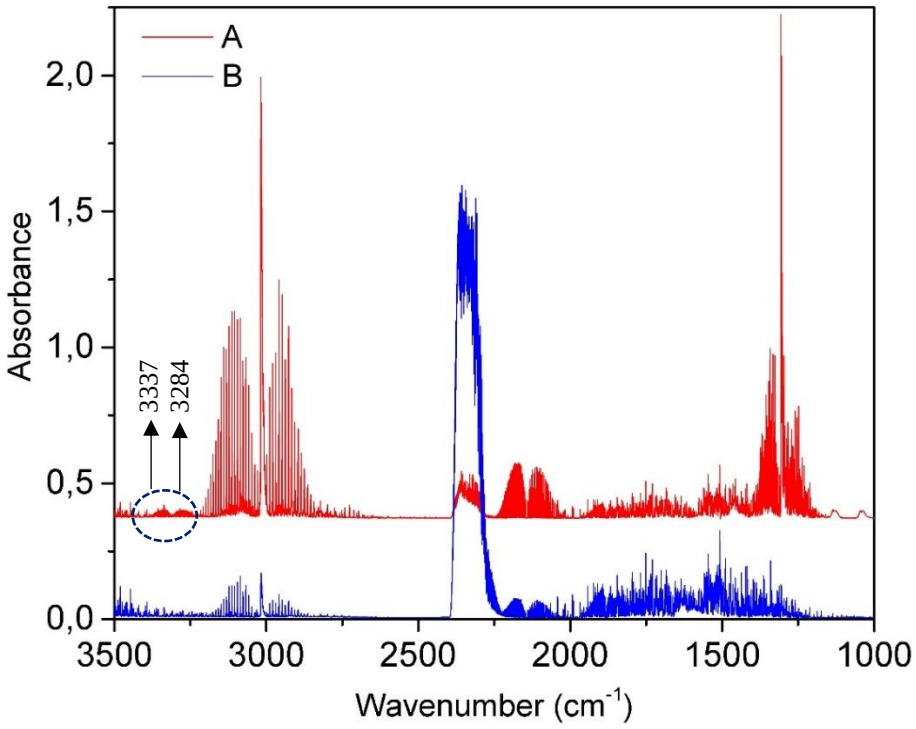

Figure 18 Spectra of the reaction products at 550 ºC. **(A):** [CH_4] = 4000 ppm, [NO] =1000 ppm, [NO_2] =111 ppm, [o-DCB] = 600 ppm, **[O_2] = 0%**, [H_2O] = 6%, GHSV= 60,000 h^{-1} **(B):** [CH_4] = 4000 ppm, [NOx] = 1000 ppm, [o-DCB] = 600 ppm, **[O_2] = 10%**, [H_2O] = 6%, GHSV= 60,000 h^{-1}

3.2 Catalyst characterization

Fresh and used catalysts samples were characterized by several techniques in order to explain the catalytic performance. Nitrogen adsorption isotherms, temperature programmed reduction by H_2, XPS and *in-situ* FTIR adsorptions of NO and o-DCB of fresh samples are presented below. Besides, additional characterizations contrasting fresh and used catalysts were also performed, the results and analyzes are part of the paper: "Catalytic activity and stability of Pd/Co catalysts in simultaneous selective catalytic reduction of NOx with methane and oxidation of *o*-dichlorobenzene", which is attached to the section 3.3.

3.2.1 Chemical composition and textural properties

In the Table 3 the chemical composition and textural properties of the catalyst are presented, the Pd and Co loadings were determined by AAS. The addition Co and Pd results in the decrease of the micropore area of the zeolite. The adsorption isotherms of the samples showed in Figure 19 reveal a solid porous texture corresponding to the type IV of the IUPAC classification, which is characteristic of mesoporous solids [203]. In all samples, the nitrogen desorption curves are deviated from the adsorption curves, this phenomenon known as hysteresis is associated with capillarity condensation taken place in the mesopores [203]. This is because the evaporation from mesopores usually takes place at a lower pressure than that of capillary condensation giving rise to a hysteresis loop [162]. The adsorption and desorption curves of all samples are close each other and nearly horizontal over an appreciable range of P/Po which suggest an H4 hysteresis type of the IUPAC classification, this hysteresis type is characteristic solids forming narrow slit like pores with uniform size or shape [162,203].

The pore size distribution of Co-HMOR and Pd/Co-HMOR fresh samples is presented in the Figure 20, both samples showed a bimodal mesopore distribution centered at 3.9 and 6.5 nm approximately. There is no change in the pore size distribution by the addition of Pd to the catalyst which suggests that the Pd does not block the internal pores of the support. The initial point at 2 nm corresponds to the micropores present in the support.

Table 3 Chemical composition and textural properties

Sample	wt.%.		S_{BET}	External surface area	Micropore area
	Pd	Co	$m^2 g^{-1}$	$m^2 g^{-1}$	$m^2 g^{-1}$
HMOR	–	–	537,1	50,9	486,2
Co-HMOR	–	2,97	346,9	41,1	305,8
Pd/Co-HMOR	0,14	2,74	319,9	36,6	283,3

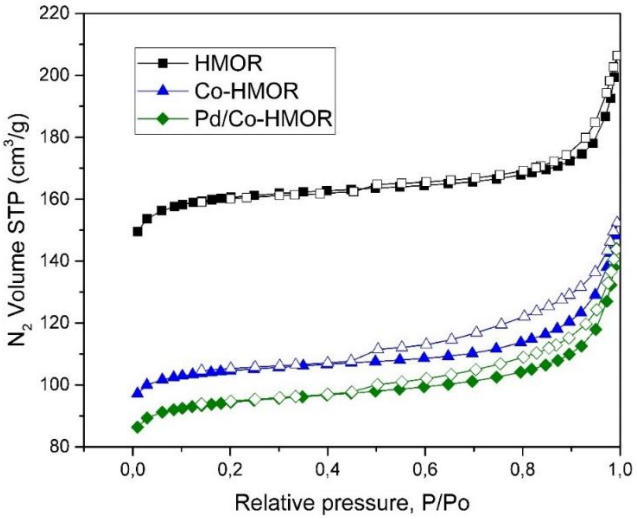

Figure 19 N_2 adsorption (filled symbols) – desorption (empty symbols) isotherms for mordenite based catalysts.

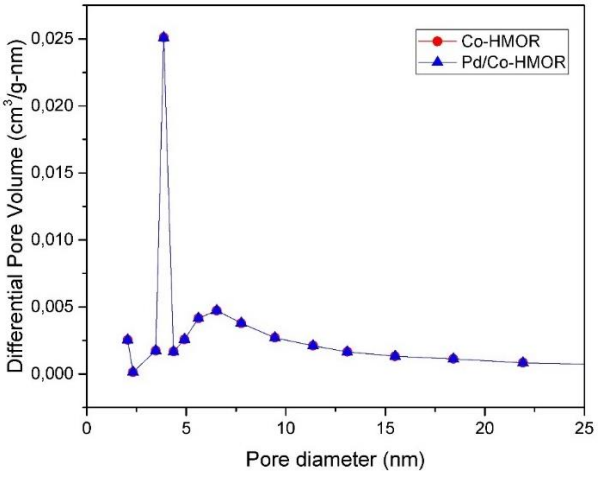

Figure 20 Pore size distribution from adsorption isotherm of nitrogen at –195 ºC for mordenite based catalysts.

3.2.2 XPS

XPS is a proven reliable spectroscopy technique to the study of the chemical valences of exterior atoms and the surface chemical composition of materials. Here XPS was used to study the Co and Pd oxidation states and the nature of the species that they form at the surface of the synthesized Co-HMOR and Pd/Co-HMOR catalysts fresh samples. The complete survey spectra of these samples (not shown) present main peaks corresponding to Co 2p, O 1s, Al 2p, Si 2s and C 1s regions and in the case of Pd/Co-HMOR sample the presence of a main peak associated to Pd 3d was also observed as expected, no other metallic nor additional impurities were detected. The high-resolution XPS spectra of the samples are displayed in Figure 21.

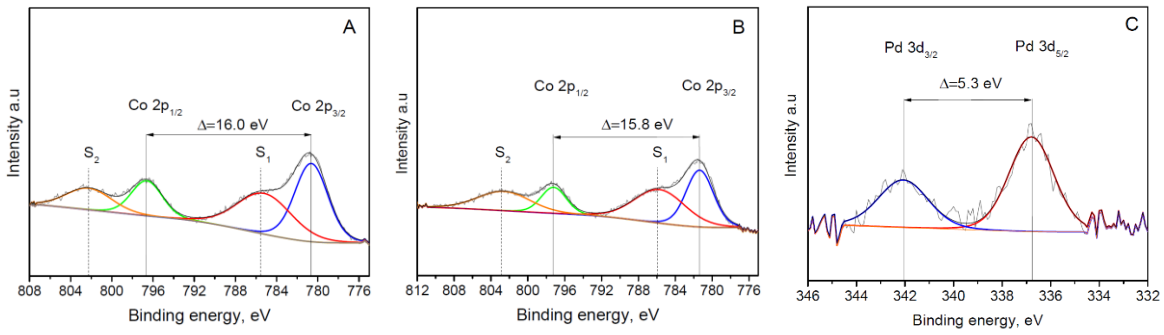

Figure 21 XPS spectra corresponding to (**A**) Co 2p for Co-HMOR, (**B**) Co 2p for Pd/Co-HMOR and (**C**) Pd 3d for Pd/Co-HMOR.

The binding energy and the Full Width at Half Maximum (FWHM) are reported in Table 4. The high-resolution XPS results for Co-HMOR and Pd/Co-HMOR samples reveal spin-orbit splitting between Co $2p_{3/2}$ and Co $2p_{1/2}$ peaks of 16.0 and 15.8 eV, respectively and show two intense satellite peaks, these data strongly suggest a Co^{2+} chemical state in the surface of the catalysts [204–207]. Previous characterization of the fresh samples by H_2-TPR [92] have also shown the presence of Co^{2+} ions revealed by high temperature reduction peaks at 769 and 875 °C in the Co-HMOR sample while in Pd/Co-HMOR were observed at 646 and 819 °C. The absence of peaks around 778.1 eV reveals that no metal cobalt is present at the surface of the catalysts [206]. Since the shake-up satellites structures of Co $2p_{3/2}$ and Co $2p_{1/2}$ in both samples are so different from the typical structures observed for the characteristic octahedral Co^{3+} component of the Co_3O_4 [207,208], the formation of this oxide in the surface

of the catalysts can be denied. The XPS profiles of the samples match both CoO and $Co(OH)_2$ oxides, however the chemical shift observed between these oxides is small (see Table 4) and the satellite structures are very similar, both exhibit two intense satellite peaks [207,209,210], therefore the Co^{2+} species found in the catalysts samples cannot be assigned to only one of these oxides, even possibly both types of oxides are present in the samples.

Table 4 XPS data corresponding to Co $2p_{3/2}$, Co $2p_{1/2}$ and Pd $3d_{5/2}$ regions for Co-HMOR, Pd/Co-HMOR, CoO, Co_3O_4 and $Co(OH)_2$.

Solids	**Binding Energy (eV)**						
	Co 2p3/2	**Co 2p3/2 Sat 1**	**Co 2p1/2**	**Co 2p1/2 Sat 2**	**Pd 3d5/2**	**Pd 3d3/2**	**Reference**
Co-HMOR	780.6 (3.8)[a]	785.2 (6.3)	796.6 (3.5)	802.2 (5.2)	-	-	This work
Pd/Co-HMOR	781.4 (3.5)	785.8 (6.5)	797.3 (3.2)	802.7 (6.7)	336.8 (2.2)	342.1 (2.4)	This work
CoO	780.0	786.3	800.8	807.5	-	-	[214]
	780.5	785.5	796.6	802.1	-	-	[207]
Co_3O_4	Co^{III}:778.9 Co^{II}:780.4	787.3	Co^{III}:794.2 Co^{II}:795.9	803.3	-	-	[208]
	779.6	N.R [b]	794.6	N.R	-	-	[209]
	779.8	788.8	795.7	804.2	-	-	[207]
$Co(OH)_2$	780.0	786.0	796.1	801.9	-	-	[209]

[a]The values in brackets correspond to the FWHM. [b]N.R: Not reported the exact value in the reference.

The binding energy of Co $2p_{3/2}$ and Co $2p_{1/2}$ peaks and its satellites in the Pd/Co-HMOR sample present slightly higher energy values regards to the monometallic Co-HMOR sample (see Table 4), similar shifts have been associated with interactions between the neighboring ions, in this case Co^{2+} and Pd^{2+} located in the HMOR framework [211]. The peak observed around 220 °C in previous H_2-TPR experiments of Co-HMOR and Pd/Co-HMOR can be associated with the reduction of Co oxocations as was already suggested [92]. The binding energy of Pd $3d_{5/2}$ for Pd/Co-HMOR catalyst (Figure 21c) was 336.8 eV, this value is higher than 336.3 eV reported for PdO [212] and lower than 337.8 eV [212] observed for $PdCl_2$ compounds reveling the presence of Pd^{2+} species in the catalyst surface, however a higher binding energy than PdO oxide implies a higher oxidation state of palladium [213], then it seems reasonably to attribute it to highly dispersed Pd^{2+} ions partially stabilized by the oxygen atoms of the zeolite framework. It was suggested [92] that the broad reduction peak

observed between 100 and 300 °C in fresh Pd/Co-HMOR corresponds to the co-reduction of Co species and Pd^{2+} ions. No peaks around 335.1 eV for $Pd_{5/2}$ were found in none of the samples, indicating that no metallic Pd is formed on the surface of the fresh catalysts [212].

3.2.3 In-situ FTIR spectroscopy study

3.2.3.1 NO adsorption experiments

FT-IR spectra obtained from HMOR in the presence of 1000 ppm of NO/Ar at 250 ºC are shown in Figure 22.

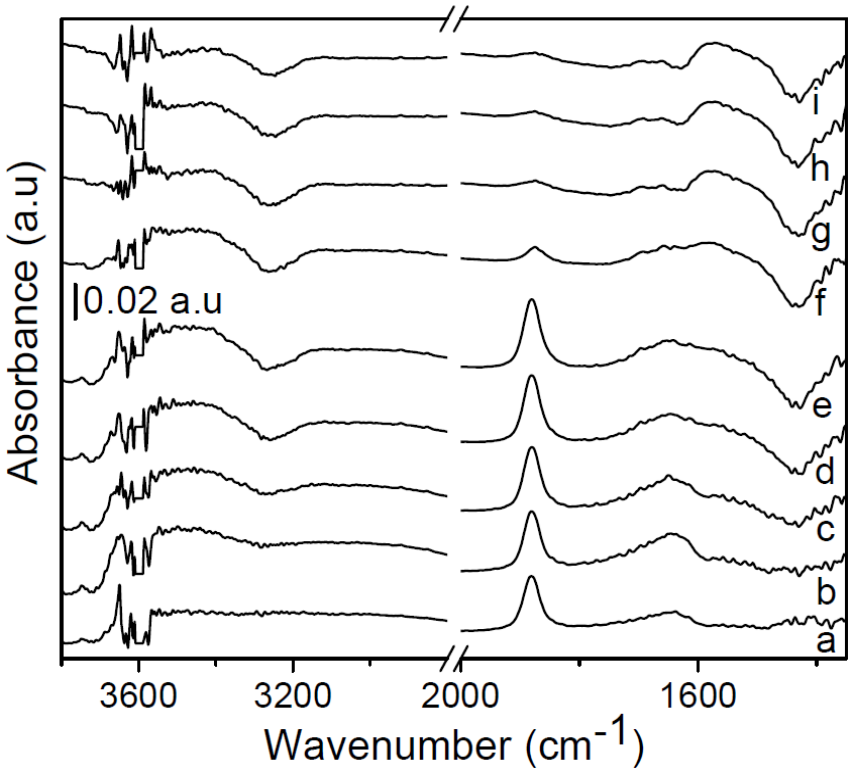

Figure 22 In situ FTIR spectra of an HMOR zeolite sample collected at 250 °C. **Stage 1:** after (a) 5 min, (b) 30 min, (c) 60 min, (d) 100 min, (e) 120 min in a 1000 ppm NO/Ar stream, **stage 2:** after (f) 5 min, (g) 20 min (h) 30 min, (i) 60 min of evacuation in Ar.

After 120 min of NO adsorption a complex spectrum structure was observed in the 3750–3000 cm^{-1} spectral region in which well-defined positive bands appear at 3650, 3615, 3610 and 3585 cm^{-1} and negative bands are observed at 3728, 3629, 3612 and 3267 cm^{-1}, all these bands can be attributed to interactions between NO and the hydroxyls groups present in the H-MOR sample. The NO stretching frequency in the gas phase appears at 1876 cm^{-1} [181]

but after the NO adsorption on the H-MOR the band was slightly shifted to 1880 cm^{-1}, this displacement to a slightly higher frequency is quite similar to the reported by Poignant et al [215] upon NO adsorption on H-ZSM-5 and in a similar way can be attributed to NO species confined in the zeolitic channels. The broads weak bands at 1650 and 1572 cm^{-1} observed during the exposition of HMOR to NO and during the evacuation in Ar respectively may be ascribed to the formation of nitrite (NO_2) or nitrate (NO_3) species [181,216,217] by reactions between adsorbed NO and surface oxygen species, which would lead to perturbations in the framework T–O bonds (T = Si, Al) of the zeolite, this might explain the negative band observed at 1429 cm^{-1}. After 5 min of evacuation in Ar the integral intensity of the 1880 cm^{-1} decreased by 83.4% and was shifted to 1876 cm^{-1} which indicate that the NO is weakly adsorbed by the acidic hydroxyl groups of the mordenite and desorbed easily as NO gas. As the evacuation time in Ar increases the intensity of the 1876 cm^{-1} band becomes smaller and broad positive bands appear around 1691 and 1583 cm^{-1} which can be associated to nitrates species that are formed when the NO desorbed as gas interacts with the hydroxyls groups located in the inner channels of the zeolite as is evidenced by the negative peak appearing around 3602 cm^{-1}.

Figure 23 and Figure 24 show the *in-situ* FT-IR spectra of Co-HMOR sample collected at 50 °C and 250 °C, respectively during the adsorption of 1000 ppm NO/Ar follow by evacuation in Ar. At 50 °C three well defined bands at 1942, 1898 and 1808 cm^{-1} are observed. The nitric oxide is a known Lewis base which can be adsorbed on cationic sites and trends to form dimers due to the presence of an unpaired electron in the molecule [216], when it is adsorbed on Co-zeolites samples a pair of bands appearing at 1900–1885 cm^{-1} and 1815–1800 cm^{-1} corresponding to Co^{2+}-dinitrosyl species has been widely reported [218]. According to this, the bands at 1898 and 1808 cm^{-1} can be safely assigned to symmetric and asymmetric stretching vibrations, respectively, of Co^{2+}–$(NO)_2$ dinitrosyl species [117,118,120,216,218,219]; these bands were slightly shifted to 1894 and 1805 cm^{-1} at 250 ºC (Figure 24). The dihedral angle (α) between the two NO molecules of Co^{2+}–$(NO)_2$ dinitrosyl species may be evaluated as [117,216]: $\alpha = 2\tan^{-1}\sqrt{I_{as}/I_s}$ where I_{as} and I_s correspond to the integral intensities of ν_{as}(NO) and ν_s(NO) bands, respectively, the average

angles obtained from spectra at 50 and 250 °C were 117 and 119°, respectively. These values are in good agreement with the dinitrosyl angles obtained by Li et al [220]: Co-Y: 119°, Co-ZSM-5: 122°, Campa et al [117]: Co-ZSM-5: 119° and Hadjiivanov et al [216] Co-ZSM-5: 124 to 130°. The formation of dinitrosyl species implies that cobalt in the fresh Co-HMOR sample is mainly as Co^{2+} cations in agreement with XPS results. The presence of Co^{2+} cations in the Co-HMOR sample was also confirmed by the H_2-TPR experiments that we reported [92] recently in which a reduction peak at 875 °C and a shoulder at 769 °C indicated the presence of Co^{2+} ions at side pockets and exchange positions in the 12-member ring (12-MR) channels of mordenite, respectively. According to the location of Co^{2+} cations in the mordenite structure they have been classified in three types denoted as Co-α, Co-β and Co-γ [119]. The Co-α cations located at the main channel of mordenite are weakly bounded to framework oxygens and present a highly tendency to form dinitrosyl species upon NO adsorption, the Co-β cations located at the compressed 8-MR channels of the mordenite cavity exhibit medium-strength bonding to framework oxygens and a high ability to form Co^{2+}-(NO) mononitrosyl species and the Co-γ ions located at the "boat-shaped" sites are the most highly coordinated Co ion bonding to framework oxygens, therefore these sites are expected to be inactive during the NO adsorption [115,119]. According to this, the formation of dinitrosyl species on the Co-HMOR sample indicates the presence of Co-α cations in the monometallic and bimetallic catalysts. At 50 ºC appears a band at 1942 cm^{-1} which increases during the first 10 min of the Co-HMOR sample exposure to flowing NO/Ar mixture, then slightly decrease up to becomes constant after 50 min of continuous adsorption. After continuous evacuation in Ar during 60 min (Figure 23 and Figure 24 trace i) the intensity of this band decreased considerably by 53% while the intensity of the bands corresponding to dinitrosyl species remained almost unalterable. The assignment of this band is not as straightforward as the pair corresponding to the dinitrosyl species, vibrations in the 1970 to 1930 cm^{-1} range in Co-zeolites have been attributed to either Co^{2+}-(NO) or Co^{3+}-(NO) mononitrosyl species [118,120,218,219,221,222]. It has been reported [221] that Co^{3+} ions are reduced to Co^{2+} by NO according to $Co^{3+} + NO = Co^{2+} + NO^+$, then as the intensity of the band corresponding to Co^{3+}-(NO) diminishes, the bands related with the Co^{2+}-(NO) and NO^+ increase (NO^+ band has been reported at 2133 cm^{-1} [218]). However, in the NO

adsorption experiments no bands related with NO^+ ions were observed, additionally according with XPS results the cobalt is mainly in Co^{2+} chemical state, thus the band observed at 1942 cm^{-1} is more likely due to Co^{2+}-(NO) than Co^{3+}-(NO) mononitrosyl complexes. The 1942 cm^{-1} band can be then attributed to mononitrosyl species formed in the Co^{2+} cations of type β, this result is in agreement with the assignment of 1940 cm^{-1} band observed by Gutierrez et al [118] upon NO adsorption on a series of Co-HMOR catalysts. At 250 ºC the Co^{2+}-(NO) mononitrosyl species were hardly evidenced by a very weak shoulder appearing at 1934 cm^{-1} which vanishes after only 5 min of evacuation in Ar indicating that these species are not stable at high temperatures. Although the dinitrosyl species were also observed at this temperature, the integral intensities of the bands associated to these species decreased by 71% and 96.5% after evacuation in Ar during 60 min and 120 min, respectively, indicating that the adsorption strength was lower than the observed at 50 ºC. The Lewis acidity of the Co^{2+} cations in Co-HMOR catalysts have been associated with the Co^{2+} cations located at exchange positions and differences in the strength of such Lewis acid sites depends on the location of the cations in the zeolitic framework [90]. The existence of Co-α and Co-β ions in the Co-HMOR and Pd/Co-HMOR samples allow us to confirm the presence of Lewis acidic Co^{2+} cations in both catalysts. Finally, the doublet centered at 1469/1413 cm^{-1} appearing at 50 ºC can be assigned to the formation of nitrate ions by interactions of the NO with the surface oxygens and the hydroxyl groups of the zeolite [223]. Indeed, the growth of nitrate ions bands is accompanied by the development of negative bands appearing at 1618 and 1307 cm^{-1} which may be associated with perturbations of the framework T–O vibrations of the mordenite structure [118] and the negative band observed in the OH stretching region at 3604 cm^{-1} can be related with acidic hydroxyl groups located in the main channels of the mordenite [90,116].

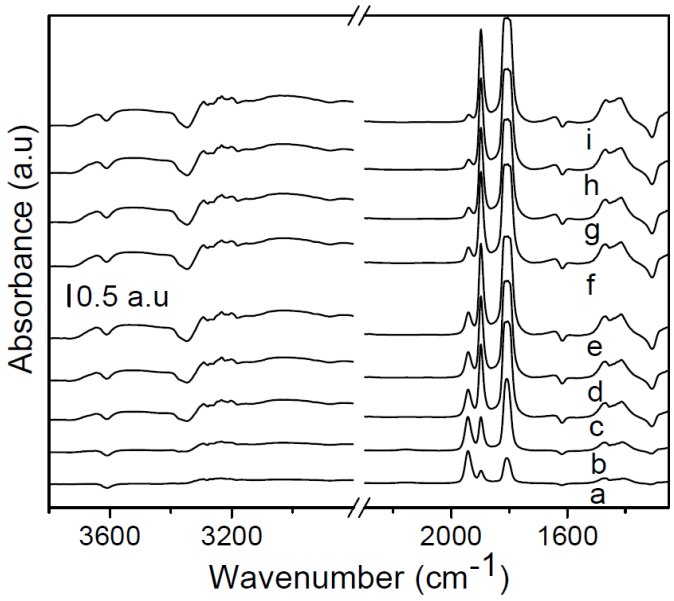

Figure 23 In situ FTIR spectra of a Co-HMOR zeolite sample collected at 50 °C. **Stage 1:** after (a) 5 min, (b) 10 min, (c) 30 min, (d) 40 min, (e) 60 min in a 1000 ppm NO/Ar stream, **stage 2:** after (f) 5 min, (g) 20 min (h) 30 min, (i) 60 min of evacuation in Ar.

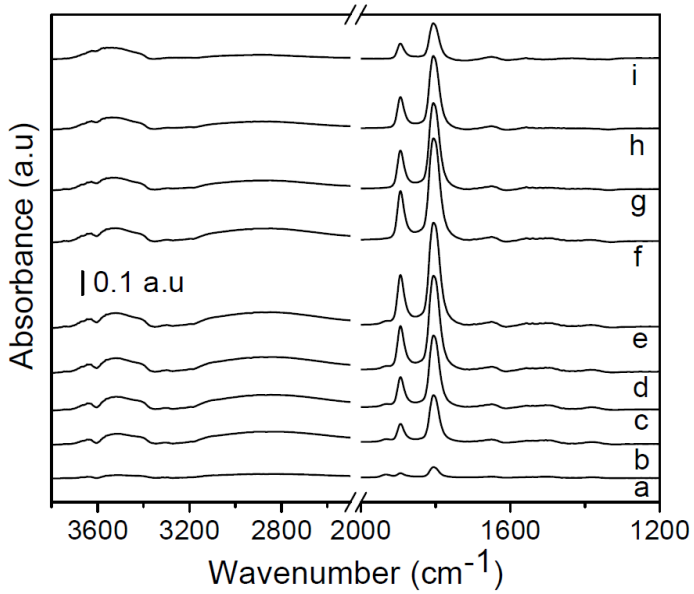

Figure 24 In situ FTIR spectra of a Co-HMOR zeolite sample collected at 250 °C. **Stage 1:** after (a) 5 min, (b) 30 min, (c) 60 min, (d) 100 min, (e) 120 min in a 1000 ppm NO/Ar stream, **stage 2:** after (f) 5 min, (g) 20 min (h) 30 min, (i) 60 min of evacuation in Ar.

The *in-situ* FT-IR spectra of Pd/Co-HMOR sample collected during the adsorption experiments of NO at 50 and 250 ºC are shown in Figure 25 and Figure 26, respectively. Similar to the observed in the monometallic sample, at 50 ºC two bands associated with the characteristic symmetric and asymmetric stretching vibrations of Co^{2+}–$(NO)_2$ dinitrosyl species appear at 1901 and 1807 cm^{-1}, at 250 ºC these bands were shifted to 1894 and 1803 cm^{-1}, respectively.

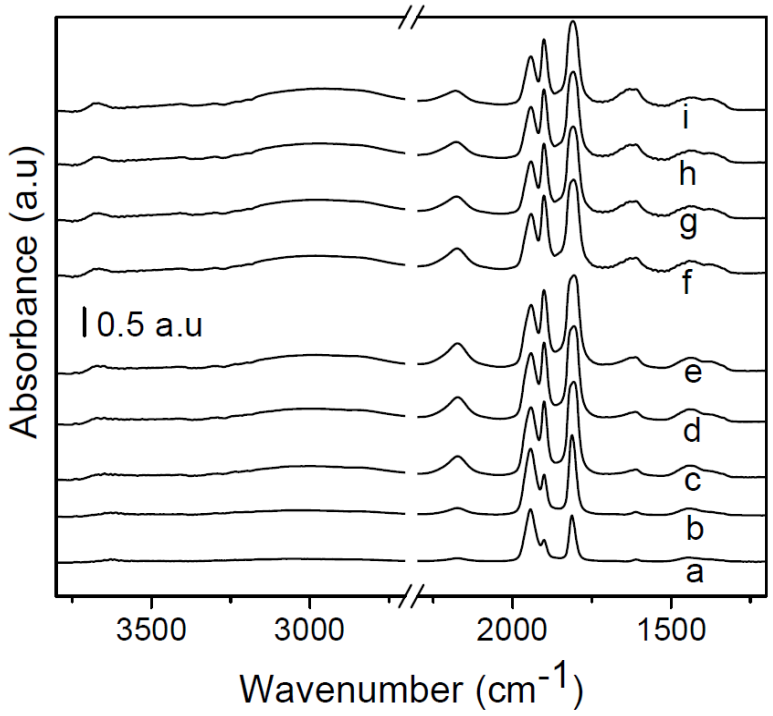

Figure 25 In situ FTIR spectra of a Pd/Co-HMOR zeolite sample collected at 50 °C. **Stage 1:** after (a) 5 min, (b) 10 min, (c) 30 min, (d) 40 min, (e) 60 min in a 1000 ppm NO/Ar stream, **stage 2:** after (f) 5 min, (g) 20 min (h) 30 min, (i) 60 min of evacuation in Ar.

The dihedral angles between the NO molecules were also evaluated as in the monometallic sample, the average angles obtained from the spectra at 50 and 250 ºC were 115º and 140º, respectively which are in good agreement with the values reported in the literature [117,216]. However, there is a considerable increase in the angle between dinitrosyl species formed on the bimetallic catalyst compared to that obtained on the Co-HMOR sample which is presumably an effect of the Pd incorporation. The relatively high angles on Pd/Co-HMOR means a greater distance for the two N atoms and consequently lower probability of N_2O

formation by interactions between the two nitrosyl groups [220], in fact no bands were evidenced in the FT-IR spectra of the products (not shown) related to this compound during the reaction. These results imply that cobalt in the bimetallic sample is also dispersed as Co^{2+} cations as was expected according with the XPS analysis. As in the monometallic sample, at 50 ºC the band at 1942 cm^{-1} can be assigned to mononitrosyl species formed in the Co^{2+} cations of type β. Comparing the spectra of Co-HMOR and Pd/Co-HMOR samples it seems that the ratio of Co-β/Co-α ions increase after the incorporation of Pd, to prove this, the ratios were estimated for each sample as $\frac{I_{1942}}{I_{1898}+I_{1808}}$ and $\frac{I_{1942}}{I_{1901}+I_{1807}}$, respectively, where I_x represents the integral intensity of the x band, the values obtained after 60 min of NO adsorption were 0.09 and 0.36 for the monometallic and bimetallic samples, respectively. According to this, it seems reasonably that the incorporation of Pd induces to a Co^{2+} migration from α to β sites.

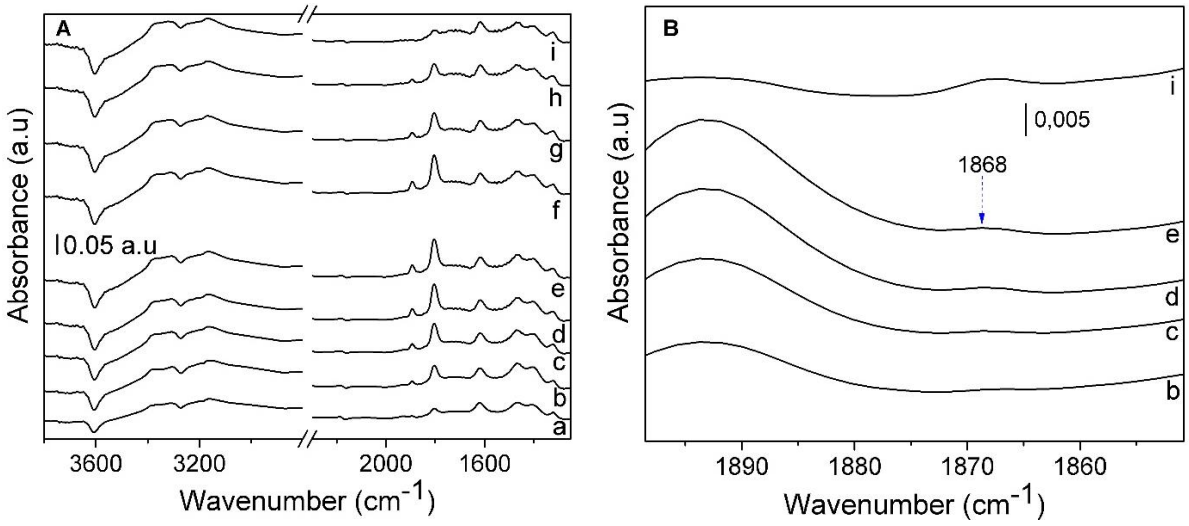

Figure 26 In situ FTIR spectra of a Pd/Co-HMOR zeolite sample collected at 250 °C. **Stage 1:** after (a) 5 min, (b) 30 min, (c) 60 min, (d) 100 min, (e) 120 min in a 1000 ppm NO/Ar stream, **stage 2:** after (f) 5 min, (g) 20 min (h) 30 min, (i) 60 min of evacuation in Ar.

The band appearing at 2173 cm^{-1} in the bimetallic sample was not observed upon NO adsorption at 50 °C in the HMOR nor Co-HMOR samples, confirming that Pd^{2+} ions are the adsorption sites. It is known [224] that due to the moderate ionization potential of NO molecule (9.5 eV) the removal of the antibonding odd electron is not difficult which allows

the formation of nitrosyl complexes with transition metals. According to this, when NO interact with transition metals the transfer of the odd electron from the NO molecule to empty *d* orbitals of transition metal ions may occur followed by lone pair donation thus generating the nitrosyl complexes which have the general structure of $M^{(n-1)+}NO^{+}$, with the oxidation state of the metal being reduced by one unit [224]. The N–O bond and the stretching frequency are strengthened by the loss of an electron to form a positive ion leading to frequencies in the 2100 cm^{-1} range [225]. Based on these facts, the band observed at 2173 cm^{-1} may be explained by the formation of the nitrosyl complex $Pd^{+}NO^{+}$ because of the reduction of Pd^{2+} ions at 50 °C according to the reaction: $Pd^{2+} + NO = Pd^{+}NO^{+}$ at 50 °C. During the evacuation in Ar at 50 °C this band was slightly shifted to 2179 cm^{-1} and after 60 min of continuous Ar flow the integral intensity decreased by 57% showing a relative stability of the complex, at this time, the intensity of the 1942 cm^{-1} band decreased by 27% indicating that the Co^{2+}-(NO) mononitrosyl species are more stable in bimetallic than in the monometallic catalyst at 50 ºC. During the NO adsorption at 250 ºC the band corresponding to $Pd^{+}NO^{+}$ complex was slightly shifted to 2185 cm^{-1} and showed a very weak absorption intensity compared to the observed at 50 °C, suggesting a higher stability of Pd^{2+} ions (which are not easily reduced at this temperature to form $Pd^{+}NO^{+}$ complex as at 50 ºC). At 1868 cm^{-1} emerges a new band (see Figure 26 B) which remains after continuous evacuation in Ar during 60 min (see Figure 26 B trace i). Che et al reported [225] a band at 1865 cm^{-1} upon the NO adsorption over Pd-Y zeolite which was a assigned to mononitrosyl complexes bonded to Pd^{2+} cations in supercages. Similarly, Aylor et al [226] observed a band at 1866 cm^{-1} after the NO adsorption on Pd-H-MFI which was assigned to NO adsorbed on molecularly dispersed PdO in ion exchange sites of MFI. On ion-exchanged Pd-H-MOR the formation of Pd^{2+}–(NO) mononitrosyl species upon NO adsorption were reported at 1860 cm^{-1} by Shimizu et al [227]. It seems then reasonably to assign the 1868 cm^{-1} band to the formation of linear Pd^{2+}–(NO) mononitrosyl species. Pd^{2+}–(NO) band was not observed at 50 ºC because of the reduction of Pd^{2+} ions by NO leading to the formation of the nitrosyl complex $Pd^{+}NO^{+}$, neither during the NO adsorptions on the HMOR and Co-HMOR samples which confirms that the formed band is related with the presence of Pd. It seems that the positive bands appearing at 1616, 1471, 1404 and 1323 cm^{-1} grow at expenses of the 3604

cm^{-1} band which corresponds to the hydroxyl groups located in the inner channels of the zeolite. The pair of bands at 1616 and 1323 cm^{-1} have been associated [228,229] with the asymmetric and symmetric stretching vibrations of NO_2, respectively and the pair of bands appearing at 1471 and 1404 cm^{-1} can be related to the formation of nitrate species [223].

The *in-situ* FTIR spectra of Pd/Co-HMOR catalyst collected during the adsorption experiments with a mixture of NO + O_2 + CH_4 at 250 ºC are shown in the Figure 27. The band appearing at 1934 cm^{-1} was previously ascribed to Co^{2+}–(NO) mononitrosyl species adsorbed on Co-β cations, similarly to the observed in the NO adsorption experiments these species vanish almost completely after only 5 min of evacuation in Ar indicating that they are weakly adsorbed to the cations. The strong band observed at 1868 cm^{-1} was previously ascribed to Pd^{2+}–(NO) mononitrosyl species [225–227]. Li et al [220] have reported that the mononitrosyl species formed on a Co-ferrierite catalyst are stabilized by O_2, even allowing the mononitrosyl species to remain on Co^{2+} cations up to 200 ºC, the stabilization would occur due to the co-adsorption of another oxygen atom on the same Co^{2+} cation and probably at higher temperatures they could be transformed into NO_2 adsorbed species. In this way, the higher intensity of Co^{2+}–(NO) and Pd^{2+}–(NO) mononitrosyl species compared to that observed during the NO adsorption experiment over Pd/Co-HMOR catalyst at the same temperature (Figure 26) suggests that both mononitrosyl species are stabilized by the presence of O_2 in the reaction mixture. The band emerging at 1631 cm^{-1} lies in the typical region of NO_2/NO_3 species [181,216,217,230]. Beutel et al [231] and Cheung et al [232] both have reported similar bands on Cu/ZSM-5 at 1628 and 1630 cm^{-1}, respectively, which were assigned to a Cu^{2+}–NO_2 adsorption species. Shimizu et al [227] assigned two bands at 1600 and 1630 cm^{-1} observed upon NO + O_2 adsorption over Pd-H-MOR to NO_2 species. Similarly Li et al [220] assigned a band observed at 1627 cm^{-1} in the spectra of Co-Ferrierite collected during the NO-TPD in O_2 to nitro adsorbed species on Co^{2+} cations. In accordance with the previous studies, the band appearing at 1631 cm^{-1} can be ascribed to the formation of NO_2 adspecies, since the band also appears in the spectra of Co-HMOR (data not shown) but not in that of HMOR (data not shown) under the same conditions, then the species are likely adsorbed on Co^{2+} cations as nitro complexes ($Co^{2+}NO_2$). After 120 min of evacuation in Ar (see Figure 27 A trace i), the intensity of the 1868 cm^{-1} corresponding to Pd^{2+}–(NO)

mononitrosyl species decreases by 55% while the intensity of the bands at 1631 cm^{-1} corresponding to Co^{2+}–NO_2 adsorption complexes remains almost unalterable. In the spectra of both Co-HMOR (data not shown) and Pd/Co-HMOR catalysts, the bands related to Co^{2+}–$(NO)_2$ dinitrosyl species were not observed with the mixture of NO + O_2 + CH_4 evidencing the absence of such species; however, as shown before the dinitrosyl species were effectively formed in the Co^{2+} cations during NO adsorption experiments. These facts suggest that during the adsorption of NO + CH_4 + O_2 mixture, the Co^{2+}–$(NO)_2$ dinitrosyl species are rapidly transformed into Co^{2+}–NO_2 complexes giving rise to the band observed at 1631 cm^{-1}, besides this explains the absence of bands related to dinitrosyl species on Co^{2+} cations. Similar results were obtained by Li et al [220] in the *in-situ* IR spectra of NO adsorbed on Co-Ferrierite after O_2 exposition. Previous works [219,220,223,233,234] have pointed out that the formation of NO_2 adspecies is the first step in the CH_4-SCR mechanism, in this sense the formation of Co^{2+}–NO_2 adsorption complexes with the concomitant absence of Co^{2+}–$(NO)_2$ dinitrosyl species during the exposure of the catalysts to NO + CH_4 + O_2 mixture is in full agreement with this hypothesis. Córdoba et al [235] have reported a shoulder at 1360 cm^{-1} in the spectra of a Pd/Co-Sulfated Zirconia during the NO desorption in O_2, it was attributed to nitro or nitrito complexes on Co^{2+} cations ($Co^{2+}NO_2$ or $Co^{2+}ONO$). Similarly, the Pd/Co-HMOR shows a weak band at 1361 cm^{-1} during NO + CH_4 + O_2 exposure, which grows in parallel to the 1868 cm^{-1} band corresponding to Pd^{2+}–(NO) species and after 120 min of evacuation in Ar the integral intensity decreases by 57% which is similar to the decrease of 55% observed for Pd^{2+}–(NO) species. Since the 1361 cm^{-1} band was not observed in the spectra of Co-HMOR (not shown) collected under the same conditions it can be assigned to nitro or nitrito complexes adsorbed on Pd^{2+} cations. In the 2300 to 2100 cm^{-1} spectral range (see Figure 27 B) two weak bands appear on both Co-HMOR (data not shown) and Pd/Co-HMOR samples at 2287 and 2191 cm^{-1}, an additional very tenuous band also appears at 2148 cm^{-1} but only in the case of Pd/Co-HMOR, all these bands were absent during the NO adsorption experiments. Similar weak bands at 2300 and 2142 cm^{-1} were reported by Lobree et al [217] over a Pd-Co-H-MOR catalyst during the NO temperature-programmed desorption (NO-TPD) in CH_4 at 450 ºC, in order to determine the nature of the species they perfomed some isotopic labeling experiments (^{15}NO + $^{12}CH_4$ or ^{14}NO + $^{13}CH_4$)

and observed the redshift for both bands when one of the gases was isotopically labeled, this led them to conclude that both species contain N and C atoms. In this way, they assigned the 2300 cm^{-1} band to NCO species and the 2142 cm^{-1} to Pd^{2+}–CN. Similar bands at 2260 and 2156 cm^{-1} were also reported by Aylor et al [230] at 350 and 500 ºC after NO_2-TPD in CH_4 over a Mn-ZSM-5 catalyst, the bands were assigned to Al^{3+}–NCO and $Mn^{3+}(O^{-})(CN)$ species, respectively. On Co-ZSM-5 catalysts Lobree et al [233] and Aylor et al [223] reported two bands at 2270 and 2173 cm^{-1} during the NO + CH_4 exposure, in both studies the bands were attributed to Al^{3+}–NCO and Co^{2+}–CN species, respectively. According to the above, it seems reasonable to attribute the band appearing at 2287 cm^{-1} to Al^{3+}–NCO species, while the very tenuous band emerging at 2148 cm^{-1} and observed only in Pd/Co-HMOR sample it is more likely due to Pd^{2+}–CN cyanide species. The band appearing at 2191 cm^{-1} in both Co-HMOR (data not shown) and Pd/Co-HMOR samples is close to that reported at 2173 cm^{-1} in Co-ZSM-5 catalyst [223,233], therefore it can be assigned to Co^{2+}–CN cyanide species, the shift in the frequency of the C-N vibration could be due to the local environment of the cations and, according to XPS results, the Co^{2+} cations are present as CoO or $Co^{2+}(OH^{-})_2$, this may explain the upscale shift in the vibrational frequency of the adsorbed CN species [223]. The very weak intensity of the 2148 cm^{-1} band corresponding to Pd^{2+}–CN cyanide species compared to the relatively higher intensity of the 2191 cm^{-1} band coresponding to Co^{2+}–CN cyanide species is probably a consquence of the lower Pd loading (0.14%) compared to that of Co (2.74%). The group of bands observed around 3016 cm^{-1} are characteristics of the CH_4 in gas phase [227] and completely disappear during the evacuation in Ar. The negative band at 3604 cm^{-1} indicates that the Brønsted acid sites are somehow involved during the reaction, likely by promoting the NO_2 generation as has also been suggested by Lónyi et al [120].

The nature of the species formed over Pd/Co-HMOR catalyst during the exposure to NO + O_2 + CH_4 at 250 °C allows to suggest that Brønsted acid sites, Pd^{2+} and Co^{2+} cations are active sites during the CH_4-SCR of NO. It is generally accepted [120,219,220,223,233] that the first step for the NO reduction over Co-zeolites catalysts is the oxidation of NO to NO_2, but there is no consensus about the nature of species involved in the oxidation. Some studies [120,236] have indicated that the Co-oxide species and/or cobalt oxide clusters are

responsible to promote the NO_2 formation. Other authors [220,223,233] have instead pointed out that the formation of NO_2 species proceeds over the Co^{2+} cations, and recently Bellmann et al [219] reported that the NO oxidation over a Co-ZSM-5 catalysts occurs over Co^{3+} cations. The Co^{2+}–NO_2 complexes were one of the most abundant species observed over Pd/Co-HMOR catalyst and presumably formed from the Co^{2+}–$(NO)_2$ dinitrosyl species located in α-type Co^{2+} cations, these facts reinforce the hypothesis of NO oxidation over Co^{2+} cations as was elucidated in the mechanistic studies of CH_4-SCR occurring in monometallic Co-zeolites [220,223,233]. Although the Co^{2+}–(NO) mononitrosyl species were stabilized under the presence of oxygen, they were very weakly bounded to the Co-β cations, therefore these could be inactive species for the CH_4-SCR in agreement with earlier findings [120]. According to this, the active cobalt species for CH_4-SCR over Pd/Co-HMOR catalyst are mainly α-type Co^{2+} cations, the NO reduction proceeds likely as follow, the Co^{2+}–$(NO)_2$ dinitrosyl species bounded to Co-α cations are quickly transformed into Co^{2+}–NO_2 complexes in the presence of CH_4 and O_2. As has been suggested [220], the adsorbed NO_2 complexes play a key role in activating the CH_4 since NO_2 contain an unpaired electron which can remove hydrogen from saturated hydrocarbons, as in the nitration of CH_4 to form CH_3NO_2. In this way, Lobree et al [233] proposed a Eley-rideal mechanism in which the Co^{2+}–NO_2 complexes reacts with gas-phase CH_4 giving rise to $Co^{2+}(CH_3NO)$ and H_2O, a further dehydrogenation of $Co^{2+}(CH_3NO)$ by OH• radicals would lead to the formation of $Co^{2+}(CH_2NO)$ and H_2O, then the ligated CH_2NO is decompose by heat into Co^{2+}–CN cyanide and H_2O. The final step would be the reduction of NO_2 by Co^{2+}–CN cyanide species to produce Co^{2+} + N_2 + CO_2. The Co^{2+}–CN cyanide species detected during the CH_4 + NO + O_2 exposure of Pd/Co-HMOR catalyst at 250 ºC allows to suggest that this is likely the reduction mechanism occurring over Co-α cations. On the other hand, high abundance of Pd^{2+}–(NO) mononitrosyl species were detected in the Pd/Co-HMOR sample which showed a relatively stability at 250 °C in the presence of CH_4 and O_2, it was also observed the simultaneously development of a very weak band related to the formation of Pd^{2+}–CN cyanide species which vanished during evacuation in Ar. According to this, it is likely that Pd^{2+}–(NO) species play a role in the activation of CH_4 molecules as the first step in the CH_4-SCR over Pd^{2+} ions, this agrees with an earlier study [237] of a Pd-H-ZSM-5 catalyst in

which the evidences indicate that the reduction of NO by CH_4 is initiated by the interaction of CH_4 with adsorbed NO on Pd cations rather than NO_2, and would be favored at temperatures above 650 K. This would also explain the growing trend in activity of Pd/Co-HMOR catalyst with increasing temperature up to 500 ºC namely, at low temperatures, the Co^{2+} cations may activate the CH_4 more effectively than Pd^{2+} cations, the latter probably becomes more active in the temperature range between 400 to 500 ºC which is consistent with the activity profile observed. Although the presence of Co-oxo species on the Pd/Co-HMOR catalyst was evidenced by the H_2-TPR experiments that we reported [92] in an earlier study, it is known [120] that these species do not adsorb NO therefore they do not appear during the in-situ FTIR experiments. However Co-oxo species have been reported [120] as effective for the oxidation of NO to NO_2, therefore these species presumably contribute in the first step of the CH_4-SCR reduction over Co-α cations.

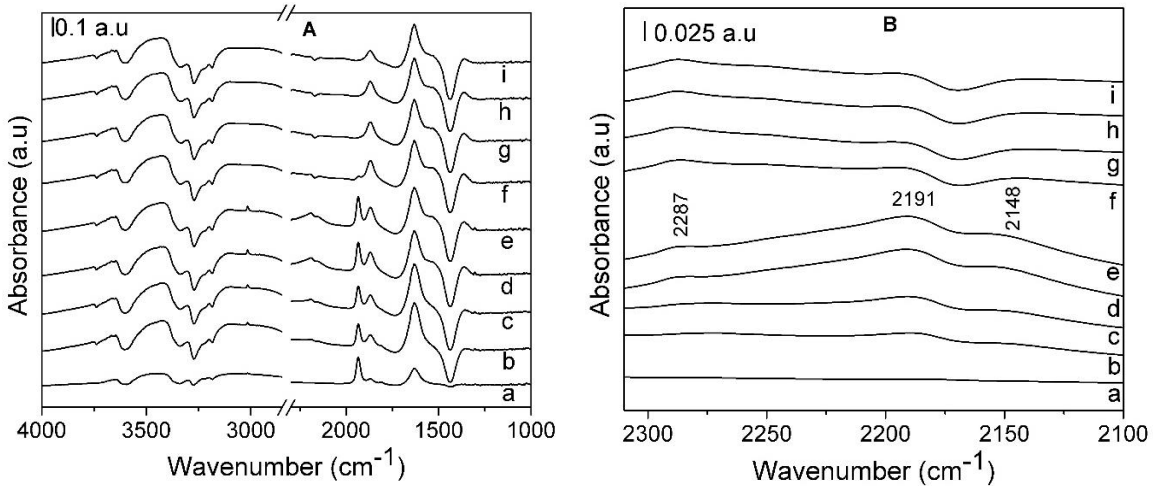

Figure 27 In situ FTIR spectra of the Pd/Co–HMOR catalyst collected at 250 °C. **Stage 1:** after (a) 5 min, (b) 20 min, (c) 30 min, (d) 100 min, (e) 120 min in a 1000 ppm NO/Ar + 4000 ppm CH_4/Ar + 10% O_2/Ar stream, **stage 2:** after (f) 5 min, (g) 20 min (h) 30 min, (i) 120 min of evacuation in Ar. **(A)** 4000–1000 cm^{-1} **(B)** 2340-2100 cm^{-1} zoom x 4

Regards to the Bronsted acid sites, the negative band appearing at 3604 cm^{-1} reveals the participation of these species during the reaction although the results here reported do not allow to assign a particular role of these sites during the reaction however, Lónyi et al [120] have reported that HMOR zeolite is active in the oxidation of NO to NO_2 reaction, on this

basis it is thought that the Bronsted acid sites contribute in this first step of the CH_4-SCR occurring over Co-α cations.

3.2.3.2 o-DCB adsorption experiments.

The FT-IR spectra of HMOR sample collected during the adsorption of 300 ppm *o*-DCB/Ar at 250 °C are shown in Figure 28. When the o-DCB is introduced in the IR cell a broad and weak negative band at 3774 cm^{-1} appears, according to the literature [141,238,239] this band corresponds to the perturbation of hydroxyl groups of extra-framework alumina of the HMOR, simultaneously a new broad band arises at 3747 cm^{-1} which can be attributed to the interaction between these hydroxyl groups and the o-DCB molecules. Another broad and more notorious band decreases around 3720 cm^{-1} while a new broad band arises around 3689 cm^{-1} at the same time. Bevilacqua et al [240] have associated a broad band in the region near 3730 cm^{-1} observed in HMOR to silanol groups, a weaker band observed also at 3730 in an H-ZSM-5 sample was assigned by Trombetta et al [241] to terminal silanol groups located on the internal pores of the zeolite. According to this, the broad negative band around 3720 cm^{-1} can be associated to the perturbation of silanol groups of the HMOR by the o-DCB molecules and the interactions between them leads to a shift to lower vibration frequency of the hydroxyl groups as reveals the positive band observed at 3689 cm^{-1}. After 10 min of exposition to *o*-DCB molecules, a well-defined negative band is observed at 3660 cm^{-1} which is even discernable from the first spectrum and reaches a constant intensity after 60 min of continuous adsorption, simultaneously a new broad band arises in the 3642–3598 cm^{-1} region. Stretching vibrations bands in the 3670–3650 cm^{-1} region have been reported [91,116,238,239,241–246] in several protonic zeolites and assigned to hydroxyls of extra-framework Al ions, in the same ways the negative band at 3660 cm^{-1} can be attributed to the perturbation of the hydroxyls of Al ions (Al-OH) partially linked to the mordenite framework at external surface. In the 3630–3600 cm^{-1} region a complex spectrum structure is observed with the bands strongly perturbed by the superimposed broad positive band in the 3642–3598 cm^{-1} region developed as consequence of the interactions between the *o*-DCB molecules and the external hydroxyls of Al ions. A weak decreasing trend around 3610 and 3625 cm^{-1} is observed, and a better-defined negative band appears at 3602 cm^{-1}. Bands within this range

have been extensively reported in zeolites [90,238,240,241,247] and related with hydroxyls bridging SiO_4 and AlO_4 tetrahedra exclusively located in the inner channels of zeolites, exhibiting strong Brønsted acidity characteristics. Since the kinetic diameter of *o*-DCB is approximately 6 Å [90] then it can only enter the main channels (12-MR) of mordenite that have a dimension of 6.5 Å x 7.0 Å dimension. Consequently, the bands at 3602, 3610 and 3625 cm^{-1} can be all assigned to the interaction of o-DCB with the bridging hydroxyls groups (Si–OH–Al) located in the main channels of the HMOR and each of the bands corresponds to a specific crystallographic positions of the hydroxyls groups in the large 12-MR channels or at the entrance of the side pockets close to the large channels of the mordenite structure as has been reported [247–249]. As result of the hydroxyl groups perturbation two broad adsorption bands at 3500 and 3260 cm^{-1} are also observed, both can be assigned to hydrogen bonding between *o*-DCB and bridging hydroxyls groups [91]. Finally, a positive band at 3068 cm^{-1} can be assigned to the aromatic C–H stretching vibrations of the adsorbed *o*–DCB [91].

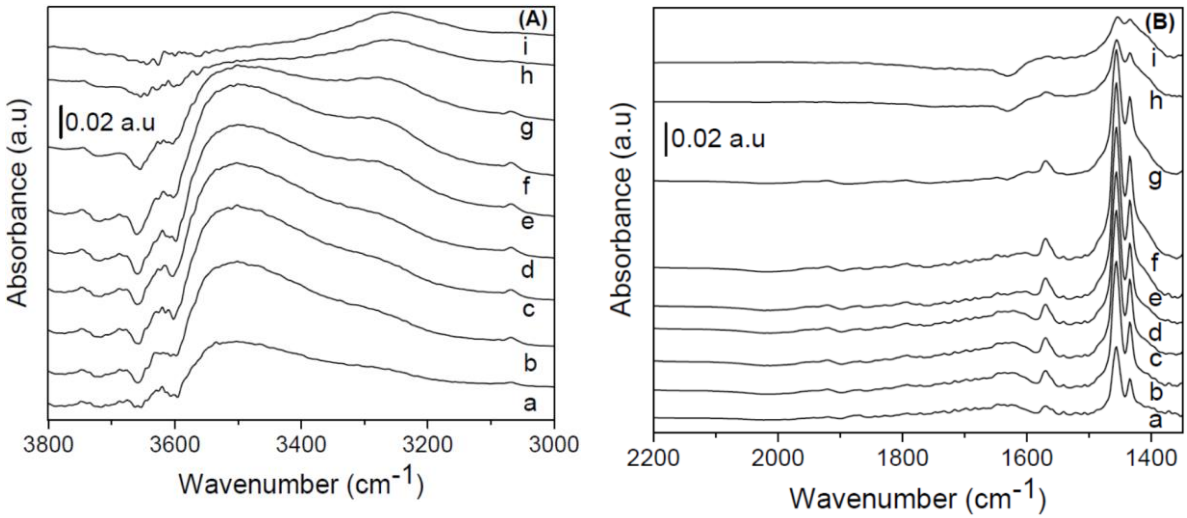

Figure 28 In situ FTIR spectra of an HMOR zeolite sample collected at 250 °C. **Stage 1:** after (a) 5 min, (b) 10 min, (c) 20 min, (d) 30 min, (e) 100 min, (f) 120 min in a 300 ppm *o*-DCB/Ar stream, **stage 2:** after (g) 5 min, (h) 20 min (i) 60 min of evacuation in Ar (A) High frequency region (3800 to 2500 cm^{-1}) and (B) Low frequency region (2200 to 1350 cm^{-1}).

At 250 °C the gas phase o-DCB present characteristic C=C stretching vibration bands at 1586, 1460 and 1442 cm^{-1} due to the benzene ring [90]. Upon the *o*-DCB these characteristics

vibrations are slightly shifted to lower values at 1570, 1456 and 1435 cm^{-1} (Figure 28 B) and can be assigned to the C=C degenerated stretching vibrations of the aromatic ring [90,250]. Similar shifts of the C=C stretching vibrations of the 2-Chlorophenol (free) towards lower frequencies when is adsorbed on oxide surfaces (α-Fe_2O_3 or α-FeOOH) have been also reported [250] and attributed to a change of the electron distribution and symmetry of the ring because of the interaction of the molecules with the oxide surfaces. In the case chlorobenzene adsorption on hydroxylated TiO_2 similar shifts were reported [251] and attributed to the interactions between hydroxyls groups with the chlorine atoms or π-electrons of the aromatic ring. In a similar way, we suggest that the adsorption of *o*-DCB on the HMOR sample proceeds by two kind of interactions, OH•••π-electrons of the aromatic ring and by hydrogen bonding between hydroxyls and chlorine atoms OH•••Cl [90,250,252]. Finally, the very weak bands observed at 1921 and 1793 cm^{-1} can be ascribed to C-H out-of-plane bending vibrations of the benzene ring [253,254].

The *in-situ* FT-IR spectra of *o*-DCB adsorption conducted on the Co-HMOR sample at 250 ºC (Figure 29 A and Figure 29 B) reveals a weak broad negative band around 3772 cm^{-1} while a positive band at 3741 cm^{-1} arises at the same time, as in the HMOR sample these bands result from the perturbation of the hydroxyl groups of extra-framework alumina by the *o*-DCB molecules [141,238,239]. Since no significant differences in the intensity of these bands were found when comparing the spectra of HMOR and Co-HMOR samples after 120 min of continuous *o*-DCB adsorption, it seems that these hydroxyls groups were not considerably affected during the ion-exchange procedure for cobalt incorporation. On the contrary, the lower intensity of the negative band at 3725 cm^{-1} compared to that observed on HMOR around 3720 cm^{-1} indicates a smaller concentration of the silanol groups after Co^{2+} exchange. In the same way, the absence of negative bands around 3660 cm^{-1} indicates that the hydroxyls groups of Al ions located at the external surface of the mordenite are strongly diminish during the Co^{2+} ion exchange. The adsorption of *o*-DCB also perturbs the bridging hydroxyls groups located in the large channels of the Co-HMOR sample as reveals the negative band at 3610 cm^{-1} [247,248], interestingly this peak exhibits a more defined structure than the observed in the HMOR sample which could be due to the absence of the superimposed broad positive band in the 3642–3598 cm^{-1} region that was presented in the

HMOR sample. The hydroxyls of extra-framework Al ions in the Co-HMOR were strongly diminished by the Co^{2+} ion exchange then no bands related to the interaction of this kind of hydroxyls and *o*-DCB molecules were formed. As in the case of the HMOR, the broad bands in the 3600–3000 cm^{-1} can be assigned to the hydrogen bonding between *o*-DCB and the remaining bridging hydroxyls groups in the Co-HMOR sample [91].

In the low frequency region, the bands appearing at 1566, 1456 and 1435 cm^{-1} correspond to aromatic ring vibrations of o-DCB interacting with the hydroxyls as was discussed in the case of HMOR sample. In the region of out-of-plane C–H bending vibrations (2000–1750 cm^{-1}) [254], the weak bands observed in the HMOR sample at 1921 and 1793 cm^{-1} were shifted to 1930 and 1811 cm^{-1} on the Co-HMOR sample, besides both peaks exhibited a marked increase in the intensity. The bands arising at 1645, 1601 and 1387 cm^{-1} are clearly observed in the spectra of the Co-HMOR sample at 250 ºC (Figure 29 B), these bands were not observed in the spectra of HMOR. Following similar assignments in previous literature reports [90,116,252,253], we have assigned these bands to the ring C=C vibration and deformation of adsorbed aromatic species. The presence of new components in the spectra of Co-HMOR sample, the shift to higher frequency values and the stronger intensities exhibited of the C-H out-of-plane bending vibrations bands with respect to the HMOR sample, suggest that the corresponding surface species are formed through the interaction of o-DCB with the Co^{2+} Lewis sites [90,254].

The intensity of all the bands were considerably decreased after exposure of the surface species formed to flowing Ar at 250 °C for 60 min (Figure 29 A and B, trace h), this was an unexpecting result since in a similar study [90] performed on a Co(4.73 wt%)-HMOR catalyst, the adsorption strength of the surfaces species formed upon the adsorption of 500 ppm *o*-DCB/He at 250 °C was found considerably higher, even after evacuation in He at 350 °C for 20 min some species remain present in the reported spectra. The strong adsorption of the surface species on that study was attributed to a confinement effect because of the size similarity between the *o*-DCB molecules and the Co-HMOR main channels. Although the similarity of both catalysts, our Co-HMOR sample has a cobalt loading of 2.97% which is much lower than the reported in the cited study, then it seems that not only the size similarity

of the Co-HMOR main channels and the *o*-DCB molecule but also the metal loading would be responsible of the confinement effect reported. In this way, the lower cobalt loading of our catalyst sample would explain the lower relative adsorption strength observed.

When the evacuation gas is shifted to 10% O_2/Ar, several bands appear in the low frequency region (Figure 29 A and B, traces i and j) suggesting the formation of several oxygenated intermediates on the Co-HMOR sample. After 60 min of exposure of the sample to the flowing oxygen, the bands related to the adsorbed species on the Co^{2+} Lewis sites result all diminished while the new broad bands corresponding to oxygenated intermediates are arising, this is an evidence of reactivity of the *o*-DCB adsorbed species on the Co^{2+} Lewis sites towards oxidation. The shoulders observed at 1610 and 1599 cm^{-1}, and the broad bands appearing at 1589, 1565 and 1410 cm^{-1} are most likely due to formates, acetates and chlorinated acetates species on the Co-HMOR surface [90,255,256].

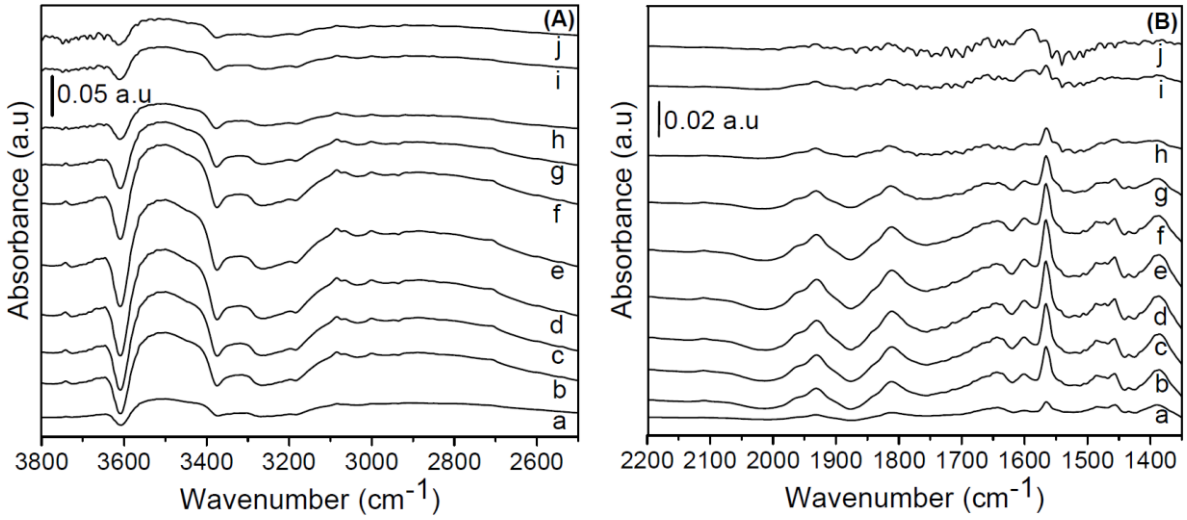

Figure 29 In situ FTIR spectra of an Co–HMOR zeolite sample collected at 250 °C. **Stage 1:** after (a) 5 min, (b) 20 min, (c) 30 min, (d) 100 min, (e) 120 min in a 300 ppm *o*-DCB/Ar stream, **stage 2:** after (f) 5 min, (g) 20 min (h) 60 min of evacuation in Ar and **stage 3:** after (i) 20 min, (j) 60 min of subsequent exposure of remain adsorbed species to a 10% O_2/Ar stream. (A) High frequency region (3800 to 2500 cm^{-1}) and (B) Low frequency region (2200 to 1350 cm^{-1}).

Figure 30 shows the *in-situ* FT-IR spectra of Pd/Co-HMOR sample collected at 250 °C during the adsorption of 300 ppm *o*-DCB/Ar follow by consecutive evacuations in Ar and 10% O_2/Ar. In the region of aromatic ring vibrations, bands at 1569, 1558, 1456 and 1435 cm^{-1} appear clearly from the spectra taken at 5 min of continuous *o*-DCB adsorption (Figure 30B trace a). As in the HMOR and Co-HMOR samples, these bands can be attributed to the interactions of *o*-DCB molecules with the OH groups of the catalyst. In the C-H out-of-plane bending vibrations region two bands appear at 1923 and 1808 cm^{-1} which correspond to slightly shifts of the bands observed at 1930 and 1811 cm^{-1} in the monometallic sample. The bands observed in the Co-HMOR sample at 1645 and 1601 cm^{-1} were observed as shoulders and slightly shifted to 1650 and 1604 cm^{-1}, respectively in the Pd/Co-HMOR sample. As in the monometallic sample, all these bands can be assigned to the interaction of *o*-DCB with the Co^{2+} Lewis sites.

After 20 min of continuous *o*-DCB adsorption (Figure 30 trace b) a broad band around 1624 cm^{-1} begins to grow as well as a series of weak bands in the 1800–1670 cm^{-1} region, after 120 min of adsorption all these bands are more clearly discernable in the spectrum and over the broad band several peaks arise at 1616, 1624, 1633, 1645, 1650 (shoulder), and 1668 cm^{-1} (Figure 30 trace e). Similar bands were observed in the Co-HMOR sample but only in the presence of gas-phase oxygen and correspond to a mixture of oxygenated intermediates. The presence of these bands in the Pd/Co-HMOR sample in the absence of gas-phase oxygen suggests that the *o*-DCB can interact with surface oxygen and initiate the oxidation process while the absence of oxygenated intermediates in the Co-HMOR sample during the *o*-DCB adsorption stage indicates that in the monometallic catalyst the lattice oxygen is strongly attached to the zeolite framework, hence is less available to react and the gas-phase oxygen is then required to begin the oxidation, these results are in agreement with the reported by Aristizábal et al [90]. The bands observed at 1616, 1624 and 1633 cm^{-1} can be ascribed to the generation of water because of the *o*-DCB oxidation [90,250].

After 60 min of continuous evacuation in Ar at 250 °C (Figure 30 trace h), no significant changes in the intensity of the peaks was observed, which indicates a higher adsorption strength than the exhibited by the Co-HMOR sample. When the gas flow to the transmission

cell was shifted to the mixtures 10% O_2/Ar, the weak bands in the 1800–1670 cm^{-1} region and the broad bands around 1624 cm^{-1} increase in intensity while the bands at 1923 and 1808 cm^{-1} are no longer discernible indicating that the species adsorbed on the Co^{2+} Lewis sites have reacted.

In the high frequency region, a new band arises at 3672 cm^{-1} which is already discernible after 5 min on stream and continuous increasing in intensity during a 2-h adsorption period. This band grows simultaneously with the observed at 1616, 1624 and 1633 cm^{-1} which were associated to water formed upon the *o*-DCB oxidation over the Pd/Co-HMOR sample. Lónyi et al [120] assigned a band at 3670 cm^{-1} to $(Co\text{-}OH)^+$ species in a Co^{IE} H-ZSM-5 catalyst, it seems then reasonable to associate the positive band arising at 3672 cm^{-1} to the formation of $(Co\text{-}OH)^+$ species. Aristizábal et al [90] have proposed that during the oxidation reaction some Co^{2+} sites may be transformed to $(Co\text{-}OH)^+$ and H^+ ions in the presence of water, this seems to explain the formation of the new band at 3672 cm^{-1}. Taken into account that the catalytic activity towards o-DCB oxidation over Co-HMOR and Pd/Co-HMOR catalysts was found to be considerably enhanced in presence of water as we reported recently [92], a plausible hypothesis to explain this behavior would be the transformation of some Co^{2+} cations into $(Co\text{-}OH)^+$ species during the course of the reaction. After 60 min of continuous *o*-DCB adsorptions (Figure 30 A trace e) negative two bands at 3610 and 3602 cm^{-1} both can be attributed to the perturbation of hydroxyls groups located at the main channel of the mordenite, as a result of this perturbation, the broad bands in the 3600 to 3100 cm^{-1} would be result of the interaction between *o*-DCB molecules and the hydroxyls through hydrogen bonds as was analyzed in the other two samples.

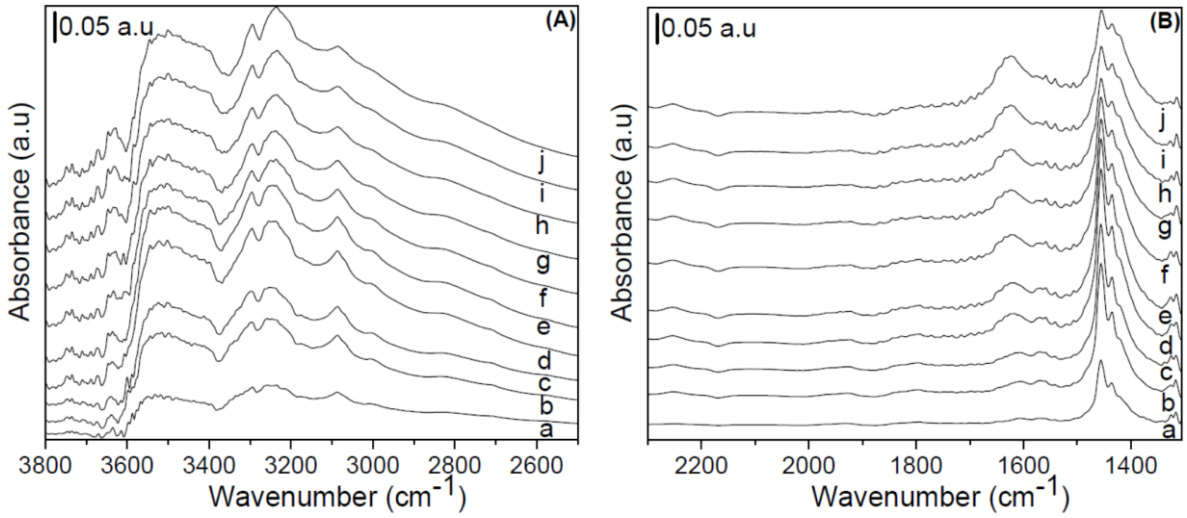

Figure 30 In situ FTIR spectra of an Pd/Co–HMOR zeolite sample collected at 250 °C. **Stage 1:** after (a) 5 min, (b) 20 min, (c) 30 min, (d) 100 min, (e) 120 min in a 300 ppm *o*-DCB/Ar stream, **stage 2:** after (f) 5 min, (g) 20 min (h) 60 min of evacuation in Ar and **stage 3:** after (i) 20 min, (j) 60 min of subsequent exposure of remain adsorbed species to a 10% O_2/Ar stream. (A) High frequency region (3800 to 2500 cm^{-1}) and (B) Low frequency region (2200 to 1300 cm^{-1}).

3.3 Catalytic activity and stability of Pd/Co catalysts in simultaneous selective catalytic reduction of NOx with methane and oxidation of o-dichlorobenzene

The results about the catalytic activity and stability of Pd/Co-HMOR and Pd/Co-SZ as also some physicochemical characterizations of the fresh and used catalysts were published in a paper currently available [92]. Next the exact copy of the paper is presented.

Catalysis Today

Catalytic activity and stability of Pd/Co catalysts in simultaneous selective catalytic reduction of NOx with methane and oxidation of o-dichlorobenzene

Volume 296, 1 November 2017, Pages 105-117

ManuelCano[a], FelipeGuarín[a], BeatrizAristizábal[b], Aída-LuzVilla[a], Lina-MaríaGonzález[a]

[a]Environmental Catalysis research group, Chemical Engineering Department, Engineering Faculty, Universidad de Antioquia, Calle 70 No. 52-21, Medellín, Colombia

[b]Hydraulic Engineering and Environmental Research Group, Universidad Nacional de Colombia Sede Manizales, Carrera 27, 64-60, Manizales, Colombia

Received 21 December 2016, Revised 19 April 2017, Accepted 13 May 2017, Available online 25 May 2017.

https://doi.org/10.1016/j.cattod.2017.05.049

Abstract

Nitrogen oxides (NOx) and polychlorinated dibenzo-p-dioxins and dibenzofurans (PCDD/Fs) are well known as hazardous pollutants that may be generated during combustion processes, and which simultaneous removal is highly desired. Here the Selective Catalytic Reduction of NO by methane (CH_4-SCR) with the simultaneous oxidation of 1,2-dichlorobenzene (o-DCB) was studied over Pd/Co-HMOR and Pd/Co-SZ catalysts under lean, dry and wet conditions. Catalysts were characterized by XRD, BET, TGA, H_2-TPR, NH_3-TPD, TEM/EDS and Raman spectroscopy. Pd/Co-HMOR showed better catalytic performance than Pd/Co-SZ in terms of activity and durability under both dry and wet conditions at 500 °C. The presence of Co^{2+} ion in both catalysts explains partially the high activity towards o-DCB oxidation. The deactivation of Pd/Co-HMOR for CH_4-SCR at reaction temperatures above 500 °C may be related with the formation of PdO specie while the loose of sulfate groups of Pd/Co-SZ can be correlated with the deactivation of this catalyst towards CH_4-SCR. According to NH_3-TPD analysis, both Pd/Co-HMOR and Pd/Co-SZ

catalysts present strong acid sites in the temperature range from 300 to 600 °C, which can be associated with their considerable active towards both reactions. The higher performance of Pd/Co-HMOR compared with Pd/Co-SZ, mainly in the CH_4-SCR reaction, can be related with the higher total acidity of the catalyst supported on HMOR. The XRD analysis of used samples showed that Pd/Co-HMOR losses crystallinity at reaction temperatures greater than 500 °C and that monoclinic phase appears in Pd/Co-SZ owing to sulfate group loss.

Keywords: Nitrogen oxides, Dioxins and furans, Selective catalytic reduction, Catalytic o-DCB oxidation, Sulfated zirconia, Zeolites.

1. Introduction

Dioxins and nitrogen oxides are well known hazardous and highly toxic compounds formed as unwanted by-products in several processes [1]. Dioxins refers to polychlorinated dibenzodioxins (PCDD) and dibenzofurans (PCDF), two families of organic solids compounds with high melting points and low vapor pressures [2]. These are highly stable molecules, which tend to bio-accumulate through the food chain and may cause a variety of toxic responses to the exposed organisms such as carcinogenicity, immunotoxicity and adverse effects on reproduction, development, and endocrine functions [3]. PCDD/Fs have been detected as side products from several industrial thermal processes including incineration of municipal [4], hazardous [5] and medical [6] wastes, combustion of coal in power plants [7], metallurgical processes such as smelting [8] and in some chemical process in which chlorine is involved as raw material [9]. On the other hand, nitrogen monoxide and dioxide (NO and NO_2) commonly named as nitrogen oxides (NOx) are the source of several environmental issues including acid rain, photochemical smog, global warming, tropospheric ozone, ozone layer weakening [10] and even have been associated with increased rates of cardiac mortality and morbidity [11]. NOx are formed during combustions processes in several stationary sources such as power plants, waste incinerators, refineries, iron ore sintering and so on, also they are generated from mobile sources during the combustion of gasoline and diesel [10,12]. NOx emissions are considered as an environmental problem of great global concern, since 1970’s emission reduction policies of pollutants in flue gases

from stationary sources have gradually evolved in several countries, especially in Japan, the United States (U.S) and Germany [10].

Although V_2O_5–WO_3/TiO_2 catalysts are widely used in stationary applications and have shown to be effective for the catalytic oxidation of PCDDs/s simultaneously with the selective catalytic reduction of NOx by ammonia (NH_3–SCR) [1,13], there are some drawbacks. The ammonia is a high corrosive, toxic and hard to handle gas and its oxidation may generate NOx. Vanadium-based catalysts are susceptible to deactivation by the deposition of ammonia salts [14], the presence of incomplete combustion products or poisoned by coke [15]. Selective catalytic reduction of NOx by methane (CH_4–SCR) is a promising alternative to the traditional NH_3–SCR technology because the high availability, ease of handling and relative low cost of methane [16]; furthermore, methane is the main component of natural gas, used in several power plants, industrial furnaces and residences with supply infrastructure in many countries [17].

Cobalt and palladium loaded zeolites have been studied for the CH_4–SCR of NOx [18–21]. Co loaded ZSM-5, FER and MOR have been reported [22–24] as highly active and selective, however Co-zeolite catalysts are sensitive to water vapor which severely decrease the NOx reduction activity and catalyst durability. As reported [25], on CoZSM-5 the primary cause of irreversible deactivation during NOx reduction by methane is the lattice dealumination induced by the steam, causing losses in the ion-exchange capacity of the zeolite and altering the nature of Co species, although the zeolite does not loss crystallinity. On the other hand, catalysts of palladium (Pd^{2+}) exchanged with H-ZSM-5 and HMOR are also highly active and selective for CH_4-SCR of NOx [18,19,26], but the presence of water vapor promotes the agglomeration of the Pd^{2+} to form bulky PdO particles which are only active for methane combustion thereby causing catalyst deactivation [17]. Since steam is unavoidably present as a product of combustion gases and considering potential practical applications, any candidate catalyst for CH_4–SCR must show long durability under wet conditions. In this sense, catalyst durability under hydrothermal conditions remains a current research topic for CH_4–SCR.

On the other hand, the catalytic oxidation of PCDD/Fs is commonly studied using chlorinated aromatics as model compounds due to the high toxicity of dioxins, in particular ortho-dichlorobenzene (o-DCB) is widely used because its structural similarity with 2,4,7,8 TCDD, the most toxic dioxin congener [27]. The catalytic oxidation of chlorinated aromatic compounds has been studied [28–30] over noble metals (Pt, Pd) and transition metal oxides (Cr_2O_3, V_2O_5, MoO_3, Fe_2O_3, and Co_3O_4) based catalysts, among the most promising alternatives are the Pd/Co loaded sulfated zirconia and mordenite catalysts which were found to be highly active for o-DCB oxidation under dry and wet conditions [27]. Although noble metals present high activity for the oxidation, they usually undergo poisoning in the presence of Cl [28,31]. Otherwise, transition metal oxides are more resistant to deactivation despite its lower activity [31,32]. It seems that the interaction between chlorine and the catalyst remains as one of the major problems in the catalysts used for the oxidation of chlorinated compounds [32]. Not only the catalysts, but also the support-type plays a key role for both reactions. In this sense, Pd catalysts supported on non-acidic materials are totally unselective for NO reduction and very active for methane combustion, while low loading Pd catalysts supported on acidic materials such as HZSM-5, H-Mordenite (HMOR) or sulfated zirconia (SZ) present high selectivities [33,34]. Strong Brønsted acid sites are known to be excellent chemisorption sites which activate chlorinated molecules in oxidation reactions [27,35,36]. Lewis acid sites are also reported as active for the oxidation of this kind of molecules, in this sense, Larrubia and Busca [37] showed that the reaction mechanism for o-DCB oxidation over V_2O_5–MoO_3/TiO_2 involves a weak and reversible interaction of the molecules with the Lewis acid sites through its chlorine atom(s) at the catalyst surface and near oxide or hydroxide nucleophilic species. Additionally, cooperative effects between Lewis and Brønsted acid sites have been found in the chlorobenzene oxidation over Pt/zeolite catalysts [38]. The presence of Lewis and Brønsted acid sites on H-MOR and SZ materials has been extensively reported [36,39–41] making them very interesting as catalyst supports for the reaction of our interest.

Synergistic effects between Pd and Co bimetallic catalysts supported on zeolites and SZ for CH_4–SCR have been extensively reported [24,42–47]. Ogura and coworkers [42] found that incorporation of Co to Pd/H–ZSM-5 resulted in a marked increase of catalytic activity and

durability, leading to stable NO conversion lasting more than 40 h in presence of steam, later they proposed that Co incorporation into Pd/H-zeolites enhances the zeolite acidity, stabilizing the isolated Pd^{2+} and minimizing the residual ion-exchangeable sites, which avoids zeolite framework collapse and dealumination from the zeolite framework, maintaining ion-exchange sites for the isolated Pd^{2+} [43]. Pieterse and coworkers [44] tested Co–Pd bimetallic catalysts supported on different H–zeolites structures (ZSM-5, MOR, FER and BEA) in presence of water and oxygen, the catalyst based on MOR and ZSM-5 were the most active. Although initially ZSM-5 supported catalyst showed higher activity than HMOR it was severe deactivated during the first 50 h on stream while HMOR based catalyst maintained the highest SCR activity over the longest period.

In the combined abatement of NOx and PCDD/Fs, few works are reported [14,48–50], some of these studies [14,50] are dedicated to investigate the simultaneous reactions over the commercial V_2O_5–WO_3/TiO_2 catalysts using the traditional NH_3-SCR technology. Recently, new catalysts based on ZSM-5 zeolite are proposed for the simultaneous removal of NO (by SCR) and o-DCB as model molecule of PCDD/Fs (by catalytic total oxidation); however, the NH_3 is also used as reducing agent [48,49].

Since both Pd/Co–HMOR and Pd/Co–SZ catalysts are highly active for o-DCB oxidation under dry and wet conditions [27] and active for the CH_4-SCR of NOx under lean and wet conditions [24,46,51–56], in the present work we studied the feasibility of the use of these catalysts for the simultaneous o-DCB oxidation during the CH_4-SCR of NOx under lean and wet conditions. The catalytic activity was compared over a temperature range of 150–550 °C and the stability was evaluated at the best performance temperature.

2. Experimental

2.1. Catalysts preparation

Sulfated zirconia catalyst was prepared following a previous reported procedure [47], 6.5 mL of zirconium butoxide $Zr(OC_4H_9)_4$ (Aldrich) was added to 22.5 mL of cyclohexane at 60 °C. The solution was stirred for 1 h and then cooled down to 3 °C. Then, a solution of distilled water (4 mol/mol Zr) and sulfuric acid (0.48 mol/mol Zr) was added dropwise with constant

stirring, until the mixture became hard to stir. The resulting gel was aged for 24 h at room temperature without stirring. Then, the aged gel was dried at 70 °C and calcined in static air at 600 °C during 4 h. Co–SZ samples were obtained with a similar procedure using a solution of 0.2 g of cobalt acetate in 5.5 mL of ethanol added to a mixture of 17 mL of cyclohexane and 6.5 mL of zirconium butoxide.

Pd/Co–HMOR catalyst was prepared according to the procedure described elsewhere [55]. Na-MOR (Si/Al = 6.5 from Zeolyst) was first transformed into NH_4–form by ion exchange with 100 mL of 1 M NH_4Cl per gram of zeolite at 80 °C for 24 h under reflux. Co–HMOR was prepared by ion exchange of NH_4–MOR with 100 mL g^{-1} of 0.09 M cobalt acetate solution per g of zeolite for 20 h at 70 °C under reflux. After the ion exchange procedure, the sample was rinsed with deionized water, filtered and heated in flowing He up to 500 °C at a rate of 2 °C min^{-1} and held at this temperature for 4 h.

Both Pd/Co–HMOR and Pd/Co–SZ catalysts were obtaining by incipient wetness impregnation with an aqueous solution containing the required amount of $Pd(NH_3)_4Cl_2 \cdot H_2O$ to obtain a Pd loading of about 0.1–0.15 wt.%. After drying at 60 °C, catalysts samples were heated in flowing argon at 2 °C min^{-1} up to 500 °C and held 4 h at this temperature and then allowed to cool at room temperature.

2.2. Catalyst characterization

Pd and Co elemental content of the catalysts were determined by atomic absorption spectroscopy. X-ray powder diffraction (XRD) patterns were obtained in a XPert PANalytical X-ray diffractometer Empyrean Series II equipped with a PIXcel 3D detector using Cu Kα radiation (λ = 1.54 nm) with a Ni filter at 45 KV and 40 mA, the scan step was 0.039°, the rate 2°/min and the scanning ranges were 2θ=5–50° and 2θ=20–80° for HMOR and SZ samples, respectively. The sulfur content in the SZ supported catalysts was determined by temperature gravimetric analysis (TGA) from the weight loss between 500 and 800 °C using a TGA Q500 V20.13 build 39 instrument. Single BET specific surface area, temperature-programmed reduction under hydrogen (H_2–TPR) and temperature-programmed desorption of ammonia (NH_3–TPD) experiments were carried out in an AutoChem II 2920 instrument (Micromeritics) equipped with a Thermal Conductivity

Detector (TCD). Specific surface areas of samples were measured by nitrogen adsorption at 77 K and data were interpreted by using the Brunauer–Emmett–Teller (BET) modeling equation. N_2 adsorbed was previously calibrated by injecting known amounts of a mixture of 30% N_2/He and correlating them with the respective integrated TCD profiles. H_2–TPR of fresh samples were obtained by flowing 50 mL min^{-1} of a mixture 10% H_2/Ar and heating from 100 to 1000 °C using a heating rate of 5 °C min^{-1}. Before H_2–TPR analysis, the samples were calcined under 50 mL min^{-1} of a flowing mixture of 5% O_2/Ar at 500 °C for 1 h. Then, the fresh samples were cooled to room temperature under a constant flow rate of pure Ar (50 mL min−1). In the case of used catalysts, the samples were only dried at 150 °C in flowing He for 1 h and then cooled to room temperature before TPR experiment run. NH_3–TPD was used to determine the total acidity of the samples. Before analysis the samples were flushed with flowing Ar (50 mL min^{-1}) for 1 h at 250 °C then the sample was cooled to 50 °C in flowing Ar. The saturation adsorption of ammonia was performed at 50 °C by flowing 50 mL min^{-1} of a gas mixture 0.3% NH_3/He for 90 min. In order to remove any physical adsorbed ammonia, the samples were flushed with 50 mL min^{-1} of He for 1 h. Desorption of ammonia was obtained by rising the temperature (10 °C min^{-1}) up to 1000 °C. Some H_2-TPR and NH_3-TPD curves of the Pd/Co-HMOR presented convoluted peaks, in such cases the curves were fitted by two or even three Gaussian functions to separate each peak. In all cases the correlation coefficient was at least 0.9.

Transmission electron microscopy (TEM) was performed on a Tecnai F20 Super-Twin TMP instrument with FEG (Gatan UltraScan® 1000XP-P camera, 0.1 nm point resolution operated at 200 kV), the chemical analyzes were performed by Energy-dispersive X-ray spectroscopy (EDS) with a detector Oxford Instruments X-MaxN. The samples for the TEM/EDS analysis were dispersed in ethanol and kept in an ultrasonic bath for 20 min, a drop of this suspension was spread out onto a TEM cooper grid (200 Mesh) covered by a holey carbon film followed by drying under room conditions. Raman spectra were collected in a Horiba Jobin Yvon Labram HR spectrometer using a 633 nm He–Ne laser.

2.3. Activity measurements

Catalytic reactions were carried out in a quartz tube fixed–bed reactor containing a quarts frit to hold the powder catalysts samples. The reactor was operated at atmospheric pressure (0.84 atm) in steady state plug–flow mode. Reactor temperature was varied from 150 to 550 °C. Durability tests were carried out for 30 h of continues operation at the temperature of the highest conversion of each catalyst. The reactant gases were fed using electronic mass flow controllers (Brooks 5850E) and mixed in line before entering the reactor (Supplementary information Fig. S1). Gas composition of the reactant mixture was 0.4% CH_4, 0.1% NOx (90% NO and 10% NO_2), 0.06% o-DCB, 10% O_2, 0–6% H_2O and balance Ar. o-DCB and water vapor were introduced into the reaction system by means of two saturators at 25 and 60 °C, respectively, using Ar as carrier gas. The tubing between the saturators and the reactor were thermally well isolated. The volumetric gas flow rate through the catalyst bed was 200 mL min−1 and the gas hour space velocity (GHSV) was fixed in 60.000 h^{-1} for each catalyst. About 100 mg of Pd/Co–HMOR and 200 mg of Pd/Co–SZ powder catalysts (30–40 mesh) were used in each experiment (apparent support bulk densities of Pd/Co–HMOR and Pd/Co–SZ: 0.5 g cm^{-3} and 1 g cm^{-3} respectively).

The concentration of the gases was analyzed online by a FTIR gas analyzer (Thermofisher scientific, model AntarisTM IGS–USB) equipped with a MCT detector, KBr beamsplitter, 2 m pathlength gas cell, 200 mL gas cell volume and a ZnSe window. Data were collected with a spatial resolution of 0.5 cm^{-1} with 32 scans for each sampling. Gas cell was operated at atmospheric pressure and the temperature was fixed at 150 °C to avoid condensation of the reactants inside the gas cell. A quantification model was developed by taking several spectrums of known gas mixtures and adjusting the absorbance and concentrations data by means of a classical least square model, the software TQ Analyst 9.4.45 (Thermo Fisher Scientific Inc.) was used for this purpose. The o-DCB, NO and CH_4 conversions were calculated as follow (Eqs. (1)–(3)):

$$x_{NO} = \frac{[NO]_0 - [NO]_f}{[NO]_0} * 100 \quad (1)$$

$$x_{CH_4} = \frac{[CH_4]_0 - [CH_4]_f}{[CH_4]_0} * 100 \quad (2)$$

$$x_{o-DCB} = \frac{[o-DCB]_0 - [o-DCB]_f}{[o-DCB]_0} * 100 \quad (3)$$

Where the subscript 0 represents the concentration at the entrance of the reactor and f represents the effluent concentration.

3. Results and discussion

3.1. Catalyst characterization

3.1.1. Chemical composition and textural properties

Elemental Co and Pd compositions, single BET surface area and total pore volume for Pd/Co–HMOR and Pd/Co–SZ catalysts are shown in Table 1. The sulfate contents of SZ supported catalysts determined from the weight loss between 500 and 800 °C are given in Table 1. As it was expected, the Pd incorporation onto Co–HMOR and Co–SZ catalysts slightly decreases their surface area and total pore volume which suggest a possible incorporation of Pd inside the pores. DTG profiles for Co–SZ and Pd/Co–SZ (Fig. 1) showed a peak below 150 °C which corresponds to the removal of physically adsorbed water while peaks above 600 °C are attributed to the sulfate groups (SO_4^{2-}) decomposition [57]. Co–SZ and Pd/Co–SZ fresh catalysts presented maximum decomposition temperatures at 673 °C and 664 °C, respectively; therefore not too much sulfate losses are expected at the calcination temperature (600 °C). In Fig. 1 it is also observed that used catalysts presented an evident reduction in the sulfur content, which can be due to losses of sulfur as SO_2 during the reaction. Formation of SO_2 was confirmed by its presence in the FTIR spectra (data not shown) of the exhaust gas products stream during a durability test for this catalyst.

The high content of sulfate groups in our prepared catalysts implies sulfate migration into the bulk solid phase, notwithstanding it has been reported [58] that a calcination temperature above 575 °C ensure that the support crystallizes and transfer the sulfate onto its surface. As

reported [59], when H_2SO_4 is used as sulfatation agent, pyrosulfate species ($S_2O_7^{-2}$) are formed on the surface of zirconia. Although in this work these species were not determined, in a previous work they were detected on SZ prepared following a similar synthesis procedure, therefore presence of pyrosulfate species is expected on our SZ synthesized [27]. It has been reported [39,59,60] that pyrosulfate is a possible stable structure on the tetragonal zirconia (101) face. The oxoanions create additional electron deficient regions that may generate new acid sites and increase the strength of Brønsted acidity [59]. Furthermore, sulfate groups protect the metastable tetragonal phase of zirconia avoiding its transformation to monoclinic phase, which is more stable but less catalytically active; as it is known the tetragonal phase make zirconia suitable for redox catalysis [27].

Table 1. Physicochemical properties of Pd/Co catalysts

Catalyst	wt%.		T_d[a] (ºC)	wt%.		S_{BET}	TPV[b]	SO_4^{2-} surface covarage[c]	
	S	SO_4^{2-}		Pd	Co	$m^2\ g^{-1}$	$m^3\ g^{-1}$	SO_4^{2-}/nm^2	%
Co–HMOR (Fresh)	--	--	--	–	2.97	379	0.1796	--	--
Pd/Co–HMOR (Fresh)	--	--	--	0.14	2.74	338	0.1599	--	--
Co–SZ (Fresh)	4.2	12.6	673	–	1.96	165	0.0777	4.79	120
Pd/Co–SZ (Fresh)	3.3	9.9	664	0.15	1.92	139	0.0724	4.06	113
Pd/Co–SZ (Used dry feed)	2.5	7.5	688	n.d	n.d	n.d	n.d	n.d	n.d
Pd/Co–SZ (Used wet feed)	2	6	676	n.d	n.d	n.d	n.d	n.d	n.d

[a]Td: Temperature of sulfate decomposition [b] TPV: Total pore volume, [c] Estimated value of a statistical monolayer is 4 SO_4^{-2}/nm^2 [47], n.d: No determined.

3.1.2. XRD results

X-ray diffraction (XRD) patterns at 2θ between 5° and 50° of Na-MOR zeolite, Pd/Co-HMOR fresh and used catalysts are shown in Fig. 2A. The characteristic diffraction peaks of mordenite crystal phase are observed in all the samples. No evidences of new phases due to palladium and cobalt incorporation into the mordenite were found. The XRD diffraction peaks of Co_3O_4 at 2θ = 31.3 and 31.8° [24,61] were not detected in the analysis, due to unmasking by the mordenite, or a concentration below the detection limit; however, the presence of this cobalt oxide was detected in the fresh Pd/Co–HMOR according with the TPR results. No diffraction peaks (33.9° and 42.3°) related with Pd and PdO aggregates were found in the Pd/Co–HMOR samples, this could be due to the low Pd loading and its high

dispersion [62]. The detected peaks of the used Pd/Co–HMOR catalysts, even after the durability tests under dry and wet conditions, remained almost as the fresh Pd/Co–HMOR sample which indicates that the structure and crystallinity were preserved.

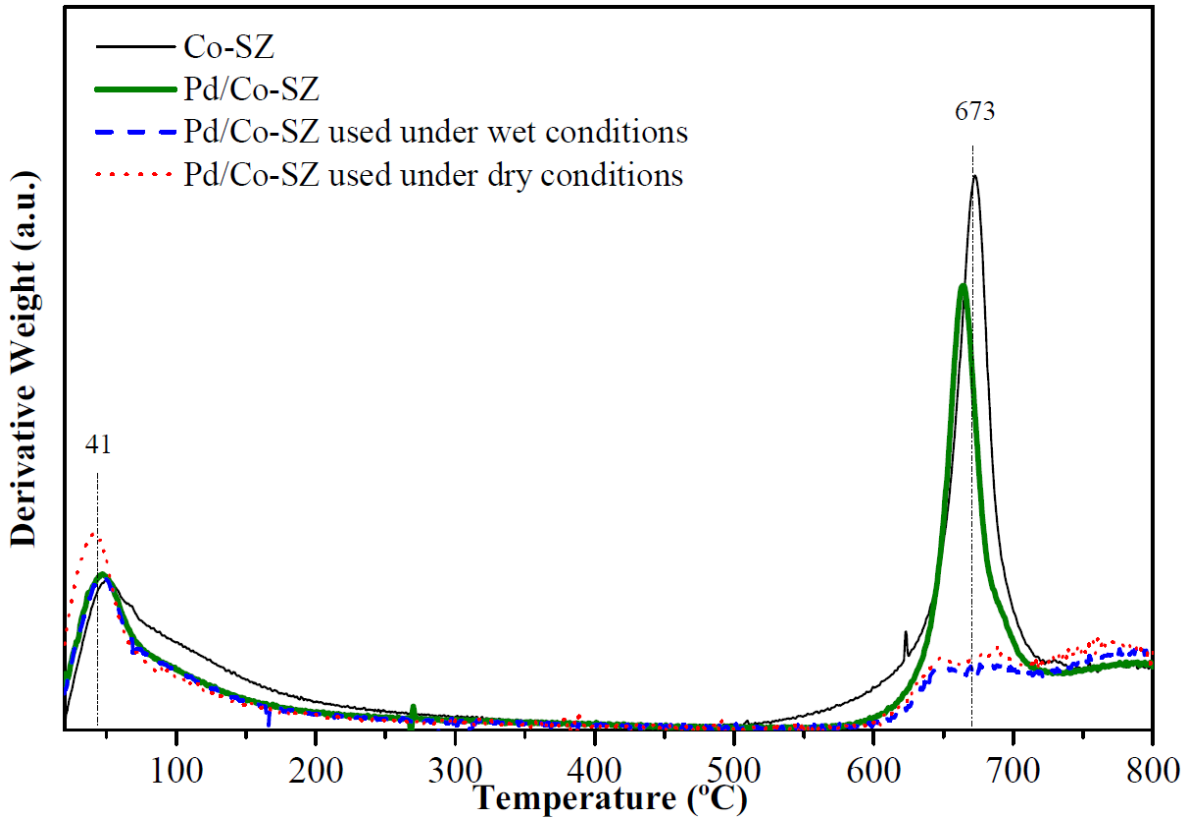

Fig. 1. DTG profiles of Co–SZ and Pd/Co–SZ catalysts before and after reaction. Reaction conditions: [CH_4] = 4000 ppm, [NOx] = 1000 ppm, [o-DCB] = 600 ppm, [O_2] = 10%, [H_2O] = 0 or 6 %, GHSV = 60,000 h, 150 – 550 ºC.

In the case of zirconia is widely known [63] that monoclinical and tetragonal crystalline structures may coexist and the phase distribution greatly depends on the calcination temperature at which ZrO_2 is prepared. After incorporation of sulfate species during the synthesis of zirconia, the tetragonal phase resulted favored and no monoclinical phase was formed at calcination temperatures between 550 and 700 °C [64]. Fig. 2B shows the XRD patterns of the Co-SZ and Pd/Co-SZ fresh and used catalysts. The fresh catalysts showed characteristic peaks at 2θ = 30°, 35°, 50°, 60° and 65° reveling the presence of only the tetragonal phase, as it was expected according with the synthesis calcination temperature

(600 °C). In contrast to the Pd/Co–HMOR, the intensity of the main peaks of fresh and used Pd/Co–SZ catalysts are quite similar, which indicates that support crystallinity is preserved at the maximum reaction temperature tested (550 °C). Notwithstanding, in the used catalysts a new peak appears at 2θ = 28° and in the both used catalysts samples for durability test under dry and wet conditions at 2θ= 28° and 32° which correspond to the monoclinic phase [65]. As it was identified by the DTG profiles, the used Pd/Co–SZ catalysts presented a reduction in the sulfur content, which was release as SO_2 in the gas products stream as consequence of the reaction temperature. The formation of the monoclinic phase can be attributed then to the loss of these sulfate groups [66] which are responsible not only for the stabilization of the tetragonal phase but also for the promotion of Pd and Co dispersion and avoid the formation of PdO and Co_3O_4 species as has been reported previously [46,65].

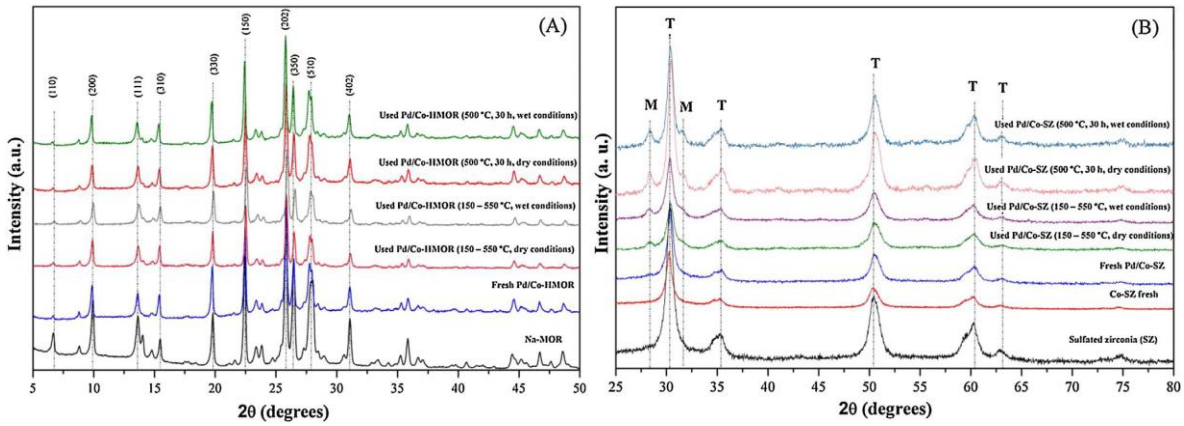

Fig. 2. XRD patterns of (A) Na-MOR, Pd/Co-HMOR catalyst before and after reaction, and (B) SZ, Co-SZ, Pd/Co-SZ catalyst before and after reaction (Reaction conditions: [CH_4] = 4000 ppm, [NOx] = 1000 ppm, [o-DCB] = 600 ppm, [O_2] = 10%, [H_2O] = 0 or 6 %, GHSV = 60000 h^{-1}). T: Tetragonal, M: Monoclinical.

3.1.3. NH_3–TPD

NH_3–TPD profiles of NaMOR, HMOR, Co–HMOR and Pd/Co–HMOR fresh samples are shown in Fig. 3A, and ammonia desorption for each catalyst are presented in Table 2. According with the ammonia desorbed peaks above 100 °C, the acid–strength distribution in the catalyst can be determined. All samples exhibit a large peak in the low temperature range between 100 and 300 °C which can be assigned to weak Brønsted and or Lewis acid sites

[36]. NaMOR only presents a broad peak achieving the maximum at 223 °C, which correspond to a protonic zeolite. Supported catalysts presented two additional desorption peaks, HMOR around to 550 °C, Co–HMOR a broad peaks with maximums at 350, 550 and 670 °C, and Pd/Co–HMOR presented also a broad peak with maximums around to 441 °C, and 580 °C. The third desorption peak above 700 °C, has the lowest concentration of acid sites around of 0.02 mmol g^{-1}. High desorption temperatures peaks indicate stronger interactions between the acid sites and the adsorbed NH_3 molecules. It is well accepted [67] that the bridging hydroxyl groups Al–(OH)–Si located in the walls of the zeolitic cavities are responsible of the strong acidic sites of protonic zeolites. According to the results reported by López-Fonseca and coworkers [36], the second desorption peaks can be assigned to strong Brønsted acid sites, while third desorption peak correspond to whatever Brønsted or Lewis acid sites; however, since these peaks are no present in the NaMOR they can be more related with Brønsted than with Lewis acid sites. The addition of Co and Pd metals on the H-MOR has led to an increase in the surface acidity, a similar effect by the addition of another metals into a H-ZSM5 zeolite has been also reported [48].

NH_3–TPD profiles of Co–SZ and Pd/Co–SZ catalysts are shown in Fig. 3B, Co–SZ catalysts present a broad desorption curve between 50–550 °C which is attributed to a weak acidity [64]. The total amount of NH_3 desorbed was pretty similar in both samples (see Table 2) which suggests that Pd incorporation does not affect the total acidity of the catalyst. However, the incorporation of Co and Pd generates a shift to left in desorption peaks respect to SZ. Pd incorporation into Co–SZ produced a higher peak between 400–550 °C which can be associated to strong acid sites [64]. Although the total amount of adsorbed NH_3 decreased after Pd impregnation. Therefore after Pd incorporation there was a shift in the acid distribution at this temperature moving from weak to strong acidity (see Fig. 3B). Although the presence of Lewis and Brønsted acid sites has been extensively reported [39–41] in these kind of catalysts, they cannot be distinguished by this technique. In spite of that, it has been reported that the amount of Lewis and Brønsted acid sites depends on the sulfate loading in the support and the formation of Brønsted acid sites on SZ based catalysts starts when at least 50% of a monolayer of sulfate groups is present on the surface [39]. The estimated sulfate monolayer coverage values of Co–SZ and Pd/Co–SZ were greater than 50% for each catalyst

(Table 1), therefore presence of both Brønsted and Lewis acid sites is highly presumable in our synthesized SZ based catalysts. In accordance with the TGA analysis of the SZ based catalysts, the desorption peak at 620 °C can be ascribed to the sulfate decomposition and no to the NH_3 desorption, therefore these data were no considered in the acidity analysis.

Table 2. Ammonia consumption and total acidity from TPD of mordenite and SZ materials.

Sample	Acidity (mmol/g)			
	Peak 1	Peak 2	Peak 3	Total acidity (mmol/g)
NaMOR	1.39 (100–340 ºC)	–	–	1.39
HMOR	0.47 (100–280 ºC)	0.37 (300–680 ºC)	0.03 (700–820 ºC)	0.87
Co–HMOR	0.82 (100–290 ºC)	0.38 (300–700 ºC)	0.02 (750–900 ºC)	1.22
Pd/Co–HMOR	0.78 (100–290 ºC)	0.28 (300–610 ºC)	0.02 (700–820 ºC)	1.08
Co–SZ	0.56 (50–550 ºC)	–	–	0.56
Pd/Co–SZ	0.46 (50–550 ºC)	–	–	0.46

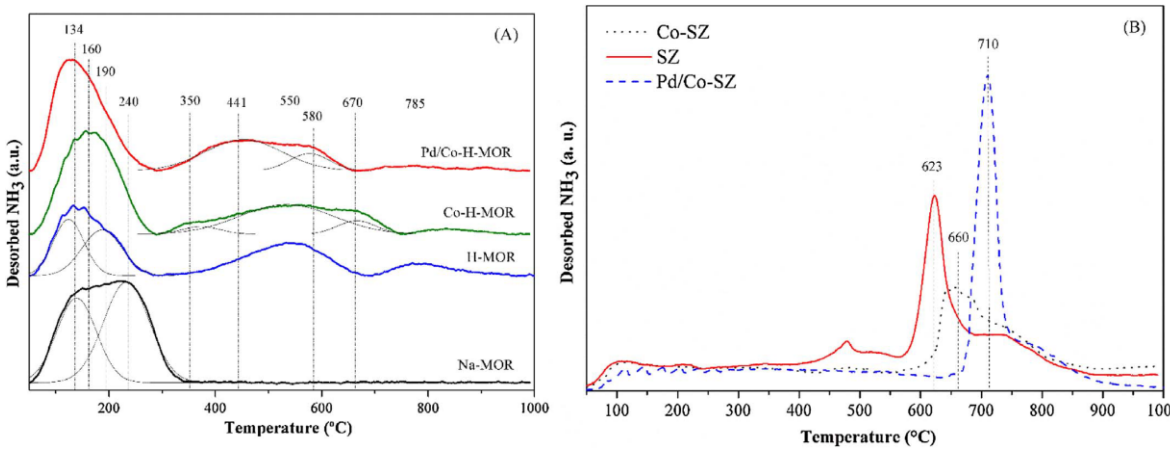

Fig. 3. NH3–TPD profiles of (A) Mordenite (B) Sulphated zirconia materials.

3.1.4. H_2–TPR

The H_2–TPR profiles for Co–HMOR and Pd/Co–HMOR fresh catalysts are presented in Fig. 4A. Co–HMOR has a weak desorption peak at 136 °C, a shoulder around 769 °C and a high temperature peak at 875 °C. Wang et al. [68] attributed the peak at 705 °C in Co-ZSM-5 to reduction of Co^{2+} ions. In the case of Co–HMOR, Bustamante and coworkers [24] assigned the peaks at 793 and 856 °C to reduction of Co^{2+} ions at exchange positions of mordenite. Therefore, the shoulder at 769 °C and the peak centered at 875 °C can be assigned to reduction of Co^{2+} ions located at the main parallel 12-ring channels and the interconnecting array of 8-ring channels of mordenite, respectively [24,27,55]. It has been reported that peaks

between 200 and 400 °C correspond to reduction of either Co oxocations $[Co–O–Co]^{2+}$ or to highly dispersed Co_3O_4 crystallites located outside zeolite pore structure [24,68,69]. The peak around 220 °C can be associated [68,69] to Co oxocations rather than with Co_3O_4 crystallites, however the presence of the latter cannot be rule out. Pd incorporation enhances the reducibility of isolated Co^{2+} ions, consequently the temperatures of maximum Co^{2+} ions reduction in Co–HMOR go down in fresh Pd/Co–HMOR from 760 °C and 873 °C to 646 °C and 819 °C respectively.

The broad desorption curve between 100 and 300 °C in the fresh Pd/Co-HMOR can be attributed to the co-reduction of Co species and Pd^{2+} ions [21] in accordance with the previous TPR of Co-HMOR. The used Pd/Co–HMOR catalysts under wet and dry conditions show a first reduction peaks at 125 °C each one, which did not appear in the fresh catalyst. Oliveira et al. [62] associated a TPR peak at 85 °C in a Pd–MOR catalyst to reduction of PdO, therefore the reduction peaks at 125 °C present in the used Pd/Co–HMOR catalysts can be attributed to the reduction of PdO particles interacting strongly with the protonic mordenite support and/or with large PdO particle sizes. The negative desorption curves in used Pd/Co–HMOR indicate the decomposition of Pd β–hydrides suggesting that Pd was formed during the PdO reduction [21]. Weak and broad signals from 300 to 500 °C appear in the TPR of used Pd/Co–HMOR catalysts, which may indicate the presence of Co-oxo species (CoOx) as it has been reported [24].

Table 3 shows both the quantification of hydrogen consumption and the reduction temperature for fresh Co-SZ and Pd/Co-SZ according to the TPR profiles of Fig. 4B. The high H/(Co + S) ratio obtained in both materials, suggests a complete reduction of Co^{2+} ions and most of the sulfate groups to H_2S or S^{2-} [47]. In addition, the presence of palladium facilitates the reduction of the catalyst as the reduction temperature appeared at a lower value in the bimetallic catalyst. The hydrogen consumption curves of the temperature programmed reduction analysis are presented in Fig. 4B. For Co-SZ a single peak is shown around 500 °C attributed to the reduction of Co and S species in the sample. No evidence of Co_3O_4 was found on fresh SZ based catalysts, it is known [65] that the presence of SO_4^{2-} improve the dispersion of Co species preventing the formation of Co_3O_4 which is more easily reducible

than dispersed Co species. Fresh Pd-Co/SZ reveals a broad peak with a maximum at 455 °C, with a shoulder at 370 °C assigned to Co^{2+}, which suggests that the presence of palladium improves the reduction of isolated cobalt ions in the fresh catalyst [47]. The curves of the used samples under both dry and wet conditions exhibit a very similar behavior with a broad peak and a maximum at 485 °C, clearly indicating that the active phase is modified, which is in accordance with the fact that sulfur content decreased and alters the reducibility of the catalyst [45].

Table 3 Hydrogen consumption of Co-SZ and Pd/Co-SZ

Catalysts	TPR	
	H/(Co+S) molar ratio	Reduction temperature (°C)
Co-SZ	9.6	503
Pd/Co-SZ	10.3	457

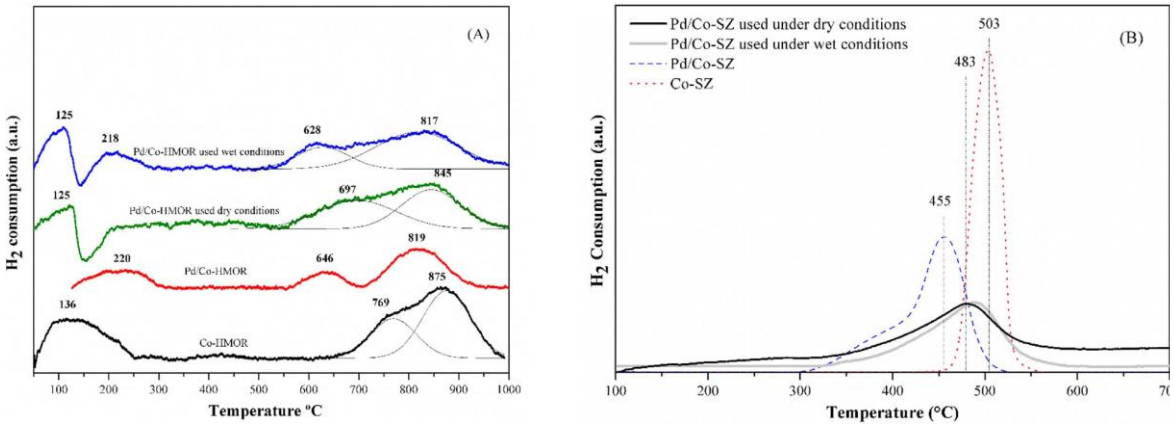

Fig. 4. H_2–TPR of (A) Co–HMOR, Pd/Co–HMOR before and after reaction, and (B) Co–SZ, Pd/Co-SZ before and after reaction. Reaction conditions: [CH_4] = 4000 ppm, [NOx] = 1000 ppm, [o-DCB] = 600 ppm, [O_2] = 10%, [H_2O] = 0 or 6%, GHSV= 60,000 h, 150–550 °C.

3.1.5. TEM and EDS

The presence of small metal particles (dp ≈ 5 nm) of Pd and Co in Pd/Co–HMOR and Pd/Co–SZ was evidenced by TEM/EDS analysis. In the fresh materials metallic Pd^0 was detected by EDS (Supplementary information, Tables S1 and S2), which indicates that the thermal

treatment with argon leads to the formation of small and homogeneously dispersed metal particles of Pd. Those particles can be oxidized to Pd^{2+} as was evidenced by H_2-TPR analysis (Fig. 4A).

EDS analysis of Pd/Co-HMOR catalyst after durability test under dry conditions showed the simultaneous presence of Cl and Pd with a Cl/Pd atomic ratio of 1.7, which could suggest the formation of $PdCl_2$ in the catalyst. On the other hand, if the Cl quantified by EDS corresponds to adsorbed o-DCB or products derived from its oxidation then the calculation may indicate that the oxidation of o-DCB is favored over the CH_4-SCR of NO. EDS analysis (Supplementary information Table S1) of the cluster in Pd/Co-MOR, Fig. 5C, reveals an increase of the % Pd from 0.05 to 2.62%, since Cl atoms were no detected in this located area, then is highly probably that the cluster corresponds to PdO. EDS analysis of Pd/Co-HMOR after durability test under wet conditions does not show the presence of Cl atoms; probably under tested conditions the excess of water can act as a hydrogen–supplier and react with Cl atoms. The presence of presumable PdO clusters was also evidenced as is shown in Fig. 5E.

TEM images of Pd/Co-SZ fresh catalyst samples (Fig. 6A and B) present some aggregates of particles with sizes lower than 10 nm. The presence of Pd^0 was evidenced by EDS (Supplementary information Table S2). Co and S atoms where found in all the EDS analysis taken over the different sampled areas, which suggests a homogenous distribution of Co and sulfate groups in the material. EDS of Pd/Co-SZ after testing under dry conditions, circles A and B in Fig. 6C, reveal that the Pd content is 75.62% and 13.51% respectively, furthermore in the region A 6.9% of sulfur was detected while in region B sulfur atoms were not detected. By DTG analysis (Fig. 1) it was found that the Pd/Co-SZ catalyst after reaction had a reduction of the sulfur content owing to its release as SO_2, as was evidenced by FTIR analysis of the gas product stream.

The combined TEM/EDS analysis seems to show that the loss of sulfate groups from the SZ structure does not occur homogenously. It has been reported [46,65] that the key roles of these groups are to stabilize the tetragonal phase of the zirconia and promote both the Pd and Co dispersion. As palladium and sulfur rich zone coexist (region A in Fig. 6C), while the Pd

poor zone is found where no sulfur atoms were detected (region B in Fig. 6D) then it seems that Pd^{2+} ions migrate to the zones where the sulfate groups remain, and once the sulfur groups are lost, the Pd cluster are formed. These clusters are likely to be formed by PdO, which is known to be highly active for oxidation reactions, especially for the CH_4 combustion.

On the other hand, the Co content in the regions A and B was 3.66 and 3.97% respectively, this may indicate that sulfate groups would have a more significant effect in the promotion of Pd rather than Co dispersion and not on both, contrary to the reported in the literature [46,65]. TEM analysis of a Pd/Co-SZ used under wet conditions (Fig. 6D) shows that the continuity of the channels that showed the fresh catalyst (Fig. 6 B) was lost; additionally no Pd was detected by EDS analysis (Supplementary information Table S2). The simultaneous presence of Pd and Cl was detected with a Cl/Pd ratio of ≈ 0.2; then probably no $PdCl_2$ was formed and the Cl content could be related with chloride compounds as o-DCB or its oxidation products.

3.1.6. Raman analysis

Raman spectra of mordenite materials, as well Pd/Co-HMOR before and after use are presented in Fig. 7A. In the Pd/Co-H-MOR catalysts is evident the presence of two peaks at 1374 and 1401 cm^{-1}, but they are more intense in the Pd/Co-H-MOR used under wet conditions. These bands are associated with the presence of C-C, C-H and C-Cl vibrations [70], than can be affected by the presence of water [71]. As it is known the PdO shows a peak around 643 cm−1 [17], although none of the used catalysts show an evident peak in this band, the used Pd/Co-HMOR under wet conditions shows a small shoulder (Fig. 7A). Taken into account the low Pd loading on the catalysts, the PdO related peak in the used samples may be not evident because its low concentration.

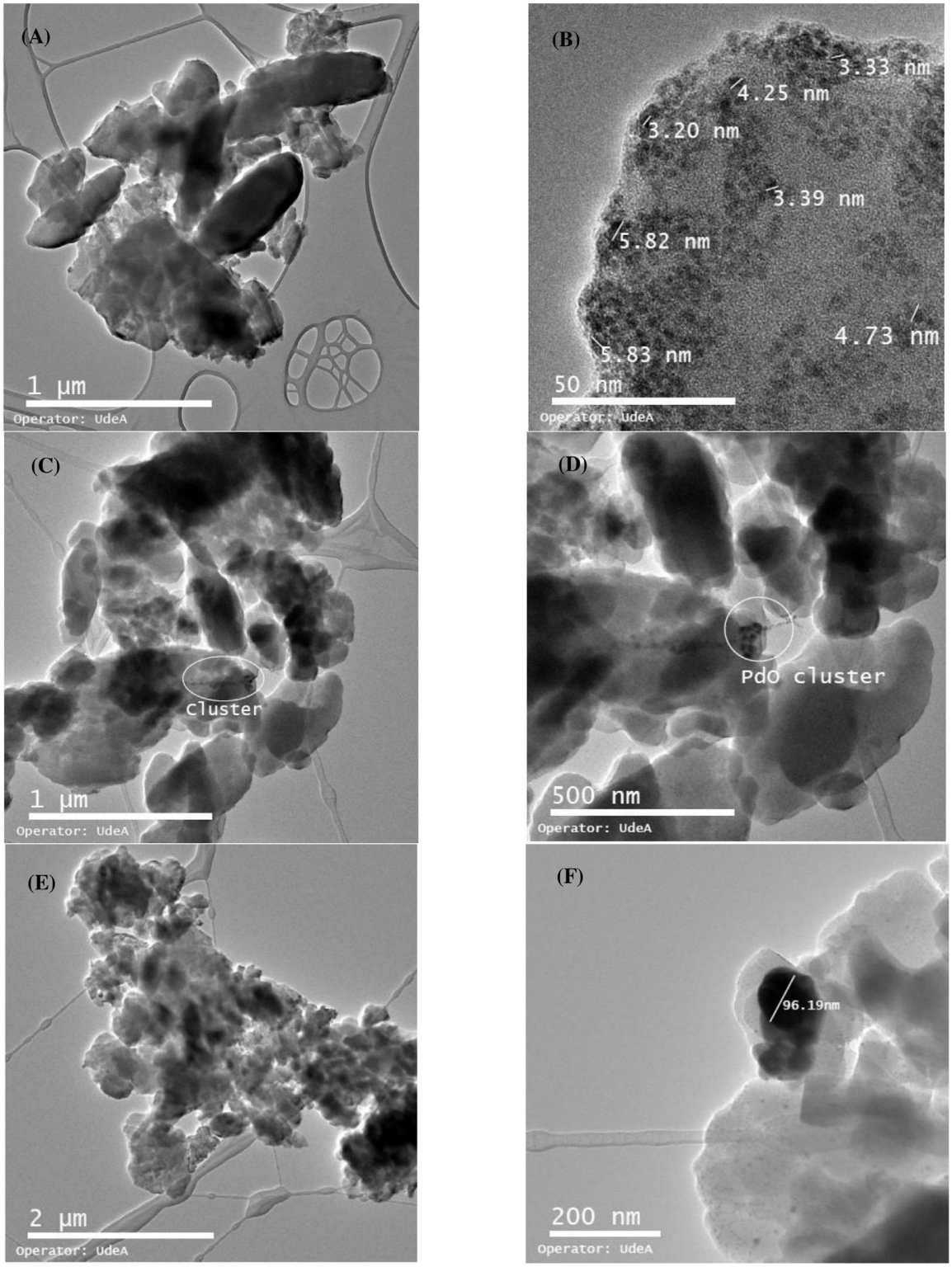

Fig. 5. TEM analysis of the Pd/Co-MOR fresh (A and B), used under dry conditions (C and D), and used under wet conditions (E and F).

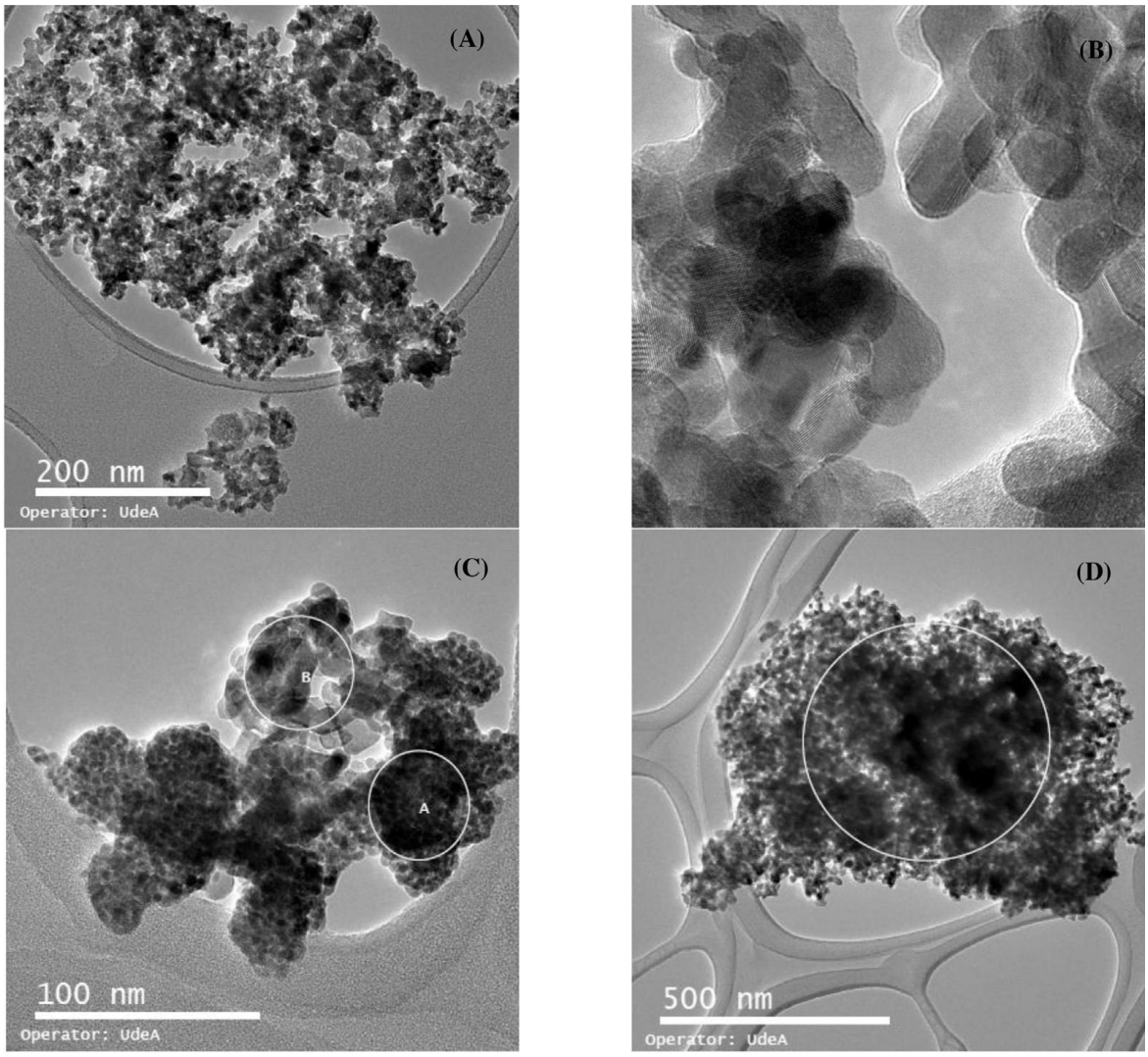

Fig. 6. TEM analysis of the Pd/Co-SZ fresh (A and B), used under dry conditions ©, and used under wet conditions (D).

Raman spectra of fresh Co-SZ and Pd/Co-SZ and used catalyst under wet conditions are presented in Fig. 7B. All samples evidenced similar behavior in the region between 100 and 700 cm^{-1} showing characteristic bands of both tetragonal and monoclinic phase. Bands at 178, 189, 338, 378 and 476 cm^{-1} are ascribed to monoclinic whereas 148, 268 and 640 cm^{-1} are assigned to tetragonal phase [72]. This finding is in contrast with XRD results where only tetragonal phase and no monoclinic was observed in fresh samples and the appearance of monoclinic was detected in used samples (Fig. 2B). Similar results reported previously [66],

propose that in sulfated zirconia samples a phase transition begins at the surface and proceeds into the bulk support. This is in agreement with the results obtained in our research as the monoclinic phase was only observed through the more surface sensitive Raman spectroscopy and not in the bulk sampling XRD [66]. In the 800–1500 cm^{-1} spectral region, lines of the sulfate species are visible. In that sense, the band centered at 1002 cm^{-1} in both fresh samples and no detected in the used catalyst evidences the loss of sulfate species in the support [46].

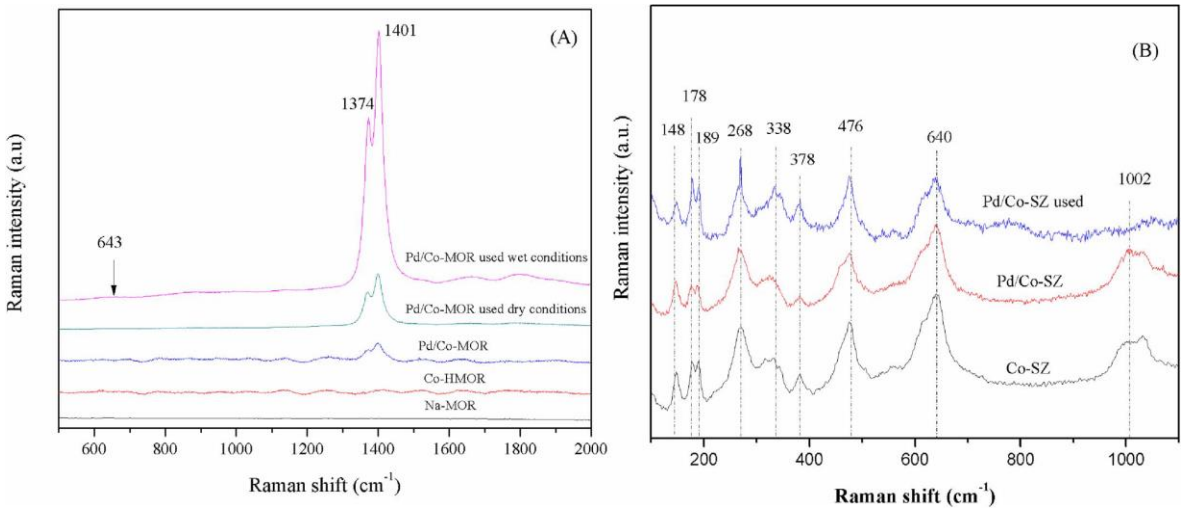

Fig. 7. Raman spectroscopy analysis of Pd/Co-MOR (A) and Pd/Co-SZ (B) catalysts.

3.2. Activity measurements

The conversion profiles of NO as a function of temperature (Fig. 8), during the o-DCB oxidation (Fig. 9), under lean, dry and wet conditions over Pd/Co–HMOR or Pd/Co–SZ catalysts are compared. Below 350 °C both catalysts presented low NO conversions under both conditions. In the temperature range from 450 to 500 °C, the presence of water significantly improves the NO conversion over Pd/Co–HMOR, since methane conversion (Fig. 10) is also enhanced by presence of water in the same temperature range for this catalyst, probably the water affects the methane combustion leading to the molecules to react more selectively with NO instead of oxygen molecules. Conversely, no relevant changes in the NO, nor o-DCB nor CH_4 conversions (Fig. 9 and Fig. 10) were observed over Pd/Co–SZ under dry or wet conditions in the overall temperature range tested. Results of o-DCB oxidation over Pd/Co–HMOR and Pd/Co–SZ are compared in Fig. 9. Although Pd/Co–

HMOR shows some activity even from the starting temperature, it decays at 250 °C but above this temperature o-DCB conversion tends to raise with increasing temperature, this might be explained by o-DCB physisorption in the catalyst at low temperatures (below 150 °C) and the subsequent desorption at 250 °C resulting in a lower conversion at this temperature. Above 250 °C o-DCB conversion tends to rise with increasing temperature. The presence of water increases significantly the o-DCB oxidation in the temperature range of 250–475 °C, above this temperature no significant differences in the o-DCB conversions were found with respect to the dry conditions. This coincides partially with the results reported by Aristizabal and coworkers [27], who studied the oxidation of o-DCB over a similar catalyst system, although they observed significant differences in the o-DCB conversion between dry and wet conditions even at high reaction temperatures (above 450 °C). To explain this difference, we must consider that in the present study the o-DCB oxidation occurs simultaneously with the SCR of NO by CH_4 and above 475 °C, both the CH_4 oxidation and the NO reduction produce water. Considering that CH_4 is in excess for the NO-SCR, about 8000 ppm of H_2O are expected to be generated, which are so high comparing with the expected 500 ppm of H_2O under the dry conditions due to the oxidation of o-DCB alone, as in the referenced study [27]. Although the amount of water expected in our reaction system (8000 ppm) is not enough to turn the dry condition into an in-situ wet condition (60,000 ppm), probably is enough to emulate the effect that the water have into the catalysts. It seems that the presence of water in the reactor play an important role to improve the o-DCB oxidation probably because it can act as a hydrogen-supplier suitable to react with the chlorine atoms to give HCl as product.

In the case of Pd/Co–SZ catalyst, the three components showed an increase in the conversion as temperature function. Notwithstanding, the majority of the o-DCB conversion was reached rapidly obtaining 85% at 400 °C while the NO and the CH_4 conversions rose slowly reaching higher NO values than CH4 between 150 and 500 °C. Only above 500 °C the conversion of CH_4 overcame the NO conversion. Aristizabal and coworkers [27] did not observe significant differences in the o-DCB conversions under dry or wet conditions over the Pd/Co–SZ catalytic system; however in this work we found a positive effect in the conversion and at 350 °C the conversion was near to 70%, in presence of CH_4 and NOx. This conversion of o-

DCB could be related to the strong metal-support interaction [73], as well to the effect of the NO_2 as oxidant.

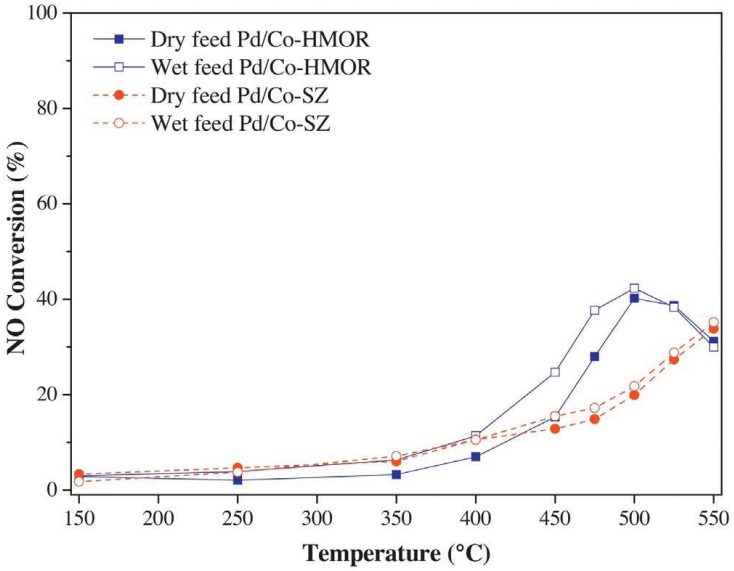

Fig. 8. NO reduction by CH_4 over Pd/Co–HMOR and Pd/Co–SZ catalysts simultaneously with o-DCB oxidation. Reaction conditions: [CH_4] = 4000 ppm, [NOx] = 1000 ppm, [o-DCB] =600 ppm, [O_2] = 10%, [H_2O] = 0 or 6%, GHSV= 60,000 h^{-1}.

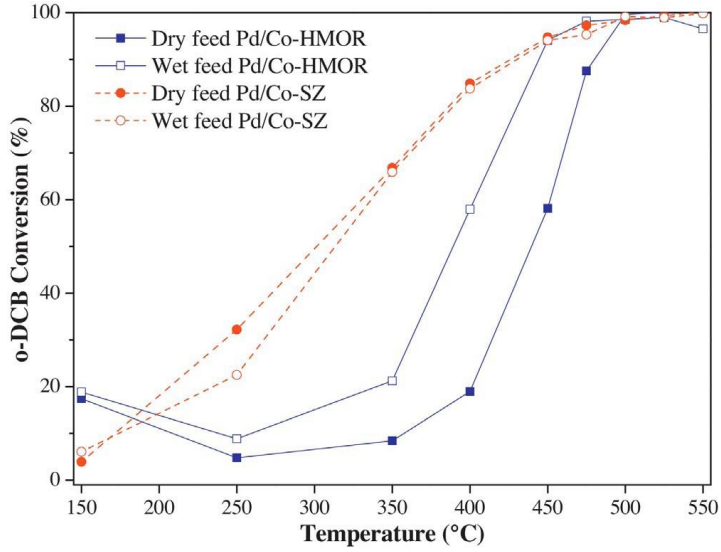

Fig. 9. o-DCB conversion over Pd/Co–HMOR and Pd/Co–SZ catalysts during NO SCR CH4. Reaction conditions: [CH_4] =4000 ppm, [NOx]= 1000 ppm, [o-DCB] = 600 ppm, [O2] = 10%, [H_2O] = 0 or 6%, GHSV =60,000 h^{-1}.

One of the main cause of deactivation of Pd catalysts in the catalytic oxidation of chlorinate compounds is generally attributed to the strong adsorption of chlorine on Pd surface, but the abundant surface hydroxyl groups of ZrO_2 support may act as the adsorption sites to transfer chlorine from the Pd surface, which alleviates the detrimental effects from chlorine adsorption on the Pd surface [73] and may explain the catalytic stability observed for the o-DCB oxidation. In the case of NO conversion (Fig. 9), a promotional effect of the temperature in the reduction reaction has been reported using palladium cobalt bimetallic sulfated zirconia [47]. However, in our research lower conversions were achieved when comparing the results at the same temperatures, which may due to either differences in Pd and Co loadings or to competitive reactions. Moreover, no a decrease effect was found in the NO conversion when water vapor was introduced in the feed stream [45,47,74]. The abrupt increment in the CH_4 conversion at 550 °C (Fig. 10) has been ascribed to the inhibiting effect of the water vapor into the Pd active sites [45], and the formation of cobalt oxides which favor the methane combustion. Formation of CO_2 and CO was detected in the system (Fig. 11), concentration of CO_2 increased significantly above 400 °C and it is higher with the Pd/Co-HMOR in agreement with the NOx, o-DCB and CH4 conversions. Below 400 °C the activity of both catalysts toward the reactions was low, consequently the concentration of CO and CO_2 in the outlet exhaust gas product stream was also poor, as expected. The production of CO in the case of Pd/Co-HMOR was higher at 475 °C (Fig. 11A) when conversion of CH_4 increased markedly. Above 500 °C the catalysts presented opposite behaviors regarding to the production of CO, in the case of Pd/Co-SZ the CO formation was favored at temperatures higher than 500 °C (Fig. 11B), inversely over Pd/Co-HMOR the production of CO decreased at elevated temperatures while the CO_2 production increased. Interesting, the CO_2 concentration increased while the CO concentration decreased by the presence of water up to 500 °C in the case of Pd/Co-HMOR catalyst. Evidently the water has a chemical influence in the activity and the product distribution over this catalyst, under wet condition besides of the hydrogens from the Brønsted acid sites of the catalyst, probably there are additional hydrogens sourced from the water which could participate in the reaction. On the other hand, not significant differences in the CO_2 and CO production between dry and wet condition were found in the case of Pd/Co-SZ.

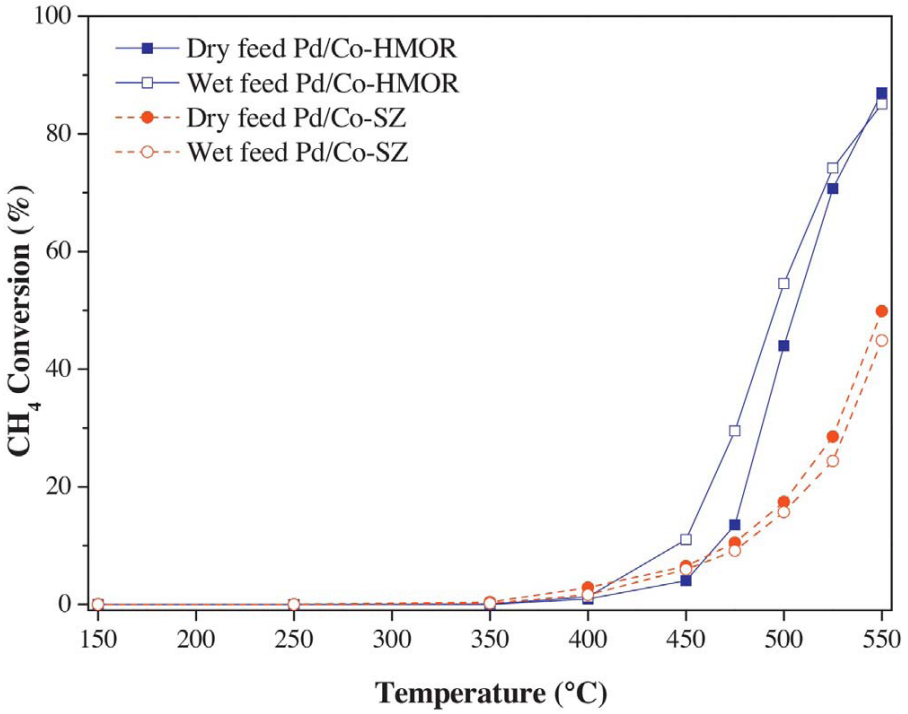

Fig. 10. CH_4 conversion over Pd/Co–HMOR and Pd/Co–SZ catalysts during NO SCR simultaneously with o-DCB oxidation. Reaction conditions: [CH_4] =4000 ppm, [NOx] = 1000 ppm, [o-DCB] =600 ppm, [O_2] =10%, [H_2O] =0 or 6%, GHSV =60,000 h^{-1}.

The Pd/Co-HMOR catalyst presented an optimum operation temperature at 500 °C for NO activity (Fig. 8), above this temperature the methane conversion increased considerably, and the NO conversion decayed indicating that methane combustion prevailed over the SCR of NO. At 550 °C although CH_4 conversion continued increasing o-DCB conversion was quite constant and NO conversion dropped. As was revealed by the TPR analysis, PdO was formed in the used Pd/Co–HMOR catalysts used under dry or wet conditions (Fig. 4A). PdO species have been widely associated with CH_4 combustion and it has a poor activity in the NO reduction [17,21,33,75]. Although, Adelman and coworkers [21] showed that formation of Pd^{2+} ions in Pd/H-ZSM-5 is favored by an oxidation reaction mixture of $CH_4 + NO_2 + O_2$ at 500 °C, in our case the Pd^{2+} ions were confirmed by TPR on fresh catalyst samples pretreated in an oxidation atmosphere (O_2 at 500 °C), however the used Pd/Co–HMOR catalysts showed peaks associated with PdO clusters, it appears that above 500 °C the oxidizing reaction

mixture (CH_4 + NO + NO_2 + o-DCB + O_2 + H_2O) turns Pd^{2+} into PdO clusters (Fig. 4A). The presence of strong Brønsted acid sites on protonic zeolites based catalysts has been associated with the oxidation activity of chlorinated hydrocarbons [29,36] and also with a high activity for CH_4–SCR of NOx of Pd–zeolite based catalysts [33,34], in this sense, the second desorption curve in the NH_3-TPD of Pd/Co–HMOR between 300 and 600 °C presenting a maximum at 441 °C is very likely that is due to the presence of Brønsted instead of Lewis acid sites in the protonic form of the zeolite (Fig. 3A), interestingly a remarkable enhance in the NO and o-DCB conversion in the temperature range between 400–500 °C which could be correlated with the presence of the strong acid sites in Pd/Co-HMOR as reveled the NH_3–TPD analysis (Fig. 3A). A similar relationship between the surface acidity and the catalytic activity for the combined NH_3-SCR of NO and o-DCB oxidation over a series of metal loaded ZSM5 (Cu/ZSM5, Fe/ZSM5, MnOx/ZSM5 and VOx/ZSM-5) catalysts was recently reported by Aranzabal and coworkers [48], as the authors also point out, it seems that the high amount of acid sites provided by the zeolite can be correlated with higher NO conversions [48,49]. The H_2–TPR peak at 646 °C in fresh Pd/Co–HMOR was shifted to 628 and 697 °C in used Pd/Co–HMOR under wet and dry conditions, respectively, which indicates a possible Co^{2+} ion migration to more accessible sites in the zeolite structure in the case of the catalyst evaluated under wet conditions, and may explain the higher catalytic activity for o-DCB oxidation compared with results under dry conditions (Fig. 9). Cobalt oxide phases formed in the used Pd/Co–HMOR has been proposed as active sites not only for o-DCB but also for CH_4 combustion and oxidation of NO which may explain the high performance of the catalyst towards o-DCB oxidation and the lower performance to NO reduction [24,27]. XRD patterns of used HMOR supported catalysts have revealed a loss of crystallinity in the zeolite framework structure at temperatures higher than 500 ºC; the relative losses in the crystallinity were calculated based on changes in peaks heights from XRD data. Pd/Co–HMOR used after 30 h in stream at 500 °C showed that the crystallinity remains almost unchanged; crystallinity losses were only 5 and 0.2% under wet and dry conditions respectively. However, in the case of the Pd/Co-HMOR used up to 550 °C the crystallinity losses were 88.2 and 88.8% under wet and dry conditions respectively. Probably the Al-O bonds in the zeolite framework can

be attacked by the HCl produced by o-DCB oxidation and may lead to the formation of volatile $AlCl_3$ causing the partial collapse of the zeolite framework structure [36].

Pd/Co-HMOR and Pd/Co-SZ showed highest activity performance at 500 and 550 °C respectively in lean and wet conditions, although in the temperature range from 250 to 400 °C, o-DCB oxidation over Pd/Co–SZ is higher than over Pd/Co–HMOR, above 400 °C not significant differences were found in the activity of both catalyst (Fig. 9). In the case of NO, Pd/Co–HMOR showed, in the temperature range of 450–525 °C, a considerable better catalytic activity than Pd/Co–SZ achieving the maximum (42.2%) at 500 °C, in the case of Pd/Co-SZ the maximum NO conversion was 35.2% at 550 °C (Fig. 8). According with these results a durability test for each catalyst was performed at the corresponding operation temperatures.

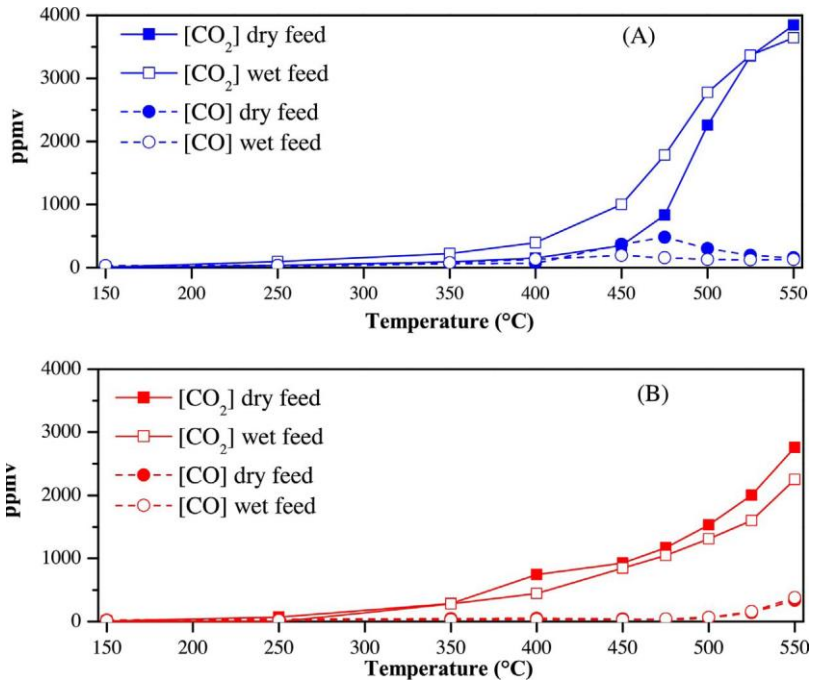

Fig. 11. CO_2 and CO outlet concentration over Pd/Co–HMOR and Pd/Co–SZ catalysts during NO SCR simultaneously with o-DCB oxidation (A) Pd/Co-HMOR and (B) Pd/Co-SZ. Reaction conditions: [CH_4] = 4000 ppm, [NOx] = 1000 ppm, [o-DCB] = 600 ppm, [O_2] = 10%, [H_2O] = 0 or 6%, GHSV =60,000 h^{-1}.

Results of the durability test for Pd/Co–HMOR are shown in Fig. 12. During the first 30 min of continuous reaction under wet conditions there was a noticeable increase in the o-DCB conversion moving from 86% to 97%, this improvement in the catalytic activity may be due to Co^{2+} ion migration to more accessible sites in the mordenite structure before the operation temperature was reached; however in the dry feed a conversion of 97% was collected just when the reactor achieved the operation temperature, this suggests that the presence of water in the feed slows down the Co^{2+} ion migration. After 30 h of continuous operation a slow decrease in the NO and CH_4 conversions were observed while activity towards o-DCB oxidation remains almost unchanged. Although PdO was formed in the used catalysts in the temperature range of 150–550 °C, this could not be found in the TPR (not shown) of the used Pd/Co-HMOR tested in the durability experiment.

The nature of Pd and Co species formed in this catalyst during the durability test will be subject of a next work. On the other hand, the durability test for Pd/Co–SZ catalyst (Fig. 13) revealed that o-DCB conversion remains also stable during the 30 h of operations; however, NO conversion abruptly decays after 1.5 h of continuous operation while the CH_4 conversion increases, this fact can be associated with the sulfate loss during the reaction.

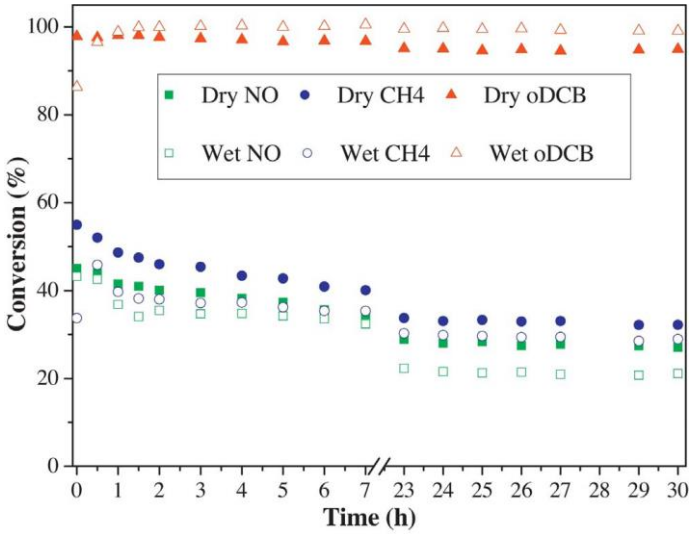

Fig. 12. Durability test for Pd/Co–HMOR catalyst. Reaction conditions: 500 °C, [CH_4] = 4000 ppm, [NOx] = 1000 ppm, [o-DCB] = 600 ppm, [O_2] = 10%, [H_2O] = 0 (fully black symbols) or 6% (open symbols), GHSV= 60,000 h^{-1}.

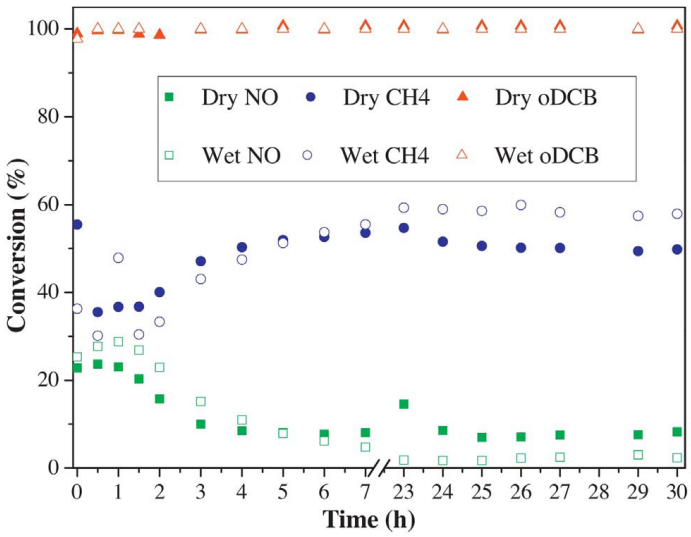

Fig. 13. Durability test for Pd/Co–SZ catalyst. Reaction conditions: 550 °C, [CH_4] = 4000 ppm, [NOx] = 1000 ppm, [o-DCB] = 600 ppm, [O_2] = 10%, [H_2O] =0 (fully black symbols) or 6% (open symbols), GHSV =60,000 h^{-1}.

4. Conclusions

Under the reaction conditions evaluated in this work it was found that at 500 ºC or higher temperatures, the presence of water does not affect significantly the o-DCB, NO, and CH_4 conversions with the Pd/Co catalysts. Activity of Pd/Co-SZ for o-DCB was relevant even at low temperatures (from 350 °C), in both dry and wet conditions. In both catalysts, the Co^{2+} ions revealed by H_2–TPR explains the high activity observed towards o-DCB oxidation. Presence of water in the feed slightly favors the activity of Pd/Co–HMOR towards o-DCB oxidation.

Independent of the catalysts NOx conversion was similar under dry and wet conditions. Used Pd/Co–SZ samples revealed the apparition of monoclinical phase related with the losses in the sulfate groups. Formation of PdO explains the catalytic deactivation of Pd/Co–HMOR for CH_4–SCR at reaction temperatures above 500 °C while losses in the sulfate groups present in Pd/Co–SZ can be correlated with the deactivation of this catalyst towards CH_4–SCR. Both catalysts present strong acid sites in the temperature range from 300 to 600 °C,

the same temperature range at which both catalysts were considerable active towards both reactions and suggest that the acidity of the support favors the catalytic activity. According with the durability tests, Pd/Co-HMOR was the most stable catalyst for the simultaneous reactions by 30 h.

Acknowledgments

The authors acknowledge financial support to Universidad de Antioquia, Universidad Nacional de Colombia sede Manizales, and Colciencias by the project 1115-569-33782 and the "Joven Investigador" program (645–2014). Part of this work was conducted during the Sabbatical Fellow of Professor Beatriz Aristizábal, sponsored by Universidad Nacional de Colombia Sede Manizales − Colombia.

Appendix A. Supplementary data

Supplementary data associated with this article can be found, in the online version, at http://dx.doi.org/10.1016/j.cattod.2017.05.049.

References

[1] R. Dvořák, P. Chlápek, D. Jecha, R. Puchýř, P. Stehlík, New approach to common removal of dioxins and NOx as a contribution to environmental protection, J. Clean. Prod. 18 (2010) 881–888, http://dx.doi.org/10.1016/j.jclepro.2010.01.024.

[2] G. McKay, Dioxin characterisation, formation and minimisation during municipal solid waste (MSW) incineration: review, Chem. Eng. J. 86 (2002) 343–368, http://dx.doi.org/10.1016/S1385-8947(01)00228-5.

[3] S. Squadrone, P. Brizio, R. Nespoli, C. Stella, M.C. Abete, Human dietary exposure and levels of polychlorinated dibenzo-p-dioxins (PCDDs), polychlorinated dibenzofurans (PCDFs), dioxin-like polychlorinated biphenyls (DL-PCBs) and non-dioxin like polychlorinated biphenyls (NDL-PCBs) in free-range eggs close to a s, Environ. Pollut. 206 (2015) 429–436, http://dx.doi.org/10.1016/j.envpol.2015.07.048.

[4] Y.-M. Chang, W.-P. Fan, W.-C. Dai, H.-C. Hsi, C.-H. Wu, C.-H. Chen, Characteristics of PCDD/F content in fly ash discharged from municipal solid waste incinerators, J. Hazard. Mater. 192 (2011) 521–529, http://dx.doi.org/10.1016/j.jhazmat.2011.05.055.

[5] J. Rivera-Austrui, M.A. Borrajo, K. Martinez, M.A. Adrados, M. Abalos, B. Van Bavel, J. Rivera, E. Abad, Assessment of polychlorinated dibenzo-p-dioxin and dibenzofuran emissions from a hazardous waste incineration plant using long-term sampling equipment, Chemosphere 82 (2011) 1343–1349, http://dx.doi.org/10.1016/j.chemosphere.2010.11.054.

[6] W. Liu, Z. Tian, H. Li, H. Xie, K. Xiao, C. Li, C. Tang, M. Zheng, Mono- to octa chlorinated PCDD/Fs in stack gas from typical waste incinerators and their implications on emission, Environ. Sci. Technol. 47 (2013) 9774–9780, http://dx.doi.org/10.1021/es402136s.

[7] G. Zhang, J. Hai, M. Ren, S. Zhang, J. Cheng, Z. Yang, Emission, mass balance, and distribution characteristics of PCDD/Fs and heavy metals during cocombustion of sewage sludge and coal in power plants, Environ. Sci. Technol. 47 (2013) 2123–2130, http://dx.doi.org/10.1021/es304127k.

[8] C.-C. Lee, T.-S. Shih, H.-L. Chen, Distribution of air and serum PCDD/F levels of electric arc furnaces and secondary aluminum and copper smelters, J. Hazard. Mater. 172 (2009) 1351–1356, http://dx.doi.org/10.1016/j.jhazmat.2009.07.148.

[9] S. Li, Y. Tian, Q. Ding, W. Liu, The release of persistent organic pollutants from a closed system dicofol production process, Chemosphere 94 (2014) 164–168, http://dx.doi.org/10.1016/j.chemosphere.2013.09.090.

[10] M.A. a. Gómez-García, V. Pitchon, a. Kiennemann, Pollution by nitrogen oxides: an approach to NO x abatement by using sorbing catalytic materials, Environ. Int. 31 (2005) 445–467, http://dx.doi.org/10.1016/j.envint.2004.09.006.

[11] L. Curtis, W. Rea, P. Smith-Willis, E. Fenyves, Y. Pan, Adverse health effects of outdoor air pollutants, J. Nutr. Environ. Med. 32 (2006) 815–830, http://dx.doi.org/10.1016/j.envint.2006.03.012.

[12] X. Wang, W. Wen, J. Mi, X. Li, R. Wang, The ordered mesoporous transition metal oxides for selective catalytic reduction of NOx at low temperature, Appl. Catal. B Environ. 176-177 (2015) 454–463, http://dx.doi.org/10.1016/j.apcatb.2015.04.038.

[13] J. Jones, J.R.H. Ross, The development of supported vanadia catalysts for the combined catalytic removal of the oxides of nitrogen and of chlorinated hydrocarbons from flue gases, Catal. Today 35 (1997) 97–105, http://dx.doi.org/10.1016/S0920-5861(96)00148-4.

[14] M. Goemans, P. Clarysse, J. Joannès, P. De Clercq, S. Lenaerts, K. Matthys, K. Boels, Catalytic NOx reduction with simultaneous dioxin and furan oxidation, Chemosphere 54 (2004) 1357–1365, http://dx.doi.org/10.1016/S0045-6535(03)00255-8.

[15] J. Lichtenberger, M.D. Amiridis, Deactivation of V_2O_5/TiO_2 catalysts during the oxidation of meta-dichlorobenzene in the presence of methyl-naphthalene, Catal. Today 98 (2004) 447–453, http://dx.doi.org/10.1016/j.cattod.2004.08.001.

[16] X. Cheng, X.T. Bi, A review of recent advances in selective catalytic NOx reduction reactor technologies, Particuology 16 (2014) 1–18, http://dx.doi.org/10.1016/j.partic.2014.01.006.

[17] H. Ohtsuka, T. Tabata, Effect of water vapor on the deactivation of Pd-zeolite catalysts for selective catalytic reduction of nitrogen monoxide by methane, Appl. Catal. B Environ. 21 (1999) 133–139, http://dx.doi.org/10.1016/S0926-3373(99)00014-4.

[18] M. Misono, Y. Nishizaka, M. Kawamoto, H. Kato, Progress in zeolite and microporous materials, Preceedings of the 11th International Zeolite Conference, Elsevier, 1997, http://dx.doi.org/10.1016/S0167-2991(97)80792-6.

[19] G. Koyano, S. Yokoyama, M. Misono, States of Pd in Pd/H-ZSM-5 and Pd/Na-ZSM-5 catalysts and catalytic activity for the reduction of NO by CH_4 in the presence of O_2, Appl. Catal. A Gen. 188 (1999) 301–312, http://dx.doi.org/10.1016/s0926-860x(99)00222-7.

[20] A.W. Aylor, L.J. Lobree, J.A. Reimer, A.T. Bell, Investigations of the dispersion of Pd in H-ZSM-5, J. Catal. 172 (1997) 453–462, http://dx.doi.org/10.1006/jcat.1997.1893.

[21] B.J. Adelman, W.M.H. Sachtler, The effect of zeolitic protons on NOx reduction over Pd/ZSM-5 catalysts, Appl. Catal. B Environ. 14 (1997) 1–11, http://dx.doi.org/10.1016/S0926-3373(97)00007-6.

[22] J. Armor, Catalytic reduction of nitrogen oxides with methane in the presence of excess oxygen: a review, Catal. Today 26 (1995) 147–158, http://dx.doi.org/10.1016/0920-5861(95)00134-2.

[23] Y. Li, Effect of water vapor on the selective reduction of NO by methane over cobalt-Exchanged ZSM-5, J. Catal. 142 (1993) 561–571, http://dx.doi.org/10.1006/jcat.1993.1231.

[24] F. Bustamante, F. Córdoba, M. Yates, C. Montes de Correa, The promotion of cobalt mordenite by palladium for the lean CH_4-SCR of NOx in moist streams, Appl. Catal. A Gen. 234 (2002) 127–136, http://dx.doi.org/10.1016/S0926-860X(02)00211-9.

[25] P. Budi, R.F. Howe, Steam deactivation of CoZSM-5 NOx reduction catalysts, Catal. Today 38 (1997) 175–179, http://dx.doi.org/10.1016/S0920-5861(97)00063-1.

[26] H. Uchida, K. Yamaseki, I. Takahashi, NOx reduction with methane over mordenite supported palladium catalyst, Catal. Today 29 (1996) 99–102, http://dx.doi.org/10.1016/0920-5861(95)00286-3.

[27] B.H. Aristizábal, C. Maya, C.M. de Correa, Ortho-dichlorobenzene oxidation over Pd/Co loaded sulfated zirconia and mordenite catalysts, Appl. Catal. A Gen. 335 (2008) 211–219, http://dx.doi.org/10.1016/j.apcata.2007.11.026.

[28] S. Krishnamoorthy, Catalytic oxidation of 1,2-dichlorobenzene over supported transition metal oxides, J. Catal. 193 (2000) 264–272, http://dx.doi.org/10.1006/jcat.2000.2895.

[29] B.H. Aristizábal, C.M. de Correa, A.I. Serykh, C.E. Hetrick, M.D. Amiridis, In situ FTIR study of the adsorption and reaction of ortho-dichlorobenzene over Pd promoted Co-HMOR, Microporous Mesoporous Mat. 112 (2008) 432–440, http://dx.doi.org/10.1016/j.micromeso.2007.10.020.

[30] B. Aristizabal, C. Montes de Correa, A. Serykh, C. Hetrick, M. Amiridis, In situ FTIR study of the adsorption and reaction of ortho-dichlorobenzene on Pd-Co sulfated zirconia catalysts, J. Catal. 258 (2008) 95–102, http://dx.doi.org/10.1016/j.jcat.2008.06.001.

[31] B.H. Aristizábal, Degradación catalítica de precursores de dioxinas y furanos, Universidad de Antioquia (2007).

[32] R.W. Van Den Brink, M. Krzan, M.M.R. Feijen-Jeurissen, R. Louw, P. Mulder, The role of the support and dispersion in the catalytic combustion of chlorobenzene on noble metal based catalysts, Appl. Catal. B Environ. 24 (2000) 255–264, http://dx.doi.org/10.1016/S0926-3373(99)00113-7.

[33] A. Ali, W. Alvarez, C.J. Loughran, D.E. Resasco, State of Pd on H-ZSM-5 and other acidic supports during the selective reduction of NO by CH4 studied by EXAFS/XANES, Appl. Catal. B Environ. 14 (1997) 13–22, http://dx.doi.org/10.1016/S0926-3373(97)00008-8.

[34] C.J. Loughran, D.E. Resasco, Bifunctionality of palladium-based catalysts used in the reduction of nitric oxide by methane in the presence of oxygen, Appl. Catal. B Environ. 7 (1995) 113–126, http://dx.doi.org/10.1016/0926-3373(95)00023-2.

[35] R.J.I. López-Fonseca Gutiérrez-Ortiz, A. Gutiérrez-Ortiz, J.R. González-Velasco, Catalytic oxidation of aliphatic chlorinated volatile organic compounds over Pt/HBETA zeolite catalyst under dry and humid conditions, Catal. Today 107–108 (2005) 200–207, http://dx.doi.org/10.1016/j.cattod.2005.07.091.

[36] R. López-Fonseca, A. Aranzabal, P. Steltenpohl, J. Gutiérrez-Ortiz, J. González-Velasco, Performance of zeolites and product selectivity in the gas-phase oxidation of 1,2-dichloroethane, Catal. Today 62 (2000) 367–377, http://dx.doi.org/10.1016/s0920-5861(00)00438-7.

[37] M.A. Larrubia, G. Busca, An FT-IR study of the conversion of 2-chloropropane, odichlorobenzene and dibenzofuran on V2O5-MoO3-TiO2 SCR-DeNOx catalysts, Appl. Catal. B Environ. 39 (2002) 343–352, http://dx.doi.org/10.1016/S0926-3373(02)00116-9.

[38] S. Scirè, M. Simona, C. Crisafulli, Pt catalysts supported on H-type zeolites for the catalytic combustion of chlorobenzene, Appl. Catal. B Environ. 45 (2003) 117–125, http://dx.doi.org/10.1016/S0926-3373(03)00122-X.

[39] K. Föttinger, K. Zorn, H. Vinek, Influence of the sulfate content on the activity of Pt containing sulfated zirconia, Appl. Catal. A Gen. 284 (2005) 69–75, http://dx.doi.org/10.1016/j.apcata.2005.01.019.

[40] Y.M. Sani, P.A. Alaba, A.O. Raji-Yahya, A.R. Abdul Aziz, W.M.A.W. Daud, Acidity and catalytic performance of Yb-doped SO^{2-}_4/Zr in comparison with SO^{2-}_4/Zr catalysts synthesized via different preparatory conditions for biodieselproduction, J. Taiwan Inst. Chem. Eng. 59 (2016) 195–204, http://dx.doi.org/10.1016/j.jtice.2015.07.016.

[41] B.T. Loveless, A. Gyanani, D.S. Muggli, Discrepancy between TPD- and FTIR-based measurements of Bronsted and Lewis acidity for sulfated zirconia, Appl. Catal. B Environ. 84 (2008) 591–597, http://dx.doi.org/10.1016/j.apcatb.2008.05.025.

[42] M. Ogura, Y. Sugiura, M. Hayashi, E. Kikuchi, Reduction of nitric oxide with methane on Pd/Co/H-ZSM-5 catalysts: cooperative effects of Pd and Co, Catal. Lett. 42 (1996) 185–189, http://dx.doi.org/10.1007/BF00810686.

[43] M. Ogura, S. Kage, T. Shimojo, J. Oba, M. Hayashi, M. Matsukata, E. Kikuchi, Co cation effects on activity and stability of isolated Pd(II) cations in zeolite matrices for selective catalytic reduction of nitric oxide with methane, J. Catal. 211 (2002) 75–84, http://dx.doi.org/10.1016/S0021-9517(02)93722-X.

[44] J.a.Z. Pieterse, R.W. Van Den Brink, S. Booneveld, F.a. De Bruijn, Influence of zeolite structure on the activity and durability of Co-Pd-zeolite catalysts in the reduction of NOx with methane, Appl. Catal. B Environ. 46 (2003) 239–250, http://dx.doi.org/10.1016/S0926-3373(03)00213-3.

[45] C. Quincoces, S. Guerrero, P. Araya, M. Gonzalez, Effect of water vapor over Pd-Co/SZ catalyst for the NO selective reduction by methane, Catal. Commun. 6 (2005) 75–80, http://dx.doi.org/10.1016/j.catcom.2004.11.002.

[46] A.A. Rubert, C.E. Quincoces, A. Mamede, D. Gazzoli, C. Cabello, M. Gloria González, Preparation and characterization of Pd-Co/sulfated zirconia catalysts for no selective reduction by methane, Catal. Commun. 9 (2008) 1096–1100, http://dx.doi.org/10.1016/j.catcom.2007.10.031.

[47] L.F. Córdoba, W.M.H. Sachtler, C. Montes de Correa, NO reduction by CH_4 over Pd/Co-sulfated zirconia catalysts, Appl. Catal. B Environ. 56 (2005) 269–277, http://dx.doi.org/10.1016/j.apcatb.2004.09.012.

[48] M. Gallastegi-Villa, A. Aranzabal, J.A. González-Marcos, J.R. González-Velasco, Metal-loaded ZSM5 zeolites for catalytic purification of dioxin/furans and NOx containing exhaust gases from MWI plants: effect of different metal cations, Appl. Catal. B Environ. 184 (2016) 238–245, http://dx.doi.org/10.1016/j.apcatb.2015.11.006.

[49] M. Gallastegi-Villa, A. Aranzabal, J.A. González-Marcos, J.R. González-Velasco, Tailoring dual redox-acid functionalities in VOx/TiO_2/ZSM5 catalyst for simultaneous abatement of PCDD/Fs and NOx from municipal solid waste incineration, Appl. Catal. B Environ. 205 (2017) 310–318, http://dx.doi.org/10.1016/j.apcatb.2016.12.020.

[50] R. Weber, T. Sakurai, H. Hagenmaier, Low temperature decomposition of PCDD/PCDF, chlorobenzenes and PAHs by TiO2-based V_2O_5–WO_3 catalysts, Appl. Catal. B Environ. 20 (1999) 249–256, http://dx.doi.org/10.1016/S0926-3373(98)00115-5.

[51] a. Kubacka, J. Janas, E. Włoch, B. Sulikowski, Selective catalytic reduction of nitric oxide over zeolite catalysts in the presence of hydrocarbons and the excess of oxygen, Catal. Today 101 (2005) 139–145, http://dx.doi.org/10.1016/j.cattod.2005.01.011.

[52] J. Regalbuto, T. Zheng, J. Miller, The bifunctional reaction pathway and dual kinetic regimes in NOx SCR by methane over cobalt mordenite catalysts, Catal. Today 54 (1999) 495–505, http://dx.doi.org/10.1016/S0920-5861(99)00212-6.

[53] N. Li, A. Wang, L. Li, X. Wang, L. Ren, T. Zhang, NO reduction by CH_4 in the presence of excess O_2 over Pd/sulfated alumina catalysts, Appl. Catal. B Environ. 50 (2004) 1–7, http://dx.doi.org/10.1016/j.apcatb.2003.10.009.

[54] C. Montes De Correa, F. Córdoba Castrillón, Supported bimetallic Pd-Co catalysts: characterization and catalytic activity, J. Mol. Catal. A Chem. 228 (2005) 267–273, http://dx.doi.org/10.1016/j.molcata.2004.09.033.

[55] L.F. Córdoba, G.A. Fuentes, C.M. de Correa, Characterization of bimetallic Pd/Co-HMOR used for the CH_4-SCR of NOx, Microporous Mesoporous Mat. 77 (2005) 193–201, http://dx.doi.org/10.1016/j.micromeso.2004.09.003.

[56] H. Ohtsuka, The selective catalytic reduction of nitrogen oxides by methane on noble metal-loaded sulfated zirconia, Appl. Catal. B Environ. 33 (2001) 325–333, http://dx.doi.org/10.1016/S0926-3373(01)00190-4.

[57] L.M. Martínez T, C. Montes de Correa, J.A. Odriozola, M.A. Centeno, Synthesis and characterization of sol-gel zirconia supported Pd and Ni catalysts, Catal. Today 107-108 (2005) 800–808, http://dx.doi.org/10.1016/j.cattod.2005.07.012.

[58] D.A. Ward, E.I. Ko, Sol-gel synthesis of zirconia supports: important properties for generating n-butane isomerization activity upon sulfate promotion, J. Catal. 157 (1995) 321–333, http://dx.doi.org/10.1006/jcat.1995.1297.

[59] A. Hofmann, J. Sauer, Surface structure of hydroxylated and sulfated zirconia. A periodic density-functional study, J. Phys. Chem. B 108 (2004) 14652–14662, http://dx.doi.org/10.1021/jp049220f.

[60] K. Föttinger, E. Halwax, H. Vinek, Deactivation and regeneration of Pt containing sulfated zirconia and sulfated zirconia, Appl. Catal. A Gen. 301 (2006) 115–122, http://dx.doi.org/10.1016/j.apcata.2005.11.024.

[61] H. Wang, B. Li, X. Lu, C. Li, F. Ding, Y. Song, Selective catalytic reduction of NO by methane over the Co/MOR catalysts in the presence of oxygen, J. Fuel Chem. Technol. 43 (2015) 1106–1112, http://dx.doi.org/10.1016/S1872-5813(15)30033-5.

[62] A.M. de Oliveira, I.M. Baibich, N.R.C.F. Machado, M.L. Mignoni, S.B.C. Pergher, Decomposition of nitric oxide on Pd-mordenite, Catal. Today 133-135 (2008) 560–564, http://dx.doi.org/10.1016/j.cattod.2007.12.100.

[63] T. Yamamoto, T. Tanaka, S. Takenaka, S. Yoshida, T. Onari, Y. Takahashi, T. Kosaka, S. Hasegawa, M. Kudo, Structural analysis of iron and manganese species in iron- and manganese-promoted sulfated zirconia, J. Phys. Chem. B 103 (1999) 2385–2393, http://dx.doi.org/10.1021/jp984378j.

[64] W. Chen, H. Ko, A. Sakthivel, S. Huang, S.-H. Liu, A.-Y. Lo, T.-C. Tsai, S.-B. Liu, A solid-state NMR, FT-IR and TPD study on acid properties of sulfated and metal promoted zirconia: influence of promoter and sulfation treatment, Catal. Today 116 (2006) 111–120, http://dx.doi.org/10.1016/j.cattod.2006.01.025.

[65] N. Li, A. Wang, M. Zheng, X. Wang, R. Cheng, T. Zhang, Probing into the catalytic nature of Co/sulfated zirconia for selective reduction of NO with methane, J. Catal. 225 (2004) 307–315, http://dx.doi.org/10.1016/j.jcat.2004.04.026.

[66] E.M. Holmgreen, M.M. Yung, U.S. Ozkan, Pd-based sulfated zirconia prepared by a single step sol-gel procedure for lean NOx reduction, J. Mol. Catal. A Chem. 270 (2007) 101–111, http://dx.doi.org/10.1016/j.molcata.2007.01.030.

[67] T.K. Phung, G. Busca, On the Lewis acidity of protonic zeolites, Appl. Catal. A Gen. 504 (2015) 151–157, http://dx.doi.org/10.1016/j.apcata.2014.11.031.

[68] X. Wang, H.-Y. Chen, W.M.H. Sachtler, Catalytic reduction of NOx by hydrocarbons over Co/ZSM-5 catalysts prepared with different methods, Appl. Catal. B Environ. 26 (2000) L227–L239, http://dx.doi.org/10.1016/S0926-3373(00)00125-9.

[69] B. Wen, J. Jia, S. Li, T. Liu, L.X. Chen, W.M.H. Sachtler, Synergism of cobalt and palladium in MFI zeolite of relevance to NO reduction with methane, Phys. Chem. Chem. Phys. 4 (2002) 1983–1989, http://dx.doi.org/10.1039/b111200g.

[70] P. Drozdzewski, A. Brozyna, M. Kubiak, T. Lis, Synthesis, structure and vibrational spectroscopy of palladium(II) complexes with 2-thiophenecarboxylic hydrazide (tch): Crystal structure of $[PdCl_2(tch)_2]2dmf$, Vib. Spectrosc. 40 (2006) 118–126, http://dx.doi.org/10.1016/j.vibspec.2005.07.007.

[71] P.M. Fechner, S. Wartewig, M. Füting, A. Heilmann, R.H.H. Neubert, P. Kleinebudde, Properties of microcrystalline cellulose and powder cellulose after extrusion/spheronization as studied by fourier transform Raman spectroscopy and environmental scanning electron microscopy, AAPS PharmSci. 5 (2003), http://dx.doi.org/10.1208/ps050431 (E31).

[72] S. Gao, X. Chen, H. Wang, J. Mo, Z. Wu, Y. Liu, X. Weng, Ceria supported on sulfated zirconia as a superacid catalyst for selective catalytic reduction of NO with NH_3, J. Colloid Interface Sci. 394 (2013) 515–521, http://dx.doi.org/10.1016/j.jcis.2012.12.034.

[73] Y. Shao, Z. Xu, H. Wan, H. Chen, F. Liu, L. Li, S. Zheng, Influence of ZrO_2 properties on catalytic hydrodechlorination of chlorobenzene over Pd/ZrO_2 catalysts, J. Hazard. Mater. 179 (2010) 135–140, http://dx.doi.org/10.1016/j.jhazmat.2010.02.070.

[74] C. Quincoces, A. Rubert, P. Araya, D. Gazzoli, M.G. González, Characterization of Co/sulfated zirconia catalysts for selective reduction of NO by methane, Catal. Commun. 10 (2008) 74–78, http://dx.doi.org/10.1016/j.catcom.2008.07.037.

[75] M. Ogura, Determination of active palladium species in ZSM-5 zeolite for selective reduction of nitric oxide with methane, Appl. Catal. B Environ. 23 (1999) 247–257, http://dx.doi.org/10.1016/S0926-3373(99)00082-X.

Chapter 4 Kinetic study

4.1 Analysis of diffusional limitations

The kinetic study with a solid catalyst requires certain operational conditions for guarantee than the reaction step on the catalyst surface is the slowest of the entire physicochemical process, ensuring that the experimental reaction rate corresponds to the intrinsic reaction kinetic.

The external mass transfer occurs between a fluid and the catalyst surface through the external boundary layer surrounding the pellet. The rate of the external mass transfer is proportional to the product of the concentration gradient and the mass transfer coefficient according to the Equation 4-1 [182]:

$$Rate = k_C(C_{Ab} - C_{As}) \quad \text{Equation 4-1}$$

Where:

C_{Ab}: Bulk concentration of reactant A [kmol/m^3]

C_{As}: Concentration of reactant A at the external surface of the pellet [kmol/m^3]

k_C: Mass transfer coefficient, given by Equation 4-2 [m/s]

$$k_C = \frac{D_{AB}}{\delta} \quad \text{Equation 4-2}$$

Where:

D_{AB}: Coefficient of diffusion [m^2/s]

δ: Boundary layer thickness [m].

The Equation 4-2 shows that the mass transfer coefficient is inversely proportional to the boundary layer thickness and directly proportional to the coefficient of diffusion. When the velocity of the fluid over the catalyst is low, the boundary layer trends to be thick, but as the fluid velocity across the catalyst increases, the boundary layer decreases, consequently the mass transfer coefficient increases. At very high velocities the boundary layer is so small, hence it will not offer any resistance to the diffusion across the boundary layer, in this conditions $C_{Ab} \approx C_{As}$, hence there are not significant concentration gradients between the bulk fluid and the catalyst surface particle [182].

The absence of the external mass transfer limitations was carried out experimentally according to the procedure described in the section 2.5.2, the results are shown in the Figure 31. No changes in the reaction rate value of the NO and *o*-DCB disappearance were observed for volumetric rate values greater than 250 mL/min. Therefore, it can be guaranteed the absence of external mass transfer limitations for volumetric flows greater than 250 mL/min having a GHSV of 90000 h^{-1} or greater.

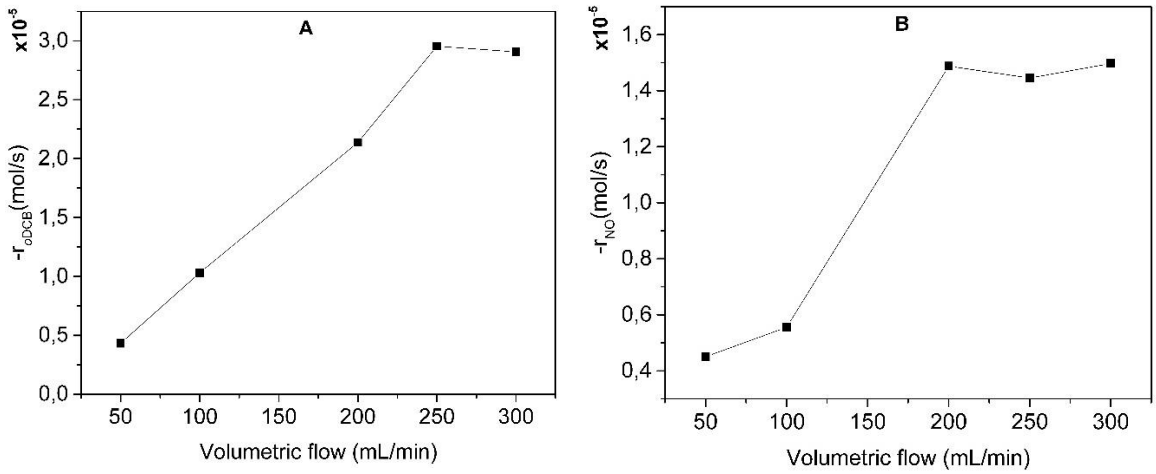

Figure 31 Reaction rates at 500 ºC varying the volumetric flow of the reactants A) For *o*-DCB oxidation and B) For the CH_4-SCR.

On the other hand, the internal diffusion occurs inside the pores of the catalyst, between the particle surface and the active sites inside the catalyst pores. In general, the catalysts pores are not perfectly straight, and the internal diffusion or the reactants is highly dependent on their morphology. In large particle size catalysts, the diffusion of the reactants to the interior

pores take time and they react only with the active sites near to the surface while the center of the catalyst particle remains untouched (wasted catalyst). As the catalyst particles size decrease, the diffusion time of the reactants to the interior also decrease until the internal diffusion no longer limits the rate of reaction [182]. If the activity of a catalyst is affected by altering the pellet size, this activity is influenced by pore diffusion [190].

The absence of the internal mass transfer limitations was experimentally tested according to the procedure described in the section 2.5.3. The particle diameter was varied in the range between 0.10 and 0.51 mm, the results are shown in the Figure 32. As can be evidenced, there are no significant changes in the reaction rate for particles diameter smaller than 0.21 and 0.33 mm for *o*-DCB oxidation and CH_4-SCR, respectively. According to this, the absence of internal diffusion limitations can be guaranteed for catalysts particles sizes equal or lower than 0.21 mm.

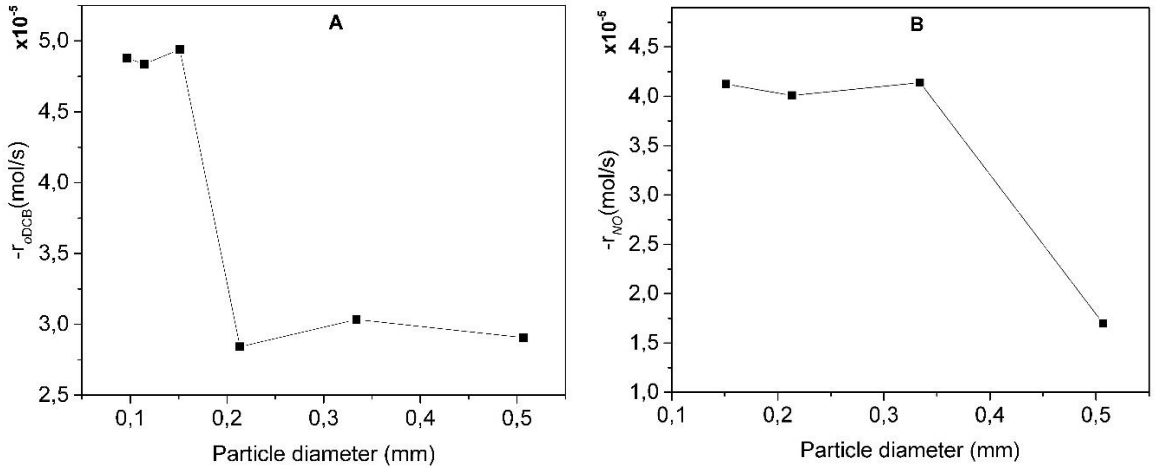

Figure 32 Reaction rates at 500 ºC varying the particle diameter in the A) For *o*-DCB oxidation and B) For the CH_4-SCR.

4.2 Analysis of kinetic parameters

4.2.1 Effect of the oxygen and water in the apparent activation energy for CH_4-SCR

In the Figure 33 is shown the effect of the water and oxygen in the apparent activation energy for the NO reduction by CH_4. In all cases, the value of the Pearson correlation coefficient was so close to –1 indicating a strong negative linear correlation between the $\ln(-r_{NO})$ and

$\frac{1}{T}$, as expected [182]. Under dry conditions Figure 33 A and B, the presence of 10% of O_2 significantly decreases the activation energy from 13 to 5 kcal/mol which suggests that the NO reduction is favored by the presence of O_2 in the feed. According to the *in-situ* FTIR experiments (see section 3.2.3.1) the oxygen participates in the first step of the CH_4-SCR over Co-α ions by the transforming the Co^{2+}–$(NO)_2$ nitrosyl species into adsorbed Co^{2+}–(NO_2) complexes, these complexes seems to play a key role in activating the CH_4 molecules by an Eley-rideal mechanism; that fact can probably decrease the apparent activation energy by the addition of oxygen to the feed under dry conditions.

The effect of the water in the activation energy for the NO reduction by CH_4 in the presence and absence of oxygen was also analyzed, the results are shown in Figure 33 C and D. In the absence of oxygen, the presence of water considerably increases the apparent activation energy by a factor of 4.5 rising from 13 to 59 kcal/mol. On the other hand, under lean conditions the presence of water increases by a factor of 3.6 the apparent activation energy from 5 to 18 kcal/mol. Cordoba has reported [257] an increase by a factor of 1.2 in the apparent activation energy of the CH_4-SCR over a Pd/Co-SZ catalyst because the addition of water, the reported values were 19.7 to 22.7 kcal/mol under dry and wet conditions, respectively. Li et al found [258] that the apparent activation energy of the NO reduction by CH_4 over a Co-FER catalyst is increased by a factor of 1.5 from 22 to 34 kcal/mol by the addition of water to the feed. Comparing the results obtained with these previous reports, it seems that the Pd/Co-HMOR catalyst is more sensible to the presence of water. The suppressing effect of the H_2O in the NO reduction has been also evidenced [97,199,200] by the decrease of the CH_4-SCR activity over other catalysts, Azambre et al [199] have suggested that such decrease is due to an inhibition effect on the NO adsorption.

There are different values reported in the literature for the apparent activation energy of the CH_4-SCR over different catalytic systems. Campa et al reported [259] values of 72 ± 5 kJ/mol (17.2 ± 1.2 kcal/mol) over a series of Mn-ZSM-5 catalysts with different Mn loading and found that the apparent activation energy was independent of the Mn loading. She et al [260] obtained a value of 113 kJ/mol (27 kcal/mol) over an Ag-alumina catalyst and Lukyanov et al reported [261] a value of 21 kcal/mol over a Co-ZSM-5 catalyst.

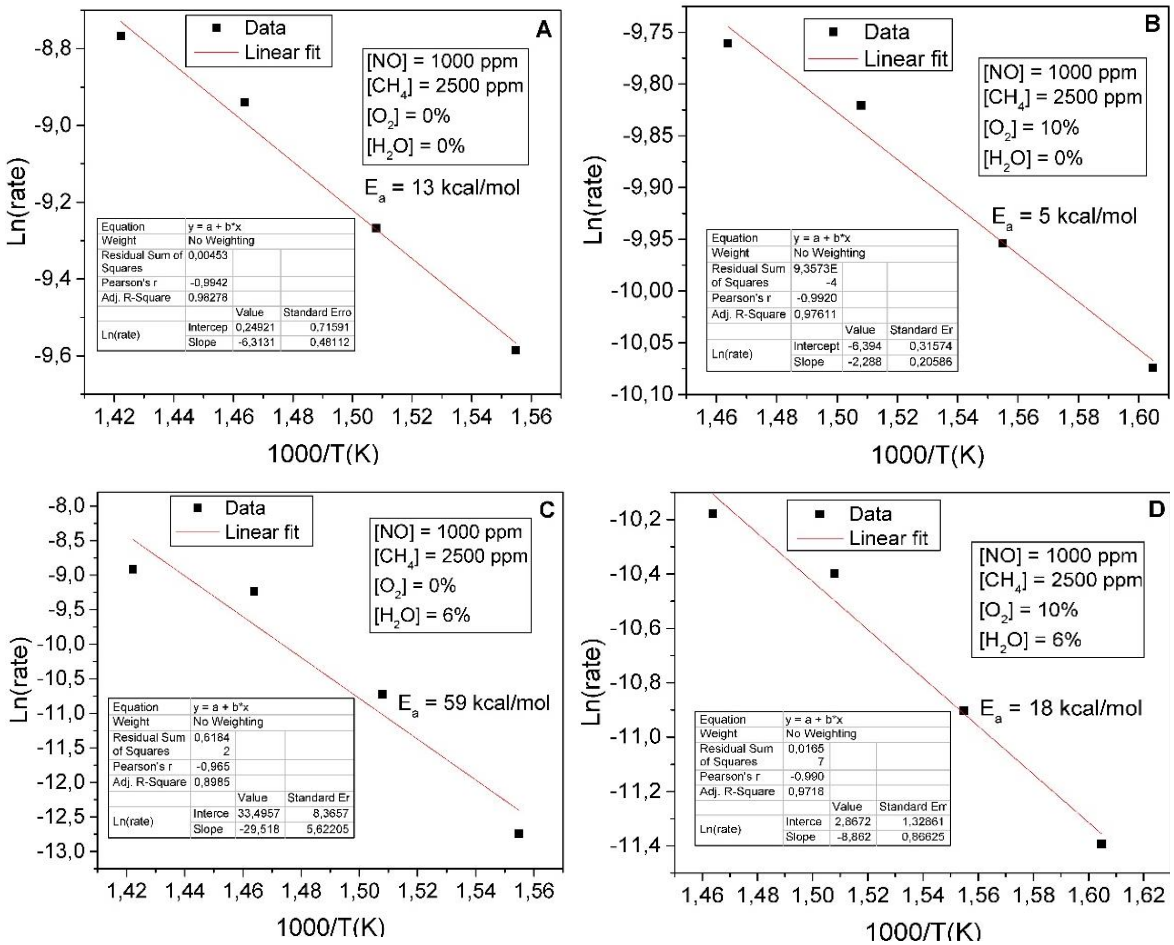

Figure 33 Effect of the H_2O and O_2 in the activation energy for NO reduction over Pd/Co-HMOR. A: In the absence of oxygen and water, B: With oxygen in the absence of water, C: Without oxygen in the presence of water, D: In the presence of oxygen and water.

4.2.2 Effect of water in the activation energy for o-DCB oxidation

The apparent activation energies for *o*-DCB oxidation under dry and wet conditions are shown in the Figure 34 A and B. The Pearson correlation was also very close to –1 indicating the good negative linear correlation between both variables. Under dry conditions (see Figure 34 A), the apparent activation energy observed was 8 kcal/mol, the addition of 6% H_2O to the feed (see Figure 34 B) resulted in a slightly increase to 12 kcal/mol. Similar values have been reported in the literature for the *o*-DCB oxidation over different catalytic systems. Ma et al reported [262] an apparent activation energy of 21.6 kJ/mol (5.2 kcal/mol) over Ca-

doped FeOx catalyst and Krisnamoorthy et al [263] have reported values from 45 to 53 kJ/mol (10.8-12.7 kcal/mol) over V_2O_5/Al_2O_3 catalysts with different vanadium loading (3.2 to 7.2%). Over a Pd/Co-SZ catalyst, Aristizábal reported [127] a value of 27 kJ/mol (6.5 kcal/mol) for the same reaction under dry conditions which is so close to the value found here over Pd/Co-HMOR catalyst under similar conditions.

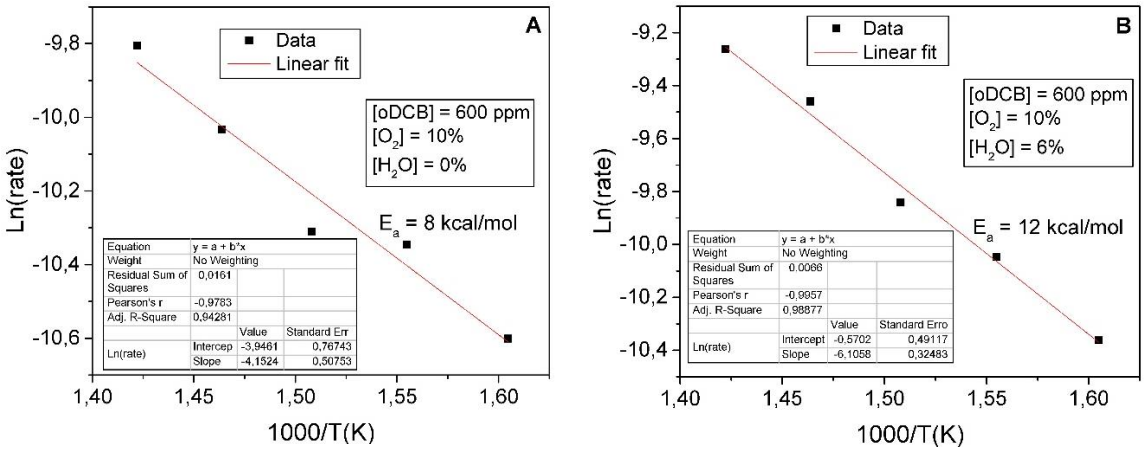

Figure 34 Effect of the H_2O in the activation energy for *o*-DCB oxidation. A: In the absence of H_2O, B: In the presence of 6% of H_2O.

4.2.3 Apparent activation energies during combined CH_4-SCR and o-DCB oxidation

The apparent activation energy for each reaction during the combined *o*-DCB oxidation and CH_4-SCR are shown in Figure 35. The results for both reactions are quite similar to the obtained previously for the independent reactions. Although the *in-situ* FTIR experiments revealed that Co^{2+} ions can catalyze both reactions, the similar values in the apparent activation energies between the single and combined reactions suggests non interferes between the reactions and that they occur independently in presence of water and oxygen in excess.

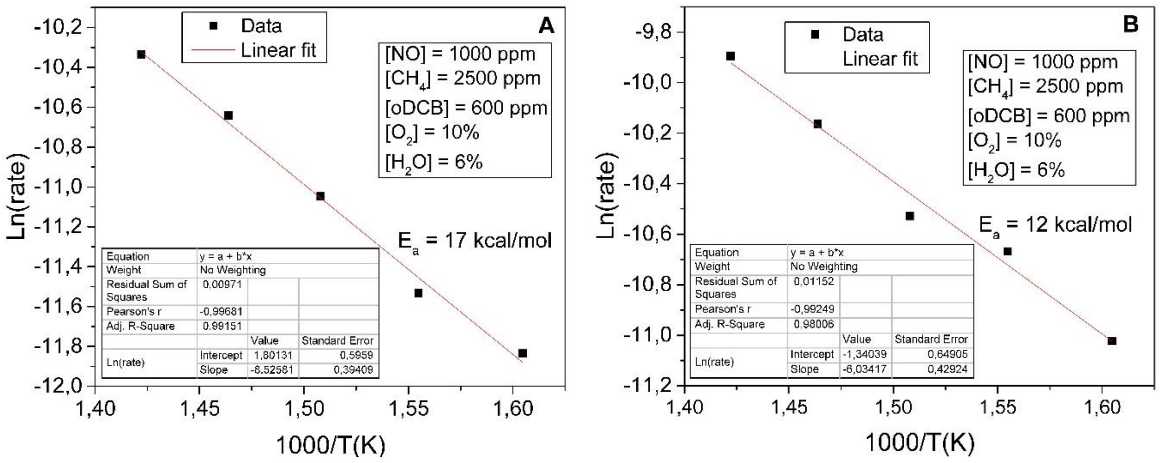

Figure 35 Effect of the simultaneous reactions in the activation energies for the NO reduction and the *o*-DCB oxidation in the presence of water and under lean conditions.

4.3 Influence of the combined reactions on the individual reaction rates

4.3.1 Effect of the o-DCB oxidation in the CH_4-SCR

The single CH_4-SCR reaction in the presence of water and oxygen in excess was evaluated between 400 and 525 °C, which corresponds to the temperature range with the most significant conversions during the simultaneous reactions. Similarly, the combined CH_4-SCR and *o*-DCB oxidation reactions were carried out under the same temperature range and conditions. The performance of both reactions (single and combined) were compared in terms of the rate of disappearance of NO, the results are shown in Figure 36. The reaction rate disappearance profile of the single CH_4-SCR exhibits a typical volcano-shaped behavior very similar to the previously found during the simultaneous *o*-DCB oxidation (see Figure 13) with a maximum reaction rate at 500 ºC. In previous studies [198,199] very similar conversion-temperature profiles have been reported for the single CH_4-SCR reaction over Pd based catalysts.

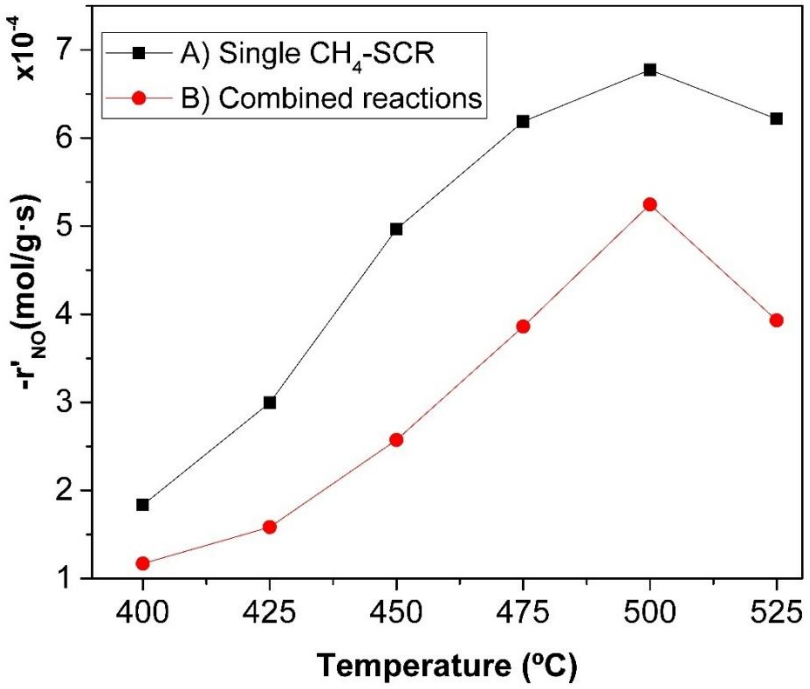

Figure 36 Reaction rates of the NO disappearance for **A)** [NO] = 1000 ppm, [NO_2] = 111 ppm, [CH_4] = 2500 ppm, [H_2O] = 6%, [O_2] = 10% and **B)** [NO] = 1000 ppm, [NO_2] = 111 ppm, [CH_4] = 2500 ppm, [*o*-DCB] = 600 ppm [H_2O] = 6%, [O_2] = 10%. GHSV = 150 000 h^{-1}

During the simultaneous reactions, the rate of disappearance of NO was lower than the observed in the single CH_4-SCR reduction under the same conditions for the temperature range tested, at 500 ºC the decrease in the reaction rate was of about 22.5% regards to the single CH_4-SCR reaction. According to the *in-situ* FTIR study, both reactions occurs with the participation of Co^{2+} Lewis sites and Brønsted acid sites, therefore the decrease in the reaction rate strongly suggests a competition between *o*-DCB and NO molecules for common active sites for the reactions.

4.3.2 Effect of CH_4-SCR on the oxidation reaction rate of *o*-DCB

The rate of *o*-DCB disappearance during the single oxidation was compared with the obtained in the simultaneous reactions in order to analyze the effect of the CH_4-SCR reaction on the *o*-DCB oxidation, the results are shown in the Figure 37. The reaction rate profiles of the single *o*-DCB oxidation and the obtained during the simultaneous reactions are quite similar and consistent with the previous results (see Figure 13) in terms of *o*-DCB conversions. It was observed a marked decrease in the reaction rate of *o*-DCB disappearance during the simultaneous reactions compared to the observed for the single *o*-DCB oxidation under the same reaction conditions, at 500 ºC such decrease was about 50%. The decrease in the reaction rate for *o*-DCB oxidation in presence of CH_4 and NO confirms the competence between NO and *o*-DCB for the active sites in the catalyst, the higher reaction rate decrease regards to the obtained for the rate of NO disappearance for the CH_4-SCR reaction (section 4.3.1) probably due to the concentration difference between NO and *o*-DCB. Similarly, Gallastegi-Villa et al [264] have reported lower conversions for NO and *o*-DCB over a VOx/TiO_2 catalyst when are co-feed together regarding the separate CH_4-SCR and *o*-DCB oxidation, they suggest also that the decrease in the conversion can be due to a possible competition of both reactions on the same active sites, specifically on the acid sites. Over a V_2O_5-WO_3/TiO_2 catalyst, Liu et al [26] have also reported a weak competitive adsorption between PCDD/Fs and NH_3 during the simultaneous catalytic oxidation of PCDD/Fs and NH_3-SCR reaction which slightly inhibits the PCDD/Fs decomposition.

4.4 Approximation to reaction rate laws

4.4.1 Approximation to reaction rate law for *o*-DCB oxidation

The kinetic parameters for *o*-DCB oxidation were calculated by fitting the experimental data to the Equation 2-22 by classical least squares. The data were treated in the statistic software R version 3.4.2, as was described in section 2.5.4.1, the results are shown in the Table 5. According to the coefficient of determination, 93.9% of the variability of the experimental reaction rate is explained by the *o*-DCB concentration. The *p*-value was lower than 0.05 indicating that the *o*-DCB concentration is a significant parameter to explain the reaction

rate. Replacing the reaction order and the specific reaction rate constant on Equation 2-21 it is obtained the reaction rate law for *o*-DCB disappearance:

$$-r'_{\mathrm{o-DCB}} = 5.12 \text{ x } 10^{-4} \cdot C_{o-DCB}^{0.7} \quad \text{Equation 4-3}$$

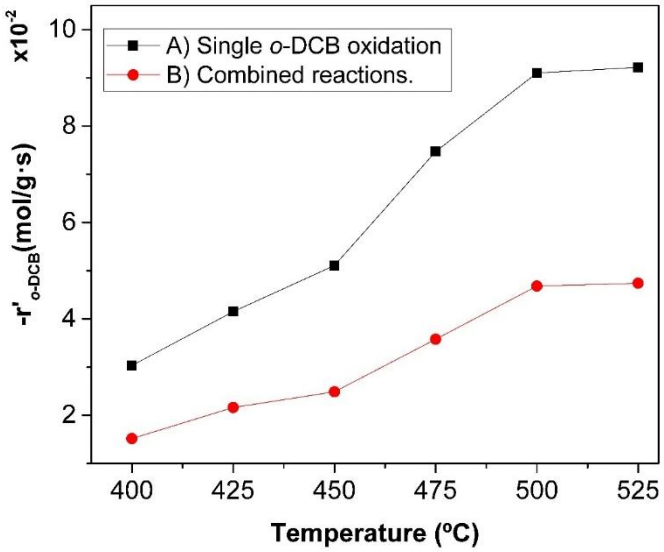

Figure 37 Reaction rates of the NO disappearance for **A)** [NO] = 1000 ppm, [CH_4] = 2500 ppm, [H_2O] = 6%, [O_2] = 10% and **B)** [NO] = 1000 ppm, [CH_4] = 2500 ppm, [*o*-DCB] = 600 ppm [H_2O] = 6%, [O_2] = 10%. GHSV = 150 000 h^{-1}

The reaction order regards to the *o*-DCB oxidation was 0.7 in the simultaneous reactions. In previous works values of 1.2 and 1.3 have been reported [29,83,263] for the single *o*-DCB oxidation over V_2O_5 supported on Al_2O_3 and TiO_2, respectively. These values were approximated to 1 and the reaction was considered as first order regards to the *o*-DCB concentration. Aristizábal reported [127] a reaction order of 1.5 for the single *o*-DCB oxidation over a Pd/Co-SZ catalyst. Although the differences in the catalytic systems, the reaction order here found is close to the reported in the literature even for the single *o*-DCB oxidation.

Table 5 Kinetic parameters *o*-DCB oxidation over Pd/Co-HMOR catalyst.

T (ºC)	k ($mol \cdot g^{-1} \cdot s^{-1} \cdot ppm^{-0.7}$)	Reaction order o-DCB	R-Squared	*p*-value
500	5.12×10^{-4}	0.70	0.9393	0.02041

4.4.2 Approximation to reaction rate law for CH_4-SCR

The reaction rate law for CH_4-SCR reaction was obtained as function of the NO and CH_4 concentrations, the experimental data were fitted to the Equation 2-22 by a multiple linear regression model according to the methodology described in section 2.5.4.2, the results are shown in Table 6. The coefficient of multiple determination shows that the 88.2% of the variability of the experimental reaction rate can be explained by the independent variables of the model, the NO and CH_4 concentrations. The p-value lower than 0.05 indicates a that the independent variables are significant for the model. The reaction rate law is obtained by replacing the parameters in Equation 2-23.

$$-r'_{NO} = 2.16 \times 10^{-8} \cdot C_{NO}^{0.89} \cdot C_{CH_4}^{0.56} \qquad \text{Equation 4-4}$$

The reaction order regards to the NO and CH_4 were 0.89 and 0.56 respectively indicating that the reaction rate increases with concentration of both compounds. Córdoba reported [257] reaction orders of 0.27 and 0.63 for NO and CH_4, respectively, over a Pd/Co-SZ catalyst. The reaction orders obtained in this work indicates that although over Pd/Co-HMOR the reaction rate depends on the concentration of both compounds, this dependence is stronger regards to the NO than the CH_4.

Table 6 Kinetic parameters for CH_4-SCR of NO over Pd/Co-HMOR catalyst.

T (ºC)	k ($mol \cdot g^{-1} \cdot s^{-1} \cdot ppm^{1.45}$)	Reaction order NO	Reaction order CH_4	Multiple R-squared	p-value
500	2.16 x 10-8	0.89	0.56	0.8827	0.0402

Chapter 5 Monolithic catalysts

A commercial cordierite monolith (Corning Inc.) was cut conveniently to obtain minimonoliths of 10 x 10 x 12 mm with 36 channels. The washcoated mini-monolithic reactors (Pd/Co-HMOR/m) were obtained after three immersion-blowing-drying cycles according to the procedure described in the section 2.2.3 in Figure 38 is presented the final aspect of a minimonolithic reactor. The percent of washcoated loading after each immersion cycle is shown in Figure 39, the washcoated loading was highly reproducible and the final average weight gain was of 16.7%.

Figure 38 Image of a cordierite mini-monolith washcoated with Pd-Co/HMOR

5.1.1 Resistance tests

The washcoated mini-monoliths samples were submitted to resistance tests which simulate the abrasive and high temperature conditions during the real process. Before and after each resistance test, the mini-monoliths samples were weight in order to analyze the strength of catalyst adhesion to the walls of the mini-monoliths based on washcoated weight losses.

Figure 39 Washcoat loading as function of the number of immersions for each minimonolith.

The percentage of washcoated weight losses after each resistance test are shown in the Figure 40. After the mechanical test (mini-monoliths treated for 1 h in ultrasonic vibration in an aqueous medium, see section 2.2.4) the weight losses were only of 2.5% which indicates a high mechanical resistance of the washcoated and suggesting a relative high adhesion of the catalysts particles to the walls of the mini-monoliths. The resistance to the thermal shock (see section 2.2.4) results in weight losses was only 1.0% which indicates a good resistance to the thermal shock of the washcoated catalyst. The mechanical test followed by thermal test resulted in weight losses of 3.9% while the thermal test followed by mechanical test result in losses of only 0.9%, this suggests that the heat treatment may appear to result in improved catalyst adhesion to the mini-monoliths walls, in accordance with previous reports [157]. The good catalyst adhesion to the walls of the mini-monoliths can be attributed to the high porosity of cordierite, this material offers many sites for the catalytic coating anchoring as has been previously reported [265].

5.1.2 Scanning electron microscopy and energy dispersive X-ray spectroscopy (SEM/EDS)

In the SEM micrographs (Figure 41 A and B) of bare cordierite mini-monoliths was evidenced the presence of homogenously distributed macropores along the channels walls, which confer to the mini-monoliths of a high internal porosity. These morphological characteristics favor the adhesion of the catalyst particles to the internal channels of the mini-

monoliths. It seems that the good results observed during the resistance tests can be largely explained by the morphological structure of the cordierite.

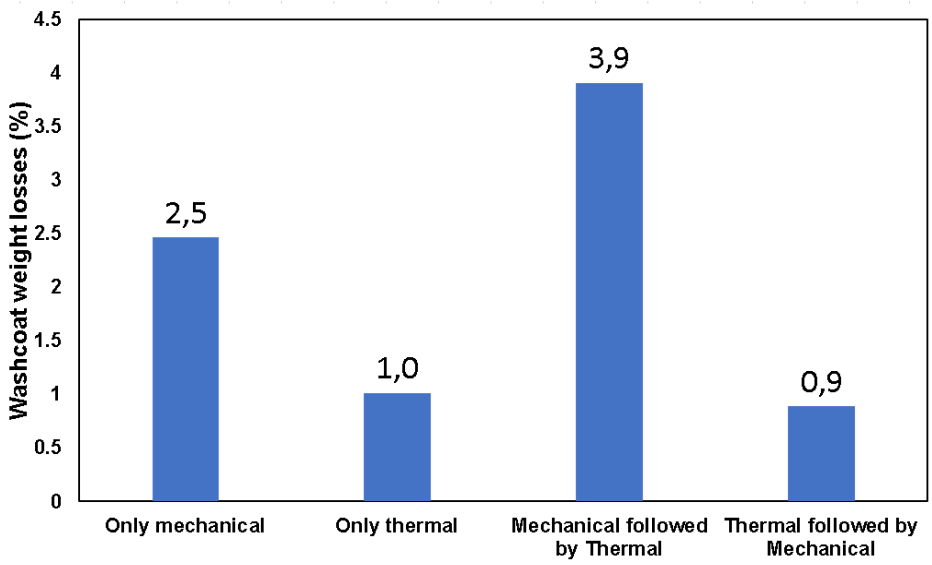

Figure 40 Percentage (%) of washcoat weight losses after each resistance test.

The coated morphology of Pd/Co-HMOR/m is shown in Figure 41 (C to F). The typical layered structure of the bare cordierite mini-monoliths is no longer observed in the images of the internal channels of the washcoated minimonoliths indicating a complete surface coverage of the cordierite with a thin layer of catalyst. Some cracks were observed close to the walls which were probably generated during the drying and calcination process. The catalyst layer thickness was not completely homogeneous along the mini-monolithic structure being a little thinner near the corners.

The chemical analysis determined by the EDS and the semi-quantitative results of the elements detected in the surface of the samples are shown in Figure 42. The surface of bare mini-monoliths (Figure 42 A and B) present elements such as O (51.27%), Mg (9.67%), Al (21.81%) and Si (27.62%) which are characteristics of a synthetic cordierite ($2MgO{\cdot}2Al_2O_3{\cdot}5SiO_2$), the EDS analysis of fresh washcoated minimonoliths (Figure 42 C and D) reveals the presence of elements as O (30.01%), Si (45.31%) and Al (6.76%), which are characteristic of the mordenite zeolite, the considerable decrease in the percentage of Mg to 0.34% regards to the 9.67% detected in the bare mini-monolith is due to the catalyst layer

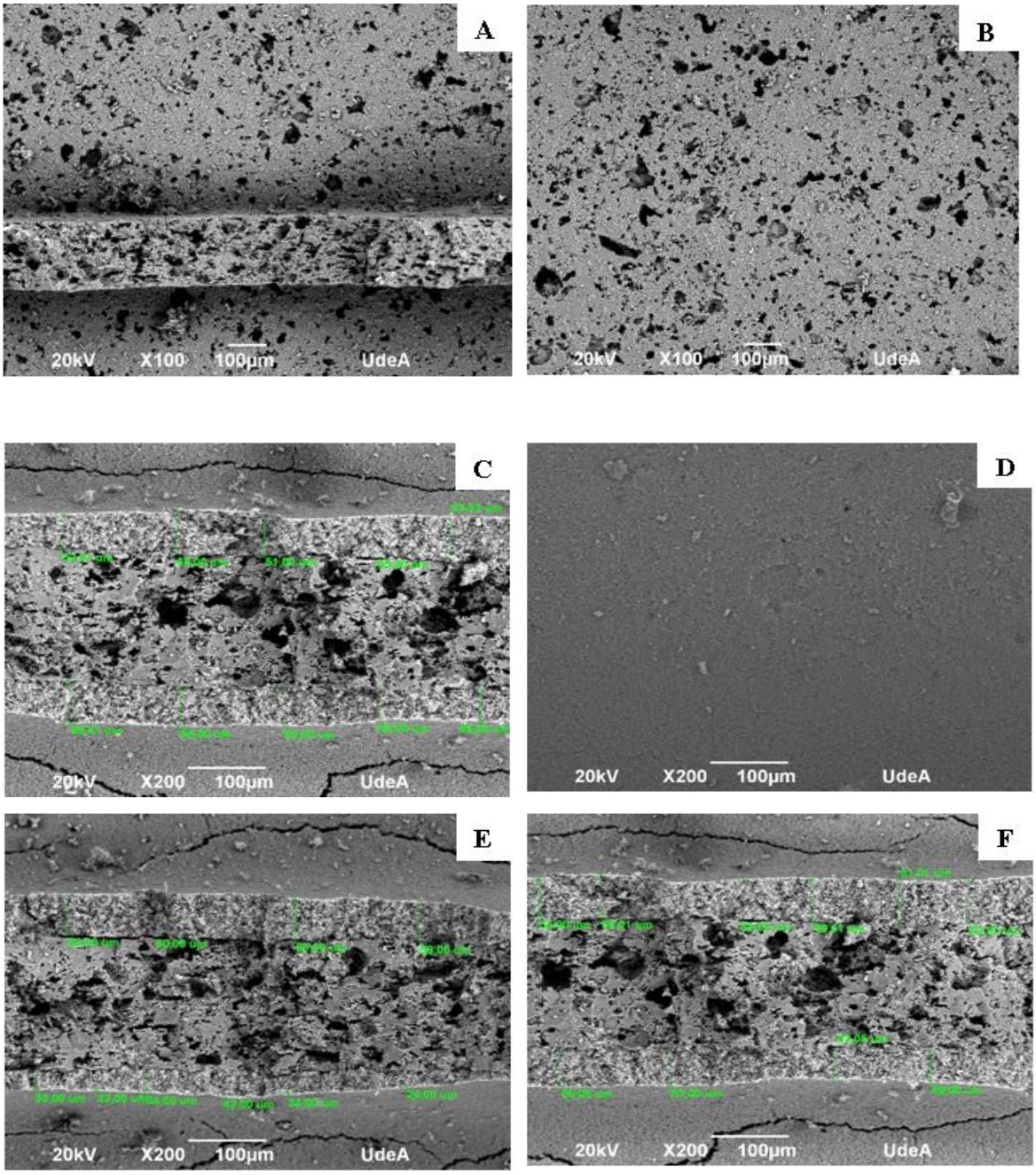

Figure 41 Micrographs of cordierite mini-monoliths. (A) Wall without catalyst, (B) Channel without catalyst, (C) Layer thickness of the washcoated mini-monolith (center), (D) Channel of the washcoated mini-monolith (center), (E) Layer thickness of the washcoated minimonolith (left), (F) Layer thickness of the washcoated mini-monolith (right).

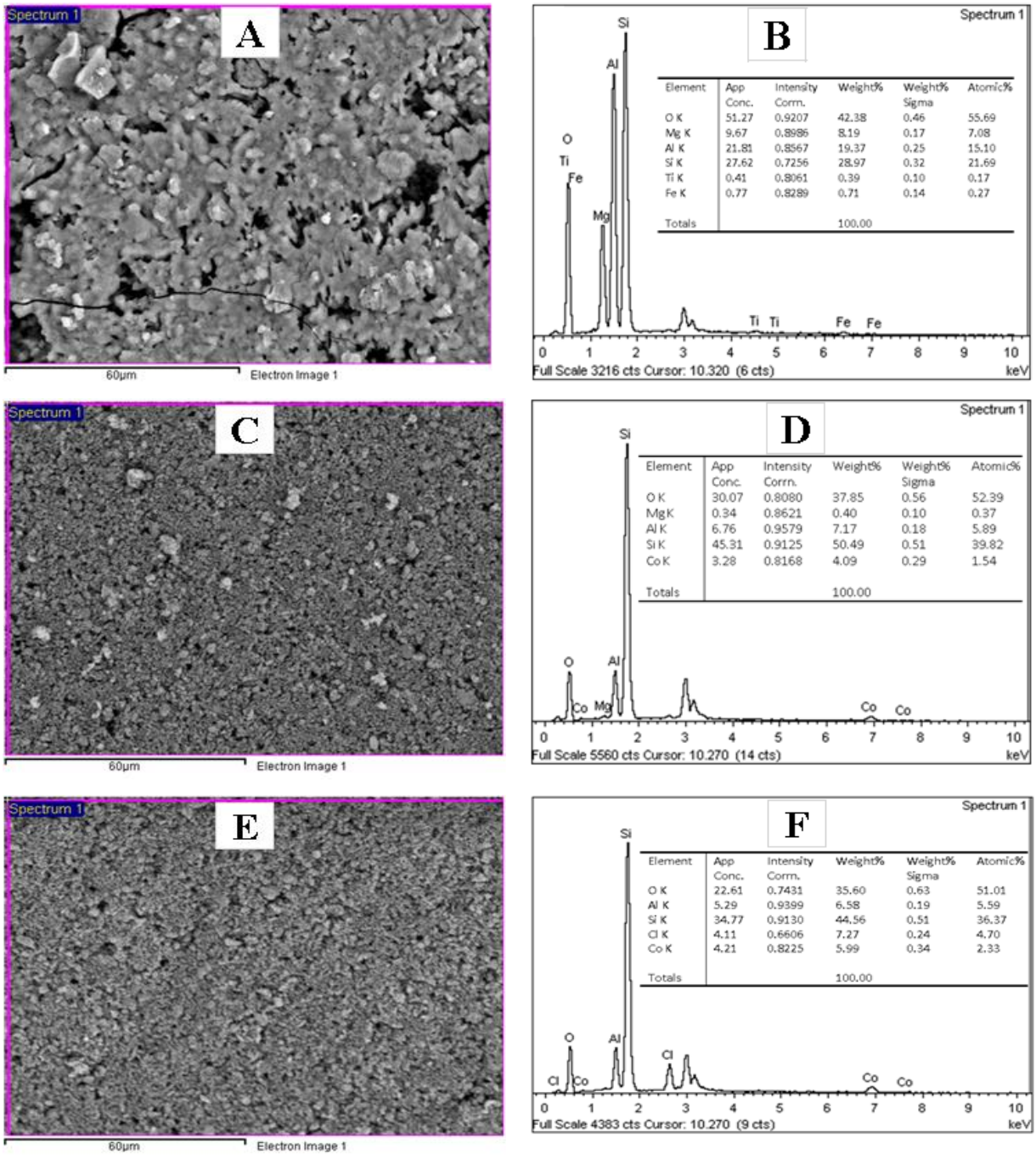

Element	App Conc.	Intensity Corrn.	Weight%	Weight% Sigma	Atomic%
O K	51.27	0.9207	42.38	0.46	55.69
Mg K	9.67	0.8986	8.19	0.17	7.08
Al K	21.81	0.8567	19.37	0.25	15.10
Si K	27.62	0.7256	28.97	0.32	21.69
Ti K	0.41	0.8061	0.39	0.10	0.17
Fe K	0.77	0.8289	0.71	0.14	0.27
Totals			100.00		

Element	App Conc.	Intensity Corrn.	Weight%	Weight% Sigma	Atomic%
O K	30.07	0.8080	37.85	0.56	52.39
Mg K	0.34	0.8621	0.40	0.10	0.37
Al K	6.76	0.9579	7.17	0.18	5.89
Si K	45.31	0.9125	50.49	0.51	39.82
Co K	3.28	0.8168	4.09	0.29	1.54
Totals			100.00		

Element	App Conc.	Intensity Corrn.	Weight%	Weight% Sigma	Atomic%
O K	22.61	0.7431	35.60	0.63	51.01
Al K	5.29	0.9399	6.58	0.19	5.59
Si K	34.77	0.9130	44.56	0.51	36.37
Cl K	4.11	0.6606	7.27	0.24	4.70
Co K	4.21	0.8225	5.99	0.34	2.33
Totals			100.00		

Figure 42 EDS of minimonoliths samples: A and B: bare cordierite monolith, C and D: Fresh washcoat minimonolith, E and F: Used minimonolithic reactor in the CH_4-SCR combined with the *o*-DCB oxidation.

deposited over the cordierite surface channels of the mini-monolith, this low percentage of Mg detected also allow to show that the washcoated surface may have some very small defects that are not noticeable in the SEM images at simple glance. In the fresh washcoated mini-monoliths it was also observed the presence of Co (3.28%) as expected but the Pd element was not detected which is due to its low concentration in the catalyst, however the Pd was evidenced in the powder samples analyzed by AAS, therefore is expected that it will be also present in the washcoated mini-monoliths. The EDS of used samples in the combined CH_4-SCR and *o*-DCB oxidation (Figure 42 E and F) reveal the presence of chlorine atoms in the surface of the washcoated channels, these atoms were also detected by TEM/EDS in the used powder Pd/Co-HMOR catalyst, the adsorption of Cl atoms on the catalyst surface has been identified as a probable cause of catalyst deactivation [92].

5.1.3 Catalytic test for mini-monolithic catalyst (Pd/Co-HMOR/m)

The NO, CH_4 and *o*-DCB conversions over Pd/Co-HMOR/m reactors were analyzed in the temperature range between 150 and 550 ºC under lean and wet conditions. Since in the Pd/Co-HMOR powder catalyst the higher activity for the NO reduction was observed for a $[CH_4]/[NO]$ ratio of 4, the same ratio was used in the mini-monolithic catalyst test, the results are shown in Figure 43. The Pd/Co-HMOR/m catalyst exhibits very similar conversion-temperature profiles than the observed in the powder catalyst for the same $[CH_4]/[NO]$ ratio under lean and wet conditions (see Figure 13).

The conversion-temperature profile of the NO displays also the typical volcano-shaped curve observed with the powder catalyst, however the maximum NO conversion temperature was observed at 525 ºC, this slight increase of 25 ºC is probably due to a resistance to the heat flow between the exterior and the interior channels of the cordierite minimonoliths, then a slightly higher oven temperature is required to achieve the equivalent temperature of the powder catalyst sample. At 550 ºC the NO conversion drops while the CH_4 continues reacting, as in the powder catalyst this behavior was already discussed and can be explained by the non-selective oxidation of methane by O_2. On the other hand, the *o*-DCB conversion shows an increasing trend with the temperature achieving a maximum conversion of 92% at 550 ºC, similar to the observed in the powder sample (96.5%). According to the results, it

seems that the active sites for both reactions remain in the catalyst after the washcoat procedure and show that it is possible to use monoliths of cordierite to support the Pd/Co-HMOR catalyst.

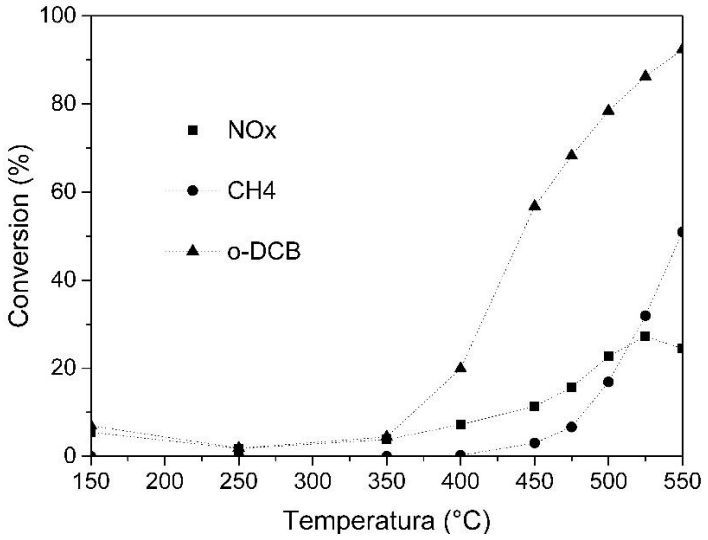

Figure 43 Catalytic activity of the monolithic catalyst. Conditions: [NO] = 1000 ppm, [NO_2] = 111 ppm, [*o*-DCB] = 600 ppm, [O_2] = 10%, [H_2O] = 6% and [CH_4] = 4000 ppm, Gas balance: Ar.

Chapter 6 General conclusions

Both Pd/Co-HMOR and Pd/Co-SZ exhibit activity towards the *o*-DCB oxidation simultaneously with the CH_4-SCR reaction however, the Pd/Co-HMOR catalyst showed a considerable higher catalytic activity and stability towards the NO reduction than the Pd/Co-SZ. For the *o*-DCB oxidation, both catalysts showed high activity and stability.

The kind of support has a highly influence in the catalytic activity and stability of the catalyst which is probably related to its acidity properties. In this way, the higher performance towards the CH_4-SCR of Pd/Co-HMOR compared with Pd/Co-SZ can be attributed to the higher total acidity of the catalyst supported on HMOR as reveled the NH_3-TPD analysis.

The Pd/Co-SZ catalyst was quickly deactivated for the CH_4-SCR reaction, the activity was almost completely lost after only 7 hours of continuous operation under wet conditions at 500 ºC, while the activity towards the *o*-DCB oxidation was hardly affected after 30 h of continuous operation. The main cause of catalyst deactivation was the losses of sulfate groups leading to the apparition of the monoclinic phase of zirconia.

The Pd/Co-HMOR catalyst was highly stable towards the *o*-DCB oxidation, however for the CH_4-SCR reaction it lost about 50% of the initial activity after 30 h of continuous operation. The main causes of catalyst deactivation were the formation of PdO clusters and the poison by chlorine leading to formation of $PdCl_2$.

The best performance temperature for CH_4-SCR over Pd/Co-HMOR catalyst was 500 ºC, at higher temperatures the non-selective oxidation of methane by oxygen prevails over the CH_4-SCR reaction.

The water in the feed can act as an hydrogen-supplier compound able to remove the surface chlorine anions adsorbed on the active sites, this explain the considerable increases in the *o*-DCB conversion over the Pd/Co-HMOR catalyst and the higher CO_2 generation regards to the dry conditions between 350 to 500 ºC. The positive effect of water vapor in the CH_4-SCR activity during the simultaneous reactions can also be ascribed to the removal of Cl^- anions by the water from the catalyst surface.

The conversion-temperature profile of the CH_4-SCR reaction over Pd/Co-HMOR catalyst reveled a high dependency between the $[CH_4]/[NO]$ ratio, the optimum NO conversion was obtained with a ratio of 4 at 500 ºC under lean and wet conditions. The dependence of the reaction rate disappearance and the concentration of both CH_4 and NO was also confirmed by the reaction rate law obtained.

The activation energy of CH_4-SCR considerably decreased in the presence of oxygen in excess regards to the absence of oxygen, which suggests that the activation of the NO and CH_4 molecules occurs easily in the presence of oxygen. According to the *in-situ* FTIR experiments, the oxygen participates in the first step of the CH_4-SCR over Co-α ions by transforming the Co^{2+}–$(NO)_2$ dinitrosyl species into adsorbed Co^{2+}–(NO_2) complexes, these complexes seems to play a key role in activating the CH_4 molecules by an Eley-rideal mechanism, this is probably the reason of the decrease of the apparent activation energy by the addition of oxygen to the feed under dry conditions.

The *in-situ* FTIR experiments revealed that Co-HMOR and Pd/Co-HMOR catalysts present Co-α and Co-β ions, since the Co-α ions (located in the main channel of the mordenite) are weakly bounded to framework oxygens of the zeolite some of them can be lost or replaced by Pd^{2+} cations during the Pd incorporation procedure, this led to a decrease in the Co-α/ Co-β ratio.

The *in-situ* FTIR study and the comparison between the reaction rates measurements of the single vs simultaneous reactions over Pd/Co-HMOR allows to conclude that Co^{2+} Lewis sites and Brønsted acid sites are common active sites for both reactions; however, although the reactions are independent there is a competition for these active sites during the simultaneous reactions.

The Pd/Co-HMOR catalyst can be successfully washcoated on cordierite mini-monoliths, the good catalyst adhesion observed was attributed to the high porosity of the cordierite which offers many sites for the catalytic coating anchoring. The activity towards the CH_4-SCR and *o*-DCB oxidation reactions were maintained in the mini-monolithic reactor.

Publications

Next is listed some of the works and events which resulted from this study.

Paper: M. Cano, F. Guarín, B. Aristizábal, A.-L. Villa, L.-M. González. Catalytic activity and stability of Pd/Co catalysts in simultaneous selective catalytic reduction of NOx with methane and oxidation of o-dichlorobenzene, Catal. Today. (2017).

Paper: Manuel Cano, Asier Aranzábal Maiztegi, Lina-María González, Beatriz Aristizábal, Juan Alberto Martínez, María Pilar González. In situ FTIR study of simultaneous CH4-SCR of NO and oxidation of o-dichlorobenzene over Pd/Co–HMOR catalyst (Draft).

Event: XXVcongresoIberoamericanodeCatálisis,Uruguay, 2016. **Work:** "Estabilidad de los catalizadores Pd/Co-HMOR y Pd/CoSZ durante la eliminación simultánea de NOx y o-diclorobenceno". **Authors:** Manuel Cano, Felipe Guarín, Julian Angel, Lina-María González, Beatriz Aristizábal, Aída-Luz Villa.

Event: The 16th International Congres on Catalysis, Beijing, 2016. **Work:** "Pd/Co based catalysts for the simultaneous elimination of NOx and chlorinated compounds under dry and wet conditions". **Authors:** Manuel Cano, Lina-María González, Beatriz Aristizábal, Aída-Luz Villa

Event: X Simposio Colombiano de Catálisis, Tunja, 2017. **Work:** "Influencia del O_2 en la reducción catalítica selectiva de NOx con CH_4 y la oxidación de o-diclorobenceno sobre el catalizdor de Pd/Co-HMOR". **Authors:** Manuel Cano, Lina-María González, Beatriz Aristizábal, Aída-Luz Villa.

Event: XXVI congreso Iberoamericano de Catálisis, Portugal, 2018. **Work:** "Desempeño de catalizadores monolíticos a base de Pd y Co en la oxidación de o-DCB en simultáneo con la reducción de NOx". **Authors:** Manuel Cano, Beatriz Helena Aristizabal, Felipe Guarín, Mateo Giraldo.

Research project: "Evaluación de la implementación de un sistema para la remoción simultánea de compuestos organoclorados y NOx generados durante la incineración de residuos". Financing entity: Colciencias.

References

[1] R. Dvořák, P. Chlápek, D. Jecha, R. Puchýř, P. Stehlík, New approach to common removal of dioxins and NOx as a contribution to environmental protection, J. Clean. Prod. 18 (2010) 881–888. doi:10.1016/j.jclepro.2010.01.024.

[2] S. Squadrone, P. Brizio, R. Nespoli, C. Stella, M.C. Abete, Human dietary exposure and levels of polychlorinated dibenzo-p-dioxins (PCDDs), polychlorinated dibenzofurans (PCDFs), dioxin-like polychlorinated biphenyls (DL-PCBs) and non-dioxin-like polychlorinated biphenyls (NDL-PCBs) in free-range eggs close to a secondary aluminum smelter, Northern Italy, Environ. Pollut. 206 (2015) 429–436. doi:10.1016/j.envpol.2015.07.048.

[3] M. a. Gómez-García, V. Pitchon, a. Kiennemann, Pollution by nitrogen oxides: An approach to NOx abatement by using sorbing catalytic materials, Environ. Int. 31 (2005) 445–467. doi:10.1016/j.envint.2004.09.006.

[4] L. Curtis, W. Rea, P. Smith-Willis, E. Fenyves, Y. Pan, Adverse health effects of outdoor air pollutants., J. Nutr. Environ. Med. 32 (2006) 815–30. doi:10.1016/j.envint.2006.03.012.

[5] A. Kelly, J. Lumbreras, R. Maas, T. Pignatelli, F. Ferreira, A. Engleryd, Setting national emission ceilings for air pollutants: policy lessons from an ex-post evaluation of the Gothenburg Protocol, Environ. Sci. Policy. 13 (2010) 28–41. doi:10.1016/j.envsci.2009.09.003.

[6] United Nations Economic Commission for Europe., Gothenburge Protocole:

Protocole to the 1979 convention on long-range transboundary air pollution to abate acidification, eutrophication and ground-level ozone, 1999.

[7] G. McKay, Dioxin characterisation, formation and minimisation during municipal solid waste (MSW) incineration: Review, Chem. Eng. J. 86 (2002) 343–368. doi:10.1016/S1385-8947(01)00228-5.

[8] S. Squadrone, P. Brizio, R. Nespoli, C. Stella, M.C. Abete, Human dietary exposure and levels of polychlorinated dibenzo-p-dioxins (PCDDs), polychlorinated dibenzofurans (PCDFs), dioxin-like polychlorinated biphenyls (DL-PCBs) and non-dioxin-like polychlorinated biphenyls (NDL-PCBs) in free-range eggs close to a s, Environ. Pollut. 206 (2015) 429–36. doi:10.1016/j.envpol.2015.07.048.

[9] M. Van Den Berg, L. Birnbaum, A.T.C. Bosveld, B. Brunström, P. Cook, M. Feeley, J.P. Giesy, A. Hanberg, R. Hasegawa, S.W. Kennedy, T. Kubiak, J.C. Larsen, F.X.R. Van Leeuwen, a. K.D. Liem, C. Nolt, R.E. Peterson, L. Poellinger, S. Safe, D. Schrenk, D. Tillitt, M. Tysklind, M. Younes, F. Wærn, T. Zacharewski, Toxic equivalency factors (TEFs) for PCBs, PCDDs, PCDFs for humans and wildlife, Environ. Health Perspect. 106 (1998) 775–792. doi:10.1289/ehp.98106775.

[10] M. Cobo, J.A. Conesa, C. Montes de Correa, Effect of the reducing agent on the hydrodechlorination of dioxins over 2wt.% Pd/γ-Al_2O_3, Appl. Catal. B Environ. 92 (2009) 367–376. doi:10.1016/j.apcatb.2009.08.016.

[11] W.F. Carroll, R.W. Johnson, S.S. Moore, R.A. Paradis, Applied Plastics Engineering Handbook, Elsevier, 2011. doi:10.1016/B978-1-4377-3514-7.10005-4.

[12] B.R. Stanmore, The formation of dioxins in combustion systems, Combust. Flame. 136 (2004) 398–427. doi:10.1016/j.combustflame.2003.11.004.

[13] Y.-M. Chang, W.-P. Fan, W.-C. Dai, H.-C. Hsi, C.-H. Wu, C.-H. Chen, Characteristics of PCDD/F content in fly ash discharged from municipal solid waste incinerators, J. Hazard. Mater. 192 (2011) 521–529. doi:10.1016/j.jhazmat.2011.05.055.

[14] K. Olie, P.L. Vermeulen, O. Hutzinger, Chlorodibenzo-p-dioxins and

chlorodibenzofurans are trace components of fly ash and flue gas of some municipal incinerators in the Netherlands, Chemosphere. 6 (1977) 455–459. doi:10.1016/0045-6535(77)90035-2.

[15] J. Rivera-Austrui, M.A. Borrajo, K. Martinez, M.A. Adrados, M. Abalos, B. Van Bavel, J. Rivera, E. Abad, Assessment of polychlorinated dibenzo-p-dioxin and dibenzofuran emissions from a hazardous waste incineration plant using long-term sampling equipment., Chemosphere. 82 (2011) 1343–9. doi:10.1016/j.chemosphere.2010.11.054.

[16] W. Liu, Z. Tian, H. Li, H. Xie, K. Xiao, C. Li, C. Tang, M. Zheng, Mono- to Octa-Chlorinated PCDD/Fs in Stack Gas from Typical Waste Incinerators and Their Implications on Emission, Environ. Sci. Technol. 47 (2013) 9774–9780. doi:10.1021/es402136s.

[17] G. Zhang, J. Hai, M. Ren, S. Zhang, J. Cheng, Z. Yang, Emission, Mass Balance, and Distribution Characteristics of PCDD/Fs and Heavy Metals during Cocombustion of Sewage Sludge and Coal in Power Plants, Environ. Sci. Technol. 47 (2013) 2123–2130. doi:10.1021/es304127k.

[18] C.-C. Lee, T.-S. Shih, H.-L. Chen, Distribution of air and serum PCDD/F levels of electric arc furnaces and secondary aluminum and copper smelters, J. Hazard. Mater. 172 (2009) 1351–1356. doi:10.1016/j.jhazmat.2009.07.148.

[19] S. Li, Y. Tian, Q. Ding, W. Liu, The release of persistent organic pollutants from a closed system dicofol production process, Chemosphere. 94 (2014) 164–168. doi:10.1016/j.chemosphere.2013.09.090.

[20] United Nations Environment Programme., Stockholm Convention on Persistent Organic Pollutants, 2001.

[21] F. Bertinchamps, C. Grégoire, E.M. Gaigneaux, Systematic investigation of supported transition metal oxide based formulations for the catalytic oxidative elimination of (chloro)-aromatics. Part II: Influence of the nature and addition protocol of secondary

phases to VOx/TiO2, Appl. Catal. B Environ. 66 (2006) 10–22. doi:10.1016/j.apcatb.2006.02.012.

[22] K. Skalska, J.S. Miller, S. Ledakowicz, Trends in NOx abatement: A review, Sci. Total Environ. 408 (2010) 3976–3989. doi:10.1016/j.scitotenv.2010.06.001.

[23] X. Zhao, L. Huang, H. Li, H. Hu, X. Hu, L. Shi, D. Zhang, Promotional effects of zirconium doped $CeVO_4$ for the low-temperature selective catalytic reduction of NOx with NH_3, Appl. Catal. B Environ. 183 (2016) 269–281. doi:10.1016/j.apcatb.2015.10.052.

[24] X. Wang, W. Wen, J. Mi, X. Li, R. Wang, The ordered mesoporous transition metal oxides for selective catalytic reduction of NOx at low temperature, Appl. Catal. B Environ. 176–177 (2015) 454–463. doi:10.1016/j.apcatb.2015.04.038.

[25] J. Jones, J.R.H. Ross, The development of supported vanadia catalysts for the combined catalytic removal of the oxides of nitrogen and of chlorinated hydrocarbons from flue gases, Catal. Today. 35 (1997) 97–105. doi:10.1016/S0920-5861(96)00148-4.

[26] X. Liu, J. Wang, X. Wang, T. Zhu, Simultaneous removal of PCDD/Fs and NOx from the flue gas of a municipal solid waste incinerator with a pilot plant., Chemosphere. 133 (2015) 90–6. doi:10.1016/j.chemosphere.2015.04.009.

[27] M.K. Camarillo, W.T. Stringfellow, J.S. Hanlon, K. a. Watson, Investigation of selective catalytic reduction for control of nitrogen oxides in full-scale dairy energy production, Appl. Energy. 106 (2013) 328–336. doi:10.1016/j.apenergy.2013.01.066.

[28] M. Goemans, P. Clarysse, J. Joannès, P. De Clercq, S. Lenaerts, K. Matthys, K. Boels, Catalytic NOx reduction with simultaneous dioxin and furan oxidation, Chemosphere. 54 (2004) 1357–1365. doi:10.1016/S0045-6535(03)00255-8.

[29] J. Lichtenberger, M.D. Amiridis, Deactivation of V_2O_5/TiO_2 catalysts during the oxidation of meta-dichlorobenzene in the presence of methyl-naphthalene, Catal. Today. 98 (2004) 447–453. doi:10.1016/j.cattod.2004.08.001.

[30] X. Cheng, X.T. Bi, A review of recent advances in selective catalytic NOx reduction reactor technologies, Particuology. 16 (2014) 1–18. doi:10.1016/j.partic.2014.01.006.

[31] H. Ohtsuka, T. Tabata, Effect of water vapor on the deactivation of Pd-zeolite catalysts for selective catalytic reduction of nitrogen monoxide by methane, Appl. Catal. B Environ. 21 (1999) 133–139. doi:10.1016/S0926-3373(99)00014-4.

[32] T.M. Butler, M.G. Lawrence, B.R. Gurjar, J. van Aardenne, M. Schultz, J. Lelieveld, The representation of emissions from megacities in global emission inventories, Atmos. Environ. 42 (2008) 703–719. doi:10.1016/j.atmosenv.2007.09.060.

[33] I. Glassman, R. a Yetter, Environmental Combustion Considerations, Combustion. (2008) 459. doi:10.1016/B978-012285852-9/50009-6.

[34] F. Normann, K. Andersson, B. Leckner, F. Johnsson, Emission control of nitrogen oxides in the oxy-fuel process, Prog. Energy Combust. Sci. 35 (2009) 385–397. doi:10.1016/j.pecs.2009.04.002.

[35] B. Ramachandran, R.G. Herman, S. Choi, H.G. Stenger, C.E. Lyman, J.W. Sale, Testing zeolite SCR catalysts under protocol conditions for NOx abatement from stationary emission sources, Catal. Today. 55 (2000) 281–290. doi:10.1016/S0920-5861(99)00252-7.

[36] F. Garin, Mechanism of NOx decomposition, Appl. Catal. A Gen. 222 (2001) 183–219. doi:10.1016/S0926-860X(01)00827-4.

[37] O. Gohlke, T. Weber, P. Seguin, Y. Laborel, A new process for NOx reduction in combustion systems for the generation of energy from waste, Waste Manag. 30 (2010) 1348–1354. doi:10.1016/j.wasman.2010.02.024.

[38] T. Rogaume, M. Auzanneau, F. Jabouille, J.. Goudeau, J.. Torero, The effects of different airflows on the formation of pollutants during waste incineration, Fuel. 81 (2002) 2277–2288. doi:10.1016/S0016-2361(02)00151-5.

[39] J.A. Miller, C.T. Bowman, Mechanism and modeling of nitrogen chemistry in

combustion, Prog. Energy Combust. Sci. 15 (1989) 287–338. doi:10.1016/0360-1285(89)90017-8.

[40] G.A. Lavoie, J.B. Heywood, J.C. Keck, Experimental and Theoretical Study of Nitric Oxide Formation in Internal Combustion Engines, Combust. Sci. Technol. 1 (1970) 313–326. doi:10.1080/00102206908952211.

[41] S.C. Hill, L.D. Smoot, Modeling of nitrogen oxides formation and destruction in combustion systems, Prog. Energy Combust. Sci. 26 (2000) 417–458. doi:10.1016/S0360-1285(00)00011-3.

[42] Y. Ninomiya, Theoretical study on the thermal decomposition of pyridine, Fuel. 79 (2000) 449–457. doi:10.1016/S0016-2361(99)00180-5.

[43] M. Piacentini, Doctoral Thesis: Fundamental Aspects of NOx Storage-Reduction Catalysts for Automotive Lean Combustion Engines., Swiss Federal Institute of Technology Zurich, 2006.

[44] C.P. Fenimore, Formation of nitric oxide in premixed hydrocarbon flames, Symp. Combust. 13 (1971) 373–380. doi:10.1016/S0082-0784(71)80040-1.

[45] E. Goos, C. Sickfeld, F. Mauß, L. Seidel, B. Ruscic, A. Burcat, T. Zeuch, Prompt NO formation in flames: The influence of NCN thermochemistry, Proc. Combust. Inst. 34 (2013) 657–666. doi:10.1016/j.proci.2012.06.128.

[46] L.V. Moskaleva, M.C. Lin, The spin-conserved reaction $CH+N_2 \rightarrow H+NCN$: A major pathway to prompt no studied by quantum/statistical theory calculations and kinetic modeling of rate constant, Proc. Combust. Inst. 28 (2000) 2393–2401. doi:10.1016/S0082-0784(00)80652-9.

[47] B.H. Aristizábal, C. Maya, C.M. de Correa, Ortho-dichlorobenzene oxidation over Pd/Co loaded sulfated zirconia and mordenite catalysts, Appl. Catal. A Gen. 335 (2008) 211–219. doi:10.1016/j.apcata.2007.11.026.

[48] K. Tuppurainen, A. Asikainen, P. Ruokojärvi, J. Ruuskanen, Perspectives on the

formation of polychlorinated dibenzo-p-dioxins and dibenzofurans during municipal solid waste (MSW) incineration and other combustion processes, Acc. Chem. Res. 36 (2003) 652–658. doi:10.1021/ar020104+.

[49] B. Aristizábal, M. Cobo, C.M. De, K. Martínez, E. Abad, J. Rivera, Dioxin emissions from thermal waste management in Medellín, Colombia: Present regulation status and preliminary results, Waste Manag. 27 (2007) 1603–1610. doi:10.1016/j.wasman.2006.08.011.

[50] K. Tuppurainen, I. Halonen, P. Ruokojärvi, J. Tarhanen, J. Ruuskanen, Formation of PCDDs and PCDFs in municipal waste incineration and its inhibition mechanisms: A review, Chemosphere. 36 (1998) 1493–1511. doi:10.1016/S0045-6535(97)10048-0.

[51] E.D. Lavric, A. a. Konnov, J. De Ruyck, Modeling the formation of precursors of dioxins during combustion of woody fuel volatiles, Fuel. 84 (2005) 323–334. doi:10.1016/j.fuel.2004.09.012.

[52] S. Jansson, Thermal formation and chlorination of dioxins and dioxin-like compounds, 2008. http://urn.kb.se/resolve?urn=urn:nbn:se:umu:diva-1881.

[53] A. Buekens, H. Huang, Comparative evaluation of techniques for controlling the formation and emission of chlorinated dioxins/furans in municipal waste incineration, J. Hazard. Mater. 62 (1998) 1–33. doi:10.1016/S0304-3894(98)00153-8.

[54] M.T. Javed, N. Irfan, B.M. Gibbs, Control of combustion-generated nitrogen oxides by selective non-catalytic reduction., J. Environ. Manage. 83 (2007) 251–89. doi:10.1016/j.jenvman.2006.03.006.

[55] D. Popp, International innovation and diffusion of air pollution control technologies: the effects of NOx and SO_2 regulation in the US, Japan, and Germany, J. Environ. Econ. Manage. 51 (2006) 46–71. doi:10.1016/j.jeem.2005.04.006.

[56] N. Popovych, P. Kirienko, S. Soloviev, S. Orlyk, Selective catalytic reduction of NOx by C_2H_5OH over Ag/Al_2O_3/cordierite: Effect of the surface concentration of silver, Catal. Today. 191 (2012) 38–41. doi:10.1016/j.cattod.2012.01.039.

[57] H. Liu, S. Kong, Y. Liu, H. Zeng, Pollution Control Technologies of Dioxins in Municipal Solid Waste Incinerator, Procedia Environ. Sci. 16 (2012) 661–668. doi:10.1016/j.proenv.2012.10.091.

[58] I. Fangmark Bavel, Bert., Marklund, Stellan,. Stromberg, Birgitta., Berge, Niklas., and Rappe, Christoffer, Influence of Combustion Parameters on the Formation of Polychlorinated Dibenzo-pdioxins, Dibenzofurans, Benzenes, and Biphenyls and Polyaromatic Hydrocarbons in a Pilot Incinerator, Environ. Sci. Technol. 27 (1993) 8. doi:10.1021/es00045a016.

[59] I. Fangmark, B. Stromberg, N. Berge, C. Rappet, Influence of Postcombustion Temperature Profiles on the Formation of PCDDs , PCDFs , PCBzs , and PCBs in a Pilot Incinerator, Environ. Sci. Technol. (1994) 624–629. doi:10.1021/es00053a014.

[60] S.B. Ghorishi, E.R. Altwicker, Formation of polychlorinated dioxins, furans, benzenes and phenols in the post combustion region of a heterogeneous combustor: Effect of bed material and post combustion temperature, Environ. Sci. Technol. 29 (1995) 1156–1162. doi:10.1021/es00005a004.

[61] H. Vogg, H. Hunsinger, A. Merz, L. Stieglitz, Influencing the production of dioxin/furan in solid waste incineration plants by measures affecting the combustion as well as the flue gas cleaning systems, Chemosphere. 25 (1992) 149–152. doi:10.1016/0045-6535(92)90500-Q.

[62] K. Watanabe, K. Tsukamoto, Emission control of dioxin compounds in plastic waste incineration, Organohalogen Compd. 19 (1994) 431–436.

[63] I. FANGMARK, The influence of fly ash load and particle size on the formation of PCDD, PCDF, PCBz and PCB in a pilot incinerator, Waste Manag. Res. 13 (1995) 259–272. doi:10.1016/S0734-242X(95)90043-8.

[64] S.P. Ryan, X.D. Li, B.K. Gullett, C.W. Lee, M. Clayton, A. Touati, Experimental study on the effect of SO_2 on PCDD/F emissions: Determination of the importance of gas-phase versus solid-phase reactions in PCDD/F formation, Environ. Sci. Technol.

40 (2006) 7040–7047. doi:10.1021/es0615369.

[65] L.C. Dickson, D. Lenoir, O. Hutzinger, K.P. Naikwadi, F.W. Karasek, Inhibition of chlorinated dibenzo-p-dioxin formation on municipal incinerator fly ash by using catalyst inhibitors, Chemosphere. 19 (1989) 1435–1445. doi:10.1016/0045-6535(89)90092-1.

[66] J.L. Bonte, K.J. Fritsky, M.A. Plinke, M. Wilken, Catalytic destruction of PCDD/F in a fabric filter: experience at a municipal waste incinerator in Belgium, Waste Manag. 22 (2002) 421–426. doi:10.1016/S0956-053X(02)00025-9.

[67] M.B. Chang, J.-J. Lin, S.-H. Chang, Characterization of dioxin emissions from two municipal solid waste incinerators in Taiwan, Atmos. Environ. 36 (2002) 279–286. doi:10.1016/S1352-2310(01)00267-9.

[68] W.M. Sierhuis, C. de Vries, J.G.P. Born, PCDD/F emissions related to the operating conditions of the flue gas cleaning system of MWI-Amsterdam, Chemosphere. 32 (1996) 159–168. doi:10.1016/0045-6535(95)00242-1.

[69] G. McKay, Dioxin characterisation, formation and minimisation during municipal solid waste (MSW) incineration: review, Chem. Eng. J. 86 (2002) 343–368. doi:10.1016/S1385-8947(01)00228-5.

[70] C.-J. Löthgren, B. van Bavel, Dioxin emissions after installation of a polishing wet scrubber in a hazardous waste incineration facility, Chemosphere. 61 (2005) 405–412. doi:10.1016/J.CHEMOSPHERE.2005.02.015.

[71] M.B. Chang, K.H. Chi, S.H. Chang, J.W. Yeh, Destruction of PCDD/Fs by SCR from flue gases of municipal waste incinerator and metal smelting plant, Chemosphere. 66 (2007) 1114–1122. doi:10.1016/J.CHEMOSPHERE.2006.06.020.

[72] K. Hirota, O. Tokunaga, T. Miyata, S. Sato, Y. Osada, M. Sudo, T. Doi, E. Shibuya, S. Baba, T. Hatomi, M. Komiya, K. Miyajima, Pilot-scale test for electron beam purification of flue gas from a municipal waste incinerator with slaked-lime, Radiat. Phys. Chem. 46 (1995) 1089–1092. doi:10.1016/0969-806X(95)00328-U.

[73] K. Hirota, T. Kojima, Decomposition behavior of PCDD/F isomers in incinerator gases under electron-beam irradiation, Bull. Chem. Soc. Jpn. 78 (2005) 1685–1690. doi:10.1246/bcsj.78.1685.

[74] R.M. Heck, Catalytic abatement of nitrogen oxides – stationary applications, Catal. Today. 53 (1999) 519–523. doi:10.1016/S0920-5861(99)00139-X.

[75] L.J. Alemany, M.A. Bañares, M.A. Larrubia, M.C. Jiménez, F. Delgado, J.M. Blasco, Vanadia-titania systems: morphological and structural properties, Mater. Res. Bull. 31 (1996) 513–520. doi:10.1016/S0025-5408(96)00029-3.

[76] G.C. Bond, S.F. Tahir, Vanadium oxide monolayer catalysts Preparation, characterization and catalytic activity, Appl. Catal. 71 (1991) 1–31. doi:10.1016/0166-9834(91)85002-D.

[77] A. Khodakov, B. Olthof, A.T. Bell, E. Iglesia, Structure and Catalytic Properties of Supported Vanadium Oxides: Support Effects on Oxidative Dehydrogenation Reactions, J. Catal. 181 (1999) 205–216. doi:10.1006/JCAT.1998.2295.

[78] L. Chen, J. Li, M. Ge, The poisoning effect of alkali metals doping over nano V_2O_5-WO_3/TiO_2 catalysts on selective catalytic reduction of NOx by NH_3, Chem. Eng. J. 170 (2011) 531–537. doi:10.1016/j.cej.2010.11.020.

[79] J.L. Sorrels, D.D. Randall, K.S. Schaffner, C.R. Fry, Chapter 2 Selective Catalytic Reduction, Econ. Cost Anal. Air Pollut. Regul. (2016). doi:10.1016/j.fertnstert.2015.01.016.

[80] E. Finocchio, G. Busca, M. Notaro, A review of catalytic processes for the destruction of PCDD and PCDF from waste gases, Appl. Catal. B Environ. 62 (2006) 12–20. doi:10.1016/J.APCATB.2005.06.010.

[81] G. Busca, L. Lietti, G. Ramis, F. Berti, Chemical and mechanistic aspects of the selective catalytic reduction of NOx by ammonia over oxide catalysts : A review, Appl. Catal. B Environ. 18 (1998) 1–36. doi:10.1016/S0926-3373(98)00040-X.

[82] P. Forzatti, Present status and perspectives in de-NOx SCR catalysis, Appl. Catal. A Gen. 222 (2001) 221–236. doi:10.1016/S0926-860X(01)00832-8.

[83] S. Krishnamoorthy, J.A. Rivas, M.D. Amiridis, Catalytic Oxidation of 1,2-Dichlorobenzene over Supported Transition Metal Oxides, J. Catal. 193 (2000) 264–272. doi:10.1006/jcat.2000.2895.

[84] J. Hahn, Technologies for dioxin control at municipal waste combustors (MWC) beyond good combustion practices (GCP) and dry scrubbers / fabric filters (DS/FF), Chemosphere. 25 (1992) 57–60. doi:10.1016/0045-6535(92)90479-B.

[85] L. Ji, X. Cao, S. Lu, C. Du, X. Li, T. Chen, A. Buekens, J. Yan, Catalytic oxidation of PCDD/F on a V_2O_5-WO_3/TiO_2 catalyst: Effect of chlorinated benzenes and chlorinated phenols, J. Hazard. Mater. 342 (2018) 220–230. doi:10.1016/J.JHAZMAT.2017.07.020.

[86] R. Weber, M. Plinke, Z. Xu, M. Wilken, Destruction efficiency of catalytic filters for polychlorinated dibenzo-p-dioxin and dibenzofurans in laboratory test and field operation — insight into destruction and adsorption behavior of semivolatile compounds, Appl. Catal. B Environ. 31 (2001) 195–207. doi:10.1016/S0926-3373(00)00278-2.

[87] K. Everaert, J. Baeyens, Catalytic combustion of volatile organic compounds, J. Hazard. Mater. 109 (2004) 113–139. doi:10.1016/j.jhazmat.2004.03.019.

[88] S. Krishnamoorthy, J.P. Baker, M.D. Amiridis, Catalytic oxidation of 1,2-dichlorobenzene over V_2O_5/TiO_2-based catalysts, Catal. Today. 40 (1998) 39–46. doi:10.1016/S0920-5861(97)00117-X.

[89] R. López-Fonseca, J.I. Gutiérrez-Ortiz, M.A. Gutiérrez-Ortiz, J.R. González-Velasco, Catalytic oxidation of aliphatic chlorinated volatile organic compounds over Pt/H-BETA zeolite catalyst under dry and humid conditions, Catal. Today. 107–108 (2005) 200–207. doi:10.1016/j.cattod.2005.07.091.

[90] B.H. Aristizábal, C.M. de Correa, A.I. Serykh, C.E. Hetrick, M.D. Amiridis, In situ

FTIR study of the adsorption and reaction of ortho-dichlorobenzene over Pd-promoted Co-HMOR, Microporous Mesoporous Mater. 112 (2008) 432–440. doi:10.1016/j.micromeso.2007.10.020.

[91] S. Scirè, S. Minicò, The Role of the Support in the Oxidative Destruction of Chlorobenzene on Pt/Zeolite Catalysts: An FT-IR Investigation, Catal. Letters. 91 (2003) 199–205. doi:10.1023/B:CATL.0000007155.59258.83.

[92] M. Cano, F. Guarín, B. Aristizábal, A.-L. Villa, L.-M. González, Catalytic activity and stability of Pd/Co catalysts in simultaneous selective catalytic reduction of NOx with methane and oxidation of o-dichlorobenzene, Catal. Today. (2017). doi:10.1016/j.cattod.2017.05.049.

[93] M. Taralunga, J. Mijoin, P. Magnoux, Catalytic destruction of 1,2-dichlorobenzene over zeolites, Catal. Commun. 7 (2006) 115–121. doi:10.1016/j.catcom.2005.09.006.

[94] F. Bustamante, F. Córdoba, M. Yates, C. Montes de Correa, The promotion of cobalt mordenite by palladium for the lean CH_4-SCR of NOx in moist streams, Appl. Catal. A Gen. 234 (2002) 127–136. doi:10.1016/S0926-860X(02)00211-9.

[95] Y. Li, J.N. Amor, Catalytic Reduction of Nitrogen Oxides with Methane in the Presence of Excess Oxygen, Stud. Surf. Sci. Catal. 81 (1994) 103–113. doi:10.1016/S0167-2991(08)63852-5.

[96] J. a Z. Pieterse, R.W. Van Den Brink, S. Booneveld, F. a. De Bruijn, Influence of zeolite structure on the activity and durability of Co-Pd-zeolite catalysts in the reduction of NOx with methane, Appl. Catal. B Environ. 46 (2003) 239–250. doi:10.1016/S0926-3373(03)00213-3.

[97] L.F. Córdoba, G.A. Fuentes, C.M. de Correa, Characterization of bimetallic Pd/Co-HMOR used for the CH4-SCR of NOx, Microporous Mesoporous Mater. 77 (2005) 193–201. doi:10.1016/j.micromeso.2004.09.003.

[98] J.M. Zamaro, M. a. Ulla, E.E. Miró, The effect of different slurry compositions and solvents upon the properties of ZSM5-washcoated cordierite honeycombs for the SCR

of NOx with methane, Catal. Today. 107–108 (2005) 86–93. doi:10.1016/j.cattod.2005.07.066.

[99] R. Weber, Low temperature decomposition of PCDD/PCDF, chlorobenzenes and PAHs by TiO_2-based V_2O_5–WO_3 catalysts, Appl. Catal. B Environ. 20 (1999) 249–256. doi:10.1016/S0926-3373(98)00115-5.

[100] J. Armor, Catalytic reduction of nitrogen oxides with methane in the presence of excess oxygen: A review, Catal. Today. 26 (1995) 147–158. doi:10.1016/0920-5861(95)00134-2.

[101] J.N.A. Yuenjin Li, Catalytic reduction of nitrogen oxide with methane in the presence of excess oxygen, Appl. Catal. B. 1 (1992) L31–L40.

[102] L.F. Córdoba, W.M.H. Sachtler, C. Montes de Correa, NO reduction by CH_4 over Pd/Co-sulfated zirconia catalysts, Appl. Catal. B Environ. 56 (2005) 269–277. doi:10.1016/j.apcatb.2004.09.012.

[103] L.M. González, B.H. Aristizábal, A.L. Villa, Actividad catalítica de Pd/Co-H-MOR en la eliminación simultánea de NOx y o-diclorobenceno, Congr. Iberoam. Catálisis CICat. (2014).

[104] P. Cheremisinoff, Waste Incineration Handbook, Elsevier, 1992. doi:10.1016/B978-0-7506-0282-2.50010-X.

[105] M. Carter-Whitney, Ontario's Waste Management Challenge - Is incineration an option, 2007.

[106] J.A.Z. Pieterse, H. Top, F. Vollink, K. Hoving, R.W. Van Den Brink, Selective catalytic reduction of NOx in real exhaust gas of gas engines using unburned gas : Catalyst deactivation and advances toward long-term stability, 120 (2006) 17–23. doi:10.1016/j.cej.2006.03.009.

[107] H. Ohtsuka, T. Tabata, Influence of Si/Al ratio on the activity and durability of Pd-ZSM-5 catalysts for nitrogen oxide reduction by methane, Appl. Catal. B Environ. 26

(2000) 275–284. doi:10.1016/S0926-3373(00)00127-2.

[108] H. Uchida, K. Yamaseki, I. Takahashi, NOx reduction with methane over mordenite supported palladium catalyst, Catal. Today. 29 (1996) 99–102. doi:10.1016/0920-5861(95)00286-3.

[109] M. Misono, Y. Nishizaka, M. Kawamoto, H. Kato, Progress in Zeolite and Microporous Materials, Preceedings of the 11th International Zeolite Conference, Elsevier, 1997. doi:10.1016/S0167-2991(97)80792-6.

[110] G. Koyano, S. Yokoyama, M. Misono, States of Pd in Pd/H–ZSM-5 and Pd/Na–ZSM-5 catalysts and catalytic activity for the reduction of NO by CH4 in the presence of O_2, Appl. Catal. A Gen. 188 (1999) 301–312. doi:10.1016/S0926-860X(99)00222-7.

[111] Y. Nishizaka, M. Misono, Catalytic Reduction of Nitrogen Monoxide by Methane over Palladium-Loaded Zeolites in the Presence of Oxygen, Chem. Lett. 22 (1993) 1295–1298. doi:10.1246/cl.1993.1295.

[112] X. Cheng, X.T. Bi, A review of recent advances in selective catalytic NOx reduction reactor technologies, Particuology. 16 (2014) 1–18. doi:10.1016/j.partic.2014.01.006.

[113] H. Ohtsuka, T. Tabata, Effect of water vapor on the deactivation of Pd-zeolite catalysts for selective catalytic reduction of nitrogen monoxide by methane, Appl. Catal. B Environ. 21 (1999) 133–139. doi:10.1016/S0926-3373(99)00014-4.

[114] C. Descorme, P. Gélin, M. Primet, C. Lécuyer, Infrared study of nitrogen monoxide adsorption on palladium ion-exchanged ZSM-5 catalysts, Catal. Letters. 41 (1996) 133–138. doi:10.1007/BF00811479.

[115] D. Kaucký, A. Vondrová, J. Dědeček, B. Wichterlová, Activity of Co Ion Sites in ZSM-5, Ferrierite, and Mordenite in Selective Catalytic Reduction of NO with Methane, J. Catal. 194 (2000) 318–329. doi:10.1006/jcat.2000.2925.

[116] T. Montanari, M. Bevilacqua, C. Resini, G. Busca, UV−Vis and FT-IR Study of the Nature and Location of the Active Sites of Partially Exchanged Co−H Zeolites, J.

Phys. Chem. B. 108 (2004) 2120–2127. doi:10.1021/jp034814o.

[117] M.C. Campa, S. De Rossi, G. Ferraris, V. Indovina, Catalytic activity of Co-ZSM-5 for the abatement of NOx with methane in the presence of oxygen, Appl. Catal. B Environ. 8 (1996) 315–331. doi:10.1016/0926-3373(95)00072-0.

[118] L.B. Gutierrez, E.E. Miró, M.A. Ulla, Effect of the location of cobalt species on NO adsorption and NOx-SCR over Co–mordenite, Appl. Catal. A Gen. 321 (2007) 7–16. doi:10.1016/j.apcata.2006.12.022.

[119] Z. Sobalík, J. Dědeček, D. Kaucký, B. Wichterlová, L. Drozdová, R. Prins, Structure, Distribution, and Properties of Co Ions in Ferrierite Revealed by FTIR, UV–Vis, and EXAFS, J. Catal. 194 (2000) 330–342. doi:10.1006/JCAT.2000.2926.

[120] F. Lónyi, H.E. Solt, Z. Pászti, J. Valyon, Applied Catalysis B : Environmental Mechanism of NO-SCR by methane over Co , H-ZSM-5 and Co , H-mordenite catalysts, "Applied Catal. B, Environ. 150–151 (2014) 218–229. doi:10.1016/j.apcatb.2013.12.024.

[121] J.-Y. Yan, H.H. Kung, W.M.H. Sachtler, M.C. Kung, Synergistic Effect in Lean NOx Reduction by CH_4 over Co/Al2O3and H-Zeolite Catalysts, J. Catal. 175 (1998) 294–301. doi:10.1006/jcat.1998.2012.

[122] G. Koyano, S. Yokoyama, M. Misono, States of Pd in Pd/H–ZSM-5 and Pd/Na–ZSM-5 catalysts and catalytic activity for the reduction of NO by CH_4 in the presence of O_2, Appl. Catal. A Gen. 188 (1999) 301–312. doi:10.1016/S0926-860X(99)00222-7.

[123] a. Ali, W. Alvarez, C.J. Loughran, D.E. Resasco, State of Pd on H-ZSM-5 and other acidic supports during the selective reduction of NO by CH4 studied by EXAFS/XANES, Appl. Catal. B Environ. 14 (1997) 13–22. doi:10.1016/S0926-3373(97)00008-8.

[124] R.W. van den Brink, R. Louw, P. Mulder, Formation of polychlorinated benzenes during the catalytic combustion of chlorobenzene using a Pt/γ-Al_2O_3 catalyst, Appl. Catal. B Environ. 16 (1998) 219–226. doi:10.1016/S0926-3373(97)00076-3.

[125] J.R. González-Velasco, R. López-Fonseca, A. Aranzabal, J.I. Gutiérrez-Ortiz, P. Steltenpohl, Evaluation of H-type zeolites in the destructive oxidation of chlorinated volatile organic compounds, Appl. Catal. B Environ. 24 (2000) 233–242. doi:10.1016/S0926-3373(99)00105-8.

[126] S. Scirè, Pt catalysts supported on H-type zeolites for the catalytic combustion of chlorobenzene, Appl. Catal. B Environ. 45 (2003) 117–125. doi:10.1016/S0926-3373(03)00122-X.

[127] B.H. Aristizábal, Tesis doctoral: Degradación catalítica de precursores de dioxinas y furanos., Universidad de Antioquia, 2007.

[128] R. López-Fonseca, J.I. Gutiérrez-Ortiz, M.A. Gutiérrez-Ortiz, J.R. González-Velasco, Dealuminated Y Zeolites for Destruction of Chlorinated Volatile Organic Compounds, J. Catal. 209 (2002) 145–150. doi:10.1006/JCAT.2002.3591.

[129] R. López-Fonseca, A. Aranzabal, P. Steltenpohl, J.. Gutiérrez-Ortiz, J.. González-Velasco, Performance of zeolites and product selectivity in the gas-phase oxidation of 1,2-dichloroethane, Catal. Today. 62 (2000) 367–377. doi:10.1016/S0920-5861(00)00438-7.

[130] M. Ogura, Y. Sugiura, M. Hayashi, E. Kikuchi, Reduction of nitric oxide with methane on Pd/Co/H-ZSM-5 catalysts: cooperative effects of Pd and Co, Catal. Letters. 42 (1996) 185–189. doi:10.1007/BF00810686.

[131] M. Ogura, S. Kage, T. Shimojo, J. Oba, M. Hayashi, M. Matsukata, E. Kikuchi, Co cation effects on activity and stability of isolated Pd(II) cations in zeolite matrices for selective catalytic reduction of nitric oxide with methane, J. Catal. 211 (2002) 75–84. doi:10.1016/S0021-9517(02)93722-X.

[132] P. Budi, R.F. Howe, Steam deactivation of CoZSM-5 NOx reduction catalysts, Catal. Today. 38 (1997) 175–179. doi:10.1016/S0920-5861(97)00063-1.

[133] F. Bustamante, F. Córdoba, M. Yates, C. Montes de Correa, The promotion of cobalt mordenite by palladium for the lean CH_4-SCR of NOx in moist streams, Appl. Catal.

A Gen. 234 (2002) 127–136. doi:10.1016/S0926-860X(02)00211-9.

[134] M. Gallastegi-Villa, A. Aranzabal, J.A. González-Marcos, J.R. González-Velasco, Metal-loaded ZSM5 zeolites for catalytic purification of dioxin/furans and NOx containing exhaust gases from MWI plants: Effect of different metal cations, Appl. Catal. B Environ. 184 (2016) 238–245. doi:10.1016/j.apcatb.2015.11.006.

[135] M. Gallastegi-Villa, A. Aranzabal, J.A. González-Marcos, J.R. González-Velasco, Tailoring dual redox-acid functionalities in VOx/TiO_2/ZSM5 catalyst for simultaneous abatement of PCDD/Fs and NOx from municipal solid waste incineration, Appl. Catal. B Environ. 205 (2017) 310–318. doi:10.1016/j.apcatb.2016.12.020.

[136] J. Cejka, H. Van Bekkum, A. Corma, F. Schüth, Studies in Surface Science and Catalysis 168: Introduction to Zeolite science and practice, Stud. Surf. Sci. Catal. 168 (2007) 455. doi:10.1016/S0167-2991(07)80803-2.

[137] R. Xu, W. Pang, J. Yu, Q. Huo, J. Chen, Chemistry of Zeolites and Related Porous Materials, John Wiley & Sons, Ltd, Chichester, UK, 2007. doi:10.1002/9780470822371.

[138] S.M. Auerbach, K.A. Carrado, P.K. Dutta, Handbook of zeolite science and technology, New York, 2003.

[139] J.A. Cubillos, PhD Thesis: Heterogeneous asymmetric epoxidation of cis-ethyl cinnamte over Jacobsen's catalyst immobilized in inorganic porous materials, Rheinisch-Westfalischen Technischen Hochschule/Aachen, 2005.

[140] M. Devadas, Selective Catalytic Reduction (SCR) of Nitrogen Oxides with Ammonia over Fe-ZSM5, Swiss Federal Institute of Technology Zurich, 2006.

[141] G. Busca, Acidity and basicity of zeolites: A fundamental approach, Microporous Mesoporous Mater. 254 (2017) 3–16. doi:10.1016/j.micromeso.2017.04.007.

[142] H. Van, Compendium of zeolite framework types building schemes and type

characteristics, First, Amsterdam, 2007.

[143] C.H. Bartholomew, R.J. Farrauto, Fundamentals of industrial catalytic process, John Wiley & Sons, Inc, New Jersey, 2006.

[144] T.K. Phung, G. Busca, On the Lewis acidity of protonic zeolites, Appl. Catal. A Gen. 504 (2015) 151–157. doi:10.1016/j.apcata.2014.11.031.

[145] M. Stöcker, Gas phase catalysis by zeolites, Microporous Mesoporous Mater. 82 (2005) 257–292. doi:10.1016/j.micromeso.2005.01.039.

[146] G.D. Yadav, J.J. Nair, Sulfated zirconia and its modified versions as promising catalysts for industrial processes, Microporous Mesoporous Mater. 33 (1999) 1–48. doi:10.1016/S1387-1811(99)00147-X.

[147] A. Hofmann, J. Sauer, Surface Structure of Hydroxylated and Sulfated Zirconia. A Periodic Density-Functional Study †, J. Phys. Chem. B. 108 (2004) 14652–14662. doi:10.1021/jp049220f.

[148] X. Song, A. Sayari, Sulfated Zirconia-Based Strong Solid-Acid Catalysts: Recent Progress, Catal. Rev. 38 (1996) 329–412. doi:10.1080/01614949608006462.

[149] A. Cybulski, J.A. Moulijn, The Present and the Future of Structured Catalysts, in: Struct. Catal. React., 2nd ed., CRC Press, 2006: pp. 1–16. doi:10.3109/00016486609121831.

[150] R.M. Heck, S. Gulati, R.J. Farrauto, The application of monoliths for gas phase catalytic reactions, Chem. Eng. J. 82 (2001) 149–156. doi:10.1016/S1385-8947(00)00365-X.

[151] J. a. Moulijn, F. Kapteijn, Monolithic reactors in catalysis: Excellent control, Curr. Opin. Chem. Eng. 2 (2013) 346–353. doi:10.1016/j.coche.2013.05.003.

[152] T. Nijhuis, T. Nijhuis, A. Beers, A. Beers, T. Vergunst, T. Vergunst, I. Hoek, I. Hoek, F. Kapteijn, F. Kapteijn, J. Moulijn, J. Moulijn, Preparation of monolithic catalysts, Catal. Rev. 43 (2001) 345–380. doi:10.1081/CR-120001807.

[153] V. Tomašić, Application of the monoliths in DeNOx catalysis, Catal. Today. 119 (2007) 106–113. doi:10.1016/j.cattod.2006.08.047.

[154] J. a. Moulijn, M.T. Kreutzer, T.A. Nijhuis, F. Kapteijn, Monolithic Catalysts and Reactors, in: Adv. Catal., 2011: pp. 249–327. doi:10.1016/B978-0-12-387772-7.00005-8.

[155] R.M. Heck, R.J. Farrauto, S.T. Gulati, Catalytic Air Pollution Control, John Wiley & Sons, Inc., Hoboken, NJ, USA, 2009. doi:10.1002/9781118397749.

[156] P. Avila, M. Montes, E.E. Miró, Monolithic reactors for environmental applications: A review on preparation technologies, Chem. Eng. J. 109 (2005) 11–36. doi:10.1016/j.cej.2005.02.025.

[157] A. V Boix, J.M. Zamaro, E.A. Lombardo, E.E. Miró, The beneficial effect of silica on the activity and thermal stability of PtCoFerrierite-washcoated cordierite monoliths for the SCR of NOx with CH4, Appl. Catal. B Environ. 46 (2003) 121–132. doi:10.1016/S0926-3373(03)00216-9.

[158] C.A. González, A.N. Ardila, C. Montes de Correa, M.A. Martínez, G. Fuentes-Zurita, Pd/TiO_2 Washcoated Cordierite Minimonoliths for Hydrodechlorination of Light Organochlorinated Compounds, Ind. Eng. Chem. Res. 46 (2007) 7961–7969. doi:10.1021/ie070713r.

[159] P. Worsfold, C. Poole, A. Townshend, M. Miró, B. Fernández, L. Lobo, R. Pereiro, Atomic Absorpton Spectrometry | Fundamentals, Instrumentation and Capabilities, Encycl. Anal. Sci. (2019) 137–143. doi:10.1016/B978-0-12-409547-2.14116-2.

[160] G. Perego, Characterization of heterogeneous catalysts by X-ray diffraction techniques, Catal. Today. 41 (1998) 251–259. doi:10.1016/S0920-5861(98)00054-6.

[161] P. Gallezot, X-Ray Techniques in Catalysis, in: Catalysis, 1984: pp. 221–273. doi:10.1007/978-3-642-93247-2_4.

[162] G. Leofanti, M. Padovan, G. Tozzola, B. Venturelli, Surface area and pore texture of

catalysts, Catal. Today. 41 (1998) 207–219. doi:10.1016/S0920-5861(98)00050-9.

[163] S. Brunauer, P.H. Emmett, E. Teller, Adsorption of Gases in Multimolecular Layers, J. Am. Chem. Soc. 60 (1938) 309–319. doi:10.1021/ja01269a023.

[164] M.. Reiche, M. Maciejewski, A. Baiker, Characterization by temperature programmed reduction, Catal. Today. 56 (2000) 347–355. doi:10.1016/S0920-5861(99)00294-1.

[165] A.G. Thomé, S. Peters, F. Roessner, iTPR - a new methodical approach for temperature programmed reduction of catalysts with improved sensitivity, Catal. Commun. 97 (2017) 10–13. doi:10.1016/J.CATCOM.2017.04.011.

[166] H.G. Karge, Concepts and Analysis of Surface Acidity and Basicity, in: Handb. Heterog. Catal., Wiley-VCH Verlag GmbH & Co. KGaA, Weinheim, Germany, 2008: pp. 1096–1122. doi:10.1002/9783527610044.hetcat0057.

[167] J. Weitkamp, M. Hunger, Chapter 22 Acid and base catalysis on zeolites, in: Stud. Surf. Sci. Catal., Elsevier, 2007: pp. 787–835. doi:10.1016/S0167-2991(07)80810-X.

[168] J.L. Falconer, J.A. Schwarz, Temperature-Programmed Desorption and Reaction: Applications to Supported Catalysts, Catal. Rev. 25 (1983) 141–227. doi:10.1080/01614948308079666.

[169] G. Busca, Characterization of Real Catalytic Materials, in: Heterog. Catal. Mater., Elsevier, 2014: pp. 23–35. doi:10.1016/b978-0-444-59524-9.00003-1.

[170] J.M. Thomas, C. Ducati, Transmission Electron Microscopy, in: Charact. Solid Mater. Heterog. Catal., Wiley-VCH Verlag GmbH & Co. KGaA, Weinheim, Germany, 2012: pp. 655–701. doi:10.1002/9783527645329.ch16.

[171] A.K. Datye, P.L. Hansen, S. Helveg, Electron Microscopy and Diffraction, in: Handb. Heterog. Catal., Wiley-VCH Verlag GmbH & Co. KGaA, Weinheim, Germany, 2008. doi:10.1002/9783527610044.hetcat0041.

[172] W. Zhou, Transmission Electron Microscopy, in: Met. Oxide Catal., Wiley-VCH Verlag GmbH & Co. KGaA, Weinheim, Germany, 2013: pp. 443–485.

doi:10.1002/9783527626113.ch10.

[173] G.D. Rostron Paul, Gaber Safa, Raman Spectroscopy, Review, Int. J. Eng. Tech. Res. 6 (2016) 50–64.

[174] G. Mestl, H. Knözinger, Vibrational Spectroscopy, in: Handb. Heterog. Catal., Wiley-VCH Verlag GmbH & Co. KGaA, Weinheim, Germany, 2008: pp. 932–971. doi:10.1002/9783527610044.hetcat0046.

[175] Y.-S. Li, J.S. Church, Raman spectroscopy in the analysis of food and pharmaceutical nanomaterials, J. Food Drug Anal. 22 (2014) 29–48. doi:10.1016/J.JFDA.2014.01.003.

[176] G.D. Rostron Paul, Gaber Safa, (Raman Spectroscopy), 392 (2018) 1–10.

[177] R.S. Das, Y.K. Agrawal, Raman spectroscopy: Recent advancements, techniques and applications, Vib. Spectrosc. 57 (2011) 163–176. doi:10.1016/J.VIBSPEC.2011.08.003.

[178] E. Taglauer, Surface Chemical Composition, in: Handb. Heterog. Catal., Wiley-VCH Verlag GmbH & Co. KGaA, Weinheim, Germany, 2008: pp. 1014–1029. doi:10.1002/9783527610044.hetcat0051.

[179] V.Y. Young, G.B. Hoflund, Handbook of Surface and Interface Analysis, in: J. Rivière, S. Myhra (Eds.), Handb. Surf. Interface Anal., CRC Press, 2009: pp. 19–64. doi:10.1201/9781420007800.

[180] M.R. Derrick, D. Stulik, J.M. Landry, The, Infrared Spectroscopy in Conservation Science, 1999.

[181] J. Szanyi, M.T. Paffett, The Adsorption of NO and Reaction of NO with O_2 on H-, NaH-, CuH-, and Cu-ZSM-5: Anin SituFTIR Investigation, J. Catal. 164 (1996) 232–245. doi:10.1006/jcat.1996.0378.

[182] H.S. Fogler, Elements of Chemical Reaction Engineering, Fourth, 2006.

[183] S. Vyazovkin, C.A. Wight, KINETICS IN SOLIDS, Annu. Rev. Phys. Chem. 48

(1997) 125–149. doi:10.1146/annurev.physchem.48.1.125.

[184] J.M. Smith, Chemical engineering kinetics, 2nd ed., McGraw-Hill, New York, 1970.

[185] R.J. Baxter, P. Hu, Insight into why the Langmuir–Hinshelwood mechanism is generally preferred, J. Chem. Phys. 116 (2002) 4379–4381. doi:10.1063/1.1458938.

[186] M.E. Davis, R.J. Davis, Fundamentals of Chemical Reaction Engineering, 2003.

[187] V.A. Tsipouriari, X.E. Verykios, Kinetic study of the catalytic reforming of methane with carbon dioxide to synthesis gas over Ni/La2O3 catalyst, Catal. Today. 64 (2001) 83–90. doi:10.1016/S0920-5861(00)00511-3.

[188] D.E. Mears, Tests for Transport Limitations in Experimental Catalytic Reactors, Ind. Eng. Chem. Process Des. Dev. 10 (1971) 541–547. doi:10.1021/i260040a020.

[189] H.H. Ibrahim, R.O. Idem, Kinetic studies of the partial oxidation of gasoline (POXG) over a Ni-CeO2 catalyst in a fixed-bed flow reactor, Chem. Eng. Sci. 62 (2007) 6582–6594. doi:10.1016/j.ces.2007.07.073.

[190] R. Madon, M. Boudart, Experimental Criterion for the Absence of Artifacts in the Measurement of Rates of Heterogenous Catalytic Reactions, in: Ind. Eng. Chem. Fundam., 1982: pp. 438–447.

[191] B. Li, Y. Chen, L. Li, J. Kan, S. He, B. Yang, S. Shen, S. Zhu, Reaction kinetics and mechanism of benzene combustion over the $NiMnO_3/CeO_2$/Cordierite catalyst, J. Mol. Catal. A Chem. 415 (2016) 160–167. doi:10.1016/j.molcata.2016.01.023.

[192] C.E. Hetrick, F. Patcas, M.D. Amiridis, Applied Catalysis B : Environmental Effect of water on the oxidation of dichlorobenzene over V_2O_5/TiO_2 catalysts, "Applied Catal. B, Environ. 101 (2011) 622–628. doi:10.1016/j.apcatb.2010.11.003.

[193] M. Taralunga, J. Mijoin, P. Magnoux, Catalytic destruction of chlorinated POPs—Catalytic oxidation of chlorobenzene over PtHFAU catalysts, Appl. Catal. B Environ. 60 (2005) 163–171. doi:10.1016/j.apcatb.2005.02.024.

[194] V. de Jong, A Mechanistic Study on the Catalytic Combustion of Benzene and

Chlorobenzene, J. Catal. 211 (2002) 355–365. doi:10.1016/S0021-9517(02)93762-0.

[195] J.R. González-Velasco, A. Aranzabal, R. López-Fonseca, R. Ferret, J.A. González-Marcos, Enhancement of the catalytic oxidation of hydrogen-lean chlorinated VOCs in the presence of hydrogen-supplying compounds, Appl. Catal. B Environ. 24 (2000) 33–43. doi:10.1016/S0926-3373(99)00087-9.

[196] R.. van den Brink, M. Krzan, M.M.. Feijen-Jeurissen, R. Louw, P. Mulder, The role of the support and dispersion in the catalytic combustion of chlorobenzene on noble metal based catalysts, Appl. Catal. B Environ. 24 (2000) 255–264. doi:10.1016/S0926-3373(99)00113-7.

[197] F. Bertinchamps, A. Attianese, M.M. Mestdagh, E.M. Gaigneaux, Catalysts for chlorinated VOCs abatement: Multiple effects of water on the activity of VOx based catalysts for the combustion of chlorobenzene, Catal. Today. 112 (2006) 165–168. doi:10.1016/j.cattod.2005.11.043.

[198] P. Gélin, A. Goguet, C. Descorme, C. Lécuyer, M. Primet, Catalytic Properties of Palladium Exchanged ZSM-5 Catalysts in the Reduction of Nitrogen Monoxide by Methane in the Presence of Oxygen: Nature of the Active sites, Stud. Surf. Sci. Catal. 116 (1998) 275–284. doi:10.1016/S0167-2991(98)80884-7.

[199] B. Azambre, L. Zenboury, P. Da Costa, S. Capela, S. Carpentier, A. Westermann, Palladium catalysts supported on sulfated ceria – zirconia for the selective catalytic reduction of NO x by methane : Catalytic performances and nature of active Pd species, Catal. Today. 176 (2011) 242–249. doi:10.1016/j.cattod.2010.12.026.

[200] T. Tabata, M. Kokitsu, O. Okada, Relationship between methane adsorption and selective catalytic reduction of nitrogen oxide by methane on gallium and indium ion-exchanged ZSM-5, Appl. Catal. B Environ. 6 (1995) 225–236. doi:10.1016/0926-3373(95)00016-X.

[201] B.H. Stuart, Infrared Spectroscopy: Fundamentals and Applications, John Wiley & Sons, Ltd, Chichester, UK, 2004. doi:10.1002/0470011149.

[202] W.C. Wilfong, C.S. Srikanth, S.S.C. Chuang, In Situ ATR and DRIFTS Studies of the Nature of Adsorbed CO_2 on Tetraethylenepentamine Films, ACS Appl. Mater. Interfaces. 6 (2014) 13617–13626. doi:10.1021/am5031006.

[203] K.S.W. Sing, Reporting physisorption data for gas/solid systems with special reference to the determination of surface area and porosity (Recommendations 1984), Pure Appl. Chem. 57 (1985) 603–619. doi:10.1351/pac198557040603.

[204] J.M. Stencel, V.U.S. Rao, J.R. Diehl, K.H. Rhee, A.G. Dhere, R.J. DeAngelis, Dual cobalt speciation in Co ZSM-5 catalysts, J. Catal. 84 (1983) 109–118. doi:10.1016/0021-9517(83)90090-8.

[205] P. Bazylewski, D.W. Boukhvalov, A.I. Kukharenko, E.Z. Kurmaev, A. Hunt, A. Moewes, Y.H. Lee, S.O. Cholakh, G.S. Chang, The characterization of Co-nanoparticles supported on graphene, RSC Adv. 5 (2015) 75600–75606. doi:10.1039/C5RA12893E.

[206] A. Lu, Y. Chen, D. Zeng, M. Li, Q. Xie, X. Zhang, D.L. Peng, Shape-related optical and catalytic properties of wurtzite-type CoO nanoplates and nanorods, Nanotechnology. 25 (2014). doi:10.1088/0957-4484/25/3/035707.

[207] S.C. Petitto, M.A. Langell, Surface composition and structure of Co_3O_4 (110) and the effect of impurity segregation, J. Vac. Sci. Technol. A Vacuum, Surfaces, Film. 22 (2004) 1690–1696. doi:10.1116/1.1763899.

[208] B. Ernst, S. Libs, P. Chaumette, A. Kiennemann, Preparation and characterization of Fischer–Tropsch active Co/SiO_2 catalysts, Appl. Catal. A Gen. 186 (1999) 145–168. doi:10.1016/S0926-860X(99)00170-2.

[209] Y. Xu, Z. Liu, D. Chen, Y. Song, R. Wang, Synthesis and Electrochemical Properties of Porous α-Co(OH) 2 and Co_3O_4 Microspheres, Prog. Nat. Sci. Mater. Int. 27 (2017) 197–202. doi:10.1016/j.pnsc.2017.03.001.

[210] M.C. Biesinger, B.P. Payne, A.P. Grosvenor, L.W.M. Lau, A.R. Gerson, R.S.C. Smart, Resolving surface chemical states in XPS analysis of first row transition metals,

oxides and hydroxides: Cr, Mn, Fe, Co and Ni, Appl. Surf. Sci. 257 (2011) 2717–2730. doi:10.1016/j.apsusc.2010.10.051.

[211] L.. Gutierrez, A.. Boix, E.. Lombardo, J.L.. Fierro, Study of the Co–Pt Synergism for the Selective Catalytic Reduction of NOx with CH_4, J. Catal. 199 (2001) 60–72. doi:10.1006/jcat.2000.3143.

[212] J.F. Moulder, W.F. Stickle, P.E. Sobol, K.D. Bomben, Handbook of X-ray Photoelectron Spectroscopy, Physical Electronics, Inc., Minnesotta, USA, 1992.

[213] A.L. Guimarães, L.C. Dieguez, M. Schmal, Surface Sites of $Pd/CeO_2/Al_2O_3$ Catalysts in the Partial Oxidation of Propane, J. Phys. Chem. B. 107 (2003) 4311–4319. doi:10.1021/jp0270194.

[214] K.S. Kim, X-ray-photoelectron spectroscopic studies of the electronic structure of CoO, Phys. Rev. B. 11 (1975) 2177–2185. doi:10.1103/PhysRevB.11.2177.

[215] F. Poignant, J.L. Freysz, M. Daturi, J. Saussey, Mechanism of the selective catalytic reduction of NO in oxygen excess by propane on H–Cu–ZSM-5, Catal. Today. 70 (2001) 197–211. doi:10.1016/S0920-5861(01)00418-7.

[216] K. Hadjiivanov, B. Tsyntsarski, T. Nikolova, Stability and reactivity of the nitrogen-oxo species formed after NO adsorption and $NO+O_2$ coadsorption on Co-ZSM-5: An FTIR spectroscopic study, Phys. Chem. Chem. Phys. 1 (1999) 4521. doi:10.1039/a904992d.

[217] L.J. Lobree, A.W. Aylor, J.A. Reimer, A.T. Bell, NO Reduction by CH4in the Presence of O_2 over Pd-H-ZSM-5, J. Catal. 181 (1999) 189–204. doi:10.1006/jcat.1998.2303.

[218] K. Hadjiivanov, E. Ivanova, M. Daturi, J. Saussey, J.-C. Lavalley, Nitrosyl complexes on Co–ZSM-5: an FTIR spectroscopic study, Chem. Phys. Lett. 370 (2003) 712–718. doi:10.1016/S0009-2614(03)00173-8.

[219] A. Bellmann, H. Atia, U. Bentrup, A. Brückner, Mechanism of the selective reduction

of NOx by methane over Co-ZSM-5, Appl. Catal. B Environ. 230 (2018) 184–193. doi:10.1016/J.APCATB.2018.02.051.

[220] Y.J. Li, T.L. Slager, J.N. Armor, Selective reduction of NOxby methane on co-ferrierites. II. Catalyst characterization, J. Catal. 150 (1994) 388–399. doi:10.1006/jcat.1994.1357.

[221] K. Góra-Marek, B. Gil, J. Datka, Quantitative IR studies of the concentration of Co^{2+} and Co^{3+} sites in zeolites CoZSM-5 and CoFER, Appl. Catal. A Gen. 353 (2009) 117–122. doi:10.1016/j.apcata.2008.10.034.

[222] F. Geobaldo, B. Onida, P. Rivolo, F. Di Renzo, F. Fajula, E. Garrone, Nature and reactivity of Co species in a cobalt-containing beta zeolite: An FTIR study, Catal. Today. 70 (2001) 107–119. doi:10.1016/S0920-5861(01)00411-4.

[223] A.W. Aylor, L.J. Lobree, J.A. Reimer, A.T. Bell, An infrared study of NO reduction by CH4 over Co-ZSM-5, Stud. Surf. Sci. Catal. 101 (1996) 661–670. doi:10.1016/S0167-2991(96)80277-1.

[224] C. Naccache, Y. Ben Taarit, Nature of nitric oxide and nitrogen dioxide adsorbed on chromium and nickel exchanged zeolites. Electron spin resonance and infra-red study, J. Chem. Soc. Faraday Trans. 1 Phys. Chem. Condens. Phases. 69 (1973) 1475. doi:10.1039/f19736901475.

[225] M. Che, J.F. Dutel, P. Gallezot, M. Primet, A study of the chemisorption of nitric oxide on PdY zeolite. Evidence for a room temperature oxidative dissolution of palladium crystallites, J. Phys. Chem. 80 (1976) 2371–2381. doi:10.1021/j100562a011.

[226] A.W. Aylor, L.J. Lobree, J.A. Reimer, A.T. Bell, Investigations of the Dispersion of Pd in H-ZSM-5, J. Catal. 172 (1997) 453–462. doi:10.1006/jcat.1997.1893.

[227] K. Shimizu, F. Okada, Y. Nakamura, A. Satsuma, T. Hattori, Mechanism of NO Reduction by CH_4 in the Presence of O_2 over Pd–H–Mordenite, J. Catal. 195 (2000) 151–160. doi:10.1006/jcat.2000.2964.

[228] J.E. House, Molecular Rotation and Spectroscopy, in: Fundam. Quantum Mech., Elsevier, 2018: pp. 137–158. doi:10.1016/B978-0-12-809242-2.00007-3.

[229] M. Kantcheva, Identification, Stability, and Reactivity of NOx Species Adsorbed on Titania-Supported Manganese Catalysts, J. Catal. 204 (2001) 479–494. doi:10.1006/jcat.2001.3413.

[230] A.W. Aylor, L.J. Lobree, J.A. Reimer, A.T. Bell, NO Adsorption, Desorption, and Reduction by CH_4 over Mn-ZSM-5, J. Catal. 170 (1997) 390–401. doi:10.1006/jcat.1997.1776.

[231] T. Beutel, FTIR study of the nitrogen isotopic exchange between adsorbed $^{15}NO_2$ complexes and ^{14}NO over Cu/ZSM-5 and Co/ZSM-5, Appl. Catal. B Environ. 9 (1996) L1–L10. doi:10.1016/0926-3373(95)00086-0.

[232] T. Cheung, S.K. Bhargava, M. Hobday, K. Foger, Adsorption of NO on Cu Exchanged Zeolites, an FTIR Study: Effects of Cu Levels, NO Pressure, and Catalyst Pretreatment, J. Catal. 158 (1996) 301–310. doi:10.1006/jcat.1996.0029.

[233] L.J. Lobree, A.W. Aylor, J.A. Reimer, A.T. Bell, Role of Cyanide Species in the Reduction of NO by CH4over Co–ZSM-5, J. Catal. 169 (1997) 188–193. doi:10.1006/JCAT.1997.1699.

[234] L.J. Lobree, A.W. Aylor, J.A. Reimer, A.T. Bell, NO Reduction by CH4 in the Presence of O_2 over Pd-H-ZSM-5, J. Catal. 181 (1999) 189–204. doi:10.1006/jcat.1998.2303.

[235] L.F. Córdoba, W.M.H. Sachtler, C. Montes de Correa, NO reduction by CH4 over Pd/Co-sulfated zirconia catalysts, Appl. Catal. B Environ. 56 (2005) 269–277. doi:10.1016/j.apcatb.2004.09.012.

[236] F. Lónyi, H.E. Solt, J. Valyon, A. Boix, L.B. Gutierrez, The SCR of NO with methane over In,H- and Co,In,H-ZSM-5 catalysts: The promotional effect of cobalt, Appl. Catal. B Environ. 117–118 (2012) 212–223. doi:10.1016/j.apcatb.2012.01.022.

[237] L.J. Lobree, A.W. Aylor, J.A. Reimer, A.T. Bell, NO Reduction by CH4in the Presence of O2over Pd-H-ZSM-5, J. Catal. 181 (1999) 189–204. doi:10.1006/JCAT.1998.2303.

[238] a Zecchina, S. Bordiga, G. Spoto, D. Scarano, G. Petrini, G. Leofanti, M. Padovan, C.O. Areàn, Low-temperature Fourier-transform infrared investigation of the interaction of CO with nanosized ZSM5 and silicalite, J. Chem. Soc., Faraday Trans. 88 (1992) 2959–2969. doi:10.1039/FT9928802959.

[239] A.A. Gabrienko, I.G. Danilova, S.S. Arzumanov, A. V. Toktarev, D. Freude, A.G. Stepanov, Strong acidity of silanol groups of zeolite beta: Evidence from the studies by IR spectroscopy of adsorbed CO and 1H MAS NMR, Microporous Mesoporous Mater. 131 (2010) 210–216. doi:10.1016/j.micromeso.2009.12.025.

[240] M. Bevilacqua, A.G. Alejandre, C. Resini, M. Casagrande, J. Ramirez, G. Busca, An FTIR study of the accessibility of the protonic sites of H-mordenites, Phys. Chem. Chem. Phys. 4 (2002) 4575–4583. doi:10.1039/b201886a.

[241] M. Trombetta, T. Armaroli, A. Gutièrrez Alejandre, J. Ramirez Solis, G. Busca, An FT-IR study of the internal and external surfaces of HZSM5 zeolite, Appl. Catal. A Gen. 192 (2000) 125–136. doi:10.1016/S0926-860X(99)00338-5.

[242] C. Jia, P. Massiani, D. Barthomeuf, Characterization by infrared and nuclear magnetic resonance spectroscopies of calcined beta zeolite, J. Chem. Soc. Faraday Trans. 89 (1993) 3659. doi:10.1039/ft9938903659.

[243] U. Bardi, International Encyclopedia of the Social & Behavioral Sciences, Elsevier, 2015. doi:10.1016/B978-0-08-097086-8.91047-X.

[244] Y. Guan, Y. Liu, W. Wu, K. Sun, Y. Li, P. Ying, Z. Feng, C. Li, Dibenzodioxin Adsorption on Inorganic Materials, Langmuir. 21 (2005) 3877–3880. doi:10.1021/la0468545.

[245] V.L. Zholobenko, M.A. Makarova, J. Dwyer, Inhomogeneity of Broensted acid sites in H-mordenite, J. Phys. Chem. 97 (1993) 5962–5964. doi:10.1021/j100124a030.

[246] B. Su, V. Norberg, Adsorption Behavior of Benzene in NaBeta Zeolite: An in-Situ Infrared Study of Molecular Recognition, Langmuir. 14 (1998) 7410–7419. doi:10.1021/la9809574.

[247] M. Bevilacqua, G. Busca, A study of the localization and accessibility of Brønsted and Lewis acid sites of H-mordenite through the FT-IR spectroscopy of adsorbed branched nitriles, Catal. Commun. 3 (2002) 497–502. doi:10.1016/S1566-7367(02)00196-6.

[248] T. Vazhnova, D.B. Lukyanov, Fourier Self-Deconvolution of the IR Spectra as a Tool for Investigation of Distinct Functional Groups in Porous Materials: Brønsted Acid Sites in Zeolites, Anal. Chem. 85 (2013) 11291–11296. doi:10.1021/ac4020337.

[249] N. Cherkasov, T. Vazhnova, D.B. Lukyanov, Quantitative infra-red studies of Brønsted acid sites in zeolites: Case study of the zeolite mordenite, Vib. Spectrosc. 83 (2016) 170–179. doi:10.1016/j.vibspec.2016.02.002.

[250] J. Bandara, J.A. Mielczarski, J. Kiwi, I. Adsorption mechanism of chlorophenols on iron oxides, titanium oxide and aluminum oxide as detected by infrared spectroscopy, Appl. Catal. B Environ. 34 (2001) 307–320. doi:10.1016/S0926-3373(01)00224-7.

[251] M. Nagao, Y. Suda, Adsorption of benzene, toluene, and chlorobenzene on titanium dioxide, Langmuir. 5 (1989) 42–47. doi:10.1021/la00085a009.

[252] J.N. Kondo, E. Yoda, H. Ishikawa, F. Wakabayashi, K. Domen, Acid Property of Silanol Groups on Zeolites Assessed by Reaction Probe IR Study, J. Catal. 191 (2000) 275–281. doi:10.1006/jcat.1999.2807.

[253] M.A. Larrubia, G. Busca, An FT-IR study of the conversion of 2-chloropropane, o-dichlorobenzene and dibenzofuran on V_2O_5-MoO_3-TiO_2 SCR-DeNOx catalysts, Appl. Catal. B Environ. 39 (2002) 343–352. doi:10.1016/S0926-3373(02)00116-9.

[254] A. Sahasrabudhe, V.S. Kamble, A.K. Tripathi, N.M. Gupta, FTIR Study on Molecular Motions of Benzene Adsorbed in ZSM-5 Zeolite: Role of Charge-Balancing Cations and Pore Size, J. Phys. Chem. B. 105 (2001) 4374–4379. doi:10.1021/jp010381i.

[255] J. Lichtenberger, M.D. Amiridis, Catalytic oxidation of chlorinated benzenes over V2O5/TiO2 catalysts, J. Catal. 223 (2004) 296–308. doi:10.1016/j.jcat.2004.01.032.

[256] P.S. Chintawar, H.L. Greene, Interaction of Chlorinated Ethylenes with Chromium Exchanged Zeolite Y: Anin SituFT-IR Study, J. Catal. 165 (1997) 12–21. doi:10.1006/jcat.1997.1443.

[257] L.F. Córdoba, Remoción de Óxidos de nitrógeno bajo condiciones típicas de motores diesel., Universidad de Antioquia, 2004.

[258] Y.J. Li, J.N. Armor, Selective Reduction of NO by Methane on Co-Ferrierites: I. Reaction and Kinetic Studies, J. Catal. 150 (1994) 376–387. doi:10.1006/jcat.1994.1356.

[259] M. Cristina Campa, D. Pietrogiacomi, S. Tuti, G. Ferraris, V. Indovina, The selective catalytic reduction of NO with CH_4 on Mn-ZSM5: A comparison with Co-ZSM5 and Cu-ZSM5, Appl. Catal. B Environ. 18 (1998) 151–162. doi:10.1016/S0926-3373(98)00034-4.

[260] X. She, M. Flytzani-Stephanopoulos, Activity and stability of Ag–alumina for the selective catalytic reduction of NOx with methane in high-content SO_2 gas streams, Catal. Today. 127 (2007) 207–218. doi:10.1016/j.cattod.2007.04.010.

[261] D.B. Lukyanov, E.A. Lombardo, G.A. Sill, J.L. D'Itri, W.K. Hall, Selective Catalytic Reduction (SCR) of NO with Methane over CoZSM-5 and HZSM-5 Zeolites: On the Role of Free Radicals and Competitive Oxidation Reactions, J. Catal. 163 (1996) 447–456. doi:10.1006/jcat.1996.0346.

[262] X. Ma, X. Feng, J. Guo, H. Cao, X. Suo, H. Sun, M. Zheng, Applied Catalysis B : Environmental Catalytic oxidation of 1 , 2-dichlorobenzene over Ca-doped FeO x hollow microspheres, "Applied Catal. B, Environ. 147 (2014) 666–676. doi:10.1016/j.apcatb.2013.10.003.

[263] S. Krishnamoorthy, M. D. Amiridis, Kinetic and in situ FTIR studies of the catalytic oxidation of 1,2-dichlorobenzene over V_2O_5/Al_2O_3 catalysts, Catal. Today. 51 (1999)

203–214. doi:10.1016/S0920-5861(99)00045-0.

[264] M. Gallastegi-Villa, A. Aranzabal, Z. Boukha, J.A. González-Marcos, J.R. González-Velasco, M.V. Martínez-Huerta, M.A. Bañares, Role of surface vanadium oxide coverage support on titania for the simultaneous removal of o-dichlorobenzene and NOx from waste incinerator flue gas, Catal. Today. 254 (2015) 2–11. doi:10.1016/j.cattod.2015.02.029.

[265] E.D. Banús, V.G. Milt, E.E. Miró, M. a. Ulla, Catalytic coating synthesized onto cordierite monolith walls. Its application to diesel soot combustion, Appl. Catal. B Environ. 132–133 (2013) 479–486. doi:10.1016/j.apcatb.2012.12.020.